FAA-RD-79-21

Project Report
ATC-88
Volume III, 1

MLS Multipath Studies, Phase 3 Final Report Volume III: Application of Models to MLS Assessment Issues Part 1

J. E. Evans
S. J. Dolinar
D. A. Shnidman

8 June 1981

Lincoln Laboratory
MASSACHUSETTS INSTITUTE OF TECHNOLOGY
LEXINGTON, MASSACHUSETTS

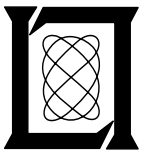

Prepared for the Federal Aviation Administration,
Washington, D.C. 20591

1. Report No.	2. Government Accession No.	3. Recipient's Catalog No.
FAA-RD-79-21		

4. Title and Subtitle	5. Report Date
MLS Multipath Studies, Phase 3. Final Report, Volume III: Application of Models to MLS Assessment Issues	8 June 1981
	6. Performing Organization Code

7. Author(s)	8. Performing Organization Report No.
James E. Evans, Samuel J. Dolinar and David A. Shnidman	ATC-88, Volume III, Part I

9. Performing Organization Name and Address	10. Work Unit No. (TRAIS)
Massachusetts Institute of Technology Lincoln Laboratory P.O. Box 73 Lexington, MA 02173	11. Contract or Grant No. DOT-FA74-WA1-461
	13. Type of Report and Period Covered Project Report
12. Sponsoring Agency Name and Address Department of Transportation Federal Aviation Administration Systems Research and Development Service Washington, DC 20591	14. Sponsoring Agency Code

15. Supplementary Notes

The work reported in this document was performed at Lincoln Laboratory, a center for research operated by Massachusetts Institute of Technology under Air Force Contract F19628-80-C-0002.

16. Abstract

This report presents work done during phase 3 of the US national Microwave Landing System (MLS) program toward developing a computer simulation model of MLS multipath effects, the experimental validation of the model, and the application of the model to investigate multipath performance of ICAO proposals for the new approach and landing guidance system.

The first two volumes of the report presented an overview of the simulation effort as well as describing in detail the propagation and MLS technique mathematical models and their validation by comparison with experimental data. In this volume, we describe the results of comparative simulations for the various MLS techniques in various scenarios and analyze in detail certain multipath performance features which were found to be significant in the scenario simulations.

Simulation results are presented for several scenarios, and shadowing of the MLS azimuth by taxiing and overflying aircraft is analyzed.

The remainder of the report focuses on multipath performance factors specific to various individual techniques. These include:

(1) the effects of angle data outlier tests and filtering in the TRSB receivers,

(2) the effects on the DMLS system due to receiver AGC, receiver motion-induced Doppler shifts, and the use of commutated reference systems, and

(3) acquisition/validation algorithms for all three techniques.

The report concludes with a summary and suggestions for future work. Part I of this volume consists of Chapters I through IV; Part II contains Chapters V through VIII and the Appendices.

17. Key Words	18. Distribution Statement
Microwave Landing System (MLS) Multipath Doppler MLS (DMLS) Time Reference Scanning Beam (TRSB) DME Based Landing System (DLS)	Document is available to the public through the National Technical Information Service, Springfield, VA 22151

19. Security Classif. (of this report)	20. Security Classif. (of this page)	21. No. of Pages	22. Price
Unclassified	Unclassified	284	

ABSTRACT

This report presents work done during phase 3 of the US National Microwave Landing System (MLS) program toward developing a computer simulation model of MLS multipath effects, the experimental validation of the model, and the application of the model to investigate the multipath performance of proposals for the new approach and landing guidance system. The model was developed by separately considering the charactertistics of the four basic elements affecting system operation in a multipath environment, i.e., airport, flight profile, propagation, and system elements. This modeling approach permits the examination of the effect on system performance of individual multipath performance factors such as: (a) reflections from terrain, aircraft, buildings with differing orientations; (b) shadowing by aircraft, buildings, and convex runways; (c) aircraft flight profiles and approach speeds; and (d) system design features to combat multipath.

The first two volumes of the report presented an overview of the simulation effort as well as describing in detail the propagation and MLS technique mathematical models and their validation by comparison with experimental data. In this volume, we describe the results of comparative simulations for the various MLS techniques in various scenarios and analyze in detail certain multipath performance features which were found to be significant in the scenario simulations.

Simulation results are presented both for the common comparative scenarios developed by the AWOP Working Group A (WG-A) multipath subgroup and for additional scenarios suggested by individual members of WG-A. Shadowing of the MLS azimuth by taxiing and overflying aircraft is analyzed analytically, by comparison of various field results and by comparative simulations.

The remainder of the report focuses on multipath performance factors specific to various individual techniques. These include:

(1) the effects of angle data outlier tests and filtering in the TRSB receivers

(2) the effects on the DMLS system due to the receiver AGC, receiver motion-induced Doppler shifts, and the use of commutated reference systems, and

(3) acquisition/validation algorithms for all three techniques.

The report concludes with a summary and suggestions for future work.

Part I of this volume consists of Chapters I through IV; Part II contains Chapters V through VIII and the appendices.

ACKNOWLEDGMENTS

The theoretical, simulation result, and field data analyses in this volume had significant contributions from several people in addition to the report authors. R. Orr contributed to the AWOP scenario result analysis as well as the TRSB shadowing and slew limiter studies. D. Shnidman analyzed the AWOP scenario multipath features and features of the DLS system performance. Steve Sussman contributed to the analysis of Doppler reference scalloping effects. Bob Burchsted, Janet Reid, and Bob Moffatt assisted in running many of the scenarios.

The studies on DMLS reference scalloping benefited from work by H. Wheeler of Hazeltine Corporation [11], J. Goodwin of ITT Gilfillan [13], and I. White of Plessey Company [140]. D. Vickers, G. Adams, J. Tracy, and R. Cleary of the Federal Aviation Administration provided the experimental data used in the shadowing studies (this included conducting a series of special field tests to address certain issues).

The AWOP WG-A multipath subgroup chaired by R. Butler was instrumental in the development and use of the comparative multipath scenarios. Other principal contributors from the subgroup included N. Hughes, J. Jones, H. Ecklundt, T. Hagenberg, and D. Cooper.

The encouragement of H. Weiss and I. Stiglitz of Lincoln Laboratory and F. Frisbie of the Federal Aviation Administration for our various studies when considerable controversy arose is gratefully acknowledged.

D. Young and N. Campbell typed the report, while C. Casazza and S. Cormney prepared the bulk of the figures.

CONTENTS

LIST OF ILLUSTRATIONS

I. INTRODUCTION AND OVERVIEW

A principal objective for the Microwave Landing System (MLS), is to reduce (as compared with ILS) the likelihood of guidance errors caused by reflections of the radio waves from terrain irregularities and objects at the airport (i.e., multipath). Thus, an important task in the MLS assessment by the International Civil Aviation Organization (ICAO) All Weather Operations Panel (AWOP) was to determine the sensitivity to multipath for the various proposed MLS techniques. In this volume of the report, we focus on the comparative behavior of the various proposals in common scenarios as well as analyzing specific multipath performance features of the systems.

Early in the AWOP assessment, it became apparent that comparative multipath performance could only be obtained by subjecting each system to identical conditions. The panel recognized that the MLS should be operational well into the 21st century, when far greater numbers of structures are expected to exist at airports. It was therefore necessary to examine system performance using airport models related to geometries found at today's airports but at the same time containing structures which one could expect to find in the future. Fully validated computer simulation of both airport multipath environments and MLS equipments was believed to be the most promising means of making the desired comparisons.

At the Melbourne meeting of the ICAO All Weather Operations Panel (AWOP) Working Group A (WG-A), it was agreed that computer simulation of the proposed techniques should be accomplished, and a number of airport scenarios* were

*A scenario specifies the siting of all ground-based equipment, the location and pertinent electrical characteristics of each reflecting and shadowing object and the aircraft flight path and approach velocity.

specified for this task [22]. These scenarios, while based upon existing airport layouts, were in most cases exaggerated in ways expected to provide more stringent tests of MLS capability than would the actual selected airports themselves. At the May 1976 Washington, D.C. meeting of WG-A, the use of computer simulation as a tool in assessing comparative multipath performance was again endorsed and a subgroup established to oversee the multipath simulation activity [111]. In particular, this subgroup:

(1) reviewed available system implementation descriptions and devised a mechanism for timely exchange of any missing data,

(2) established ground rules for system model validation,

(3) reviewed the existing set of scenarios and augmented it with several additional scenarios (based on the same airports) to address issues not foreseen at the Melbourne meeting,

(4) agreed to use the Lincoln Laboratory propagation model [29] for all the multipath simulations (consequently, the multipath signal characteristics for each scenario are identical for all implementations in a given frequency band, and

(5) established a common format for the presentation of results.

At subsequent meetings of the AWOP WG-A, additional scenario modifications were developed by the multipath subgroup. The results of these generally agreed to WG-A scenario simulations are described in chapter II. In addition, individual members of WG-A introduced scenarios which were intended to address specific performance features for one or more systems. Representative scenarios and analyses which involve reflection and shadowing phenomena are presented in chapters III and IV, respectively.

It is important to note the difference between the scenarios in this report and the simulations reported in volumes I and II of this report. Two general classes of simulation were conducted for the various interested parties: sensitivity simulations and airport-specific simulations. Sensitivity simulations are primarily concerned with identifying system sensitivities to general airport features (e.g., building and aircraft locations).

Models for the AWOP scenarios* are related to sensitivity simulations and were developed for the most part by placing simulated buildings at the locations of actual buildings at actual airports. It was agreed that the buildings assumed in some simulation runs were to be higher and/or more reflective than the actual buildings so as to compare all the systems in the more challenging environment that could exist when MLS is implemented. Also, it was agreed to simplify the airport features by representing the buildings by uniform flat plates, terrain as a horizontal flat sheet, etc. This was done because inclusion of fine detail (for example, the precise locations and shapes of windows on airport buildings) would so complicate the resulting simulation that one might never achieve the desired understanding of system behavior. Thus, although those scenarios were evolved from actual airports, the simulation results could not be directly related to MLS performance at the airport from which the scenario was derived. Although this point was well understood within AWOP [66], confusion was created outside AWOP by the (unfortunate) use of actual airport names to designate the AWOP scenarios derived from those airports.

---

*e.g., the "standard" scenarios agreed on by the AWOP [72,111] and/or the additional scenarios generated by the AWOP panel members from the FRG, Netherlands, U.K., and U.S.

Airport-specific simulations, intended to predict MLS performance at a given airport on a particular flight path, require utilization of very detailed airport data in generating the airport model. Airport-specific simulations such as are described in volumes I and II of this report were utilized to validate the multipath simulations. Careful site surveys are made to determine precise transmitter and scattering object locations, terrain features (e.g., grass height and ground contours), building surface composition, taxiing and parked aircraft locations, etc. Additionally, precise aircraft flight profile data is often necessary to give a close replication of resultant error waveform.

As noted in volume I of this report, the comparative scenario simulations have the virtue of bringing all the facets of multipath performance for a given system together to better assess the system behavior in the expected MLS environment. However, it was also necessary to analyze in depth those factors which emerged as important in yielding system performance differences. Figs. 1-1 to 1-3 show the multipath performance features* suggested as important by the respective system proposers. These suggestions were used as a starting point in the process of significant feature identification; however, many of the significant features were identified principally via the scenario simulations.

One issue identified in the scenario simulations was the means by which the TRSB receivers would reject "unreasonable" angle estimates and still time average the results to reduce noise and dynamic multipath effects. Chapter V

---

*Appendix A summarizes the specific implementations used in the simulations reported here.

1) DLS - Azimuth ground station
   - Large base interferometer system (appr. 95 wavelength for ± 40° coverage
   - Mathematical horizontal beam forming, including beam alignment to the direction of the received signal (virtual diagram)
   - Use of directional antennas
   - Growth potential:
     . use of vertical aperture antennas
     . simple modification of ground antenna arrays according to the special critical environments, i.e., sharper beam forming in vertical and/or horizontal direction, reducing of side lobes and grating lobes

2) DLS - Elevation ground station
   - Use of vertical beam forming procedures in the computer
   - Mathematical beam alignment corresponding to the elevation of the received signal
   - Lateral diversity antenna configuration for in beam multipath rejection. With the help of the lateral diversity antenna configuration a virtual horizontal antenna pattern is formed in additional to the virtual vertical pattern.

3) Common features for DLS-A and DLS-E
   - Multipath rejection due to time delay between direct and multipath signal
   - Coverage control within the computer program
   - Growth potential for improved mathemetical multipath rejection features

4) Airborne data processing
   - Elimination of outliers due to the airborne tracking gate
   - Variable airborne tracking gate width dependent on signal quality (reply efficiency, confidence level of the received signal)
   - Digital airborne data filtering, filter characteristic adapted to the interrogation rate
   - Variable airborne interrogation rate

     Normal mode: 15 Hz

     Approach mode: 50 Hz (automatically changed)

Fig. 1-1. DLS multipath immunity features.

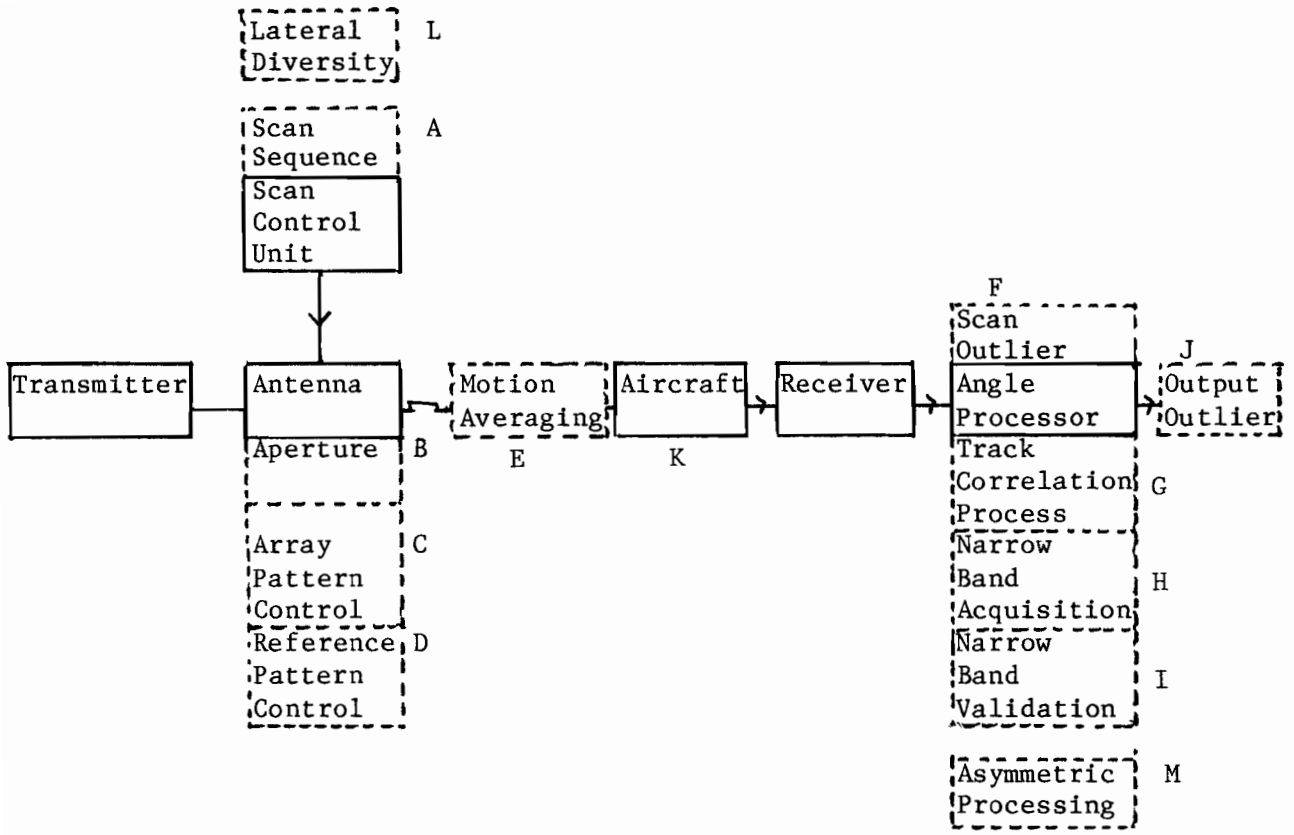

A) Scan control - use of optimum sequence of scans

B) Aperture of main array gives effective "narrow beam" coding of coverage

C) Azimuth and elevation patterns of array elements

D) Azimuth and elevation patterns of reference elements

E) Motion averaging - function of signal format and scan sequence

F) Outlier test applied to individual scans

G) Tracking processor matched to ground system aperture

H,I) Narrow band process discriminates against inconsistent signals larger than tracked signal

J) Outlier test applied to output data blocks

K) Not technique related

L) Tested on 60-wavelength elevation array

M) Can give in-beam multipath rejection to signals of known error sign, e.g., ground reflection in elevation

Fig. 1-2. Overview of DMLS multipath protection features.

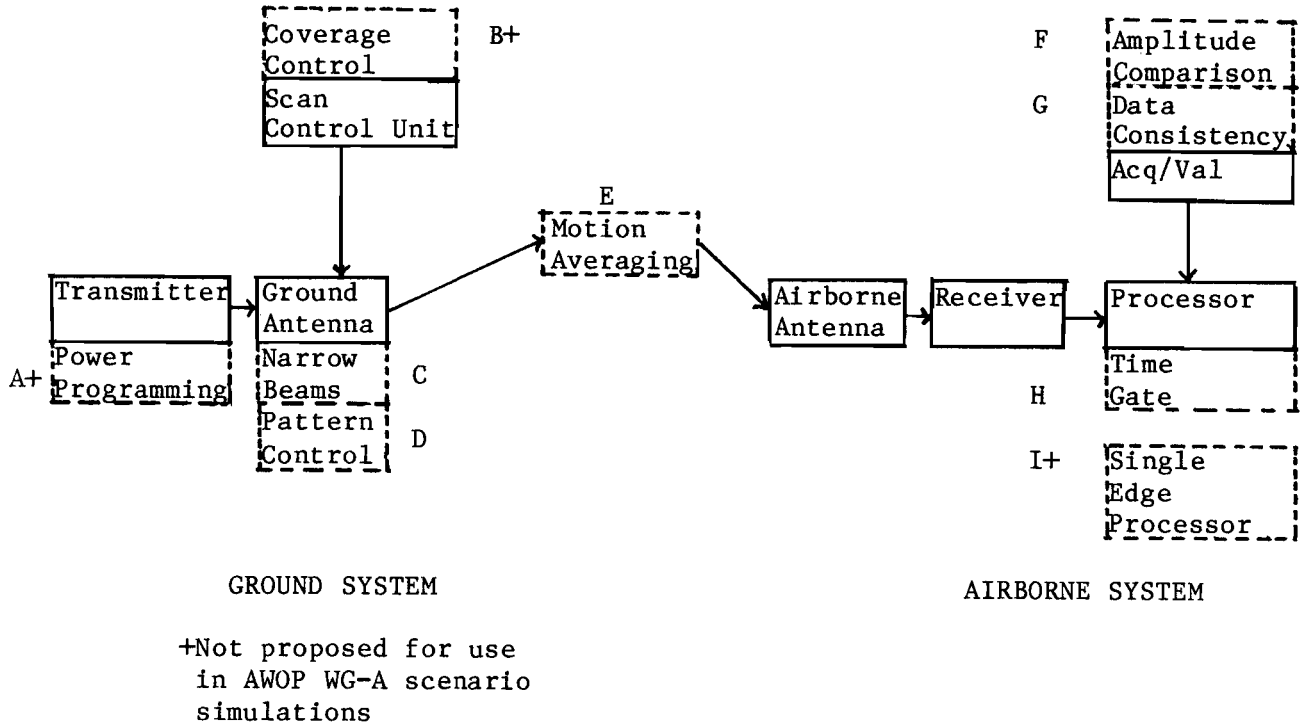

TRSB Multipath Immunity Features

TRSB Multipath Combatting Features Overview

A) Power programming - ability to vary radiated power as a function of scan angle.

B) Coverage control - ability to cutoff radiated power as a function of scan angle.

C) Narrow beams - use of wide apertures (e.g., 60) to yield narrow beam angle coding.

D) Pattern control - use of array elements which provide sharp elevation cutoff at low elevation angles to reduce ground influence. Shaped azimuth pattern of elevation arrays to provide centerline emphasis.

E) Motion averaging - optimized approximately uniform asynchronous scan spacing within data frame to provide good motion averaging down to low scalloping frequencies. High elevation/flare data rates.

F) Amplitude comparison - out of beam multipath rejected by amplitude comparison. Also, "real time" thresholding.

G) Data consistency - checks on to-fro beam symmetry, dwell gate widths, slew rate limiting on output values.

H) Time gate - Ignores out of beam multipath in making angle measurement (even if out of beam is momentarily greater than direct).

I) Single edge processor - makes measurements on clean edge of beam envelope when multipath is known to affect other edge (e.g., as in flare).

Fig. 1-3. Overview of TRSB multipath features.

describes the differences which arise when the data rejection is done prior to the filtering operation as opposed to after the filtering is accomplished.

Chapter VI discusses several multipath performance features which were unique to the DMLS concept. These include

(a) modification of the effective beam patterns due to multipath effects on the DMLS AGC circuit

(b) errors due to dynamic multipath effects on the DMLS reference signal including the performance interplay with the DMLS scan format

(c) errors due to dynamic multipath effects on the DMLS array signal

and

(d) use of lateral diversity for an elevation array to reduce the effects of multipath from vertical surfaces.

Another performance issue was the capability for acquisition and validation (ACQ/VAL) of the track on the proper angle signal. In principle, the various systems could utilize equivalent approaches to this problem. However, cost and hardware realization factors lead to suboptimal approaches in several cases. Chapter VII outlines the general ACQ/VAL problem and then discusses specific performance features of each proposed implementation. Also described is one scenario intended to explore ACQ/VAL behavior when several competing multipath signals are present.

The final chapter summarizes the results of the AWOP WG-A studies and presents some multipath performance areas which merit further investigation in the context of implementing the TRSB technique which was adopted by ICAO.

II. AWOP WG-A "STANDARD SCENARIOS"

In the preceding chapter, we indicated how a set of "standard" multipath scenarios was developed and refined by the AWOP WG-A. In this chapter, we:

(1) present the various airport scenarios

(2) describe the principal multipath characteristics (amplitude, separation angle, time delay, and scalloping frequency) for the scenarios

(3) show the resulting errors for the proposed DLS, DMLS, and TRSB implementations

The original AWOP WG-A scenarios developed in Melbourne are described in Section A.1 with the additional scenarios described in Section A.2. Section B describes the principal multipath characteristics (amplitude, separation angle, and time delay) for each of the scenarios with terrain reflectivity characteristics (dielectric constant and roughness) similar to flat, smooth snow. Also, one scenario with inhomogeneous terrain characteristics is also described. Scalloping frequency data for many of the principal reflectors is also given.

Section C describes the results of simulations of the DLS [7], DMLS [8], and TRSB [9, 10] systems for each of the AWOP WG-A simulation scenarios. We emphasize at the outset that the results here consider only multipath error; actual receiver outputs would also have a "clean environment" noise component due to front-end noise, quantization, etc.

A. Airport Scenario Descriptions

1. Scenarios described in the report of the third (Melborne) meeting of the All Weather Operations Panel Working Group A [72].

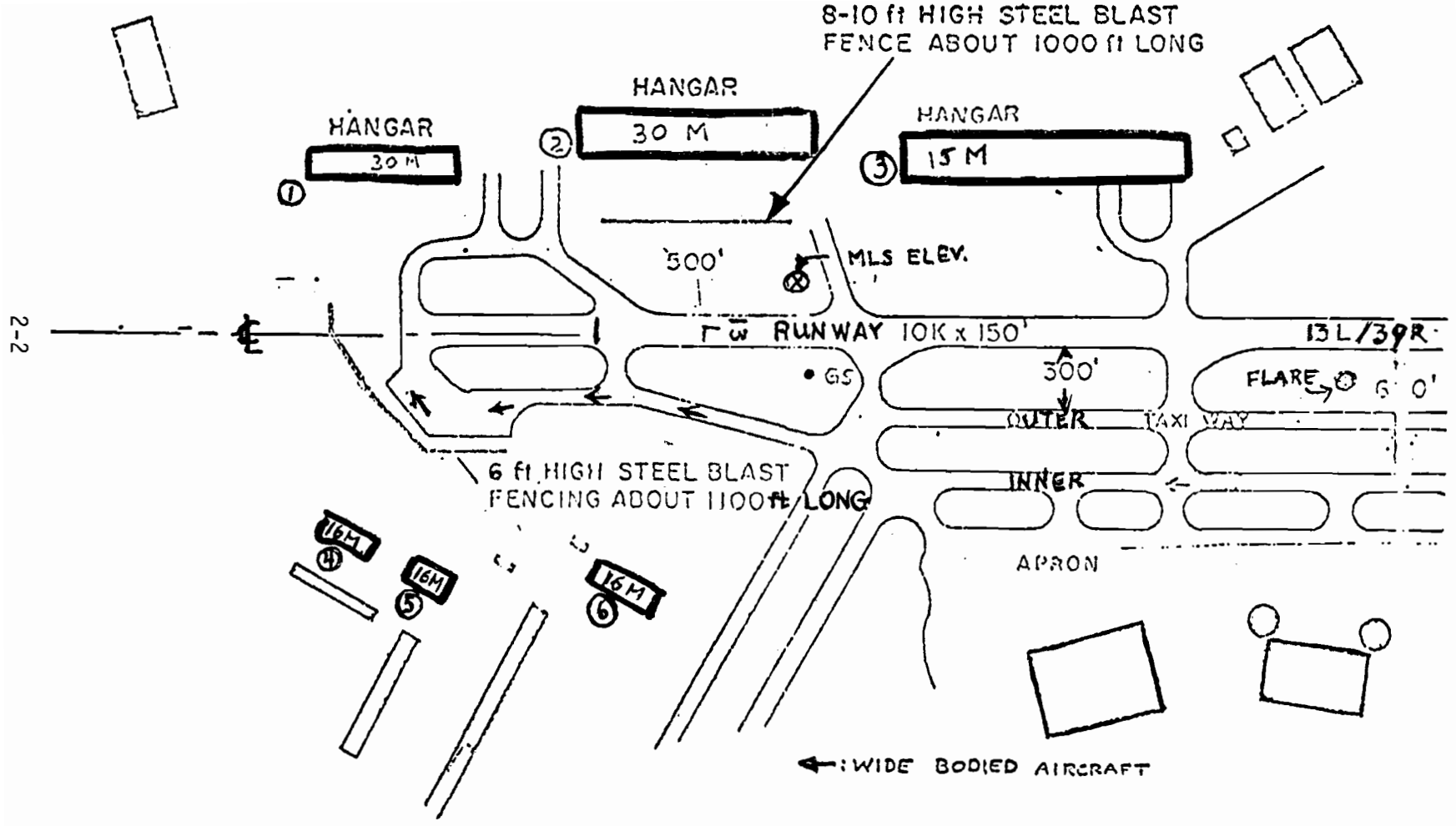

Fig. 2-1. Scenario 1: elevation/flare multipath at decision height and threshold (JFK).

Scenario 1: (Fig 2-1) Elevation/Flare Multipath at Decision Height and Threshold. Flare Multipath at Decision Height and Threshold. Flare Multipath in Touchdown Zone.

The congestion at the end of runway 13L at JFK (Fig. 2-1) demonstrates how the need for space at major metropolitan airports may create quite challenging multipath environments. The geometry of this runway end was therefore used as a starting point for the first scenario.

(1) Equipment Siting

The location of the existing ILS glide path is shown. The MLS elevation antenna to be sited at the opposite side of the runways as shown in Fig. 2-1. Similarly, the flare element will be sited on the opposite side of the runway.

(2) Flight Profiles

For this case, centerline approaches up to a 2.86° glide path (20:1) toward the existing GPIP are appropriate. The approach will begin at an altitude of 500 ft. The flare maneuver will be an exponential flare commencing at 50 ft altitude and terminating at touchdown 300 ft beyond GPIP, assuming the aircraft antenna to fly the defined path and an antenna to wheel height of 8 ft. The aircraft velocity (important for motion averaging effects) is chosen as 130 knots.

(3) Multipath Scatterer Characteristics

Buildings - the surfaces towards the runway are taken to be flat, homogeneous plates whose effective reflection coefficient is 0.7 for angles of incidence (defined as the angle between the incident ray and reflecting surface) above 20°* and 0.9 otherwise.

---

*Although the locations of the buildings in the model are in agreement with those on the airport, the panel somewhat arbitrarily specified these reflection properties and they are not necessarily of the actual buildings (see volume I of this report). However, the specified properties are not atypical for U.S. airports (see [27]).

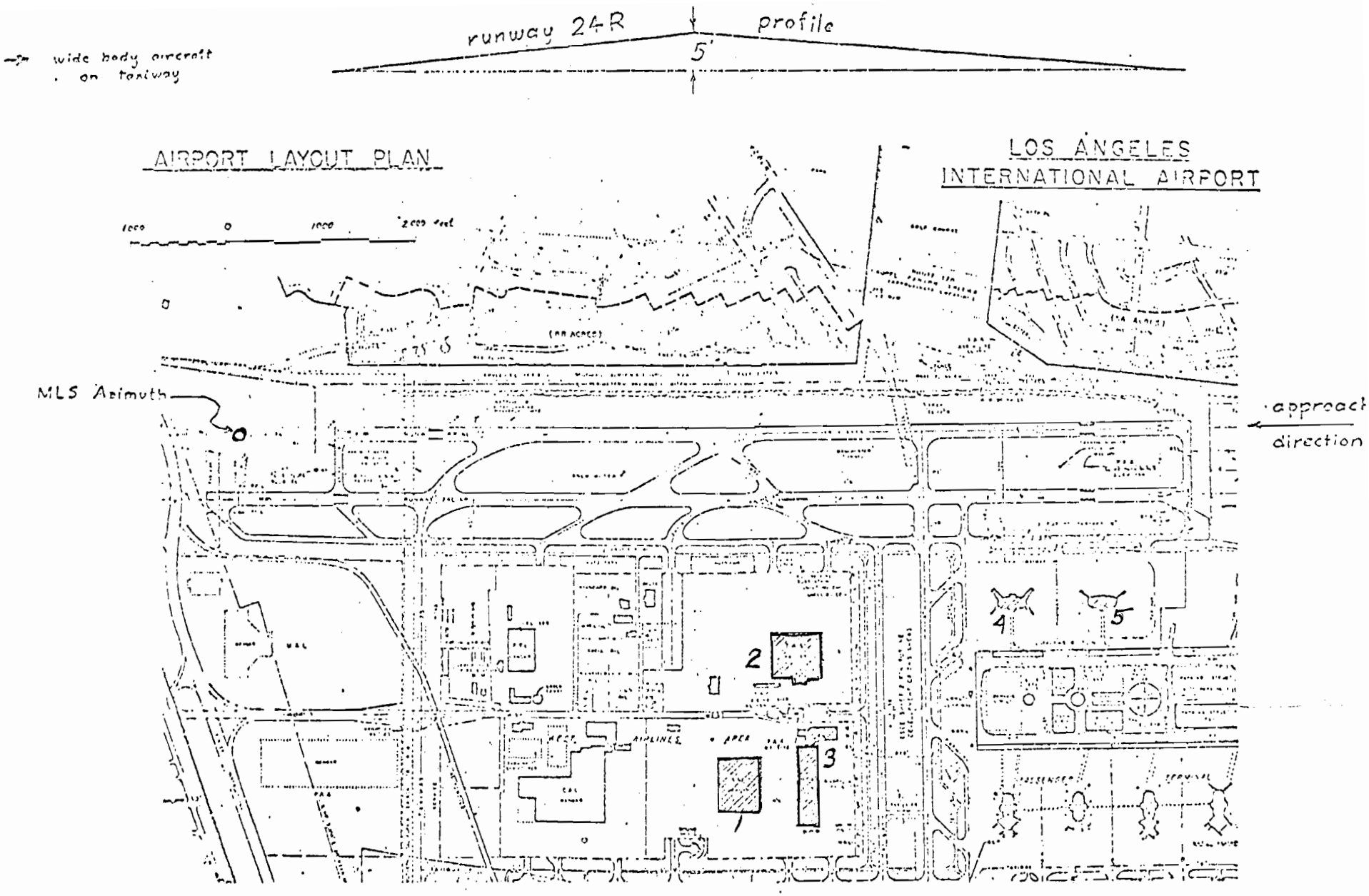

Fig. 2-2. Azimuth multipath - scenario 2 (LAX).

Aircraft - the aircraft are taken to be wide-bodied aircraft such as B747, A300, DC10 and L1011. The fuselage typically can be represented as a cylinder of diameter 20 feet which is 125 feet long. The tail fin is typically 35 feet in vertical extent and approximately 25 feet wide.

Ground reflections - the ground is taken to have a dielectric constant $\varepsilon/\varepsilon_o = 1.2$ and conductivity = 0.

(4) Multipath Conditions Generated

Multipath generated by the various scatterers in the scenario is summarized below and will be considered simultaneously.

Function	CAT I DH	CAT II DH	Threshold	Touchdown Zone
Elevation*				
In Beam	BLDG 1	ARCFT, BLDGS 2-6	ARCFT, BLDGS 2-6	
Out-of-Beam	GND	GND, ARCFT		
Flare*				
In Beam	-		BLDGS 3,6	BLDG 3
Out-of-Beam	-		GND	GND

*Note: It is recognized that the terms "In Beam" and "Out-of-Beam" may only apply to specific systems.

Scenario 2: (Fig 2-2) Azimuthal Multipath at Threshold and Rollout

The coverage region of the azimuth guidance function typically encompasses much of the airport building complex. Thus, it is not surprising that several multipath reflections may be present simultaneously near threshold. The details are as follows:

(1) Equipment Siting

Runway 24R at LAX has a category 2 ILS localizer sited some 3000 feet beyond the end of the runway. For purposes of this scenario, the MLS azimuth array will be sited 1000 feet beyond the end of the runway.

(2) Approach Profiles

As in Scenario 1, the primary concern is with the final stages of approach. Hence, a centerline approach on a 2.86° (20:1) glide slope from 500 ft altitude direct to GPIP is appropriate. As before, the aircraft velocity considered is 130 knots.

(3) Scatterer Physical Characteristics

Each of the major scatterer types is considered in turn:

Buildings: the surfaces facing the runway are taken as flat homogeneous plates whose effective reflection coefficient is 0.7 for angles of incidence above 20° and 0.9 for angles of incidence below 20°*. Buildings 1-3 are 30 meters high. Buildings 4 and 5 are 15-m-high terminal buildings with 50-m wings included some 36° with respect to a line parallel to centerline.

Aircraft: as in Scenario 1.

Ground: the ground between the transmitter and the approach end of the runway is taken to be slightly humped as shown in Fig 2-2. The ground along centerline is taken to be flat smooth concrete ($\varepsilon/\varepsilon_o = 13$) or flat snow ($\varepsilon/\varepsilon_o = 1.2$). The ground off the runway is taken to be flat smooth ground ($\varepsilon/\varepsilon_o = 13$) or snow.

---

*It should be noted that the runway facing surface of the actual building 1 which was modified (at considerable expense) to reduce the ILS localizer multipath levels so that a successful ILS installation could be accomplished [27].

(4) Multipath Conditions Encountered

The various buildings and aircraft are located such that out-of-beam azimuth multipath is more or less continually present from the Cat. II decision height to threshold.

Scenario 3: (Fig 2-3) Azimuth, DME and Elevation Multipath at STOL Port

This scenario shown in Fig 2-3 is derived from an airport layout (Crissy) which is under consideration as a civilian STOL port. The less stringent obstruction clearance criteria permits vertical surfaces to be located much nearer the runway than was the case in Scenarios 1 and 2. This scenario is also interesting in that building 1 is located and oriented much like the AWOP azimuth multipath screen test [72], and thus yields azimuth multipath over a substantial section of the flight path near threshold. The train assumed to be on the adjacent track yields multipath in this same region; thus, we have a possibility of simultaneous multipath analogous to that of Scenario 2.

(1) MLS Equipment Siting

It is assumed here that the MLS azimuth and elevation elements are not collocated so as to achieve Cat. I (or hopefully, Cat. II) performance. The elevation array is assumed to be on the opposite side of the runway from the train tracks so as to minimize the likelihood of elevation signal reflections from trains.

(2) Approach Profiles

The principal multipath here is expected to be encountered near decision height. The flight profile will be a centerline approach at

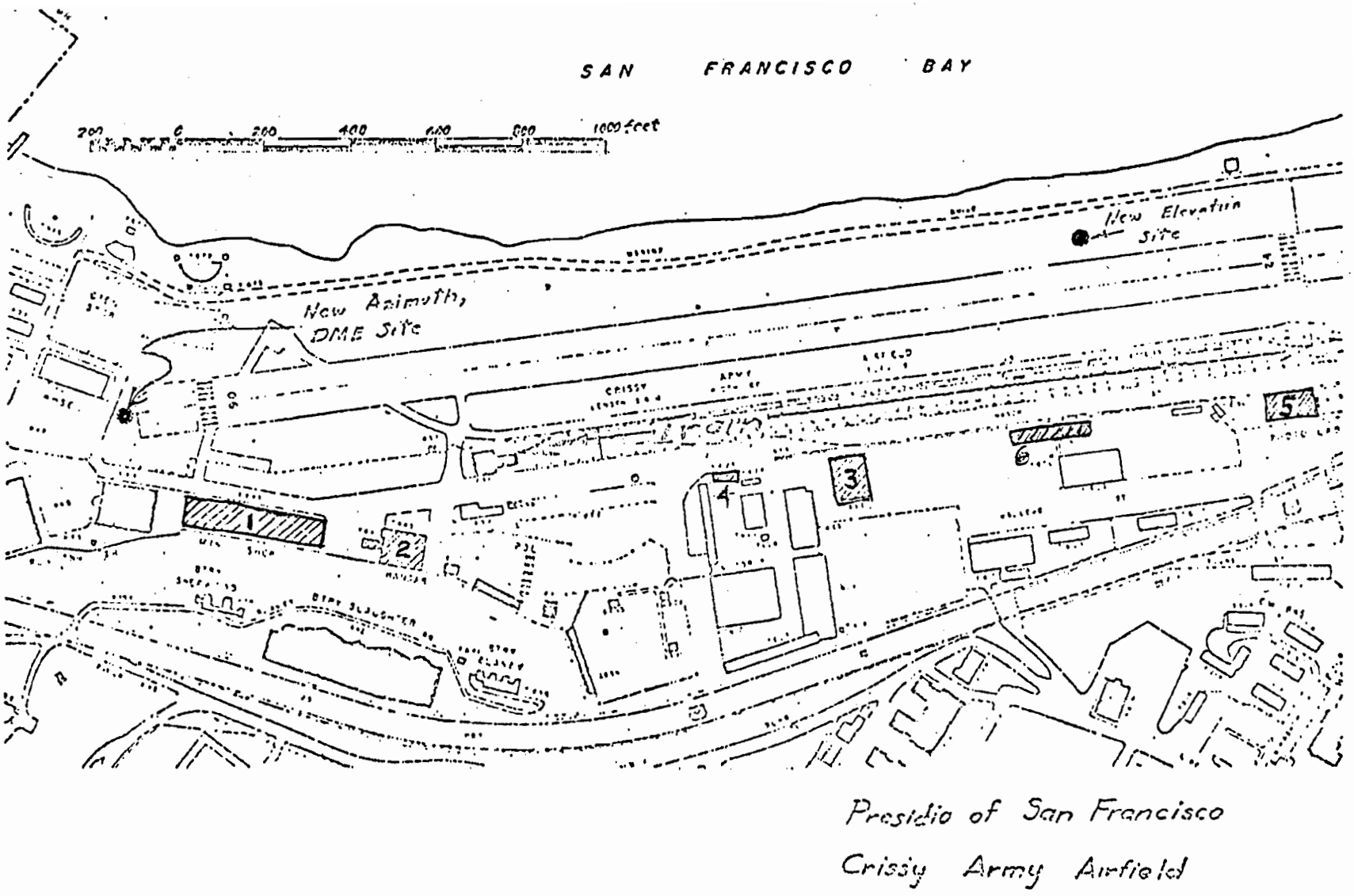

Fig. 2-3. STOL elevation/multipath - scenario 3.

a 6° glide slope from 500 ft altitude to 8 ft altitude or loss of signal. The approach velocity is 70 knots.

(3) Scatterer Physical Characteristics

Each of the major types of scatterers is considered in turn:

Buildings - the surfaces facing the runway are taken to be flat homogeneous plates whose reflection characteristics are the same as those in scenario 2. Buildings 1,3,4, and 6 are 10 meters high, while buildings 2 and 5 are 25 meters high.

Train Cars - the train car sides facing the runway are flat metal plates 5 meters high and 12 meters in length.

Ground - the runway is smooth flat concrete ($\varepsilon/\varepsilon_o = 5$ or $\varepsilon/\varepsilon_o = 13$) or snow ($\varepsilon/\varepsilon_o = 1.2$) while the terrain to the side is taken to be smooth flat ground ($\varepsilon/\varepsilon_o = 13$) or smooth fresh snow ($\varepsilon/\varepsilon_o = 1.2$).

(4) Multipath Conditions Encountered

Buildings 1-4, and 6 can generate azimuthal multipath at decision height, as can the train cars. Building 5 can generate elevation multipath between the Cat. II decision height and threshold.

2. Airport Scenarios Developed by Multipath Subgroup at the Washington Meeting (May 1976) of AWOP Working Group A. [111]

Scenario 4: Elevation/Flare Multipath at Decision Height and Threshold. Flare Multipath at Touchdown.

This scenario is a variation on scenario 1 in which the MLS elevation antenna is sited on the same side of the runway as the existing ILS glide slope (see Fig. 2-1) and at the same distance along the runway as the MLS elevation position shown on Fig. 2-1. Also, the flare antenna is placed on

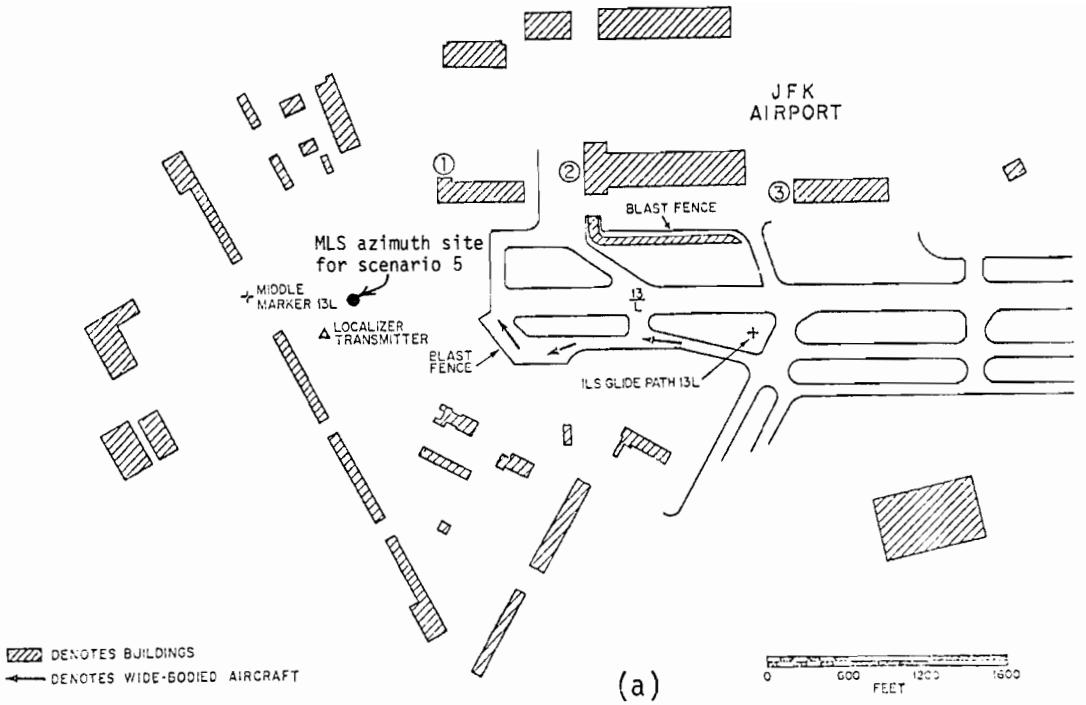

(a)

Note: flight profile distance from end of runway is not to scale

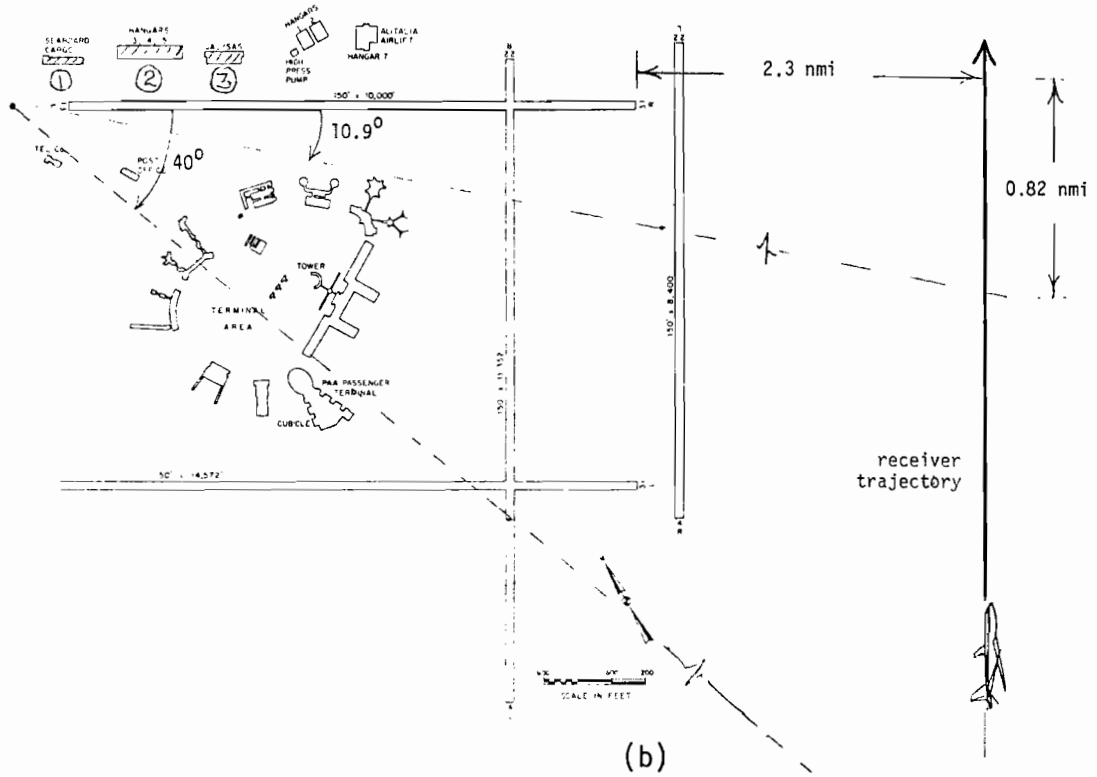

(b)

Fig. 2-4. (a) Airport map for scenario 5. (b) Flight profile for curved approach at JFK.

the opposite side of the runway from the flare location shown in Fig. 2-1. For both this scenario and scenario 1, the elevation and flare antennas are assumed to be 400 feet and 250 feet, respectively, off the centerline.

All other aspects of scenario 4 (flight profiles, scatterer characteristics) are identical to those of scenario 1. And, as in scenario 1, buildings 1 and 2 generate elevation multipath between Cat II DH and threshold.

The rationale for this variant on scenario 1 is that large buildings near threshold are either on the same side of the runway as the elevation and flare antennas or they are on the opposite side of the runway. Consequently, it was deemed desirable to compare the various systems for the two siting possibilities.

Scenario 5: Azimuth Multipath/Shadowing on Curved Approach

Large buildings located near the stop end of the runway can produce significant azimuthal multipath for large portions of a curved approach. Since one of the principal MLS requirements is high quality proportional guidance over a wide coverage volume, it was felt that one scenario should explore the off centerline capability of the various systems.

The scenario is derived from the airport layout of Fig.2-1 by siting the azimuth unit at the other end of the runway and then considering the aircraft to be flying at right angles to the extended runway centerline as shown in Fig. 2-4.

As the aircraft enters the MLS coverage volume (assumed to be ±40°), out-of-beam azimuth multipath is generated by buildings 1-3. Multipath from the various buildings could be encountered until the aircraft azimuth is less than 10°. As the aircraft crosses over centerline, buildings 1-3 can shadow the

direct signal for considerable periods. Thus, it is seen that a high degree of immunity to shadowing and out-of-beam azimuth multipath is essential for an MLS.

(1) Equipment Siting

Runway 31R at JFK airport has an ILS localizer sited 1000 ft beyond the end of the runway. For purposes of this scenario, the MLS azimuth antenna was also sited 1000 feet beyond the end of the runway as shown in Fig. 2-4(a).

(2) Flight Profile

In the section where reflections occur, the aircraft is assumed to be flying level at a height of 1200 feet and a ground velocity of 160 knots, while the portion where shadowing occurs, the aircraft height is 2000 feet*. The flight trajectory, shown in Fig. 2-4(b), is at right angles to the extended runway centerline at a distance of 2.3 n miles from the end of runway 31R (this distance is the mean of the Carnarsie approaches to JFK, which were taken as exemplifying noise abatement IFR approaches available with MLS).

(3) Scatterer Physical Characteristics

These are identical to scenario 1 except that no scattering aircraft are present.

(4) Multipath Conditions Encountered

Out-of-beam azimuthal multipath is more or less continually present from an aircraft azimuth of -40° to -10°. Similarly, shadowing (diffraction) is encountered between azimuths of +10° to +40°.

---

*It was originally planned [111] that the aircraft height would be 1200 ft in both sections; however, the shadowing loss at 1200 ft was such (-30 dB) as to make unrealistic the assumption of sufficient SNR (e.g., for function identity decoding). Consequently, it was agreed that the shadowing portion should be at a greater height.

Scenarios 6-8 - Scenario 1 Airport Geometry with "Wiggled" Flight Path

This scenario is a variant on scenario 1 where the aircraft lateral position and heading vary sinusoidally during final approach. This variation in aircraft position/heading represents typical path holding for a CTOL aircraft [110]. The effect of the heading changes is to modify the scalloping frequency along the flight path such that it no longer increases monotonically as in a straight in approach. The position variation changes the rf phase relationship between the direct and multipath components at a given location, and thus changes the errors at a given scalloping rate.

The specific lateral position and heading changes are based on the Smith's Industry studies [110]:

$$\text{longitudinal position} \triangleq x = x_o - v\,t\cos\theta_{gs}$$

$$\text{lateral position} \triangleq y = Y_M \sin(0.3t + \phi_o)$$

$$\text{vertical position} \triangleq z = z_o - vt\sin\theta_{gs}$$

$$\text{longitudinal velocity} \triangleq v_x = -v\cos\theta_{gs}$$

$$\text{lateral velocity} \triangleq v_y = 0.3\,Y_M\cos(0.3t + \phi_o)$$

$$\text{vertical velocity} \triangleq v_z = -v\sin\theta_{gs}$$

where:

$x_o = 18850$

$Y_M = 17.3$ ft

$z_o = 500$ ft

$\theta_{gs} = 0.05$ radians (2.87^o)

$\phi_o = 0$ and $\pm 2\pi/3$ radians

$v = 219$ ft/sec

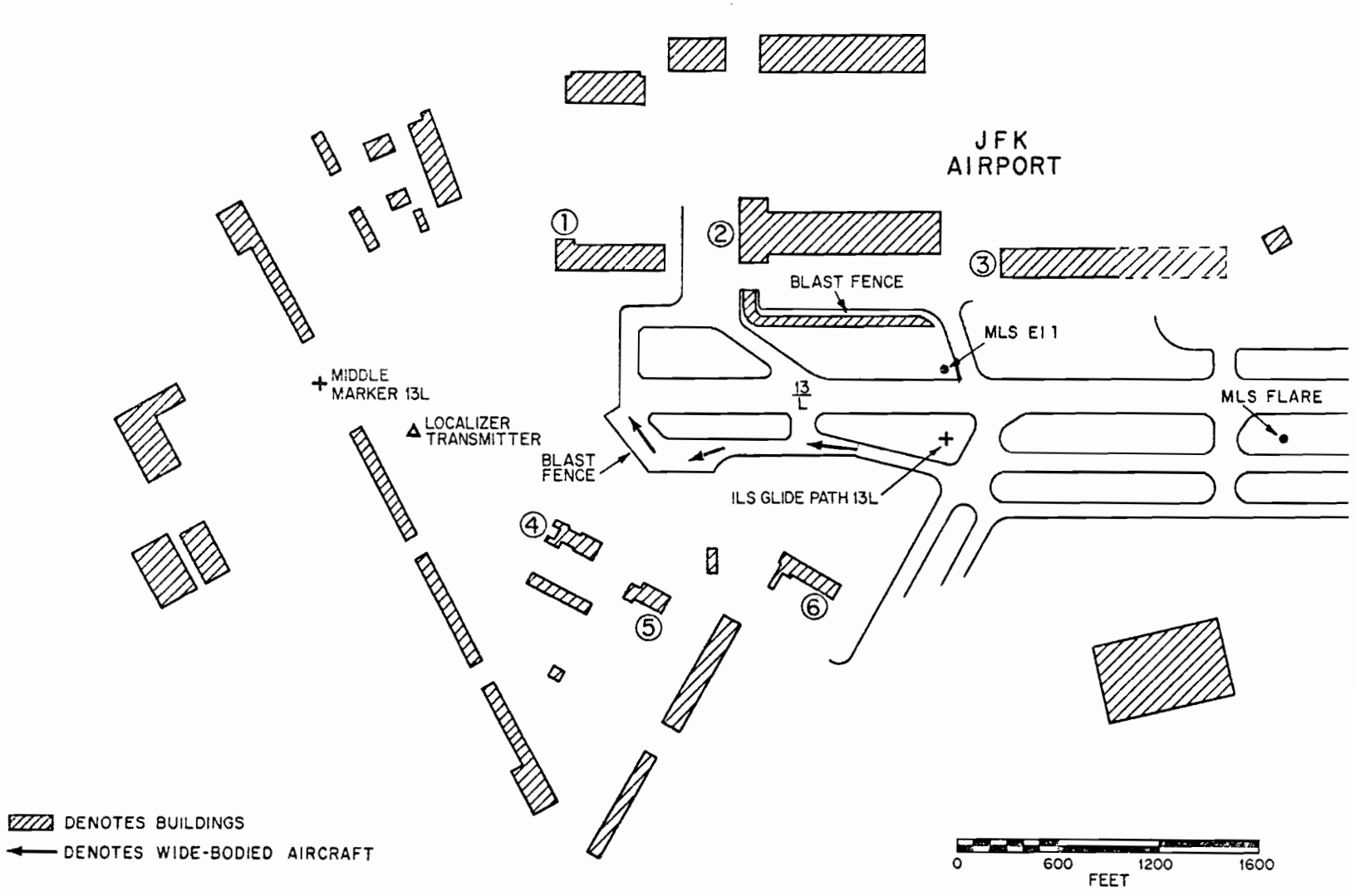

Fig. 2-5. Approach end of runway for scenario 1.

All other aspects of the scenario (ground equipment and scatterer locations, scatterer characteristics and multipath conditions) encountered are as in scenario 1.

B. Airport Models and Multipath Characteristics for Various Scenarios

In this section, unless otherwise indicated, the terrain was assumed to be a flat homogeneous surface with complex dielectric constant $[\varepsilon/\varepsilon_o = 1.2 + j.01]$ and the ground reflection multipath computed using the usual flat plane model.

1. Scenario 1

Scenario 1 is derived from runway 13L at John F. Kennedy International Airport (JFK). Fig 2-5 is a blowup of the threshold end of the runway where most of the buildings are concentrated. The six numbered buildings are those included in the scenario model. The coordinate system used has as its origin the center of the top end of the runway. The positive x direction is towards the threshold and positive y direction towards buildings 4, 5 and 6. The phase center of the elevation transmitter position is (9200, -400, 10) with the flare at (8000, 250, 10) the DME (0,120,5), and the AZ at (0,0,5) (dimensions are in feet). The six buildings and five aircraft locations are specified in Table 2-1. It is assumed that the building surfaces are flat rectangles with reflection coefficient $\rho_{RC} = 0.7$ if the grazing angle is greater than 20° (and 0.9 otherwise). The aircraft are taken to be Boeing 747's. The flight path along which multipath and errors are calculated is as follows:

> Flight Path: v = 219.56 ft/sec (130 knots)
> Starting at (18850,0,500) the path descends along four straight line segments sampled every 43.91 ft (5 Hz rate) with break points at (9850,0,50), (9350,0,29) and (9050,0,20) and ending point at (8850,0,8).

TABLE 2-1

BUILDING AND AIRCRAFT LOCATIONS FOR

SCENARIOS 1,4, and 6-8

Buildings	Building Locations		Height (ft)
B1.	(10750, -750)	(11400, -750)	100
B2.	(9100, -850)	(10300, -850)	100
B3.	(8000, -700)	(8700, -700)	50
B4.	(11150, 890)	(11400, 725)	52
B5.	(10700, 1200)	(10900, 1075)	52
B6.	(9675, 1150)	(10025, 950)	52

Aircraft Location for MLS

Plane	Tail Locations	Nose Locations
A1.	(9200, 400)	(9399.7, 390.1)
A2.	(9600, 400)	(9787.4, 469.9)
A3.	(10200, 500)	(10399.2, 517.4)
A4.	(10400, 400)	(10595.3, 443.1)
A5.	(10000, 400)	(10189.4, 464.1)

Origin at stop-end of runway
Azimuth Transmitter at (0,0,5)
Elevation Transmitter at (9200,-400,10) for C band
Elevation Transmitter at (9200,-400,16.5) for L band
Flare Transmitter at (8000,250,15)
DME Transmitter at (0,12,5)

Computer generated maps (rotated 180° relative to Fig. 2-5) for this scenario for C and L band carrier frequencies are illustrated in Figs. 2-6 and 2-7 together with peak multipath levels and the x distance along the flight path at which the peak occurred. The symbol G refers to specular ground reflections. The B's represent buildings with the appropriate numbering and the A's represent airplanes. The levels, as given, assume that both the transmitter and receiver antennas are omnidirectional (each system simulation accounts for the antenna patterns in evaluating the system errors). The computed multipath levels and separation angle for the six largest ranked reflections are presented for azimuth and elevation for C-band carrier frequency in Figs. 2-8 and 2-9 and azimuth, DME, and elevation for L-band carrier frequency in Figs. 2-10 to 2-12.

The azimuth multipath levels plotted at a given point for a scatterer represent the largest level of the four paths X-O-R, X-G-O-R, X-O-G-R and X-G-O-G-R (where X denotes transmitter, O the obstacle, G the ground and R the receiver) by which specular reflections reach the receiver [29]. The effective M/D level for that scatterer involves the (coherent) sum of these four paths taking into account the ground antenna pattern characteristics of a given MLS.

The plotted elevation multipath level is only the X-O-R path level. The rationale here is that the other path components will be heavily attenuated by the ground antenna patterns ("real" or "virtual") and/or signal processing.

Figs. 2-13(a), (b), and (c) illustrate where reflection edge rays intercept the flight path for the transmitter located at the azimuth site, EL 1, and flare sites, respectively. In almost all cases of building and aircraft

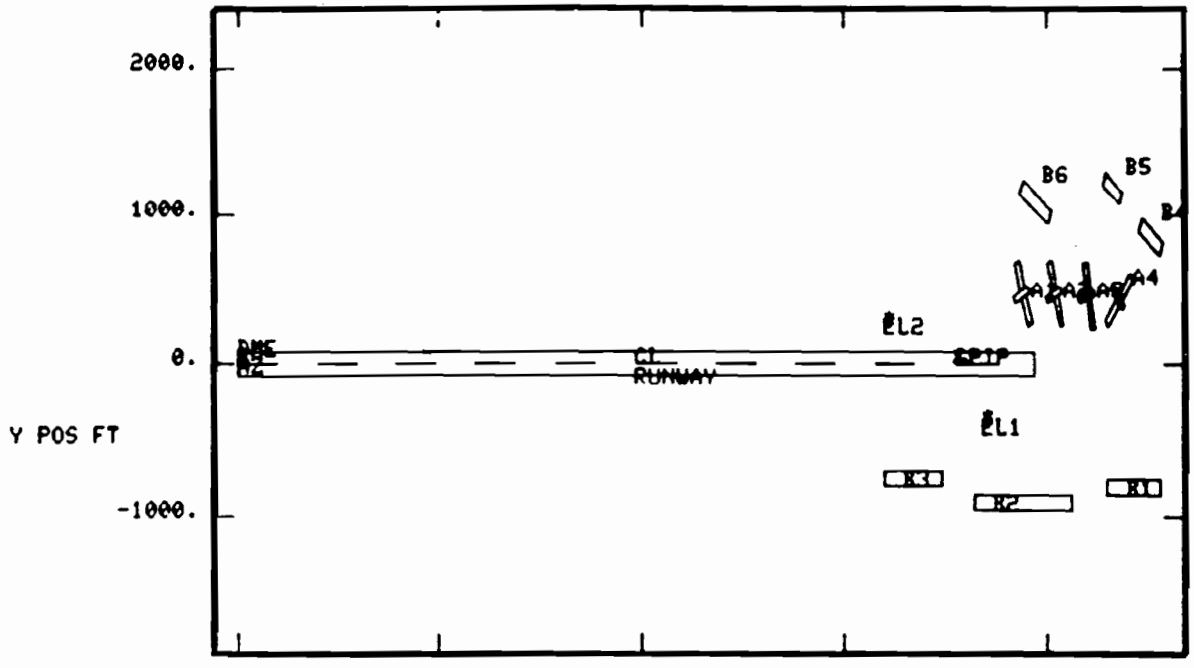

FLT PTH A

AZ SYSTEM

OBST	RANK	AMP	DIST	RDOP
G	1	0	10312.0	0.
B1	8	40	6937.5	-175.
B2	5	27	131.7	-4.
B3	4	27	2151.6	-4.
B4	7	33	7332.7	-749.
B5	6	27	7683.9	-734.
B6	2	16	8649.9	-662.
A1	11	65	10312.0	-2154.
A2	10	63	10207.0	-2180.
A3	9	58	5576.4	-4.
A4	3	20	7947.4	-1111.
D	0	80	0.0	0.

EL SYSTEM

OBST	RANK	AMP	DIST	RDOP
G	1	1	9511.7	0.
B1	2	2	4610.5	-22.
B2	3	2	6630.2	-81.
B3	4	7	9687.3	-443.
B4	10	30	7815.7	-1266.
B5	5	12	8606.0	-1435.
B6	11	31	9186.9	-1102.
A1	6	17	8474.2	-69.
A2	9	20	8298.6	-162.
A3	8	20	3995.8	-3.
A4	7	18	8649.9	-1890.
D	0	80	0.0	0.

RANK = multipath ranking

AMP = maximum -M/D ratio (dB)

DIST = distance along flight path (ft) at which maximum M/D occurred = 18850 - x pos (ft)

RDOP = relative Doppler (Hz) at point of maximum M/D

Fig. 2-6. Airport map for WG-A scenario 1 for C-band carrier and snow-covered ground.

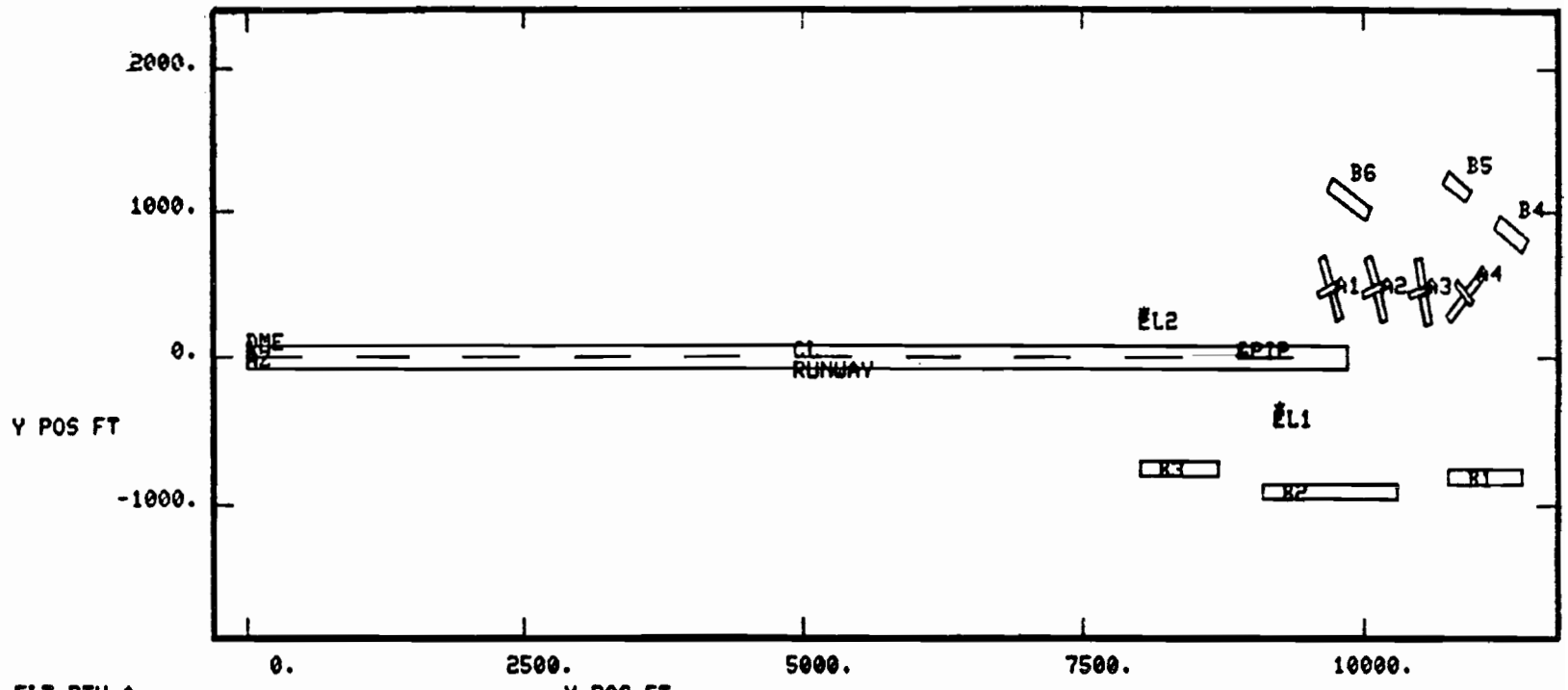

FLT PTH A

AZ SYSTEM

OBST	RANK	AMP	DIST	RDOP
G	1	0	10312.0	0.
B1	8	34	7683.9	-111.
B2	6	25	0.0	-1.
B3	7	26	2371.1	-1.
B4	5	25	7332.7	-148.
B5	4	22	7683.9	-145.
B6	2	11	8649.9	-130.
A1	11	58	10312.0	-424.
A2	10	56	10163.1	-429.
A3	9	56	10250.9	-434.
A4	3	20	8035.2	-223.
D	0	80	0.0	0.

EL SYSTEM

OBST	RANK	AMP	DIST	RDOP
G	1	1	9511.7	0.
B1	4	7	4391.0	-4.
B2	2	2	7069.2	-21.
B3	3	5	9687.3	-87.
B4	10	22	7815.7	-249.
B5	5	14	8562.1	-281.
B6	11	24	9186.9	-217.
A1	6	15	8606.0	-19.
A2	9	20	3820.2	-0.
A3	7	19	4522.7	-1.
A4	8	19	8737.7	-378.
D	0	80	0.0	0.

RANK = multipath ranking

AMP = maximum -M/D ratio (dB)

DIST = distance along flight path (ft) at which maximum M/D occurred = 18850 - x pos (ft)

RDOP = relative Doppler (Hz) at point of maximum M/D

Fig. 2-7. Airport map for WG-A scenario 1 for L-band carrier.

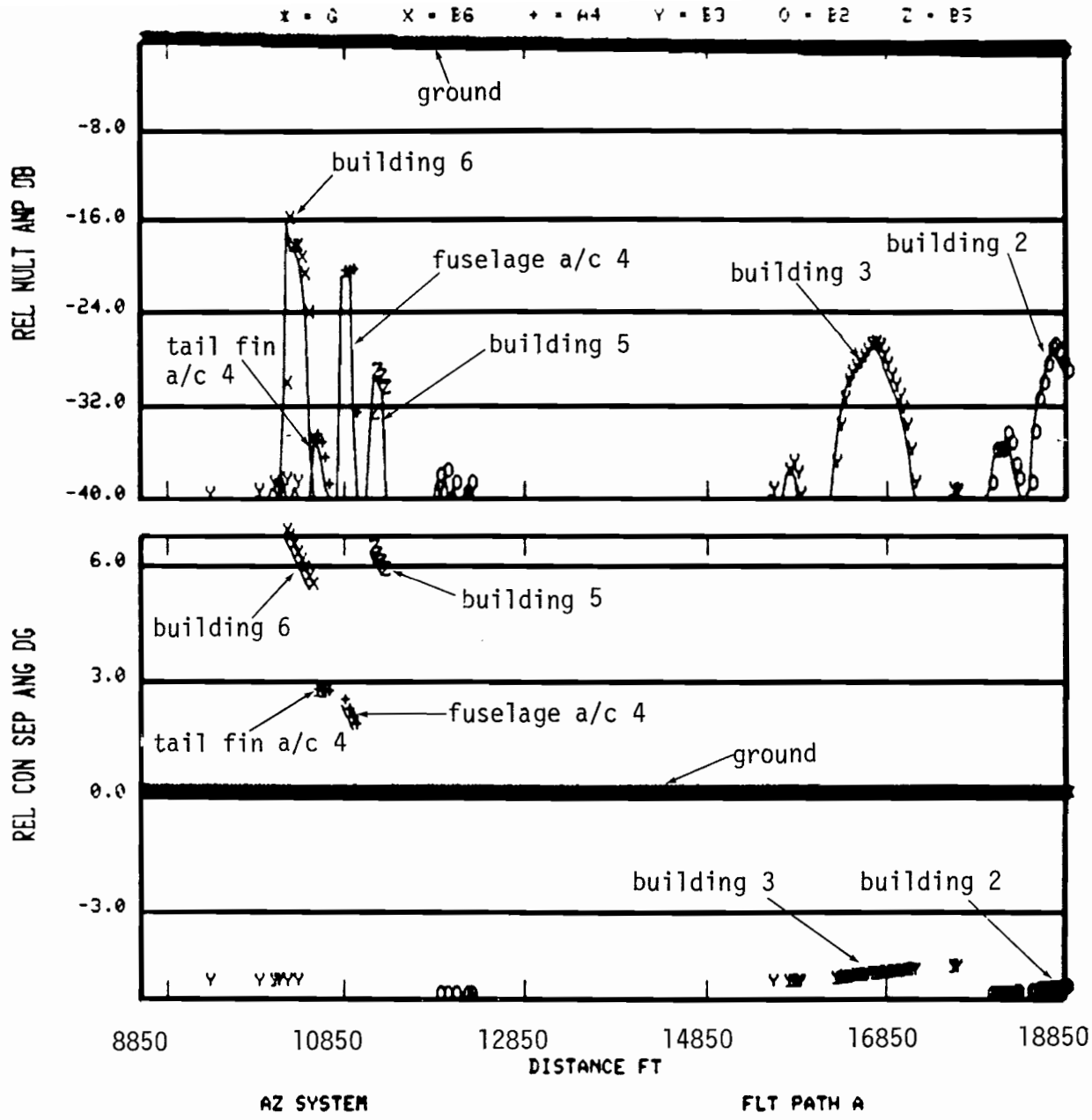

Fig. 2-8. Azimuth multipath and separation angle for scenario 1 (JFK) for C-band with snow.

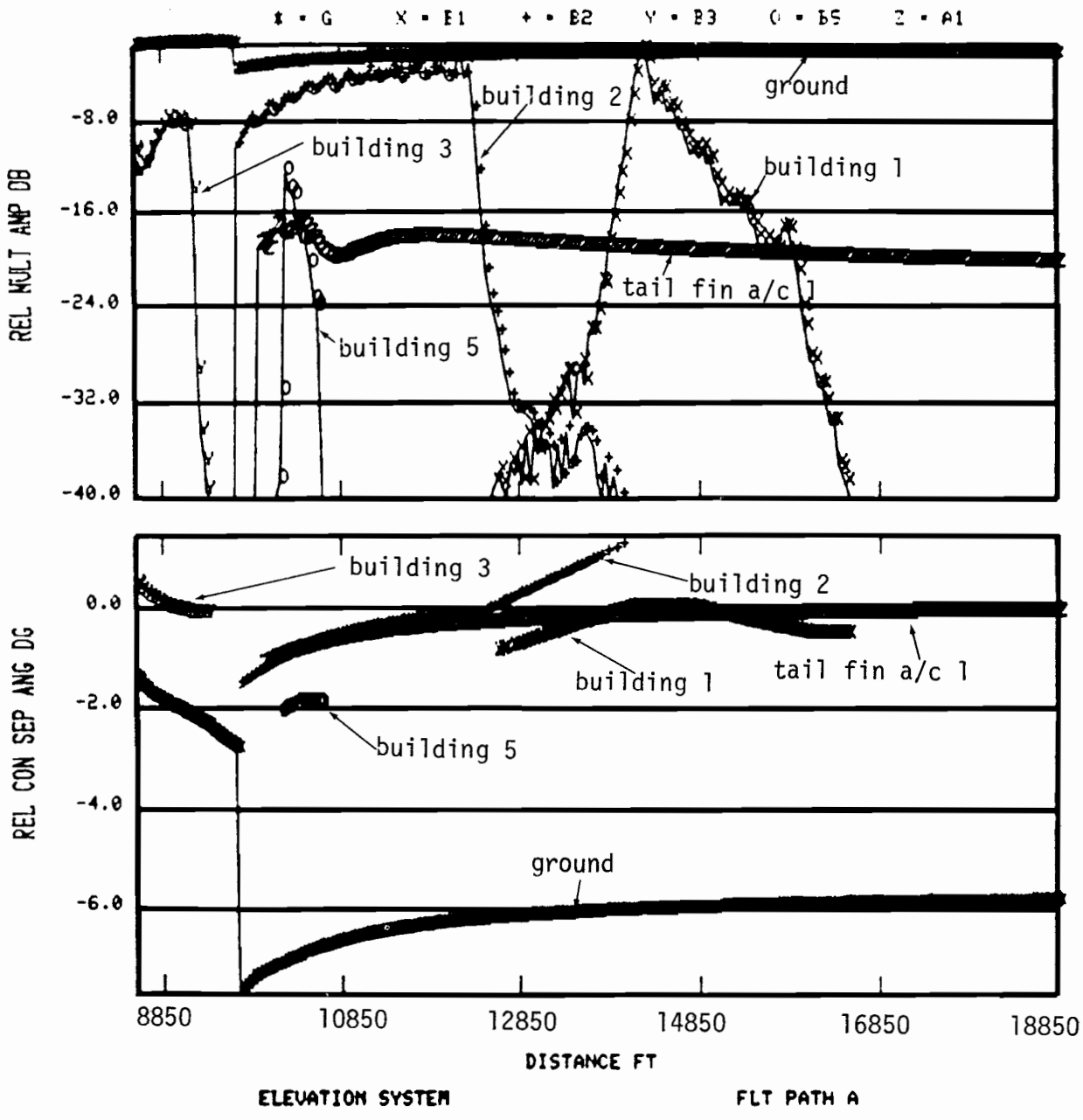

Fig. 2-9. Elevation multipath and separation angle for scenario 1 (JFK) for C-band.

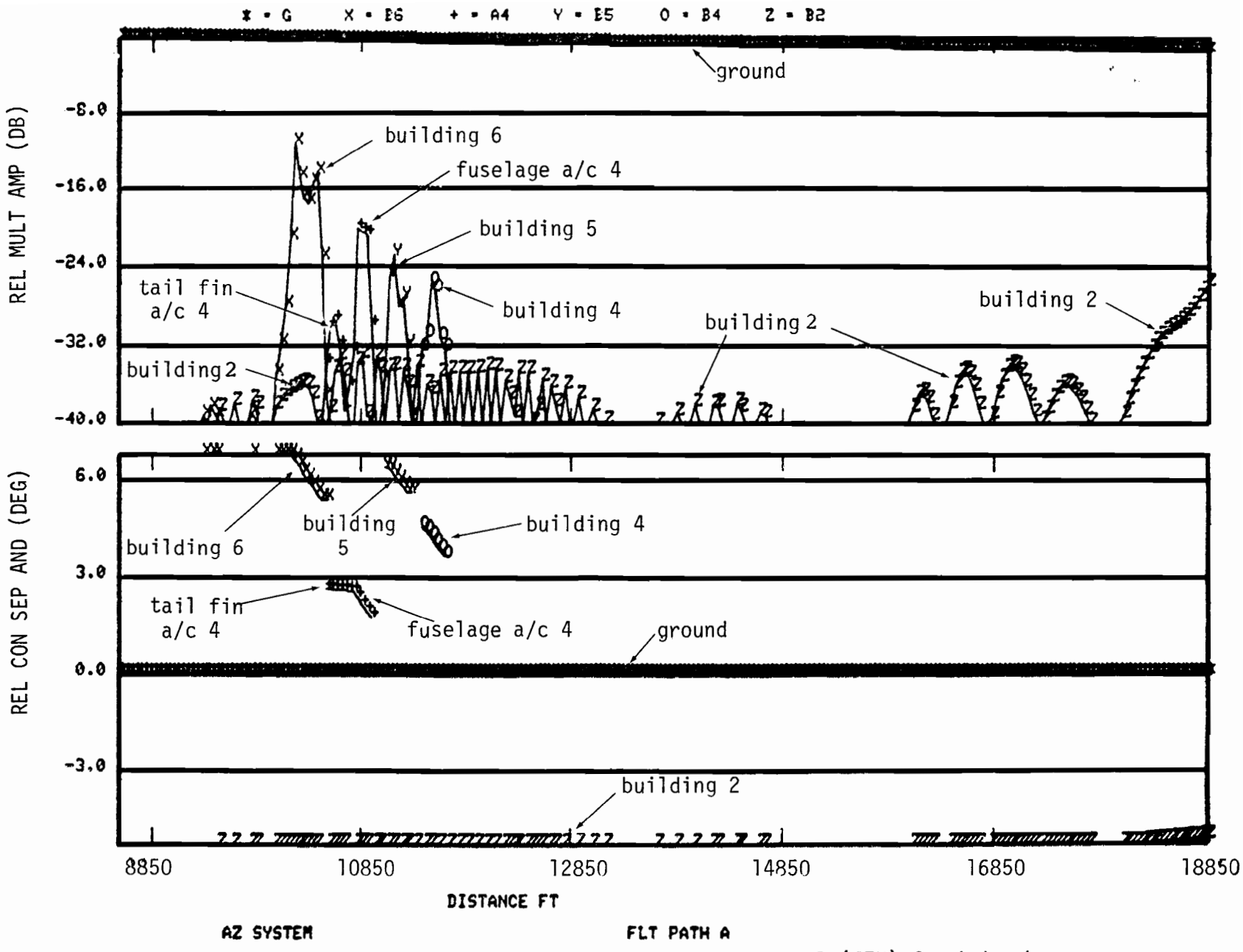

Fig. 2-10. Azimuth multipath and separation angle for scenario 1 (JFK) for L-band.

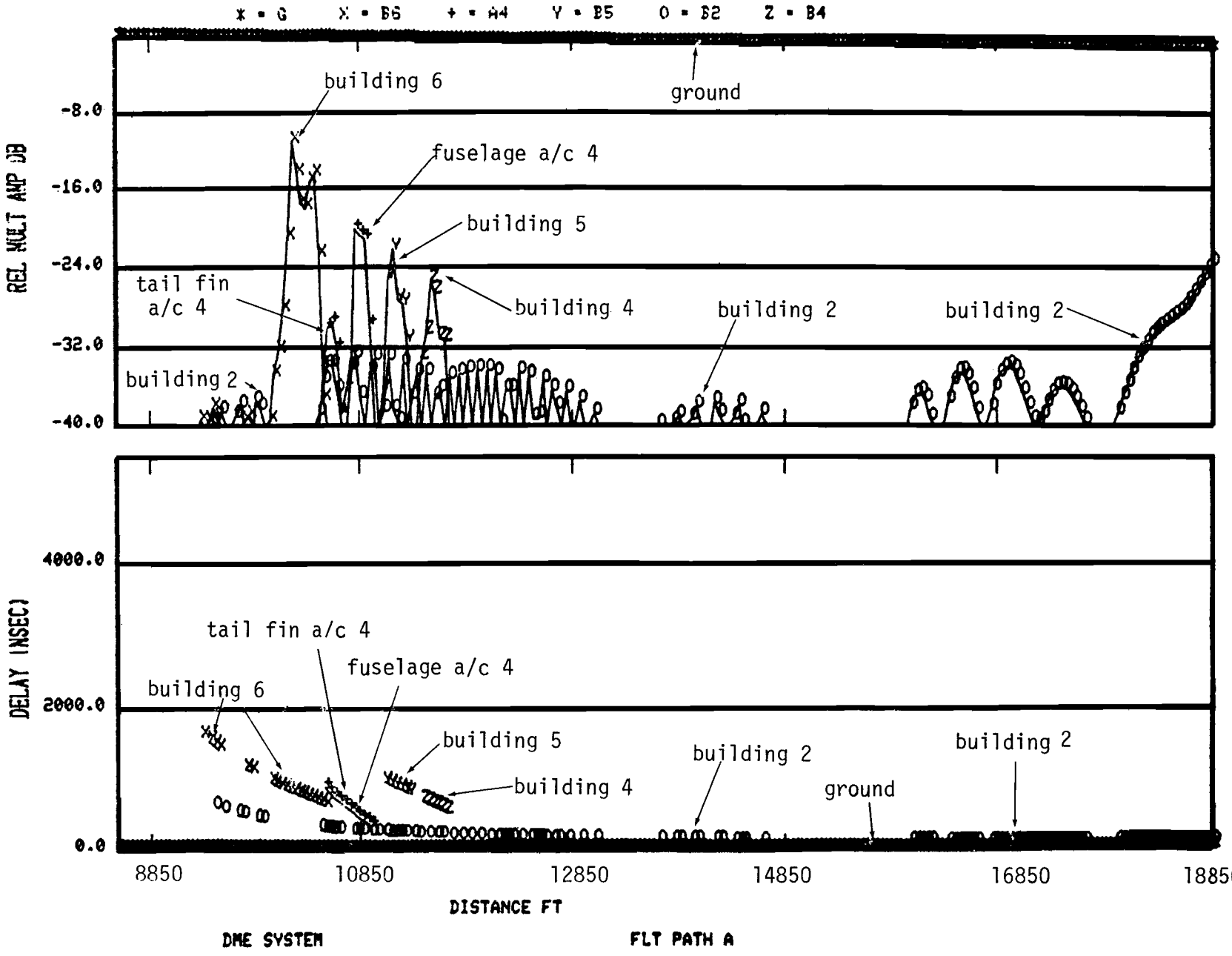

Fig. 2-11. DME multipath and delay for scenario 1 (JFK) for L-band.

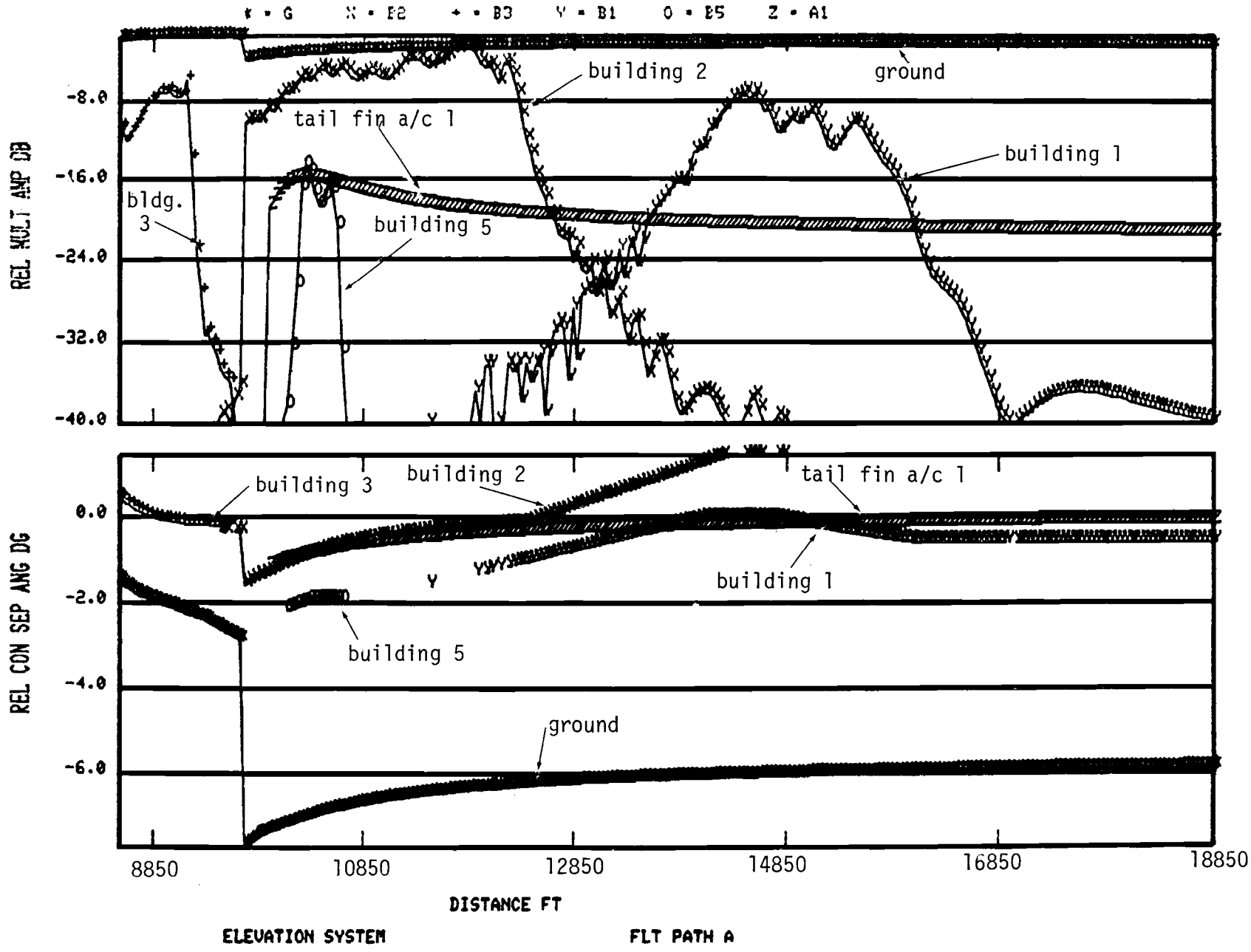

Fig. 2-12. Elevation multipath and separation angle for scenario 1 L-band.

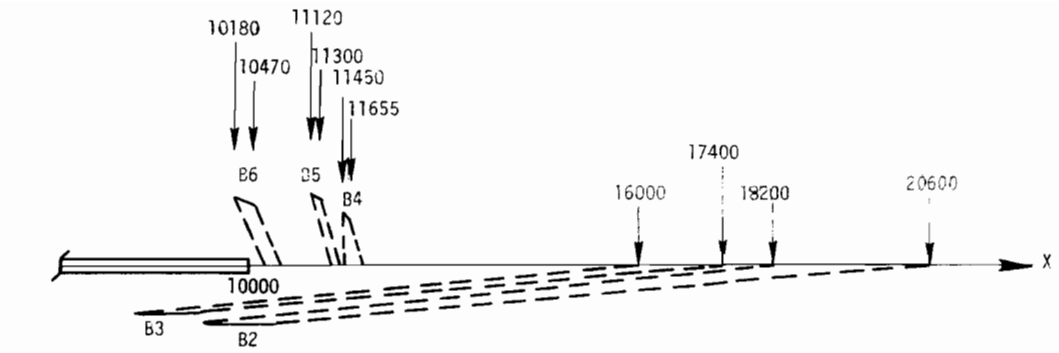

a.

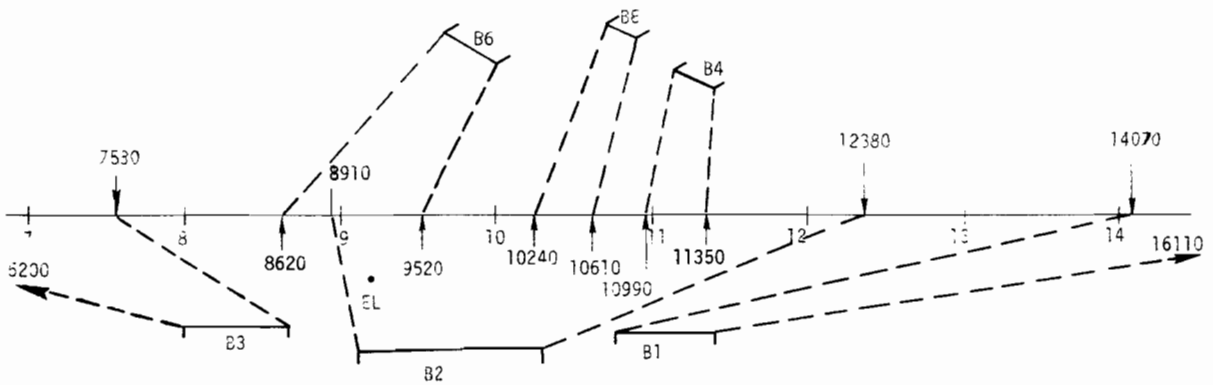

b.

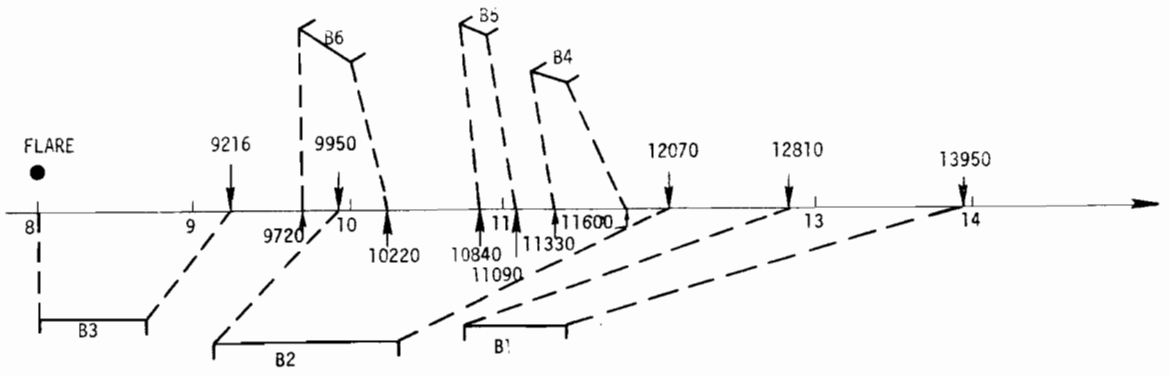

c.

Fig. 2-13. JFK map with edge reflection rays in horizontal plane for a) azimuth transmitter, b) elevation transmitter and c) flare transmitter.

fuselage reflections the multipath will peak between these two limits and be low elsewhere. An exception to this rule can occur if the height of specular point is well above the building as we see in the case of building 3 in Fig. 2-10. The peak reflection does conform to our expectations but there are other lower peaks near x = 14000 feet. These peaks correspond to the point on the flight path where the height of the specular point is in proximity to that of the building. Aircraft tail reflections are of lower level and more spread out due to the curvature of the tail.Comparing Figs. 2-13(a), (b), and (c) with the corresponding multipath plots, we see the multipath appears where expected.

Buildings 1 and 2 have elevation multipath levels, separation angles and a flight path duration such that noticeable elevation errors were produced for all three systems. Since motion averaging proved to be an important factor in the end performance, and motion averaging is closely tied to scalloping frequency [28], the scalloping frequencies are of particular interest here. Figs 2-14 and 2-15 show the scalloping frequencies for these two buildings. We see that the scalloping frequencies vary considerably within the multipath region, corresponding to a "low persistence" geometry [28].

2. Scenario 2

Scenario 2 is derived from the geometry of runway 24R at Los Angeles International Airport (LAX). Fig 2-16 is a map of the airport. With the origin of the coordinate system used at the stop end of runway 24R, the azimuth and DME transmitter sites are at (-1000,0,6), the elevation and flare transmitter sites are at (7900,-400,10), and (7000,-400,13). There are five

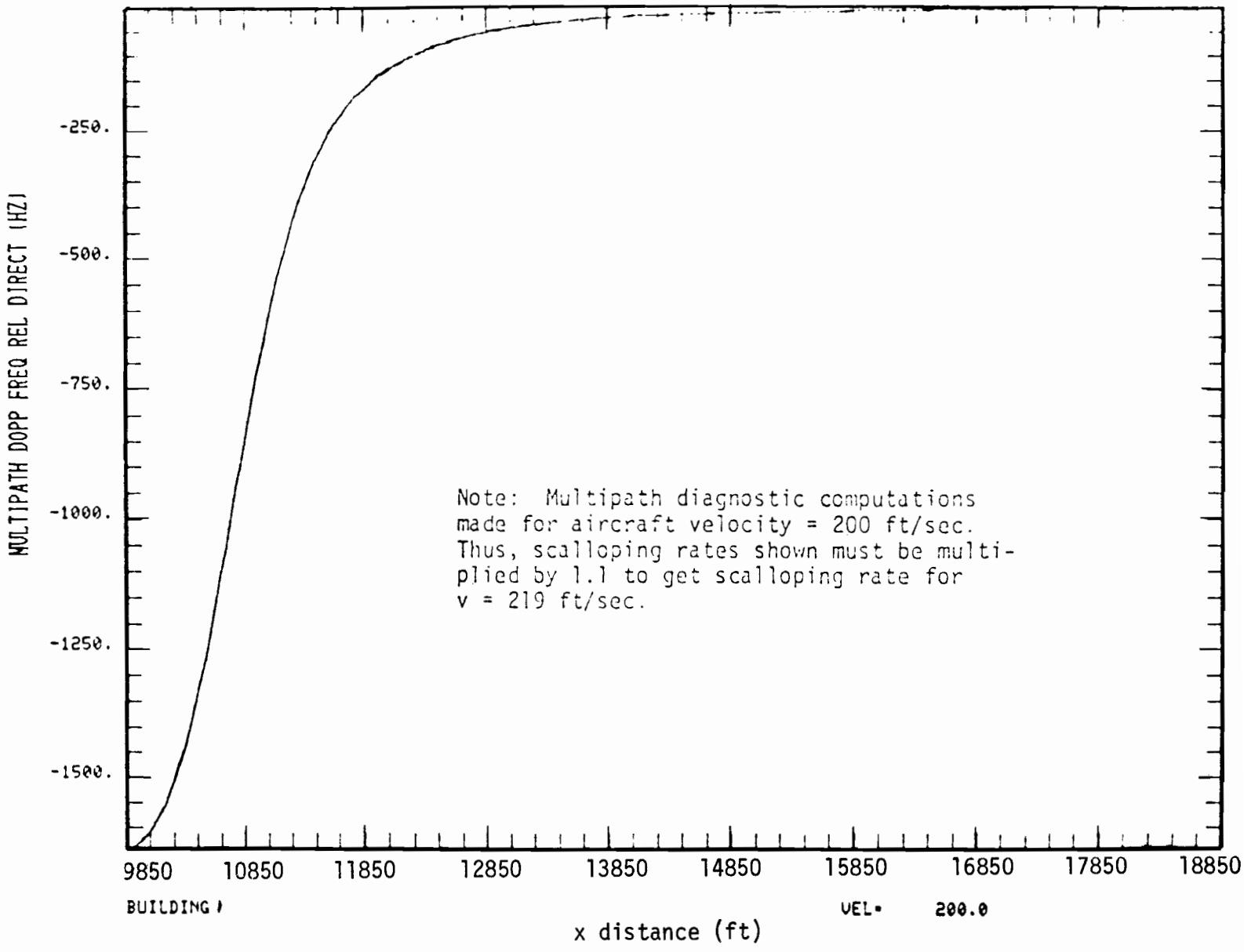

Fig. 2-14. Scalloping frequency along flight path for scenario 1, EL transmitter, Building 1.

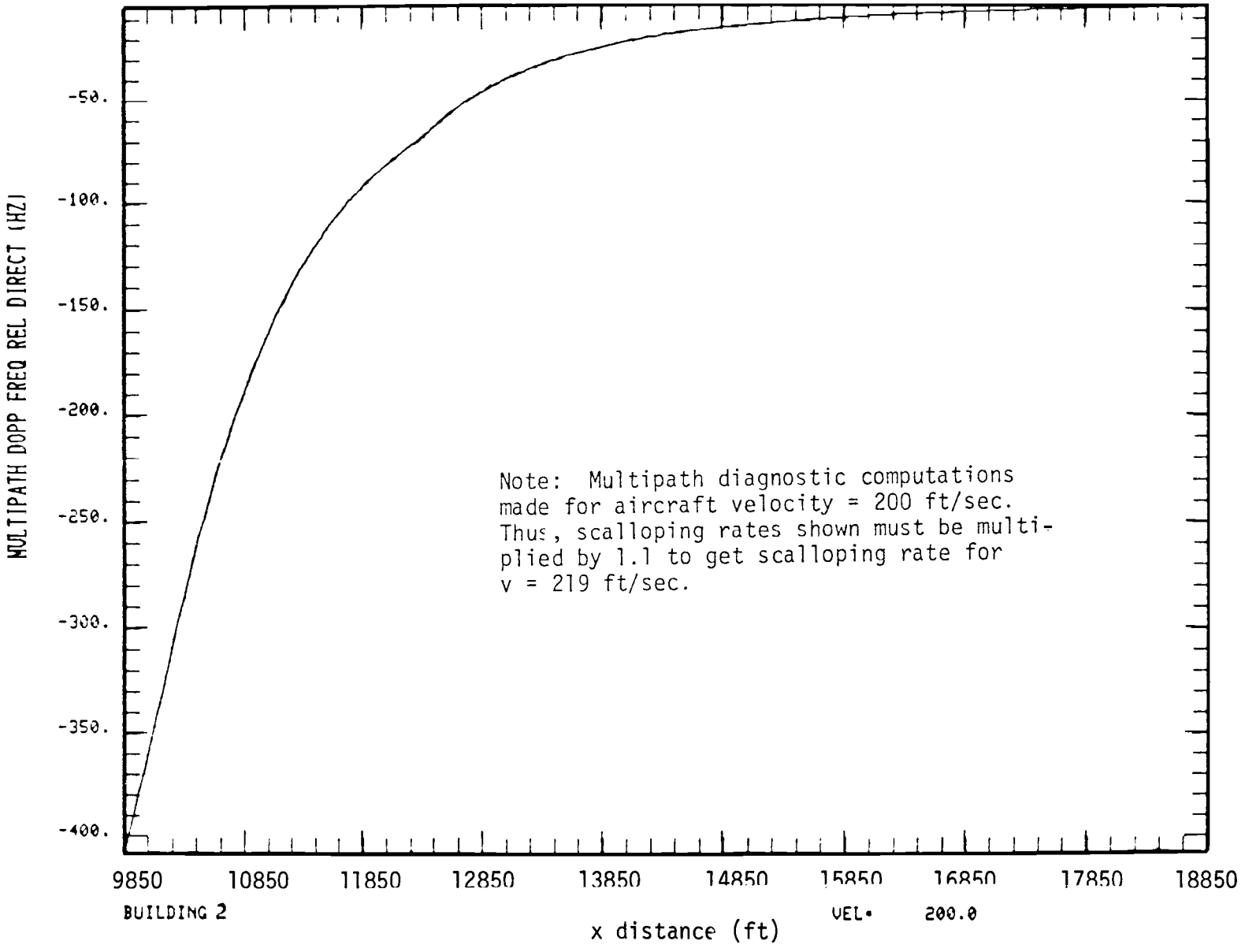

Fig. 2-15. Scalloping frequency along flight path for scenario 1, EL transmitter, Building 2

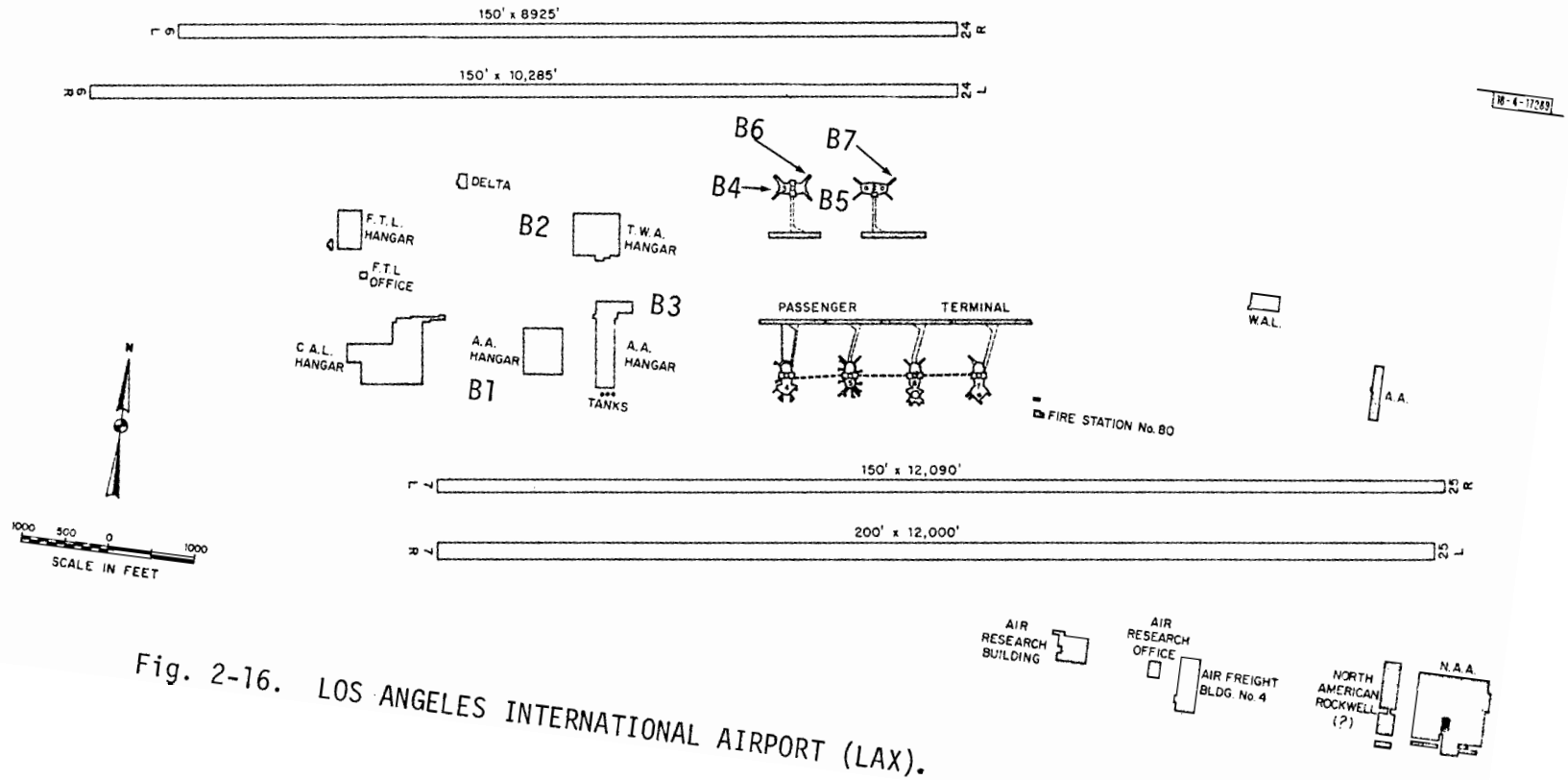

Fig. 2-16. LOS ANGELES INTERNATIONAL AIRPORT (LAX).

buildings and four airplanes included in this scenario, but two of the buildings (B4 and B5) have wings extending outwards and they are specified as B6 and B7. The locations of the buildings and aircraft are given in Table 2-2. Again the aircraft are assumed to be Boeing 747's. The flight path along which multipath levels and system errors are calculated is as follows:

Flight path: v = 219.56 ft/sec (130 knots)

Starting at (17700,0,500) and descending along a straight line toward (7700,0,0) with samples every 43.91 ft (5 Hz rate).

The runway is modeled as being humped with the hump shaped as a segment of a circular cylinder of radius 25,000 ft and centered at (3800,0,-24995).

Computer generated airport maps are given in Fig. 2-17 for C band carrier and Fig. 2-18 for L band. These are followed by multipath plots for C band for each of the transmitter sites (Figs. 2-19 and 2-20) and for L band for each of the transmitter sites (2-21 to 2-23). The reflection edge rays for the azimuth and elevation transmitter are illustrated in Figs. 2-24 and 2-25. Again, in comparing region of significant multipath levels to Figs. 2-24 and 2-25, there are no surprising results.

There is one significant difference in these multipath plots from those of scenario 1 and that is in the behavior, for azimuth and DME, of the ground reflection. This difference is due to the shadowing resulting from the hump in the runway model. Fig. 2-26 shows the diffraction results caused by the hump in the runway. We see, for C band, that at the start of the flight path at x = 17700 there is no effect from the shadowing. The receiver descends along the flight path so that the angle of the receiver above the hump gets smaller until at about x = 15000 the diffraction model takes over and the

TABLE 2-2

SCENARIO 2 BUILDING AND AIRCRAFT LOCATIONS

	Building Locations		Height (ft)
B1.	(3975, -3400)	(4400, -3400)	100
B2.	(4550, -2100)	(5080, -2100)	100
B3.	(4800, -3100)	(5200, -3100)	100
B4.	(6825, -1800)	(7125, -1800)	50
B5.	(6825, -1800)	(8080, -1800)	50
B6.	(7125, -1800)	(7524, -1706)	50
B7.	(8080, -1800)	(8209, -1706)	50

Note: Buildings 6 and 7 are wings of Buildings 4 and 5.

Aircraft Locations

Plane	Tail Location	Nose Location
A1.	(5700, -1150)	(5900, -1150)
A2.	(6700, -1150)	(6900, -1150)
A3.	(8758.58, -1150)	(8900, -1008.58)
A4.	(8900, -900)	(8900, -700)

Origin at stop-end of runway

Azimuth and DME transmitters at (-1000,0,5)

Elevation transmitter at (7900,-400,10) for C band

Elevation transmitter at (7900,-400,16.5) for L band

Flare transmitter at (7000,-400,13)

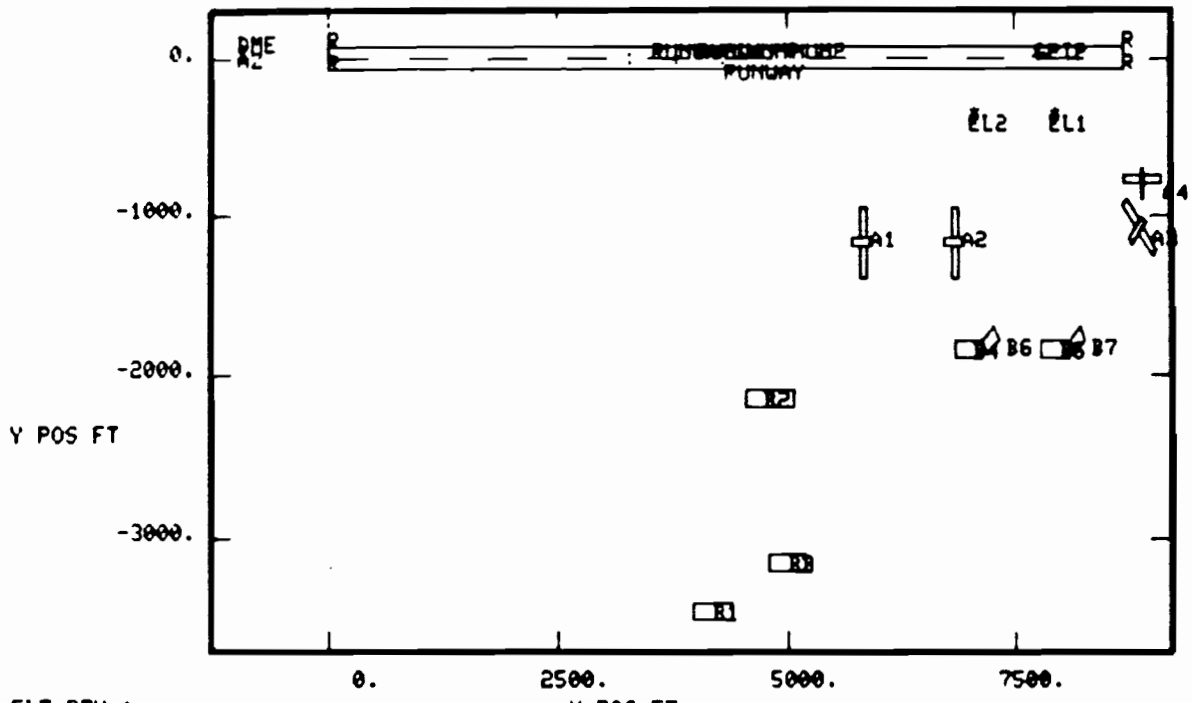

FLT PTH A

AZ SYSTEM

OBST	RANK	AMP	DIST	RDOP
G	1	0	4698.3	0.
B1	4	4	7991.3	-173.
B2	2	2	6805.8	-63.
B3	3	2	7025.3	-130.
B4	9	26	2854.1	-27.
B5	10	28	834.3	-22.
B6	11	44	9791.4	-708.
B7	5	7	9308.5	-974.
A1	8	22	4917.8	-14.
A2	7	22	8913.3	-137.
A3	6	18	8913.3	-1091.
A4	12	68	9001.1	-1396.
D	0	80	0.0	0.

EL SYSTEM

OBST	RANK	AMP	DIST	RDOP
G	1	0	10012.5	2.
B1	11	68	6542.4	-111.
B2	7	63	6366.7	-51.
B3	8	65	6542.4	-118.
B4	4	49	9835.3	-584.
B5	3	34	9045.0	-591.
B6	6	59	9176.7	-410.
B7	5	50	9879.2	-1243.
A1	10	67	131.7	-4.
A2	9	65	263.5	-6.
A3	2	20	9045.0	-1194.
A4	12	68	8913.3	-1165.
D	0	80	0.0	0.

RANK = multipath ranking

AMP = maximum -M/D ratio (dB)

RDOP = relative Doppler (Hz) at point of maximum M/D

DIST = distance along flight path (ft) at which maximum M/D occurred = 17700 - x pos (ft)

Fig. 2-17. Airport map for WG-A scenario 2 for C-band carrier.

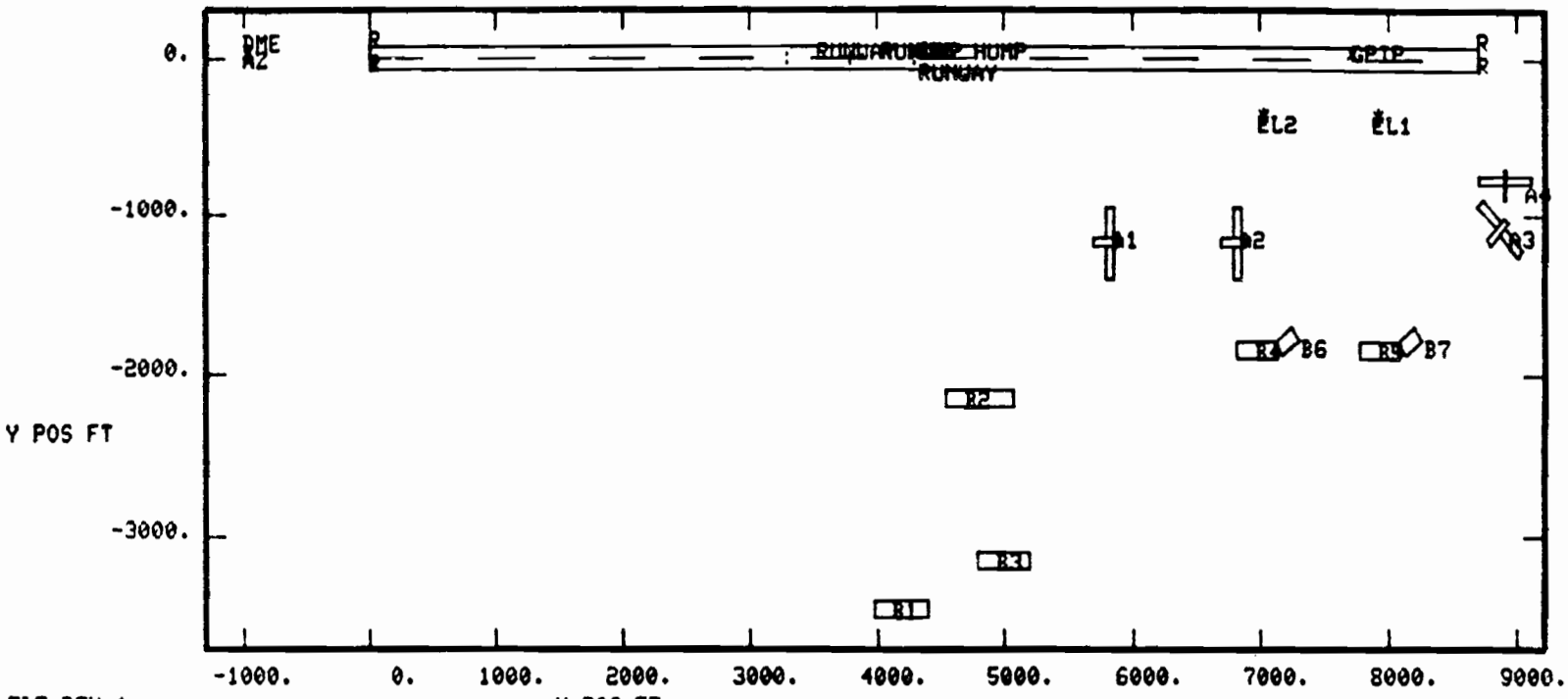

FLT PTH A

AZ SYSTEM

OBST	RANK	AMP	DIST	RDOP
G	12	80	0.0	0.
B1	1	0	8079.1	-35.
B2	2	2	7376.6	-14.
B3	4	5	6542.4	-24.
B4	6	25	2766.3	-5.
B5	7	26	790.4	-4.
B6	10	39	9747.5	-135.
B7	3	2	9352.4	-193.
A1	9	29	4961.7	-3.
A2	8	27	9132.8	-32.
A3	5	19	9045.0	-240.
A4	11	61	9001.1	-275.
D	0	80	0.0	0.

EL SYSTEM

OBST	RANK	AMP	DIST	RDOP
G	1	0	10012.5	0.
B1	11	60	7420.5	-27.
B2	7	56	6981.4	-12.
B3	9	58	7376.6	-29.
B4	4	41	9176.7	-77.
B5	3	26	9045.0	-116.
B6	6	50	9396.3	-94.
B7	5	42	9220.7	-176.
A1	10	59	0.0	-1.
A2	8	58	0.0	-1.
A3	2	22	9045.0	-235.
A4	12	62	9001.1	-253.
D	0	80	0.0	0.

RANK = multipath ranking

AMP = maximum -M/D ratio (dB)

DIST = distance along flight path (ft) at which maximum M/D occurred = 17700 - x pos (ft)

RDOP = relative Doppler (Hz) at point of maximum M/D

Fig. 2-18. Airport map for WG-A scenario 2 for L-band carrier.

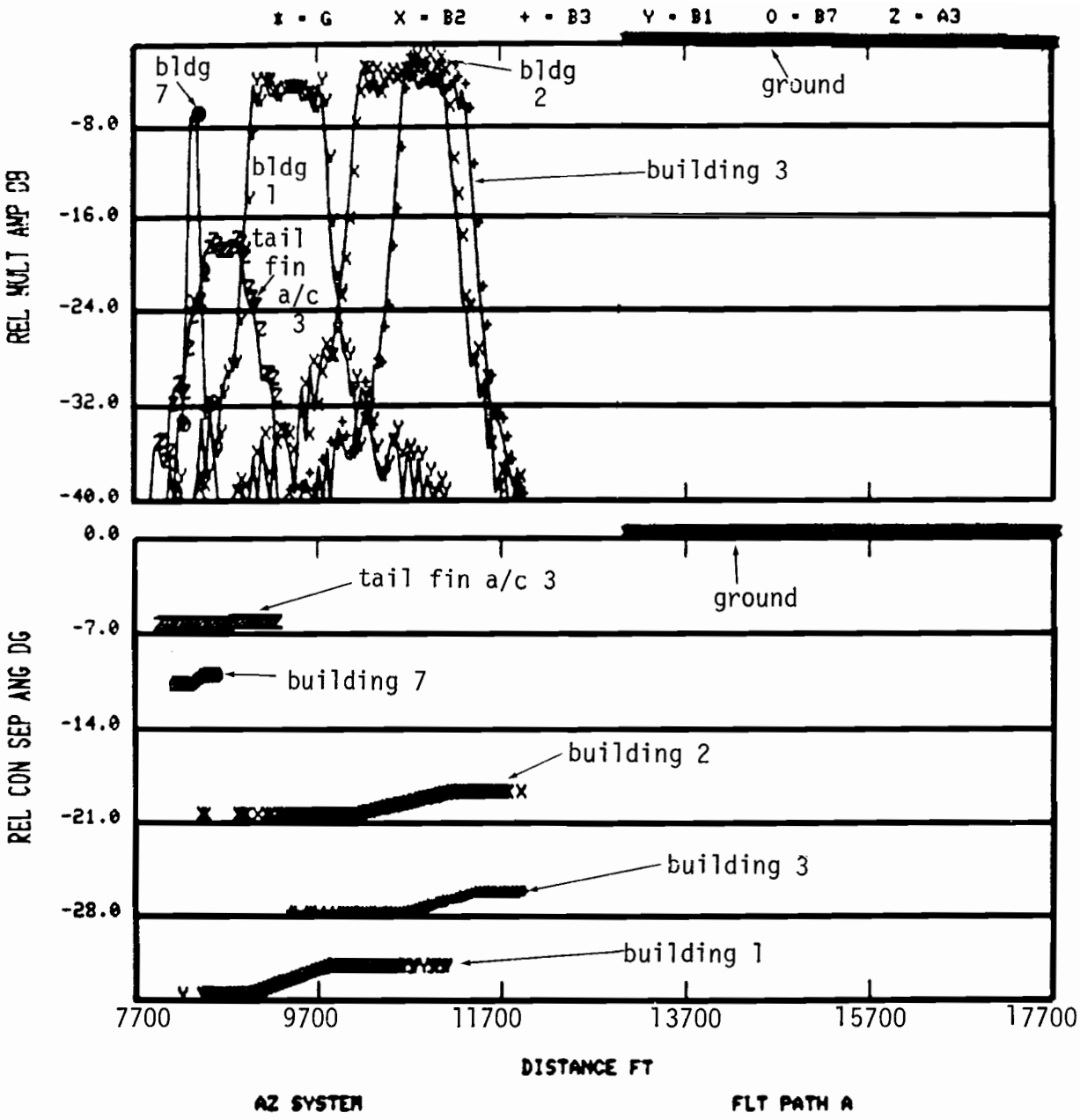

Fig. 2-19. Azimuth multipath and separation angle for scenario 2 (LAX) for C-band with snow.

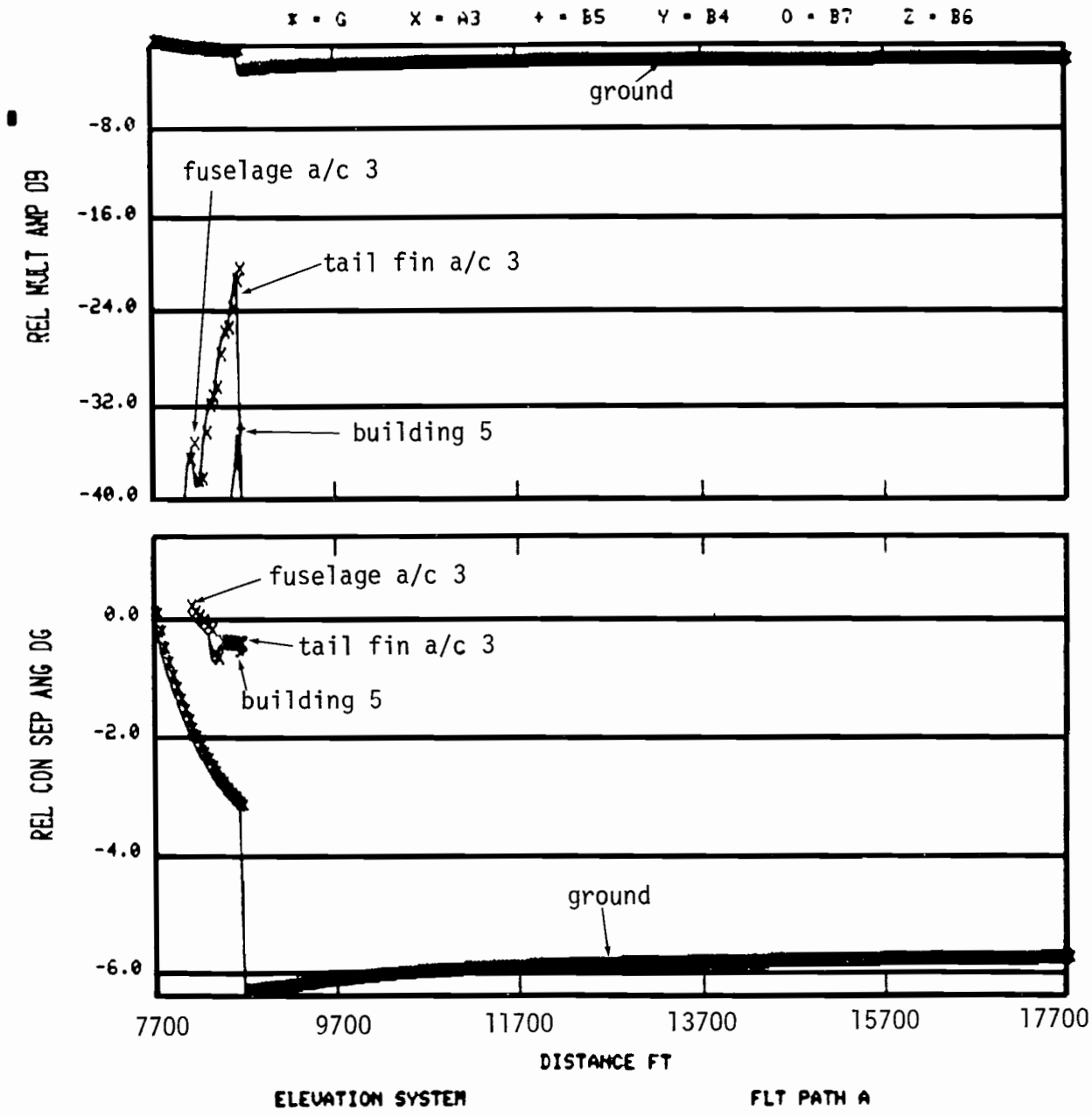

Fig. 2-20. Elevation multipath and separation angle for scenario 2 (LAX) for C-band with snow.

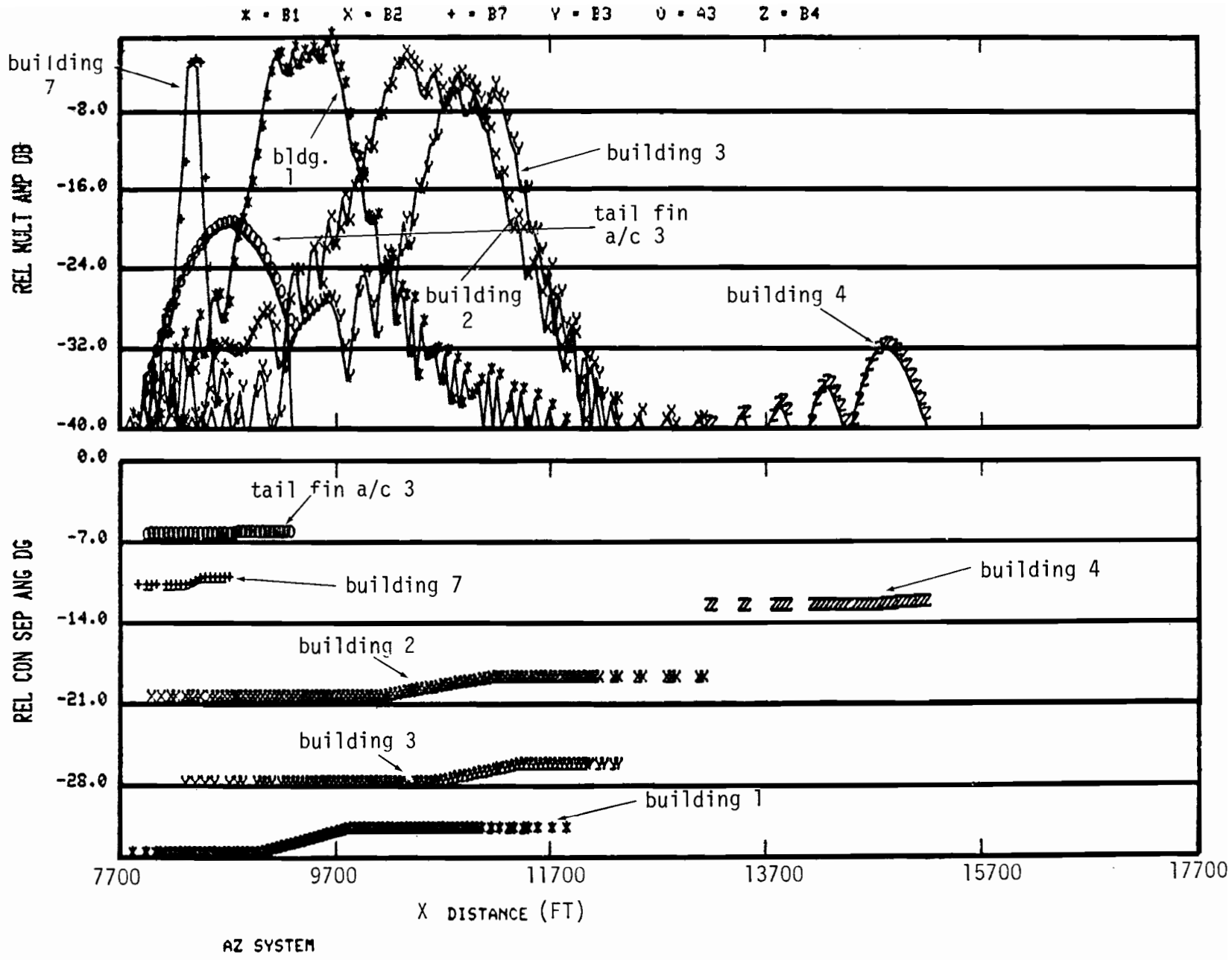

Fig. 2-21. Azimuth multipath and separation angle for scenario 2 (LAX) L-band.

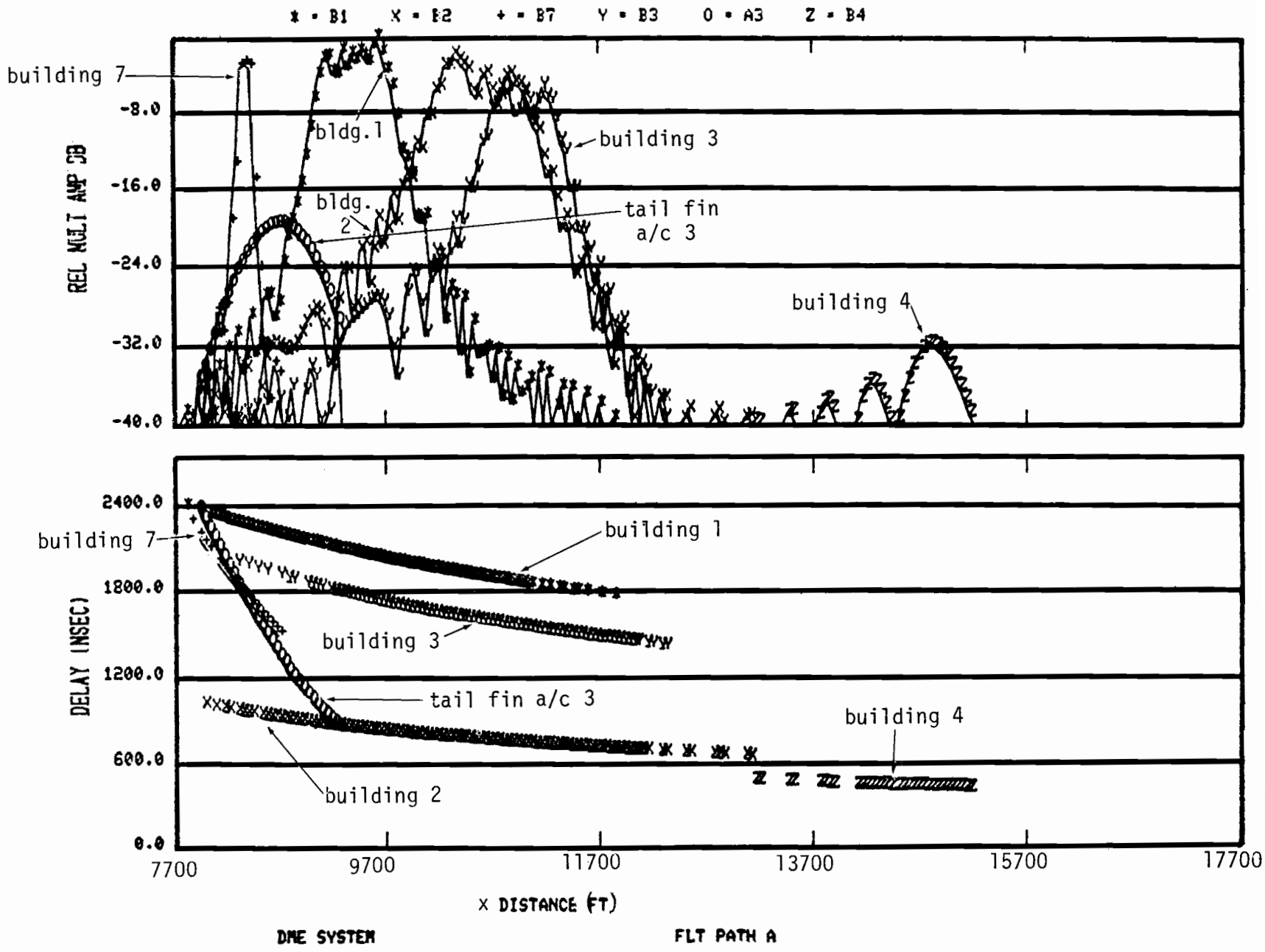

Fig. 2-22. DME multipath and delay for scenario 2 (LAX) for L-band.

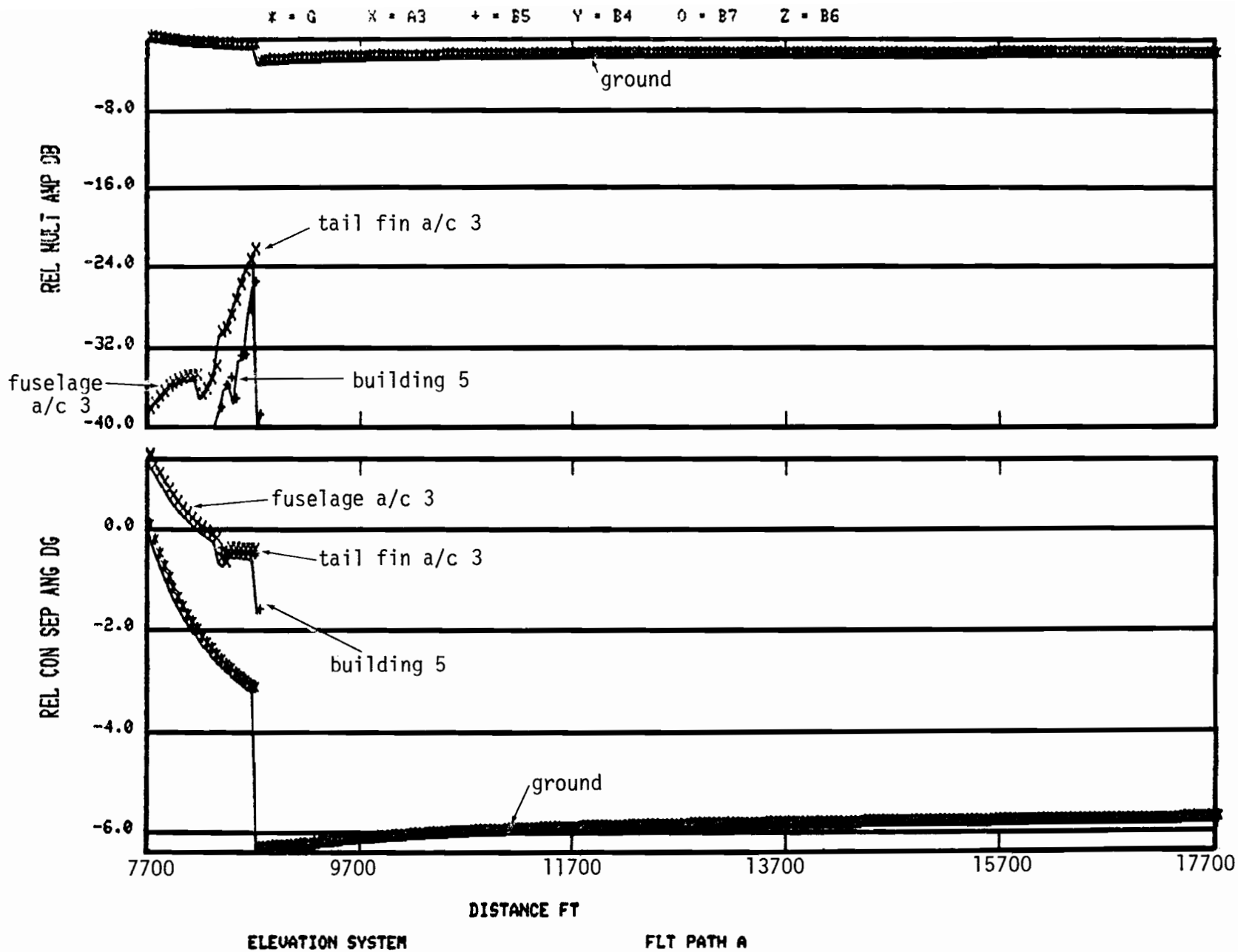

Fig. 2-23. Elevation multipath and separation angle for scenario 2 (LAX) L-band.

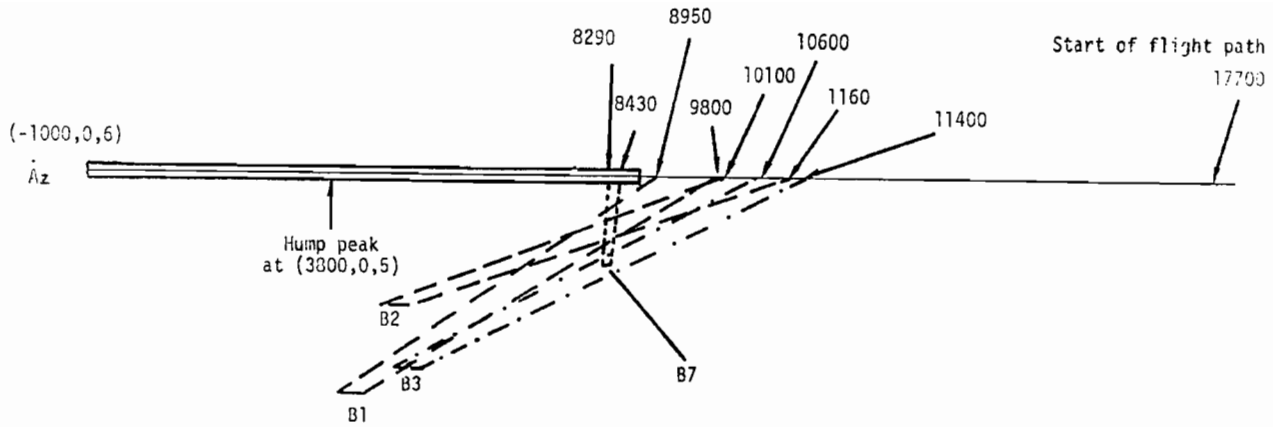

Fig. 2-24. LAX map with edge reflection rays in horizontal plane for azimuth transmitter.

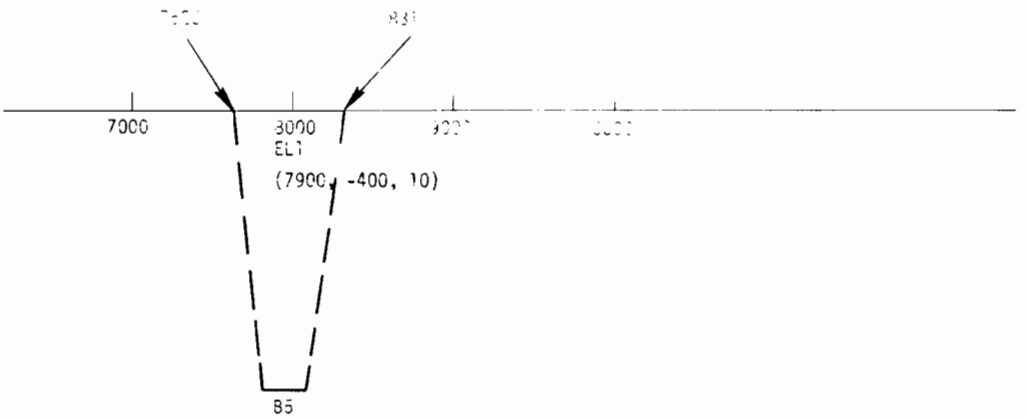

Fig. 2-25. LAX map with edge reflection rays in horizontal plane for elevation transmitter.

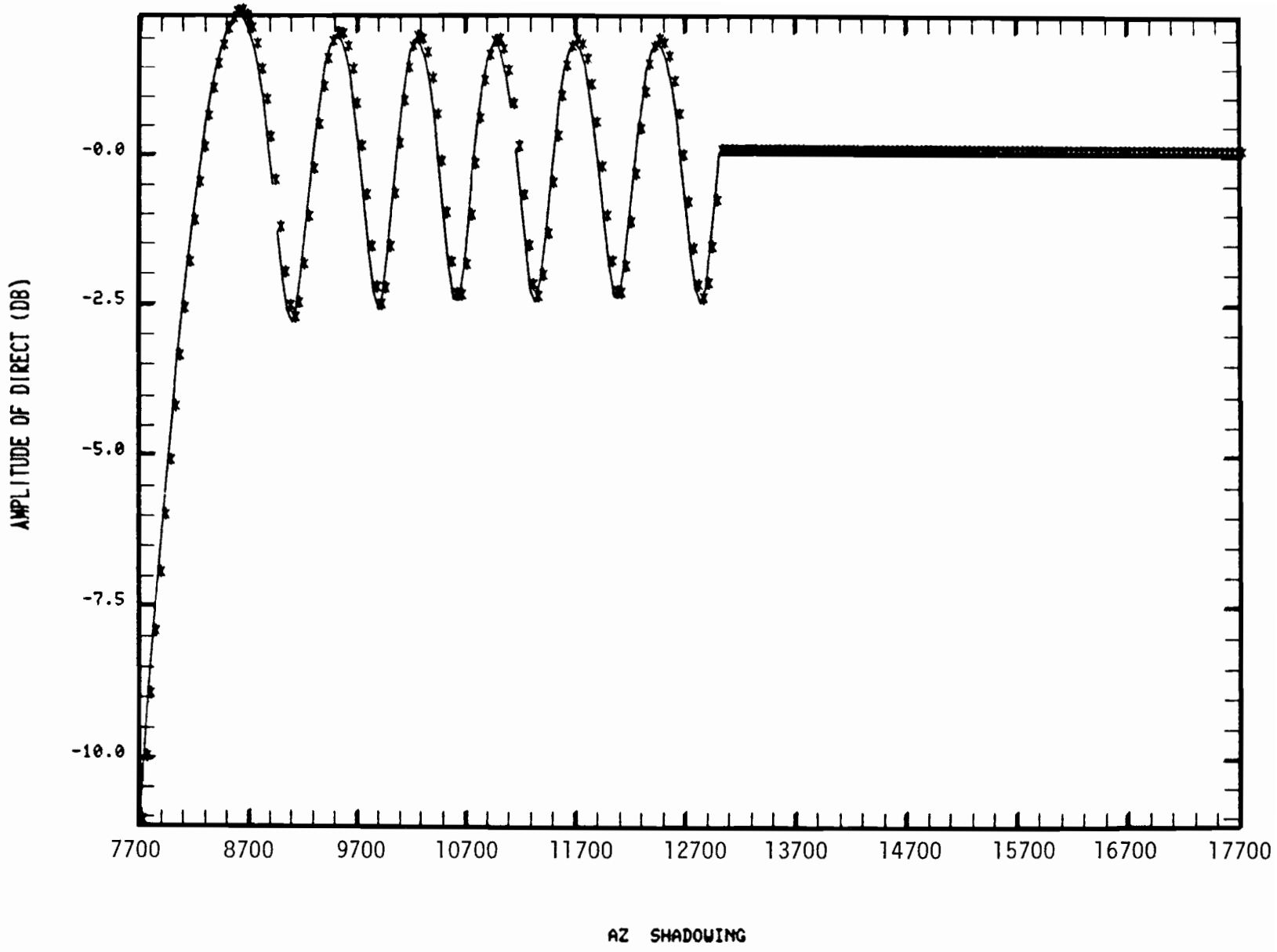

Fig. 2-26. Azimuth shadowing for WG-A scenario 2 (LAX) C-band.

combined results of the direct signal and its ground reflections is shown in Fig. 2-26. We see that as the receiver nears threshold it goes into a deep shadow of the azimuth signal.

Fig. 2-27 illustrates the same results for L band. For the lower frequency, the diffraction model takes over much sooner. In fact, even at the start of the flight path the diffraction model is used. A deep shadow of the azimuth signal near threshold is observed for L band as well.

The variation of scalloping frequency within the respective multipath regions was small for the principal multipath scatters, and hence, detailed plots are not shown.

3. Scenario 3

AWOP scenario 3 was derived from the geometry at Crissy Army Field, San Francisco. Fig. 2-28 presents a map of Crissy Field, a STOL airport. The glide slope here is chosen as 6° and the velocity as 70 knots (118.22 ft/sec). The origin of our coordinate system is again at the center of the stop-end of the runway. The transmitters are located at (-140,0,6) for azimuth (-140,12,6) for DME, and (2120,120,10) for elevation and flare. There are six buildings and a train (denoted as B7) whose specifics are given in Table 2-3. The flight path along which multipath levels and system errors are computed is as follows:

> Flight path: velocity = 118.22 ft/sec (70 knots)
> Starting at (677.18,0,500) and descending along a straight line to (2096.11,0,8.0) with samples every 23.64 ft. (= 5 Hz rate).

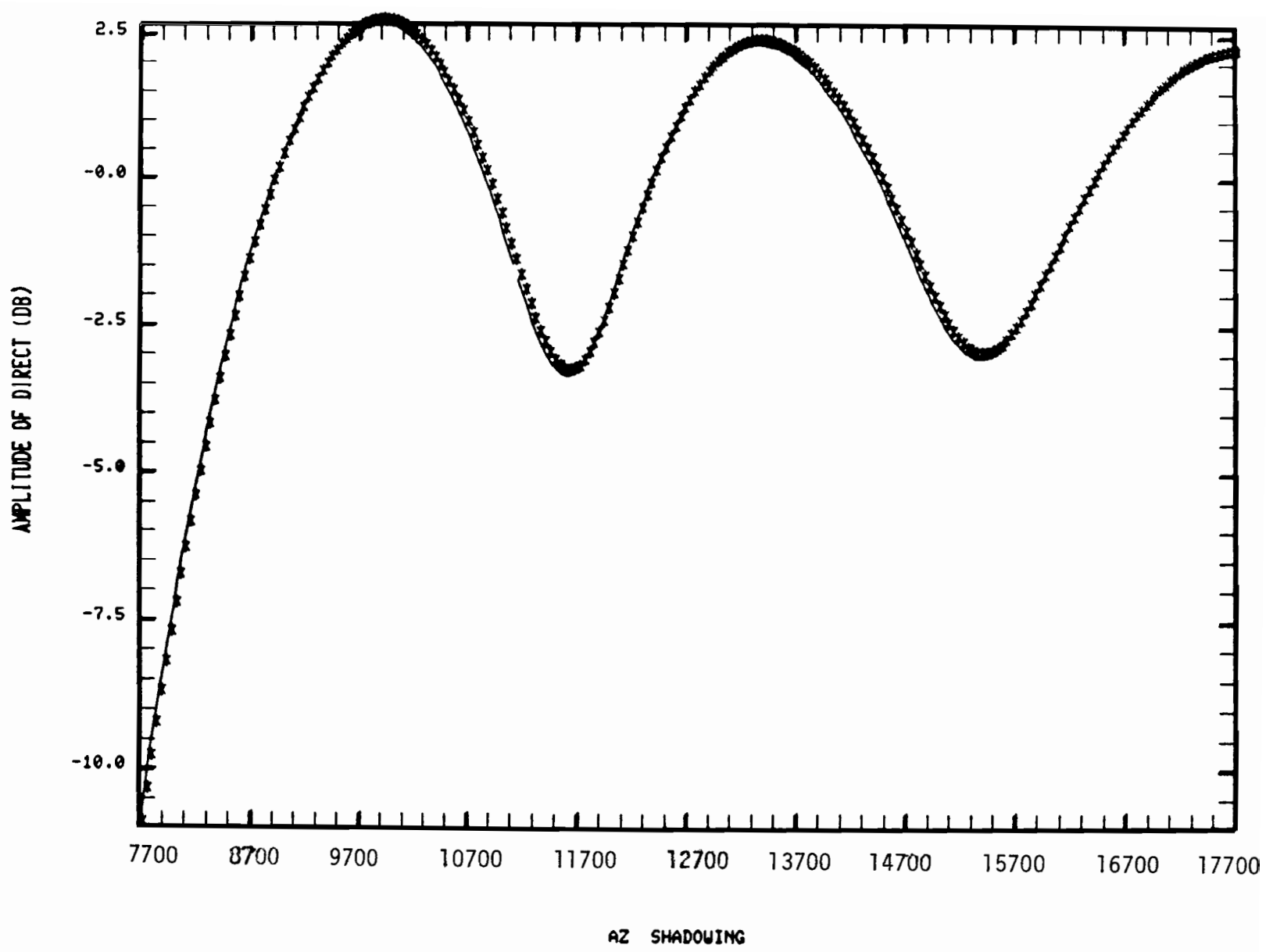

Fig. 2-27. Azimuth shadowing for WG-A scenario 2 (LAX) L-band.

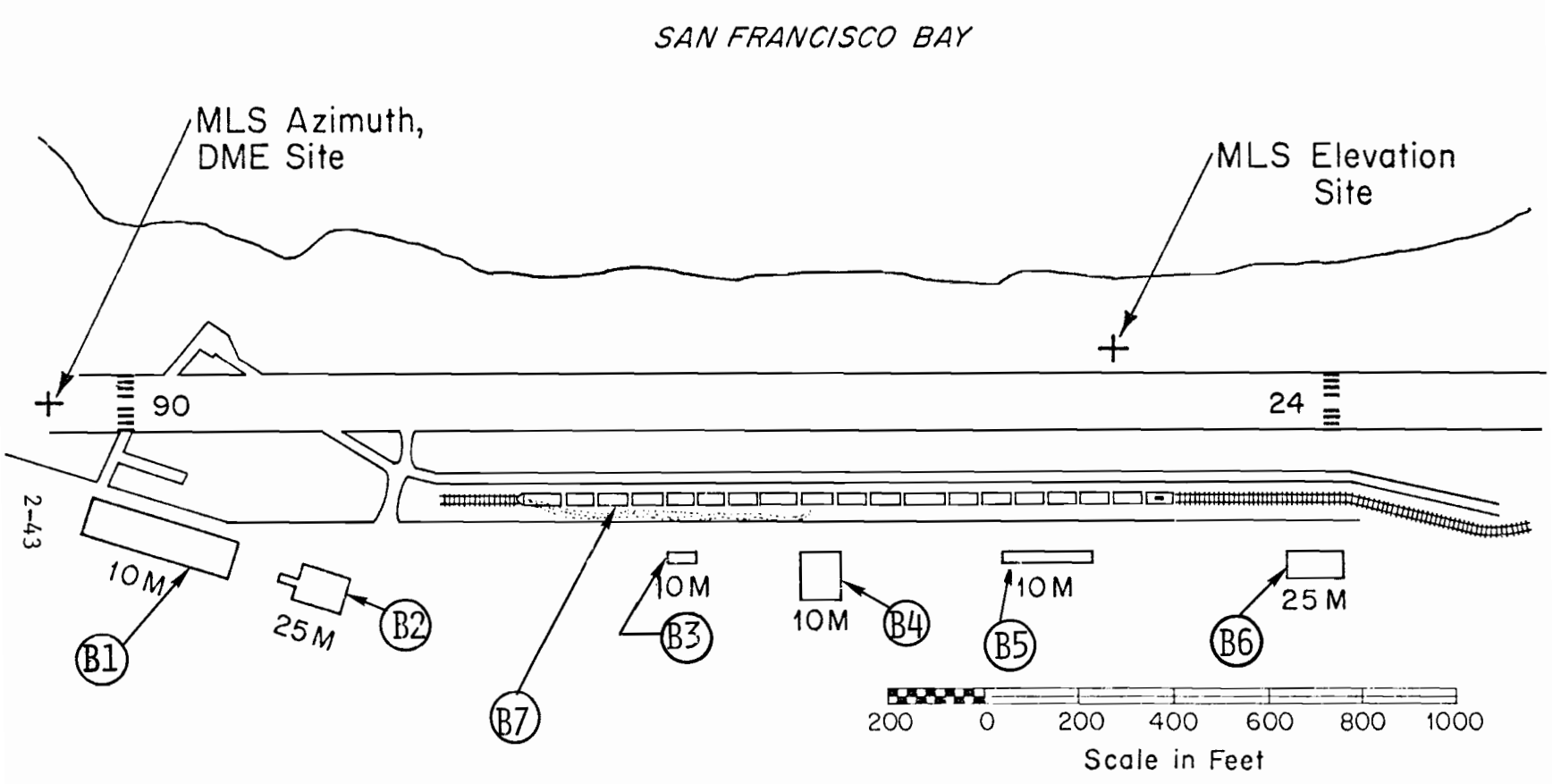

Fig. 2-28. Crissy Army Airfield in San Francisco.

TABLE 2-3

SCENARIO 3 BUILDING LOCATIONS

LOCATION OF BUILDING FRONTS

Building	From (x,y)	To (x,y)	Height
B1	(-40, -200)	(270, -290)	33'
B2	(400, 340)	(500, -370)	80'
B3	(1460, -320)	(15400, -320)	33'
B4	(1190, -320)	(1240, -320)	33'
B5	(2500, -320)	(2600, -320)	80'
B6	(1880, -320)	(2060, -320)	33'

Train (denoted as B7) is from (800, -200) to (2300, -200) and 16 ft high.

Origin at stop-end of runway

Azimuth transmitter at (-140,0,6)

DME transmitter at (-140,12,6)

Elevation transmitter at (22120,120,9) for C band

Elevation transmitter at (2120,120,16.5) for L band

The computer generated map and multipath plot results are given in Figs. 2-29 to 2-31 for C band and Figs. 2-32 to 2-35 for L band. The edge reflection rays indicated in Fig. 2-36a for azimuth and DME and in Fig. 2-36b for elevation, coincide with the regions of significant multipath reflections in Figs. 2-29 to 2-35. The principal multipath errors in this scenario arose from building 1. Fig. 2-37 shows the variation of scalloping frequency for this scatterer as a function of distance along the flight path.

This scenario was also simulated assuming inhomogeneous ground dielectric constants:

(1) $\varepsilon/\varepsilon_o = 5.0$ for the runway

(2) $\varepsilon/\varepsilon_o = 1.2$ for terrain off the runway

For this case, numerical integration over an appropriate region was used to determine the ground reflection level as opposed to the closed form (i.e., classical Fresnel) expression used in the other scenarios. Only the azimuth multipath performance was found to be affected by this change. Figs. 2-38 and 2-39 show the azimuth multipath characteristics at C band and L band respectively. The inhomogeneous terrain features and numerical integration computation procedure are seen to produce ground reflection level fluctuations considerably larger than those computed assuming homogeneous terrain.

4. Scenario 4

All aspects of scenario 4 are identical to those of scenario 1 except for the MLS elevation and flare transmitter locations. These are:

MLS elevation (9200,400,10) at C band and (9200,400,16.5) at L band

MLS flare (8000,-250,15)

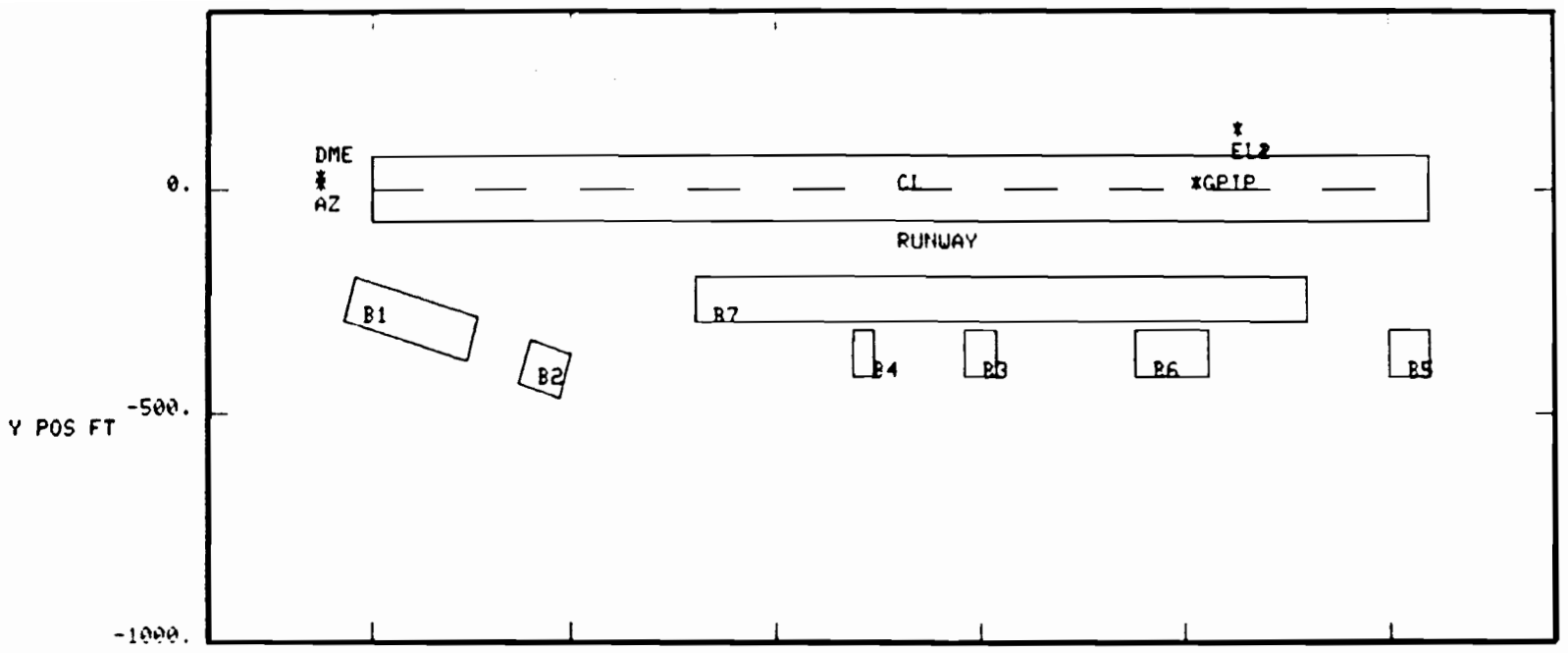

FLT PTH A

AZ SYSTEM

OBST	RANK	AMP	DIST	RDOP
G	1	0	4706.8	0.
B1	3	1	3049.5	-2.
B2	7	28	165.5	-1.
B3	5	23	3687.8	-11.
B4	4	4	4255.2	-16.
B5	8	32	1513.0	-4.
B6	6	28	2742.2	-6.
B7	2	0	4657.0	-9.
D	0	20	0.0	0.

EL SYSTEM

OBST	RANK	AMP	DIST	RDOP
G	1	5	0.0	-0.
B1	8	73	4397.0	39.
B2	6	61	3333.2	-4.
B3	5	61	4373.3	3.
B4	7	63	4397.0	23.
B5	2	5	3876.9	-157.
B6	4	48	4706.8	186.
B7	3	11	4515.2	-301.
D	0	80	0.0	0.

RANK = multipath ranking

AMP = maximum -M/D ratio (dB)

DIST = distance along flight path (ft) at which max M/D occurred = 6775 - x pos (ft)

RDOP = relative Doppler (Hz) at point of max M/D

Fig. 2-29. Airport map for WG-A scenario 3 for C-band.

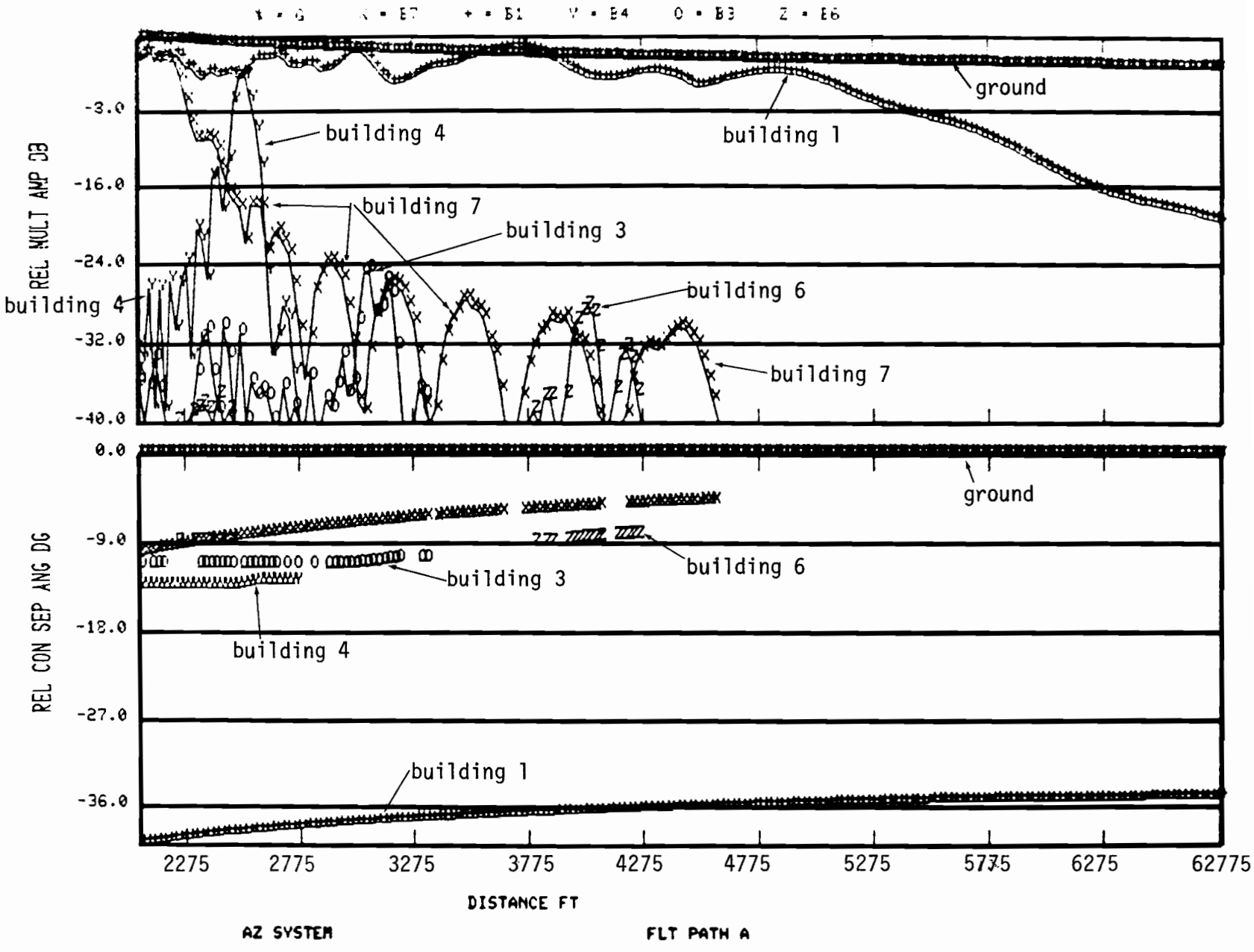

Fig. 2-30. Azimuth multipath and separation angle for scenario 3 (Crissy) for C-band.

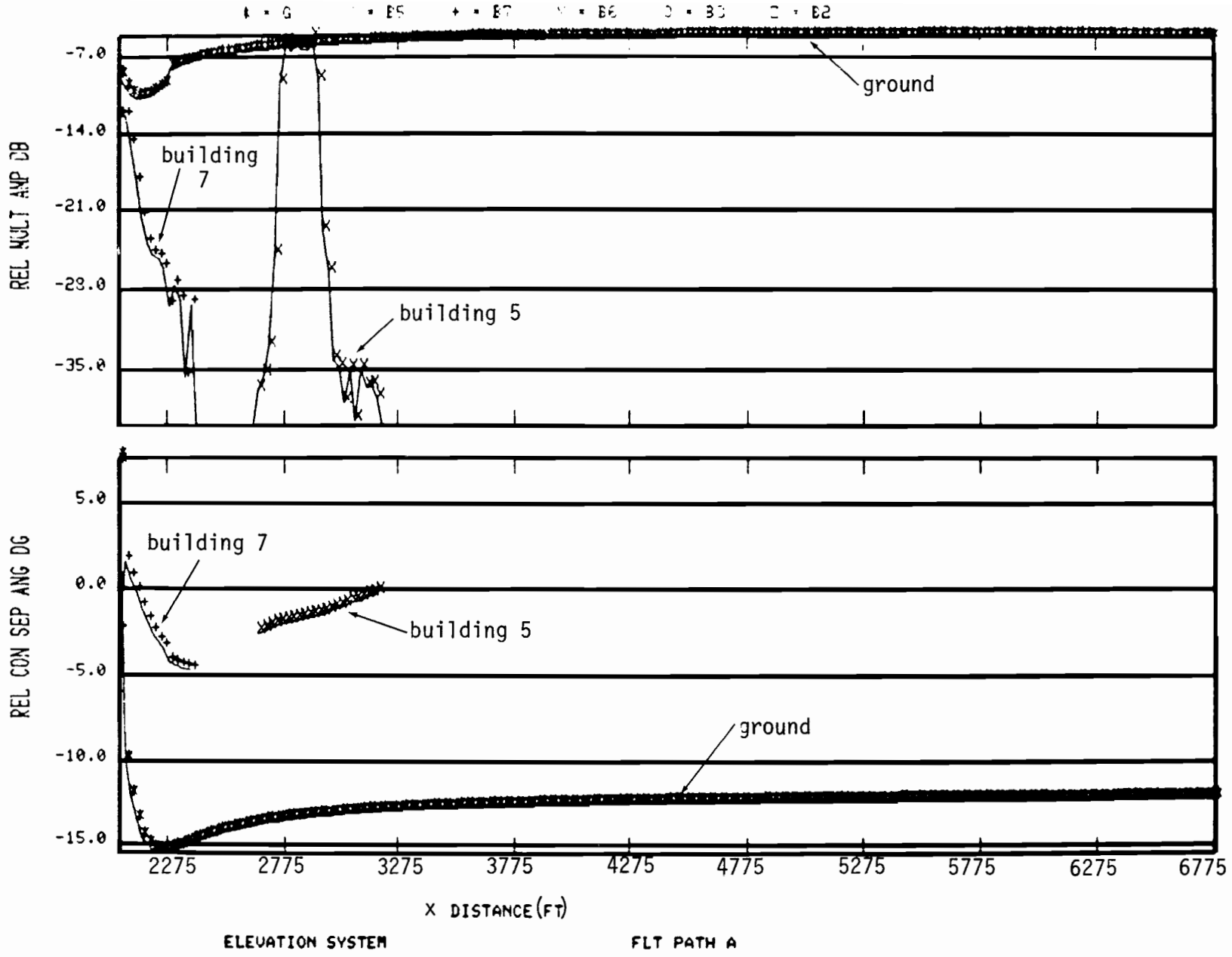

Fig. 2-31. Elevation multipath and separation angle for scenario 3 (Crissy) for C-band.

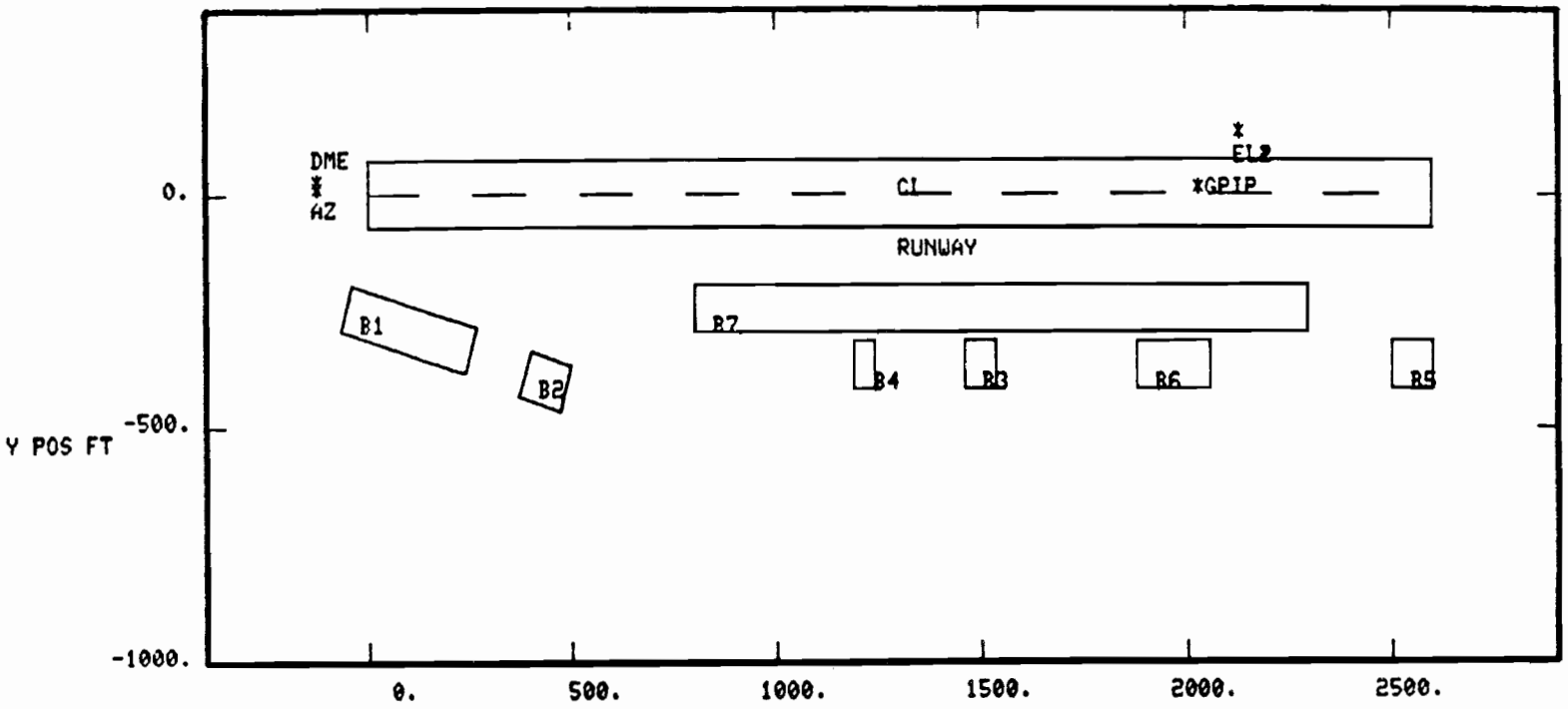

FLT PTH A

AZ SYSTEM

OBST	RANK	AMP	DIST	RDOP
G	1	0	4706.8	0.
B1	2	1	4160.6	-1.
B2	6	21	0.0	-0.
B3	5	20	3758.7	-2.
B4	4	10	4349.7	-4.
B5	8	29	3616.9	-11.
B6	7	24	2836.8	-1.
B7	3	6	4586.1	-2.
D	0	80	0.0	0.

EL SYSTEM

OBST	RANK	AMP	DIST	RDOP
G	2	5	0.0	-0.
B1	8	70	4278.8	3.
B2	5	55	3687.8	-1.
B3	6	58	4515.2	12.
B4	7	61	4515.2	17.
B5	1	4	3876.9	-31.
B6	4	40	4704.3	35.
B7	3	12	4562.4	-56.
D	0	80	0.0	0.

RANK = multipath ranking

AMP = maximum -M/D ratio (dB)

DIST = distance along flight path (ft) at which max M/D occurred = 6775 - x pos (ft)

RDOP = relative Doppler (Hz) at point of max M/D

Fig. 2-32. Airport map for WG-A scenario 3 for L-band.

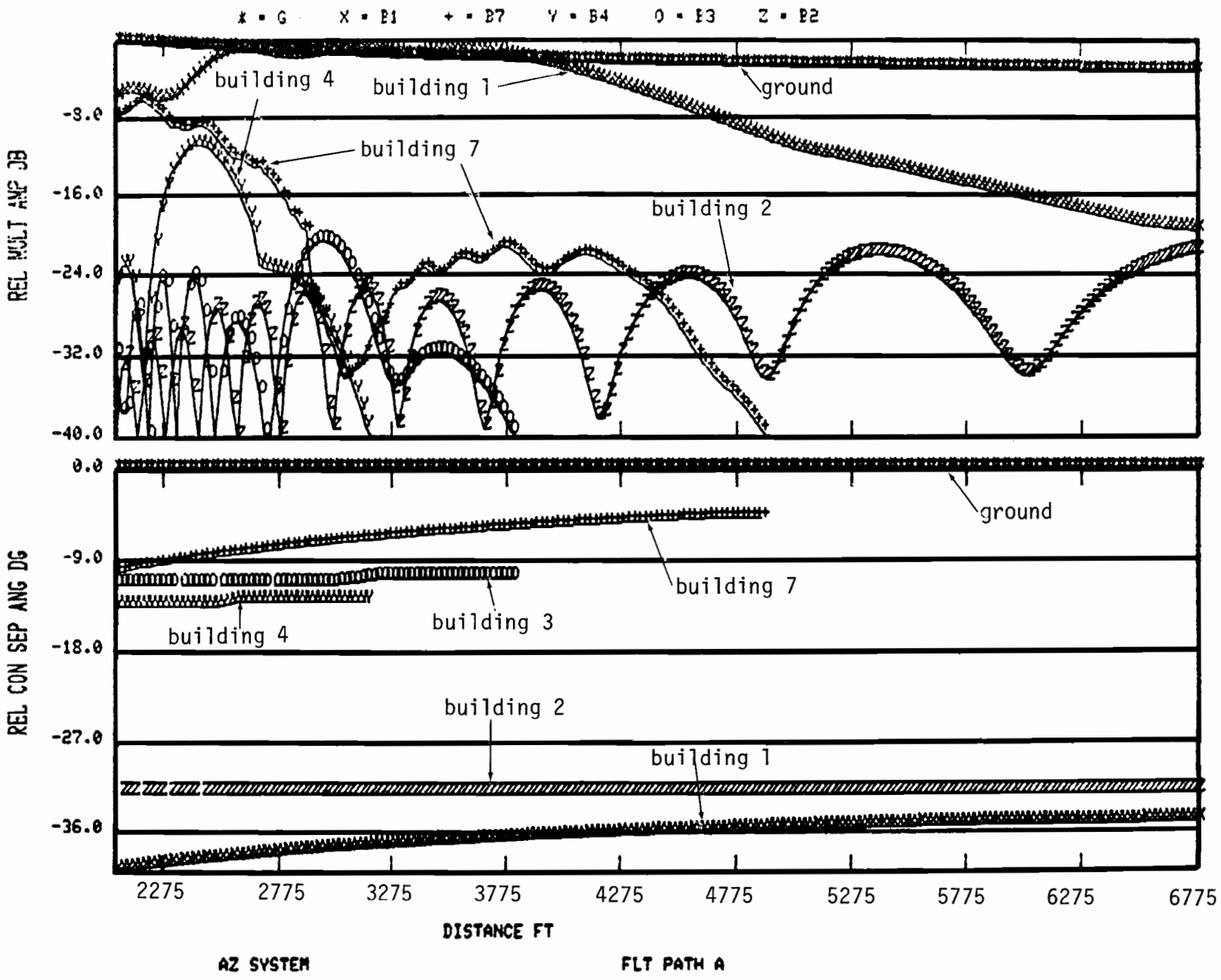

Fig. 2-33. Azimuth multipath and separation angle for scenario 3 (Crissy) for L-band.

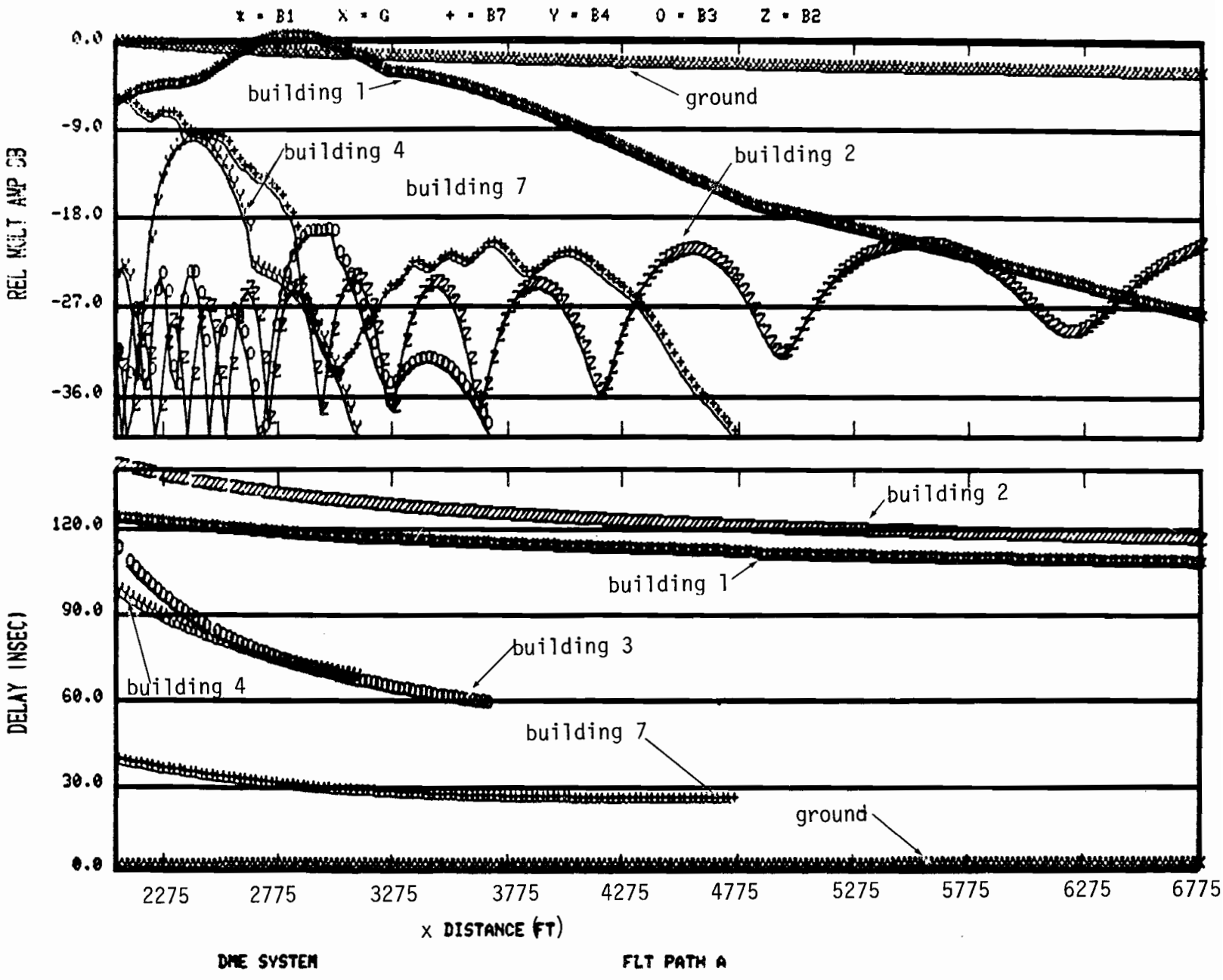

Fig. 2-34. DME multipath and delay for scenario 3 (Crissy) for L-band.

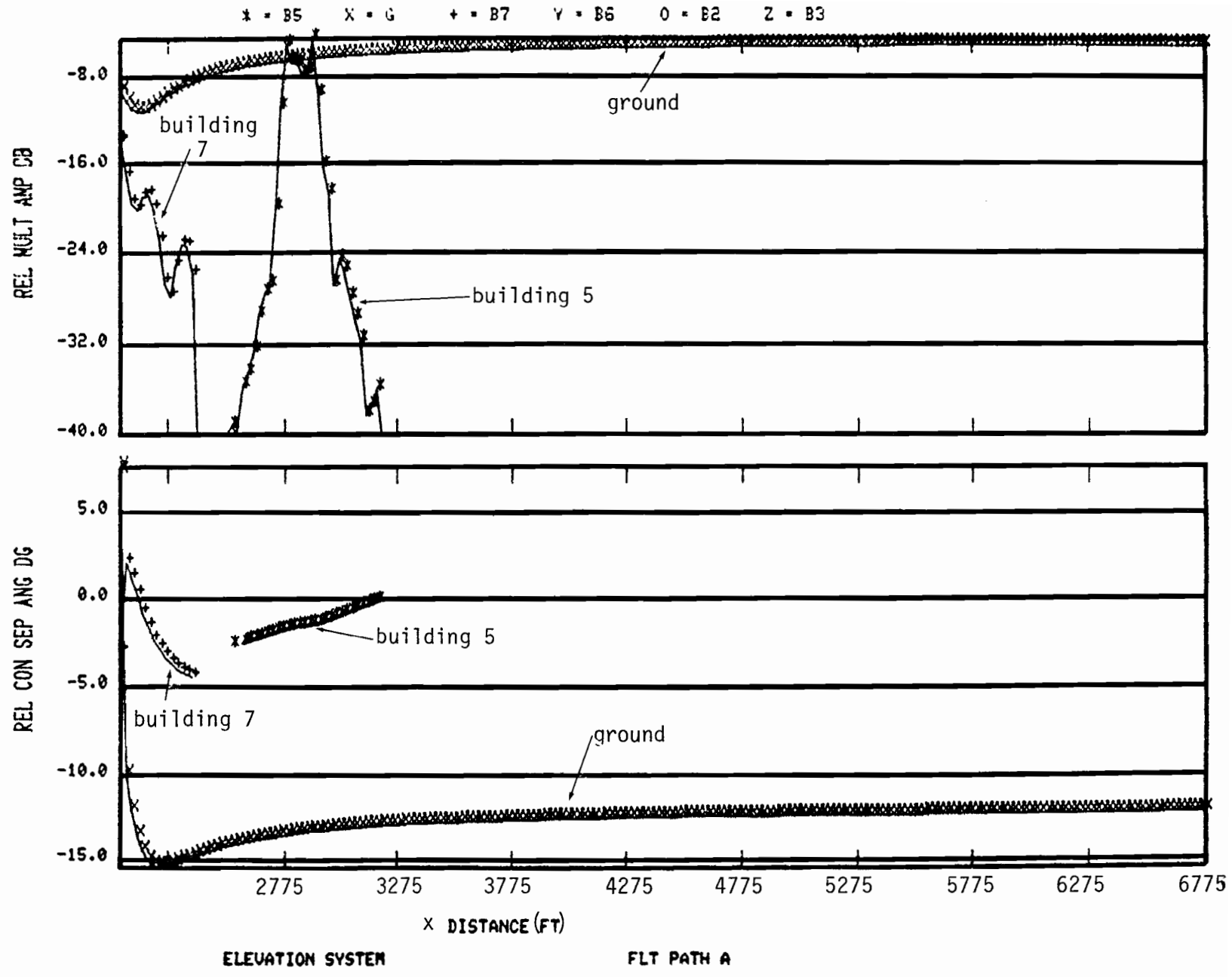

Fig. 2-35. Elevation multipath and separation angle for scenario 3 (Crissy) for L-band.

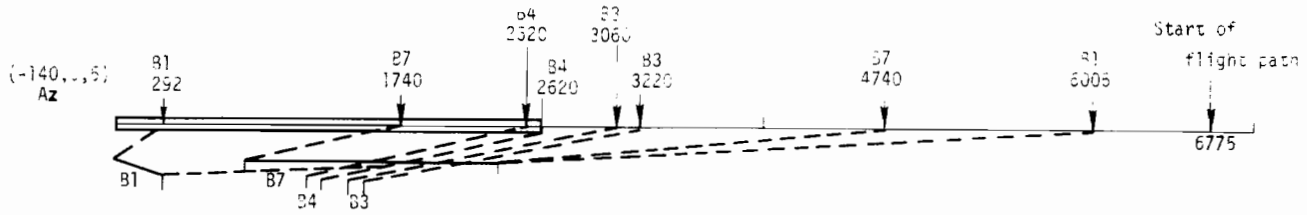

Fig. 2-36(a). Crissy Field map with edge reflection rays in the horizontal plane for azimuth transmitter.

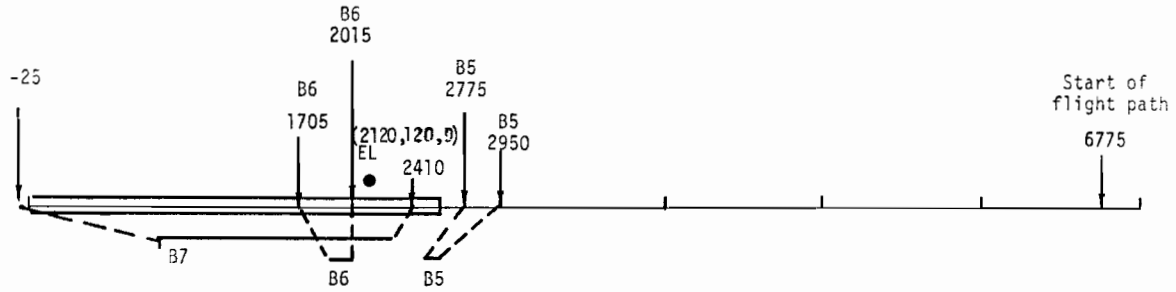

Fig. 2-36(b). Crissy Field map with edge reflection rays in the horizontal plane for elevation transmitter.

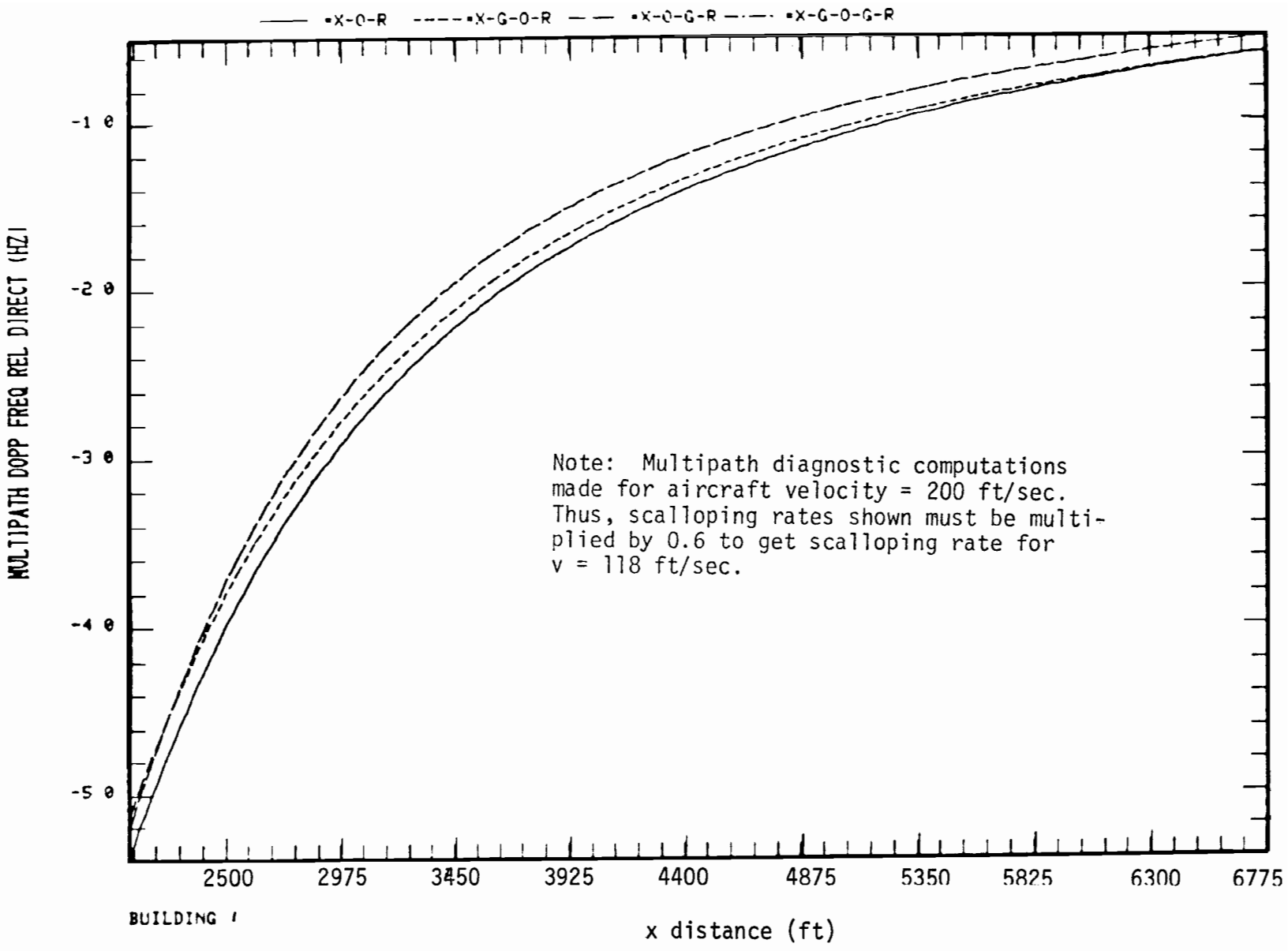

Fig. 2-37. Scalloping frequency along flight path for scenario 3, AZ transmitter, Building 1.

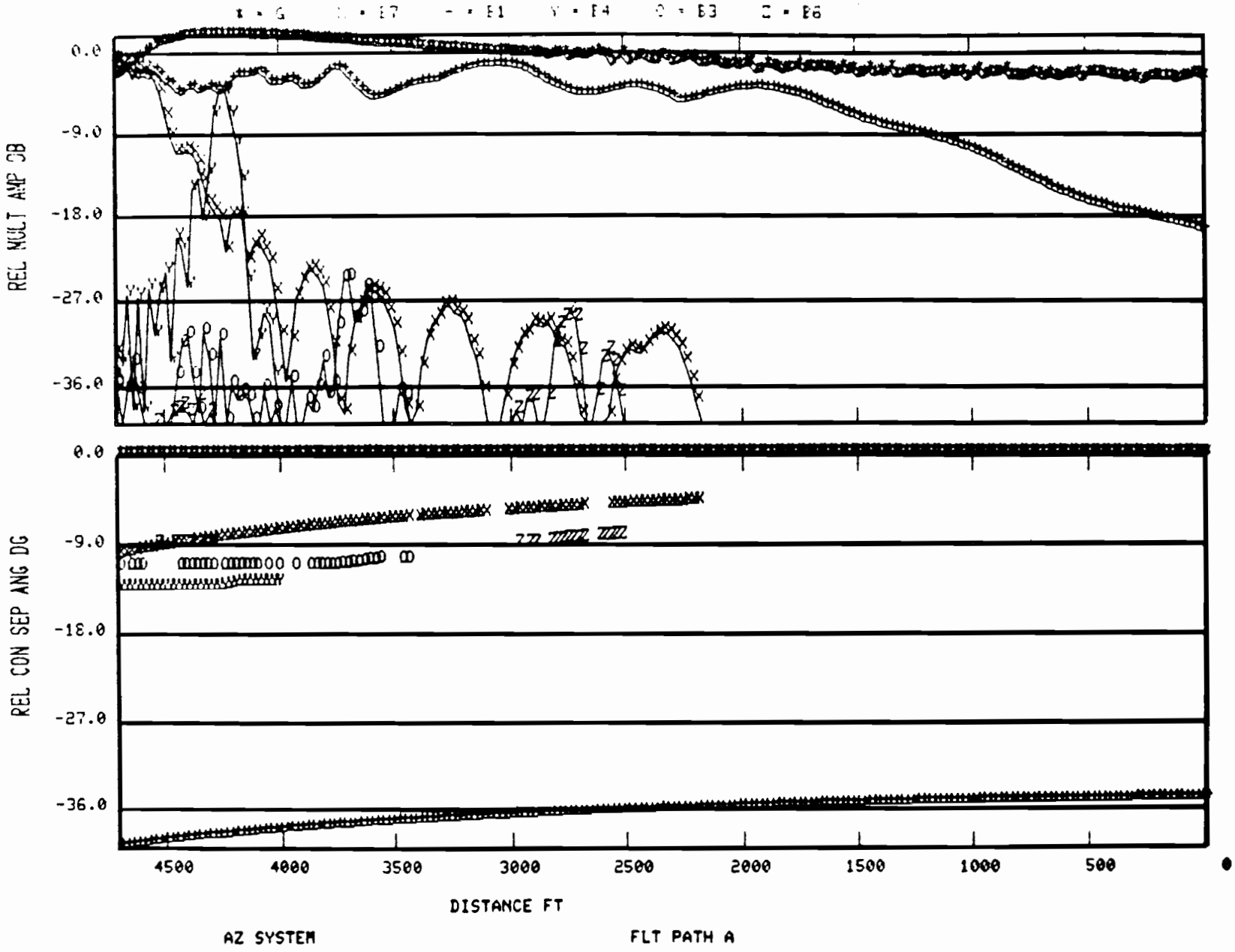

Fig. 2-38. Azimuth multipath characteristics at C-band for scenario 3 with inhomogeneous terrain.

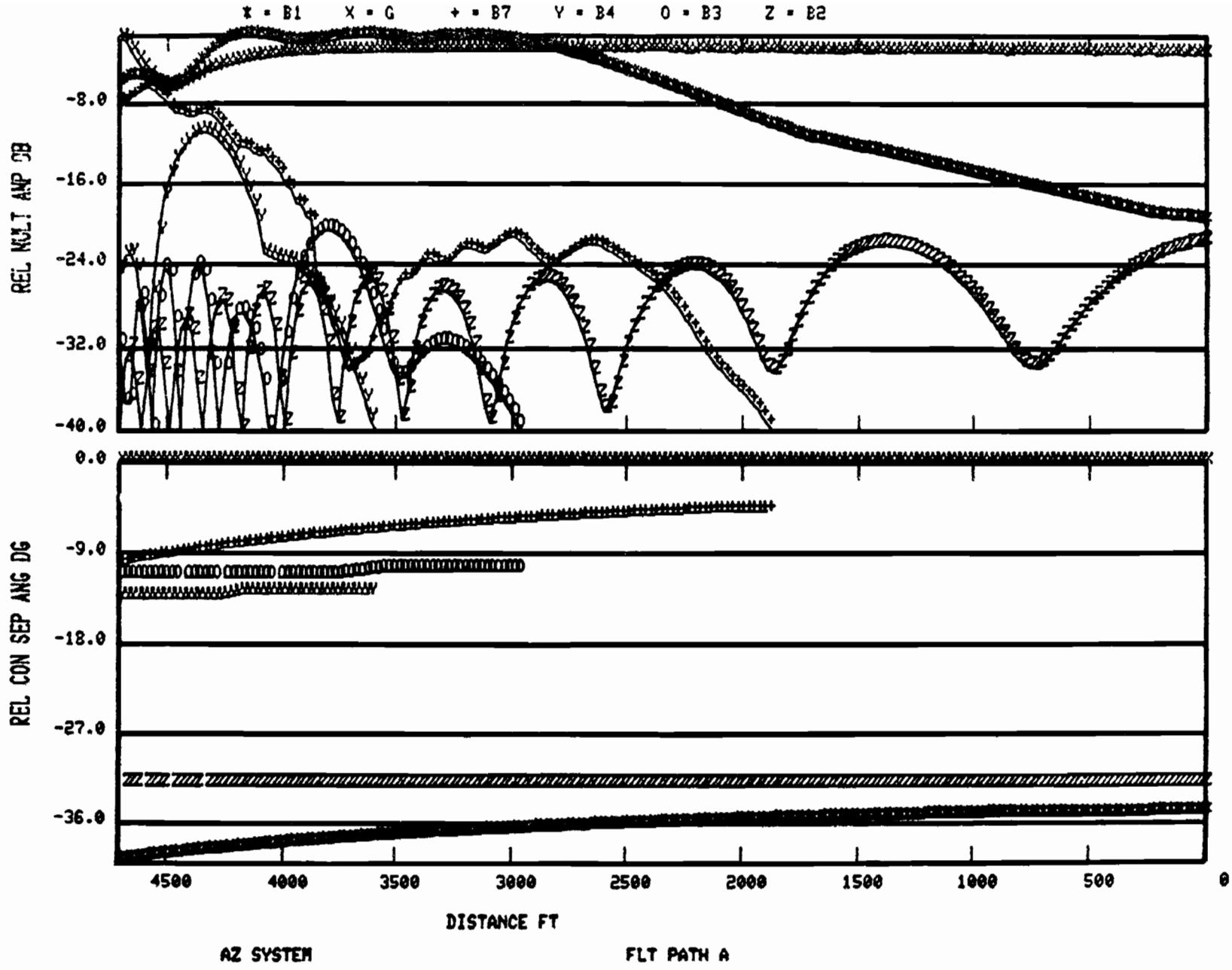

Fig. 2-39. Azimuth multipath characteristics at L-band for scenario 3 with inhomogeneous terrain.

Computer generated maps (rotated 180° relative to Fig. 2-5) for this scenario for C and L band carrier frequencies are illustrated in Figs. 2-40 and 2-41.

Plots of the multipath levels and separation angle for the six largest ranked reflections are presented for elevation for C-band carrier frequency in Fig. 2-42 and elevation for L-band carrier frequency in Fig. 2-43.*

Figs. 2-44 and 2-45 illustrate where edge reflection rays intercept the flight path for the transmitter located at the elevation and flare sites, respectively. In almost all cases of building and aircraft fuselage reflections, the multipath will peak between those two limits and be low elsewhere. Figs. 2-46 and 2-47 show the scalloping frequencies associated with the two principal multipath sources (buildings 1 and 2) for this scenario.

5. Scenario 5

Scenario 5 is based on runway 31R at JFK, a map of which was shown earlier in Fig. 2-4. Only the three buildings which will be instrumental in generating azimuth multipath and shadowing have been retained for this scenario. As before, the coordinate system has as its origin the stop end of the runway (runway 31R and not, as before, 13L) with the positive x axis in the direction of the approach end of the runway. The building positions are given in Table 2-4.

---

*Azimuth and DME characteristics are identical to those of scenario 1 and hence are not shown here.

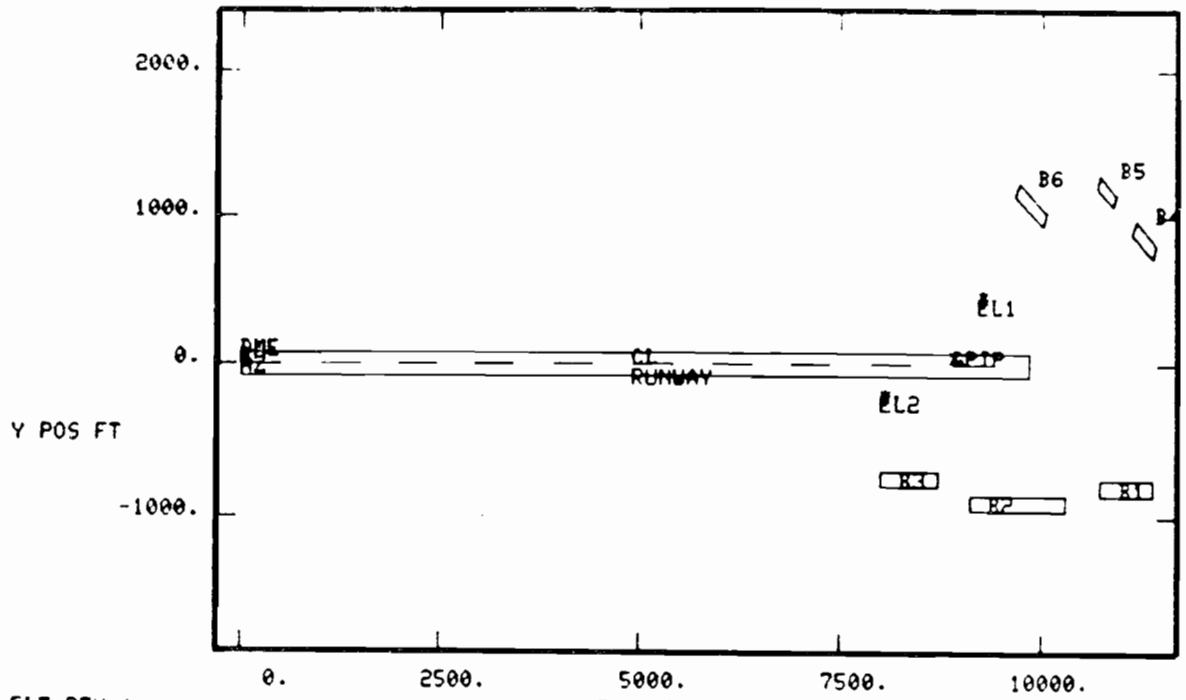

FLT PTH A

AZ SYSTEM

OBST	RANK	AMP	DIST	RDOP
G	1	0	10312.0	0.
B1	7	40	6937.5	-175.
B2	4	27	131.7	-4.
B3	3	27	2151.6	-4.
B4	6	33	7332.7	-749.
B5	5	27	7683.9	-734.
B6	2	16	8649.9	-662.
D	0	80	0.0	0.

EL SYSTEM

OBST	RANK	AMP	DIST	RDOP
G	1	1	9511.7	0.
B1	2	3	7069.2	-203.
B2	4	6	7947.4	-381.
B3	3	4	9186.9	-184.
B4	7	27	7552.2	-911.
B5	6	20	8166.9	-1101.
B6	5	8	9362.5	-1276.
D	0	80	0.0	0.

RANK = multipath ranking

RDOP = relative Doppler (Hz) at point of maximum M/D

AMP = maximum -M/D ratio (dB)

DIST = distance along flight path (ft) at which maximum M/D occurred = 18850 - x pos (ft)

Fig. 2-40. Airport map for scenario 4 (JFK) C-band carrier

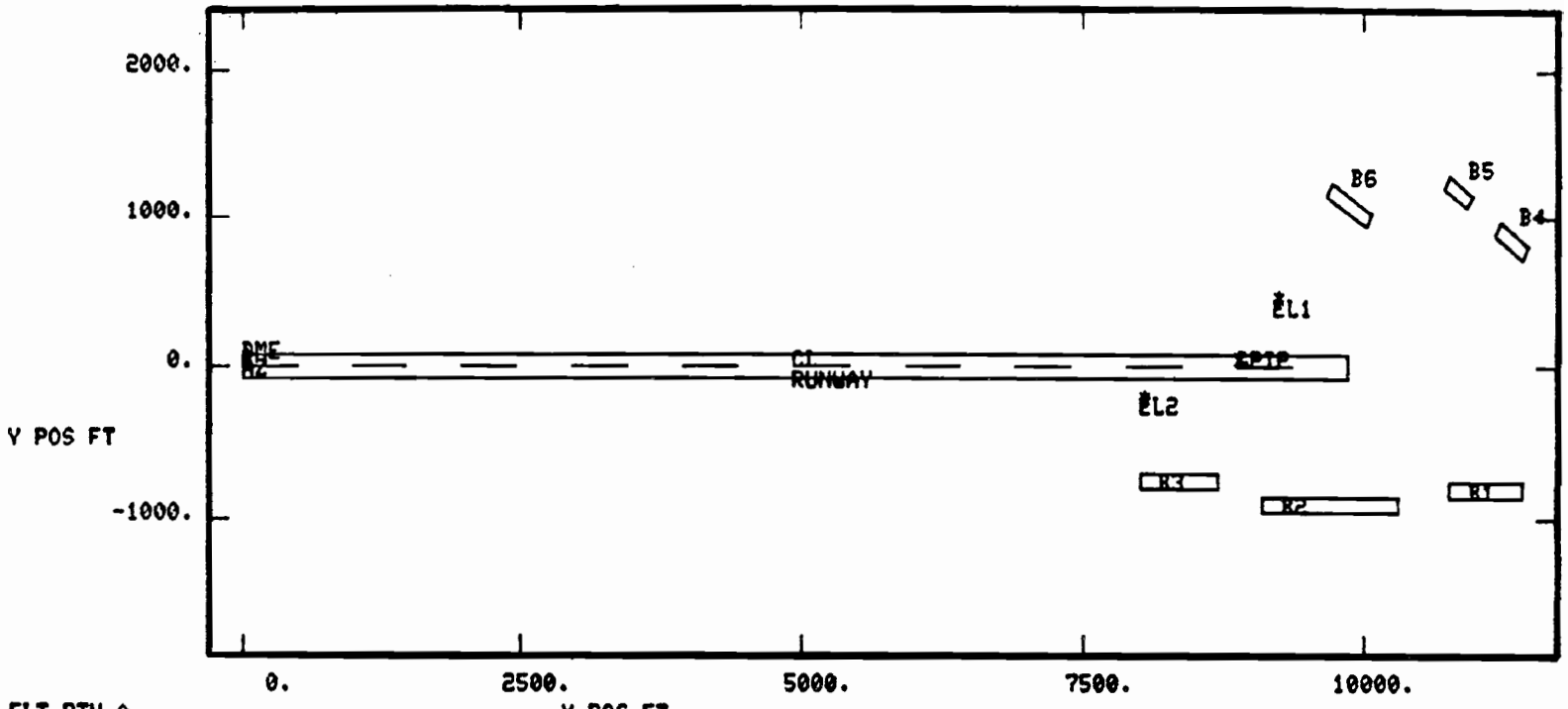

FLT PTH A

AZ SYSTEM

OBST	RANK	AMP	DIST	RDOP
G	1	0	10312.0	0.
B1	7	34	7683.9	-111.
B2	5	25	0.0	-1.
B3	6	26	2371.1	-1.
B4	4	25	7332.7	-148.
B5	3	22	7683.9	-145.
B6	2	11	8649.9	-130.
D	0	80	0.0	0.

EL SYSTEM

OBST	RANK	AMP	DIST	RDOP
G	1	1	9511.7	0.
B1	5	7	7025.3	-39.
B2	3	5	7859.6	-71.
B3	2	3	9230.8	-38.
B4	7	21	7508.3	-176.
B5	6	14	8166.9	-217.
B6	4	7	9186.9	-240.
D	0	80	0.0	0.

RANK = multipath ranking RDOP = relative Doppler (Hz) at point of maximum M/D

AMP = maximum - M/D ratio (dB)

DIST = distance along flight path (ft) at which maximum M/D occurred = 18850 - x pos (ft)

Fig. 2-41. Airport map for scenario 4 (JFK) L-band and carrier.

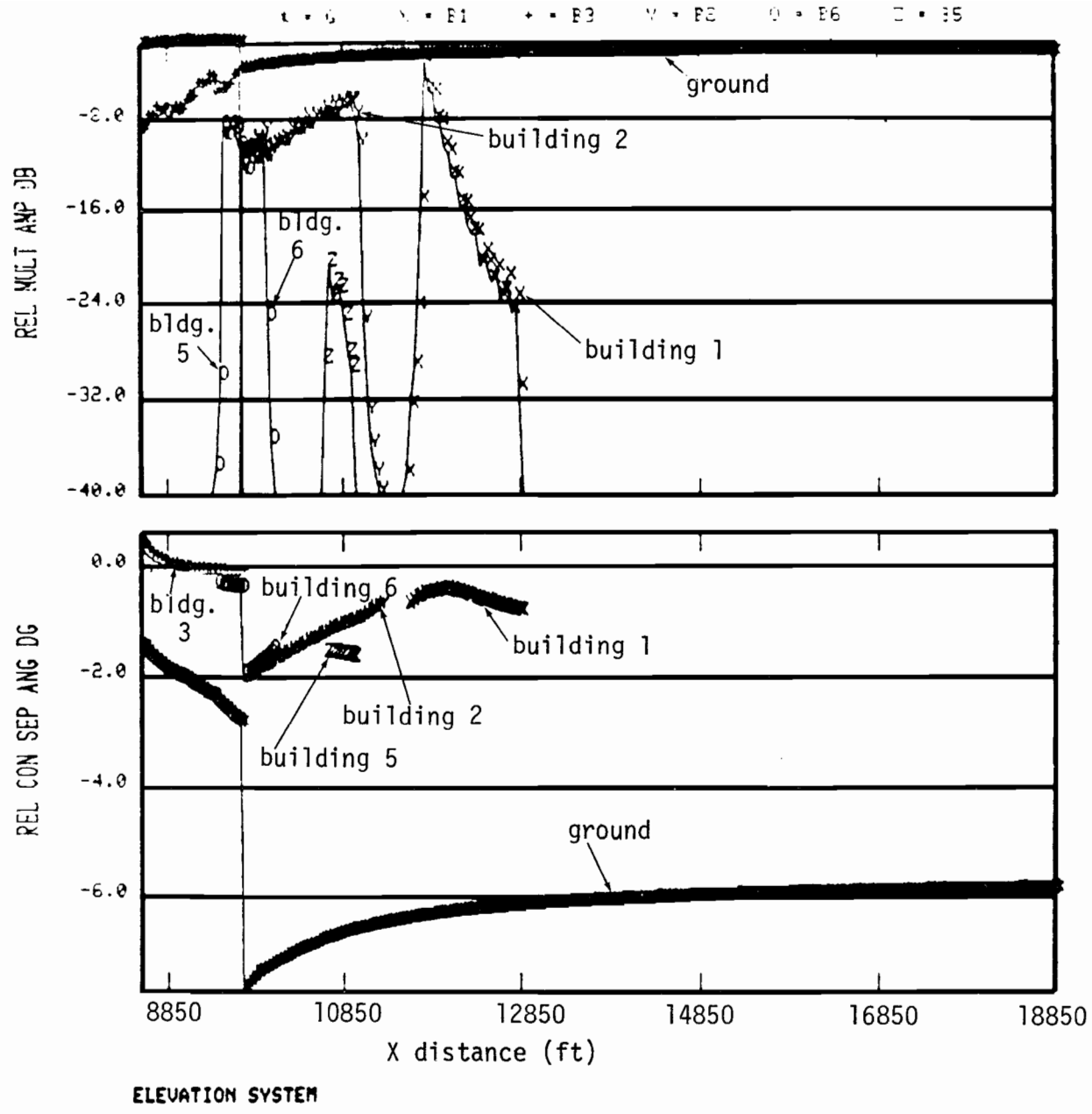

Fig. 2-42. Elevation multipath and separation angle for scenario 4 (JFK) for C-band.

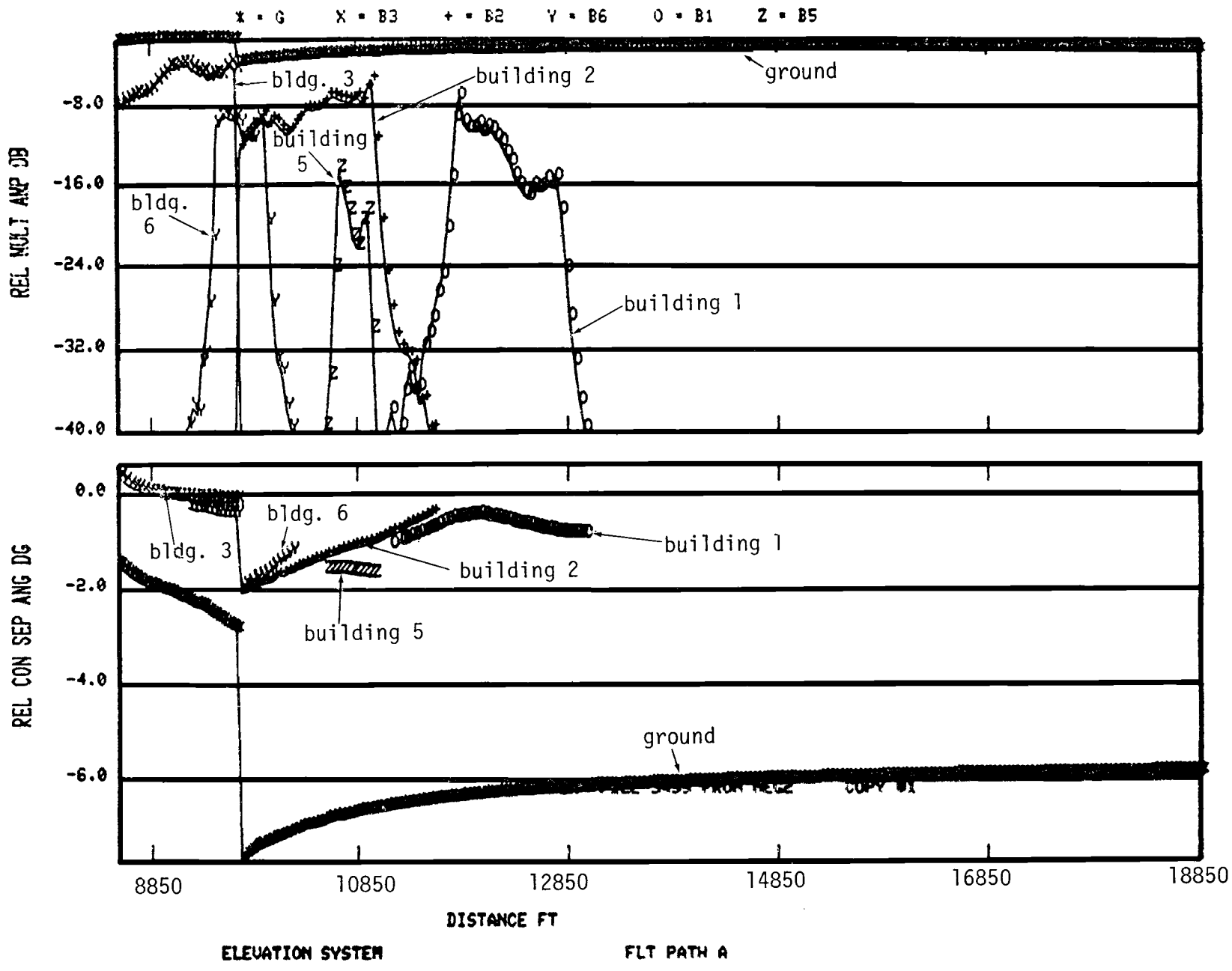

Fig. 2-43. Elevation multipath and separation angle for scenario 4 (JFK) L-band.

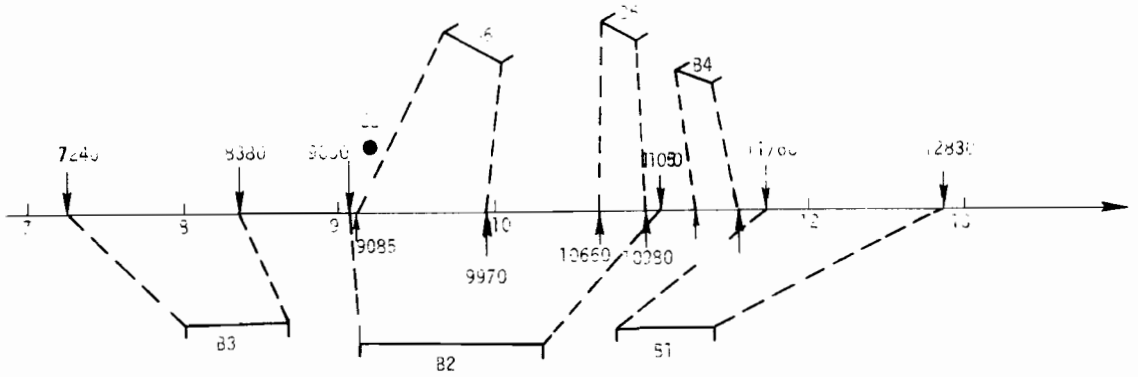

Fig. 2-44. JFK with edge reflection rays in horizontal plane for alternate EL position.

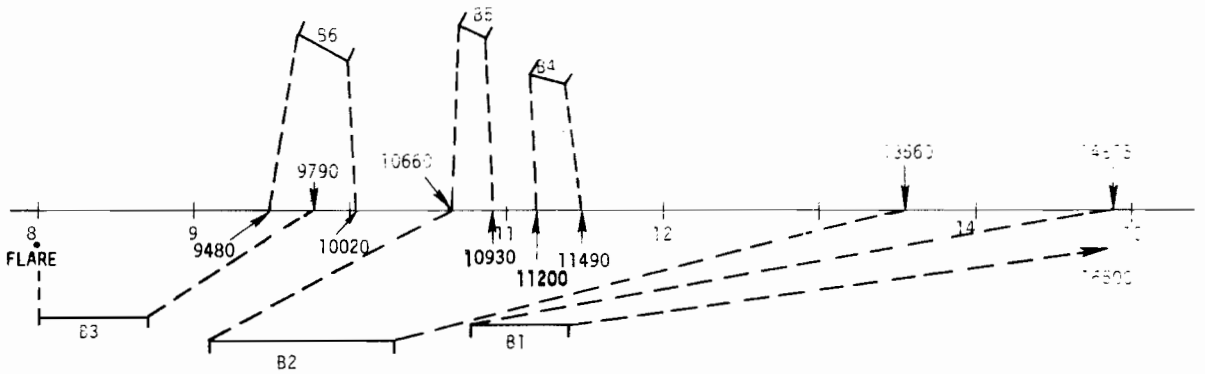

Fig. 2-45. JFK with edge reflection rays in the horizontal plane for flare in alternate position.

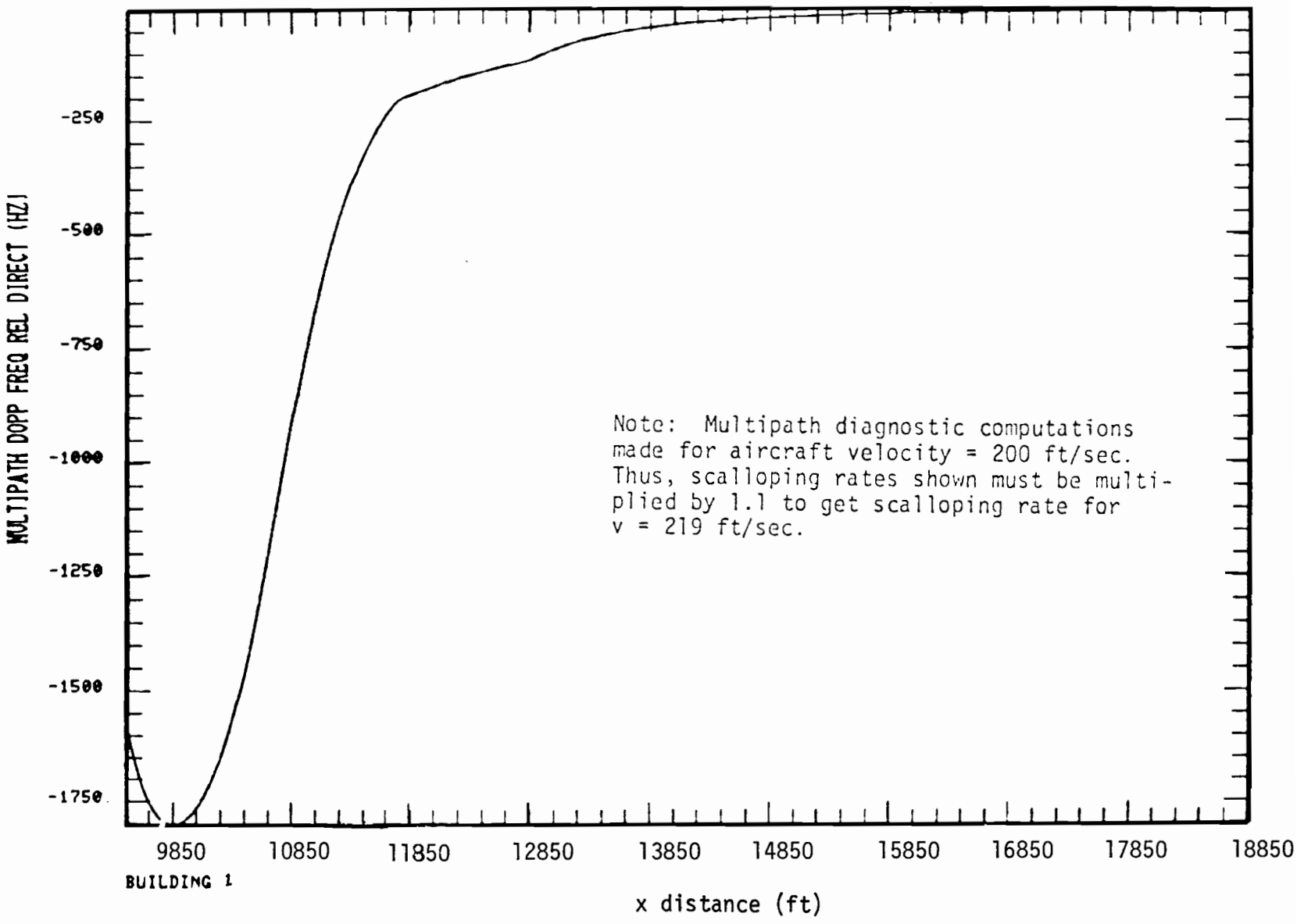

Fig. 2-46. Scalloping frequency along flight path for scenario 4, EL transmitter, Building 1.

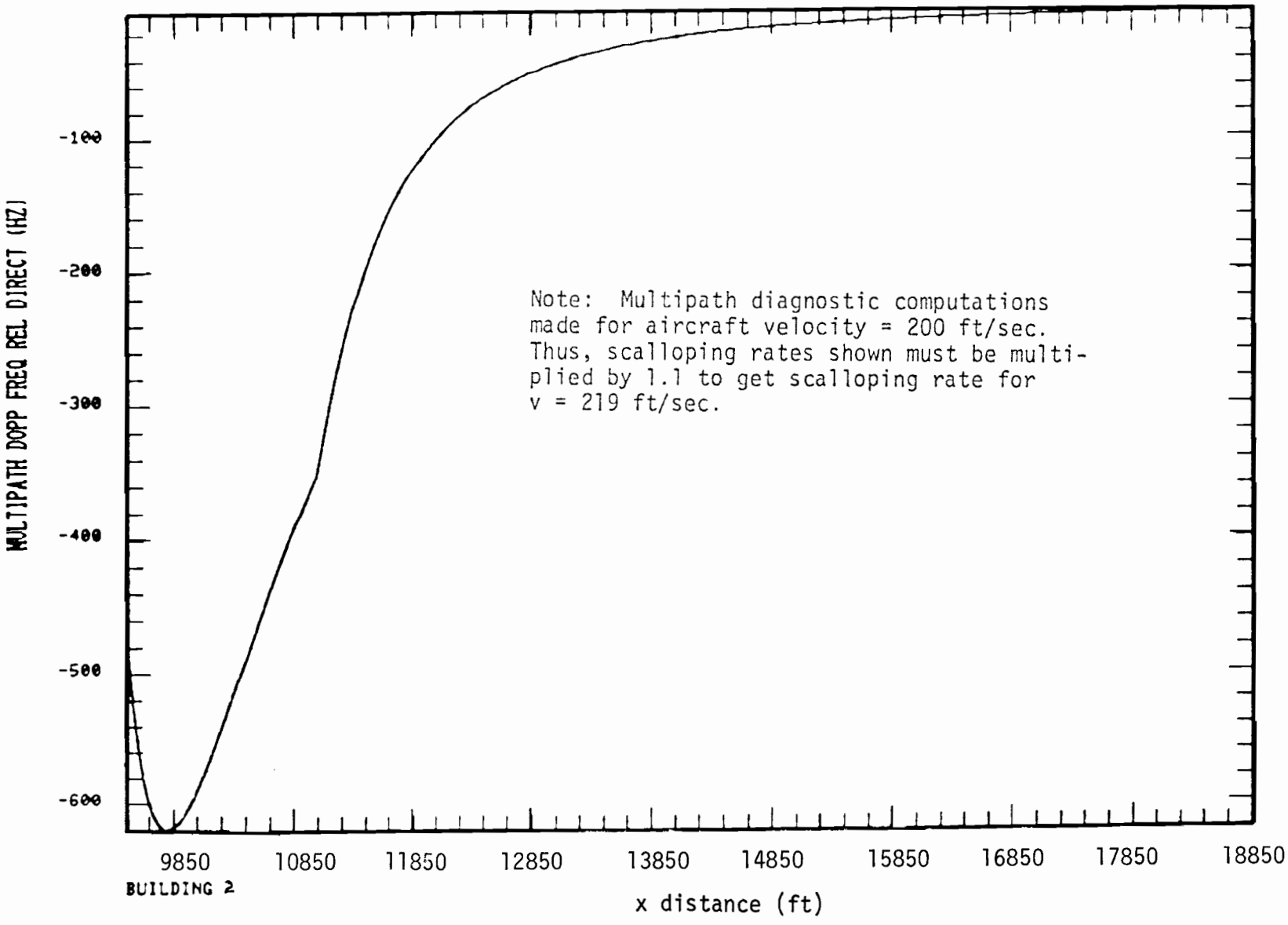

Fig. 2-47. Scalloping frequency along flight path for scenario 4, EL transmitter, Building 2.

TABLE 2-4

BUILDING LOCATIONS FOR SCENARIO 5

	Building Coordinates		Height (ft)
B1.	(-400, +750)	(250, +750)	100
B2.	(700, +850)	(1900, +850)	100
B3.	(2300, +700)	(3000, +700)	50

Origin at stop-end of runway
GPIP at (9000,0,0)
Azimuth Transmitter at (-1000,0,6)
Elevation Transmitter at (9200, -400,13)
Flare Transmitter at (7200,-400,13)
DME Transmitter at (-1000,0,6)

Flight Profile

(25000,-22000,1200) to (25000,-5000,1200) for reflection portion
(25000,0,2000) to (25000,22000,2000) for shadowing portion

Computer generated maps for the reflection portion of this scenario for C and L band carrier frequencies are illustrated in Figs. 2-48 and 2-49, together with peak multipath levels and the x distance at which the peak occurred. As before, omnidirectional antennas are assumed for these multipath calculations.

Plots of the computed multipath levels are presented in Fig. 2-50 for C-band azimuth and in Figs. 2-51 and 2-52 for L-band azimuth and DME*. Fig 2-53 illustrates when edge reflection rays intercept the flight path for the azimuth transmitter.

Fig 2-54 illustrates the C-band azimuth shadowing loss on the shadowing portion of the scenario while Fig. 2-55 shows the L-band azimuth shadowing loss. The azimuth shadowing loss plotted is the amplitude of the direct signal coded component which corresponds to the direct signal when the line of sight is not blocked. It should be noted that there is also a shadowed ground reflection with direct signal code which is combined with the plotted direct signal component in computing the system errors.

The small perturbation at y = 5000 feet is due to edge rays from the top of building 3. Similarly, the perturbation between y = 7500 and 13000 is due to edge rays from the top of building 2. In both cases, the LOS is not blocked so that fairly small signal losses occur.

---

*Elevation multipath characteristic plots are not shown since no elevation building multipath or shadowing arises in this scenario.

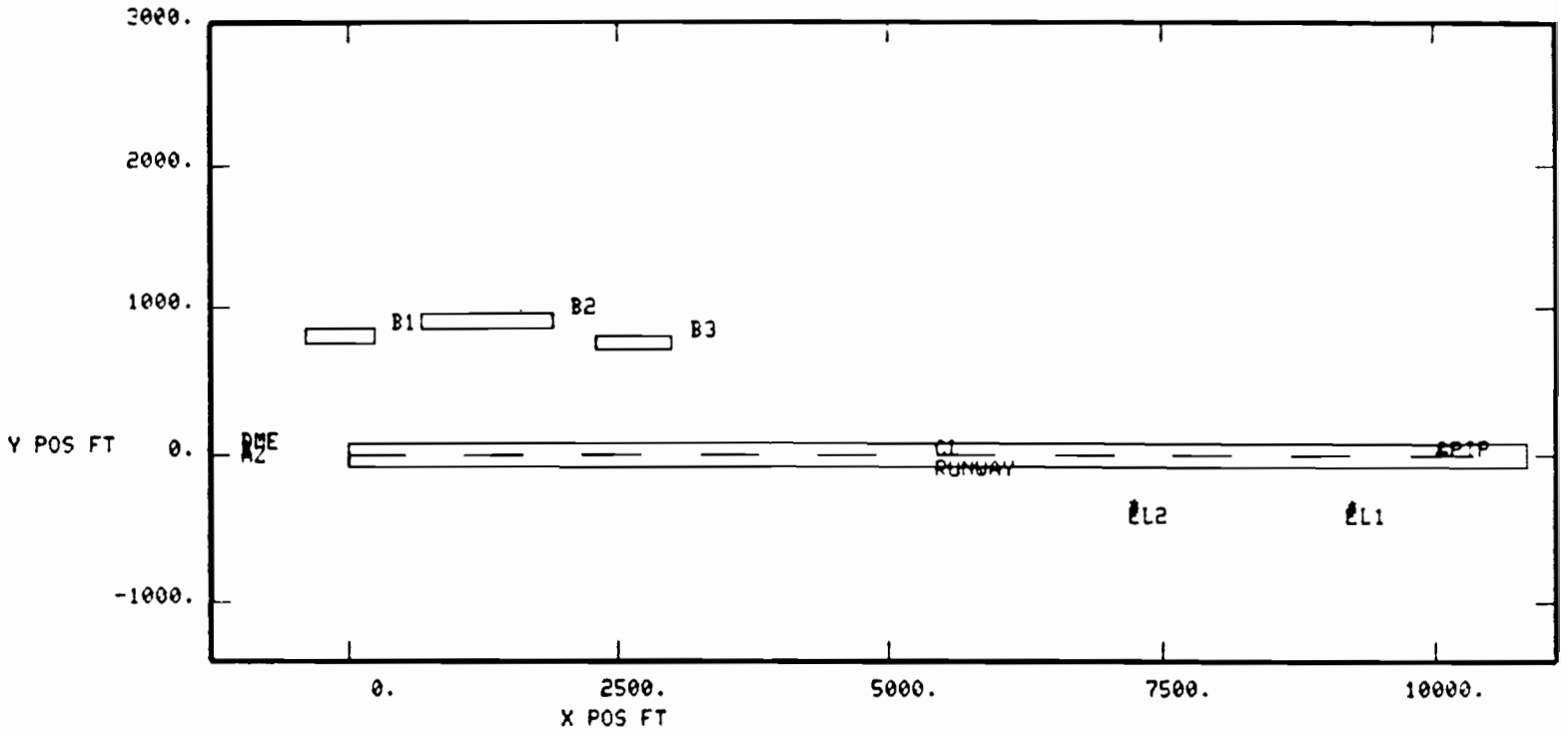

AZ SYSTEM

OBST	RANK	AMP	DIST	RDOP
G	1	-3	432.0	-0.
B1	3	1	7560.0	51.
B2	2	0	10962.0	67.
B3	4	52	4536.0	92.
D	0	80	0.0	0.

EL SYSTEM

OBST	RANK	AMP	DIST	RDOP
G	1	1	432.0	-0.
B1	3	65	5562.0	-194.
B2	2	64	3186.0	-151.
B3	4	80	270.0	-122.
D	0	80	0.0	0.

RANK = multipath ranking

AMP = maximum -M/D ratio (dB)

RDOP = relative Doppler (Hz) at point of maximum M/D

DIST = distance along flight path (ft) at which maximum M/D occurred = 22000 - y pos (ft)

Fig. 2-48. Airport map for scenario 5 (JFK, curved approach), C-band carrier.

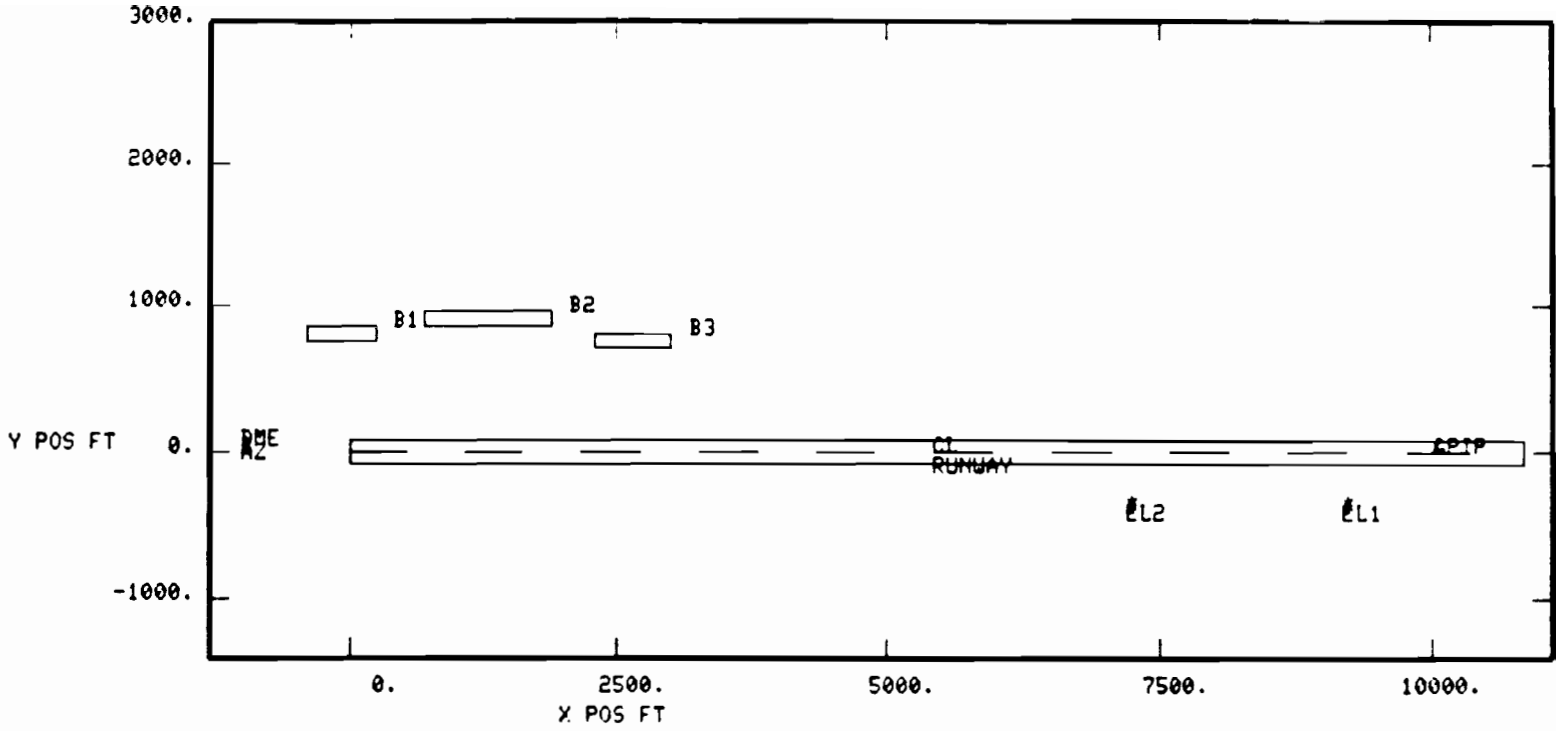

AZ SYSTEM

OBST	RANK	AMP	DIST	RDOP
G	1	0	16956.0	-0.
B1	2	0	7182.0	10.
B2	3	3	11232.0	13.
B3	4	47	15012.0	17.
D	0	80	0.0	0.

EL SYSTEM

OBST	RANK	AMP	DIST	RDOP
G	1	-2	648.0	-0.
B1	3	59	3078.0	-37.
B2	2	58	1998.0	-29.
B3	4	70	0.0	-24.
D	0	80	0.0	0.

RANK = multipath ranking

RDOP = relative Doppler (Hz) at point of maximum M/D

AMP = maximum -M/D ratio (dB)

DIST = distance along flight path (ft) at which maximum M/D occurred = 22000 -y pos (ft)

Fig. 2-49. Airport map for scenario 5 (JFK curved approach), L-band.

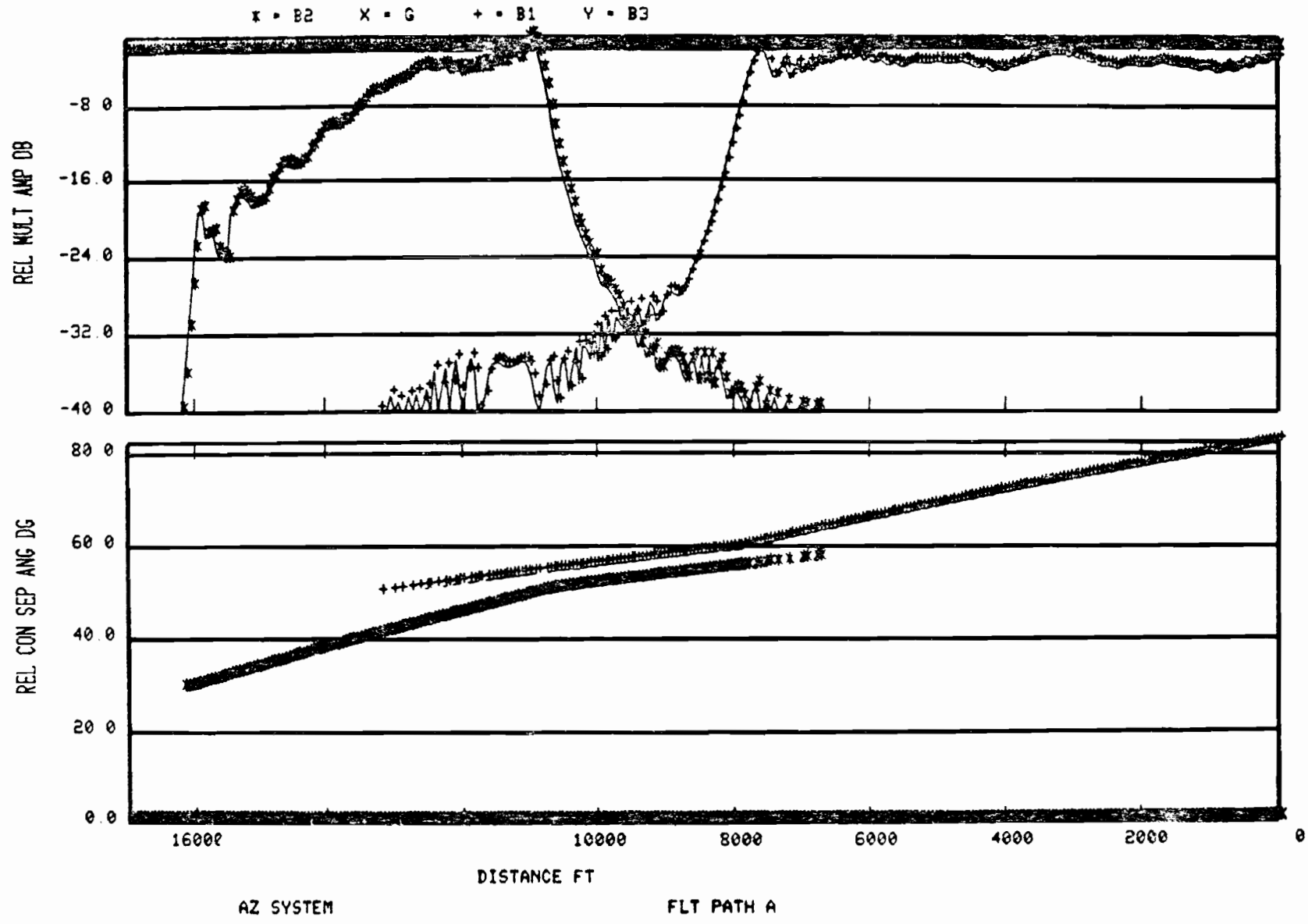

Fig. 2-50. Azimuth multipath and separation angle for scenario 5 (JFK curved approach) for C-band.

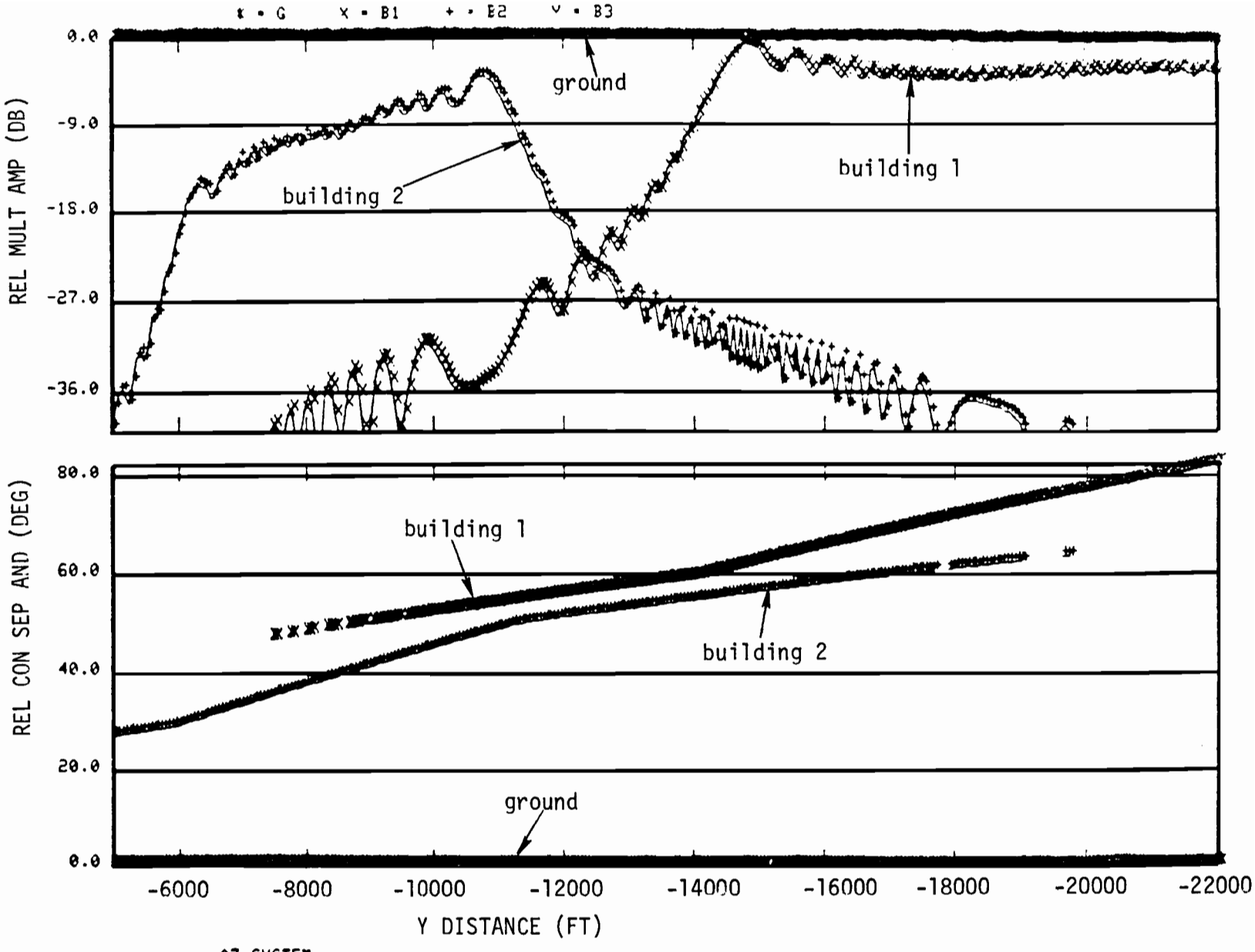

Fig. 2-51. Azimuth multipath and separation angle for scenario 5 (JFK curved approach), L-band.

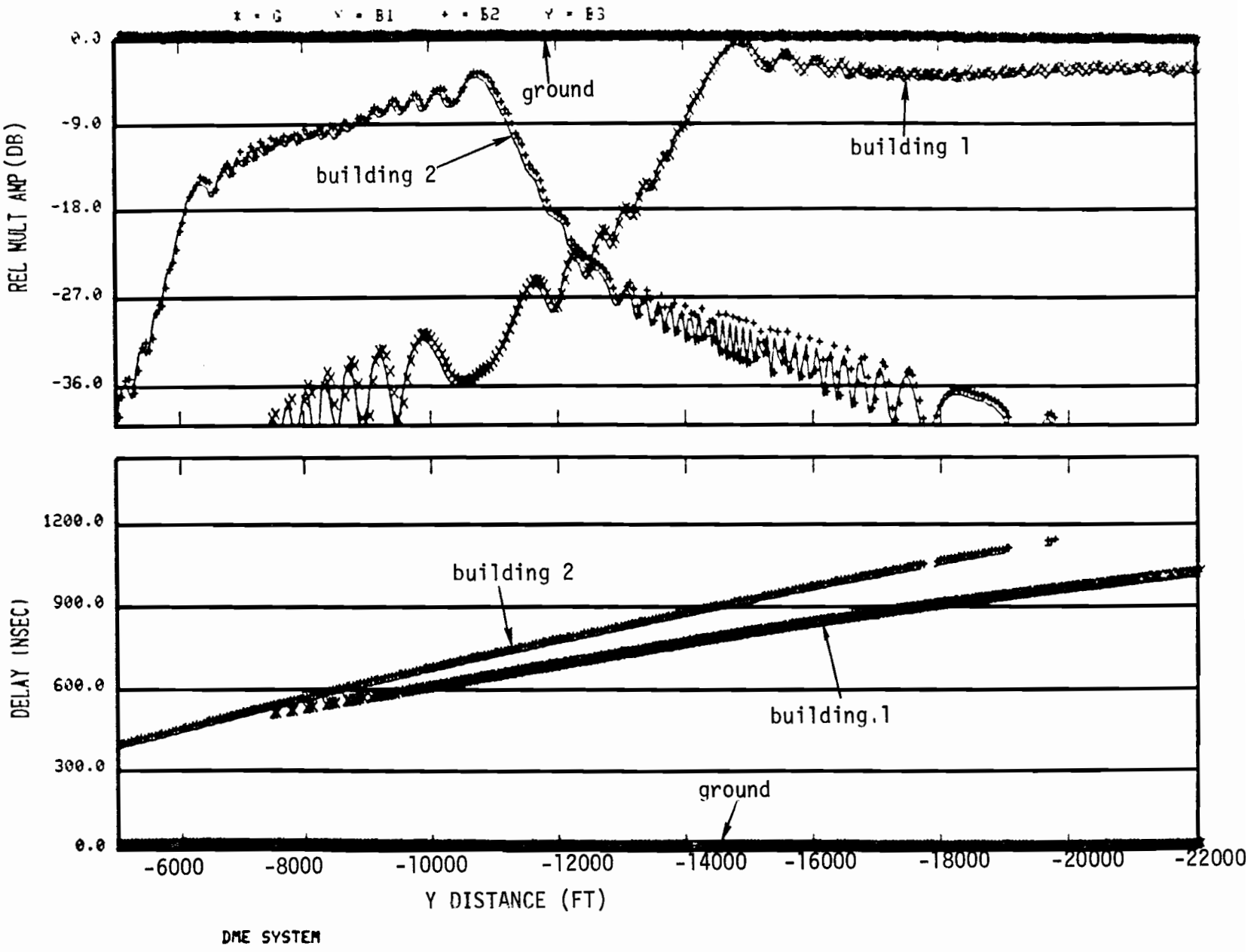

Fig. 2-52. DME multipath and delay for scenario 5 (JFK, curved approach), L-band.

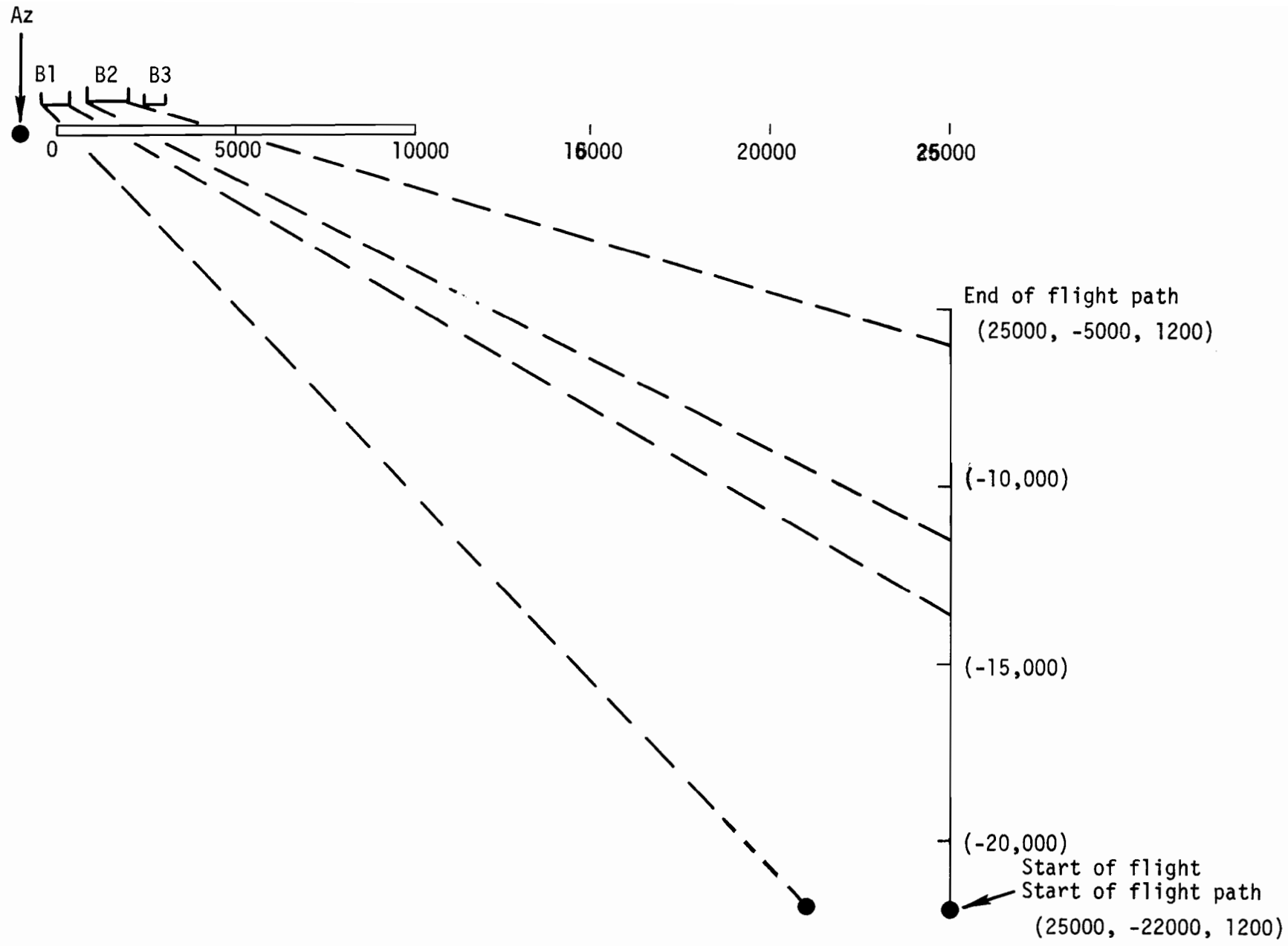

Fig. 2-53. JFK (Runway 31R) with edge reflection rays in horizontal plane for Az transmitter.

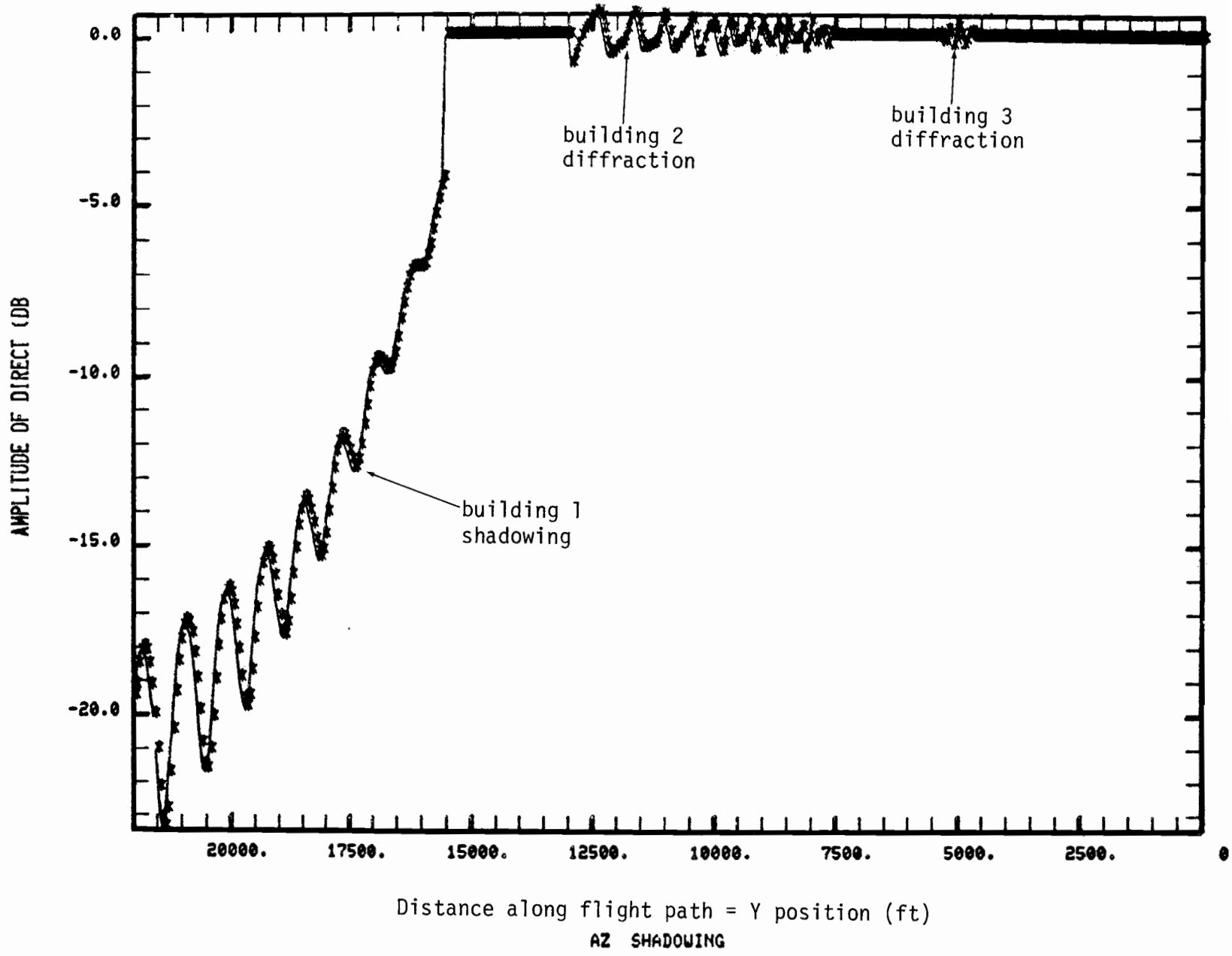

Fig. 2-54. C-band azimuth shadowing loss for shadowing portion of scenario 5.

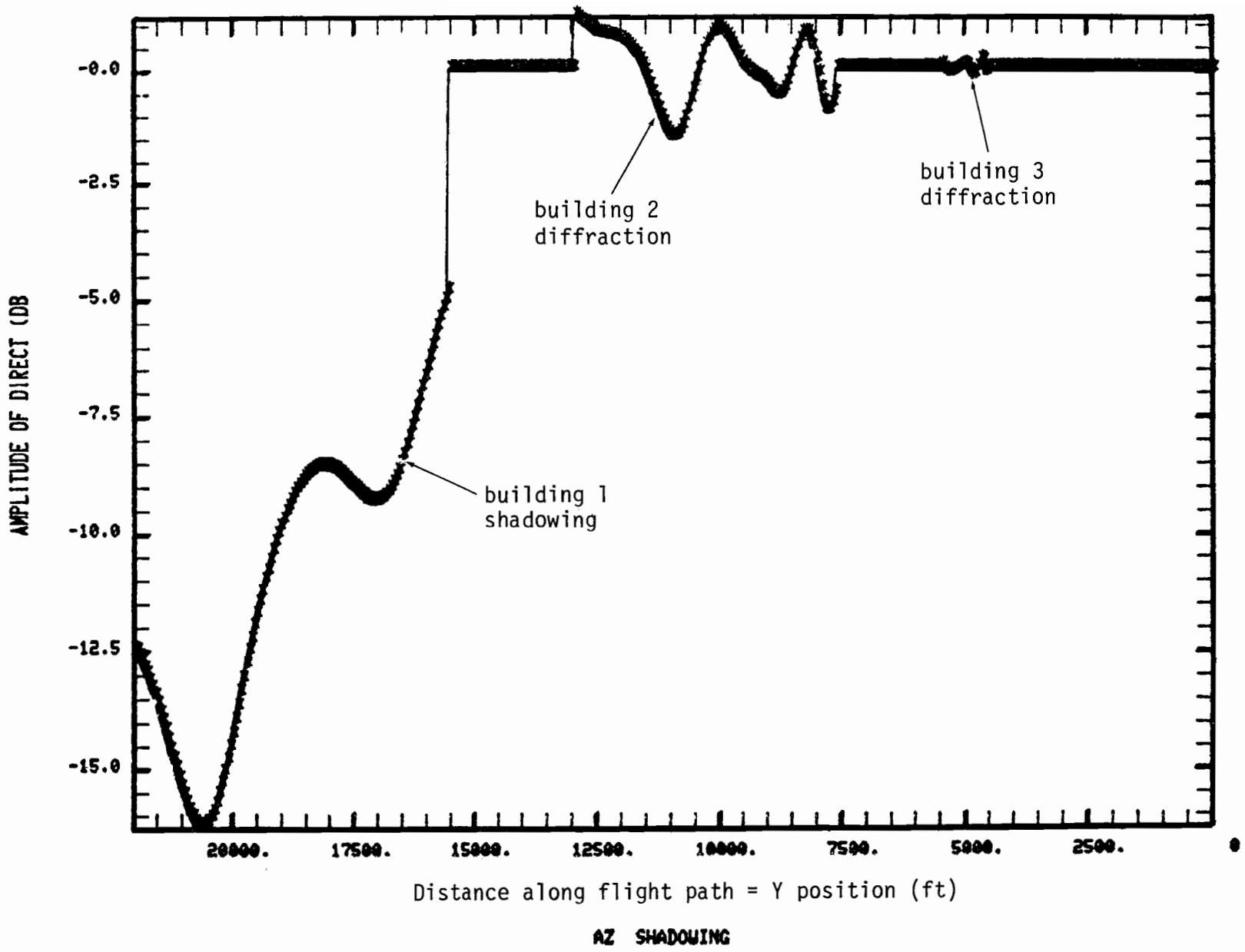

Fig. 2-55. L-band azimuth shadowing loss for shadowing portion of scenario 5.

6. Scenarios 6-8

Scenarios 6-8 were nearly identical to scenario 1 except for the sinusoidal variation introduced in the flight path and a slightly lower flight path. Fig 2-56 compares the flight path x,z coordinates with those of scenario 1.

These variations may have a noticeable effect on the system angle errors since scalloping frequencies and therefore motion averaging will be affected. The multipath plots were essentially identical to those of scenario 1, and therefore will not be shown here.

C. System Error Results

In this section, we present the computed errors for the various AWOP scenarios using the simulation models discussed in volume II of this report. The bulk of the simulation results pertain to the "most capable" system of each proposer. This highly capable system uses "any fully defined and costed features on the list of system features related to multipath protection for azimuth, elevation and flare functions." Simulation results for a "cost reduced 'basic' system proposed for normal sites for azimuth only" are shown for several of the azimuth multipath scenarios.

It was noted that some differences between TRSB and DMLS azimuth results might arise from the differences in the proposed elevation pattern of the azimuth arrays (the TRSB pattern, based on measured field data, rolls off nearly twice as fast at the horizon as does the proposed DMLS pattern). Since identical azimuth column radiator elements were assumed for the DMLS and TRSB arrays in the WG-A costing, one DMLS simulation was repeated using the azimuth antenna with the TRSB elevation pattern rolloff.

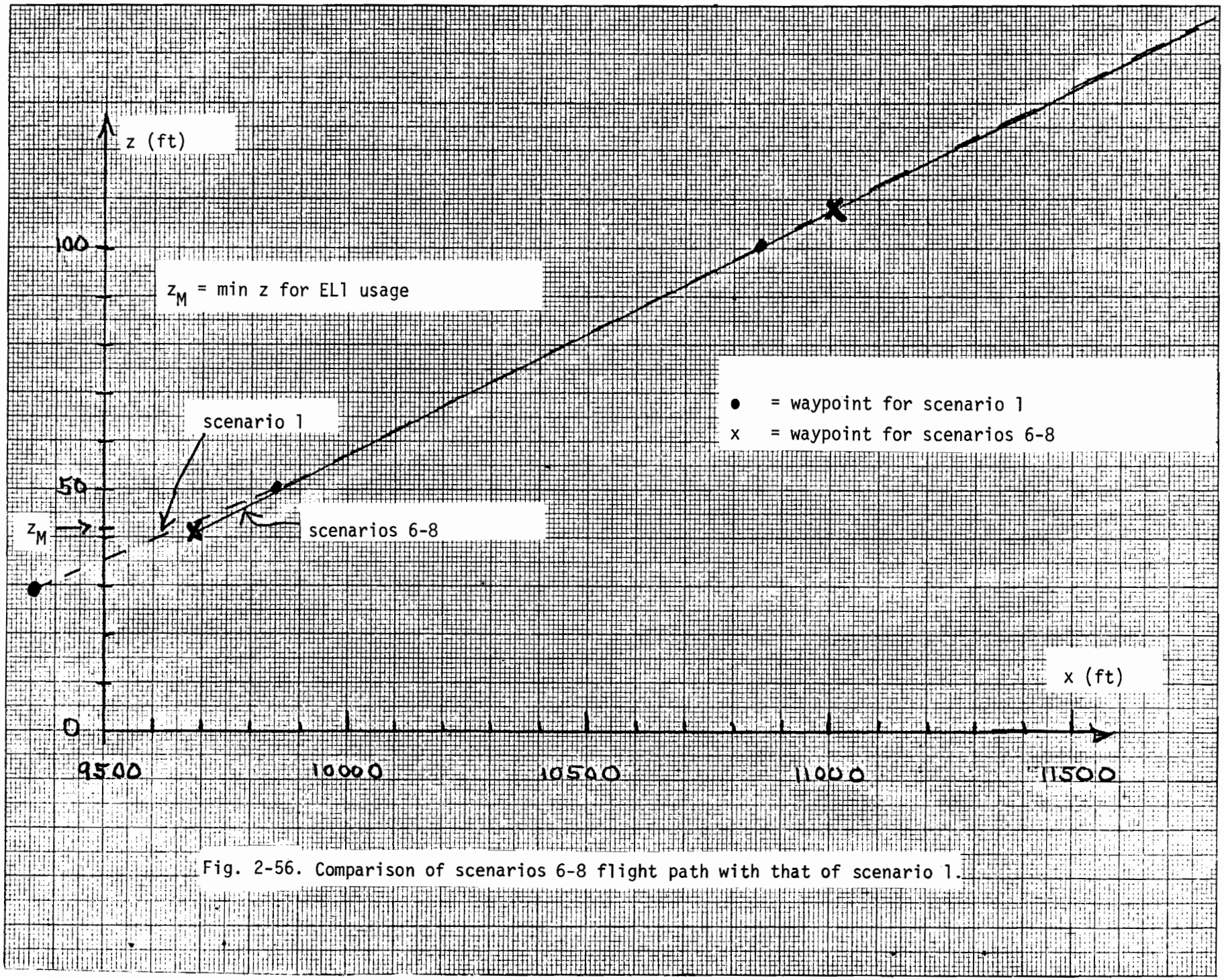

Fig. 2-56. Comparison of scenarios 6-8 flight path with that of scenario 1.

The bulk of results presented in this report consist of raw error waveforms although in some cases we also present path following error, control motion noise and rate noise waveforms. These latter three waveforms were derived by processing the raw error trace through the filters described in [72].

It had originally been planned (see Appendix C of [111]) that results for each system would be annotated by the proposing state to show contribution of each multipath combatting feature to the overall multipath protection before the results were circulated to the panel members. However, due to the late changes in system features, it was not practically possible to have these results annotated in the initially planned manner.

However, we still feel that some discussion of the salient features of the results is necessary to make the results understandable. For this purpose, the results are annotated with three types of comments/analyses:

(1) a general indication of the type of multipath present at various portions of the flight path, i.e., "in beam' or "out of beam,"

(2) comparative results for the dynamic error versus the error on single scans (or interrogations) so as to provide insight into motion averaging and/or receiver data rejection features, and

(3) discussion of the error mechanism for errors which exceed a guideline similar to that used in assessing "basic accuracy" field data.

The concepts of "in beam" and "out of beam" have proved useful in the MLS multipath discussions. However, confusion has arisen due to the two different usages of the phrase "out of beam":

(a) Rayleigh criterion [112]:

Direct signal and multipath rays have an angular separation in the scanned coordinate $\geq$ k beamwidths, i.e.,

$$\theta_{sep} \geq k/(L/\lambda) \qquad (2\text{-}1)$$

where k is a number between 1 and 2 and L/λ is the antenna aperture in wavelengths.

(b) MLS processor criterion:

The error due to multipath becomes insignificant for "reasonable" multipath levels. Also, the direct and multipath received signal components have angle code separations meeting criterion (2-1).

In our annotation, we have used the Rayleigh criterion with k = 1.5 since it is applicable independent of processor, thus bypassing any differences that arise between the various MLS processors with respect to criterion (b). For several systems, the criteria coincide under quasi-static conditions.

The relative efficacy of motion averaging for the various systems was discussed extensively (see, e.g., B.WP/7, B-BIP/5, B-BIP/9 in [113]; W.WP/35, W.WP/40, W.WP/45, W-BIP/1, W-BIP/15, W-BIP/16 in [111]; TH.WP/2, TH-BIP/1, TH-BIP/13 in [114]). Additionally, the various aircraft receivers have logic to reject "obviously bad" data. Since both these features play an important role in the overall system performance, we find it useful to display the error that would have occurred had only a single measurement (i.e., scan or interrogation) been made in a 0.2 second period and no output data consistency tests applied.

There was no clear WG-A consensus as to quantitative criteria for what constitutes an "unacceptable" MLS multipath error. Nor is there any intention to propose such a standard in this report. However, we have had to make a

decision as to the level of detail at which we discuss the various multipath errors that do occur. The rule we have used is to comment on:

(a) azimuth errors which are greater than 0.05°

and

(b) elevation errors which are greater than 0.07°.

In any case where displayed errors which reach those limits are not multipath related,* explanatory comments are made.

1. Results for Scenario 1

The results for scenario 1 with a terrain dielectric constant $\varepsilon/\varepsilon_o = 1.2$ are shown in Figs. 2-57 to 2-63. The azimuth errors are in all cases very small as expected since the azimuth multipath at nonzero separation angles was quite small as well as out of beam.

The elevation multipath diagnostics for this scenario show that multipath from two buildings is of substantial amplitude and inbeam. Consequently, it is not surprising that elevation errors arise. Figs 2-59 and 2-60 show that all three systems were able to substantially reduce their errors by motion averaging.

A principal factor causing DLS elevation error to be larger that that of the other two systems is the smaller aperture. The multipath diagnostics show that the multipath separation angle gets fairly large as the aircraft nears the threshold. Plots of elevation error as a function of separation angle (see volume II of this report) show the DLS error is larger than the other two systems at large separation angles (e.g., 1.5°); consequently, large errors may be expected here.

---

*e.g., due to receiver lags, etc.

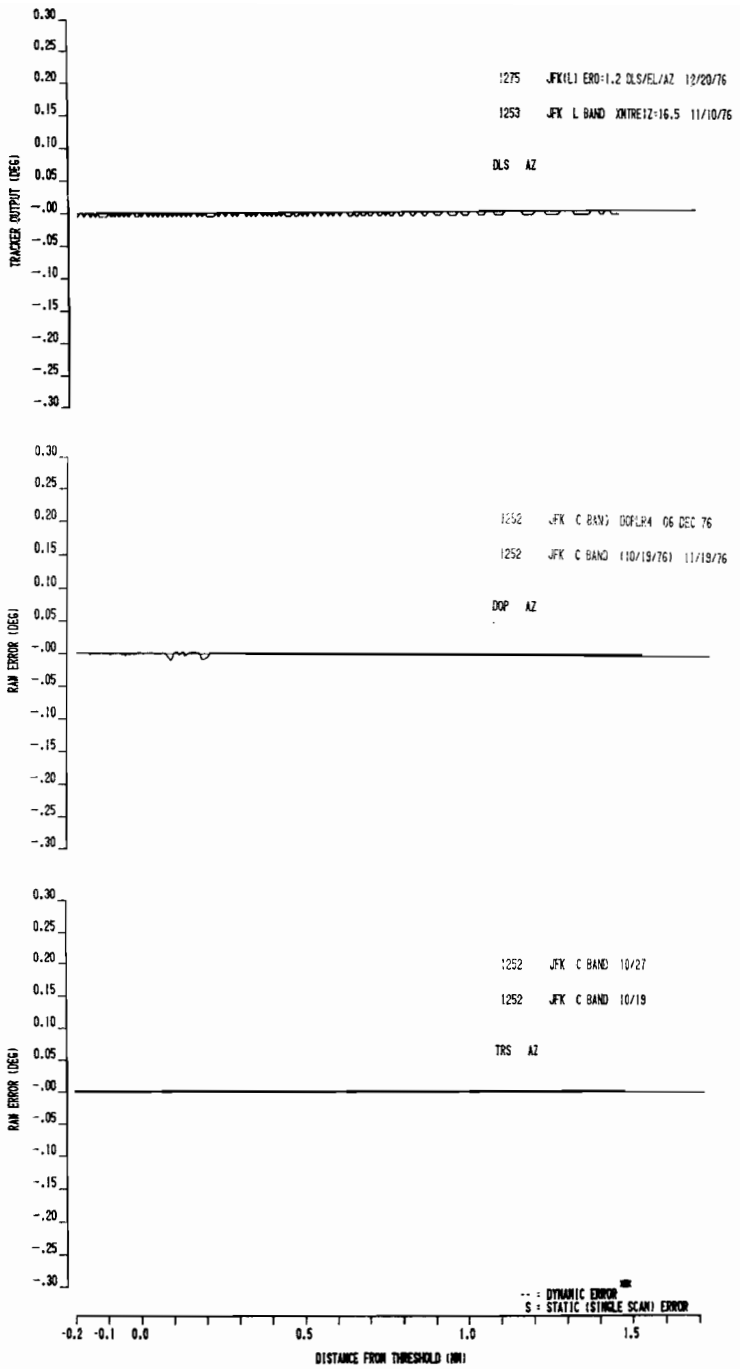

Fig. 2-57. Dynamic azimuth errors for scenario 1.

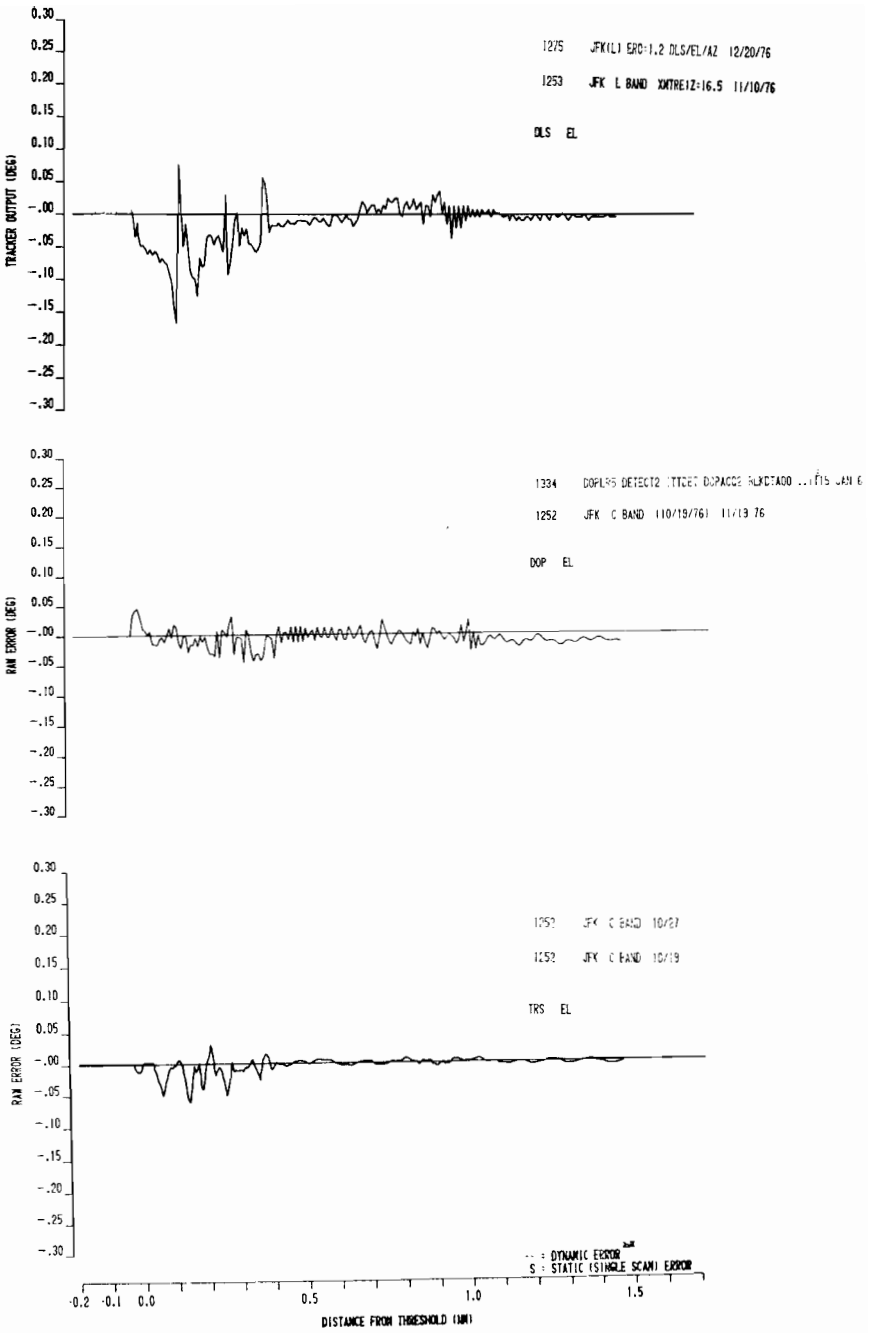

Fig. 2-58. Dynamic elevation errors for scenario 1.

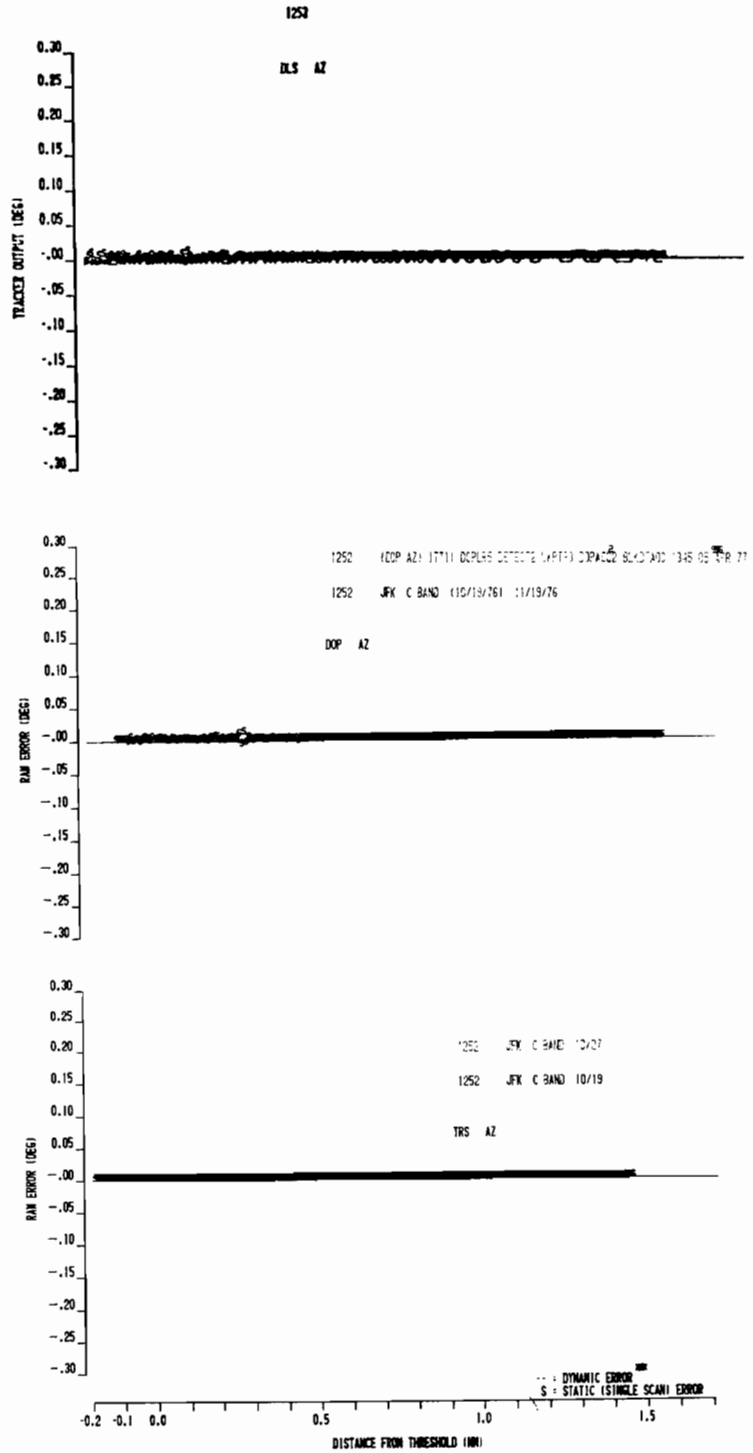

Fig. 2-59. Dynamic and single-scan azimuth errors for scenario 1.

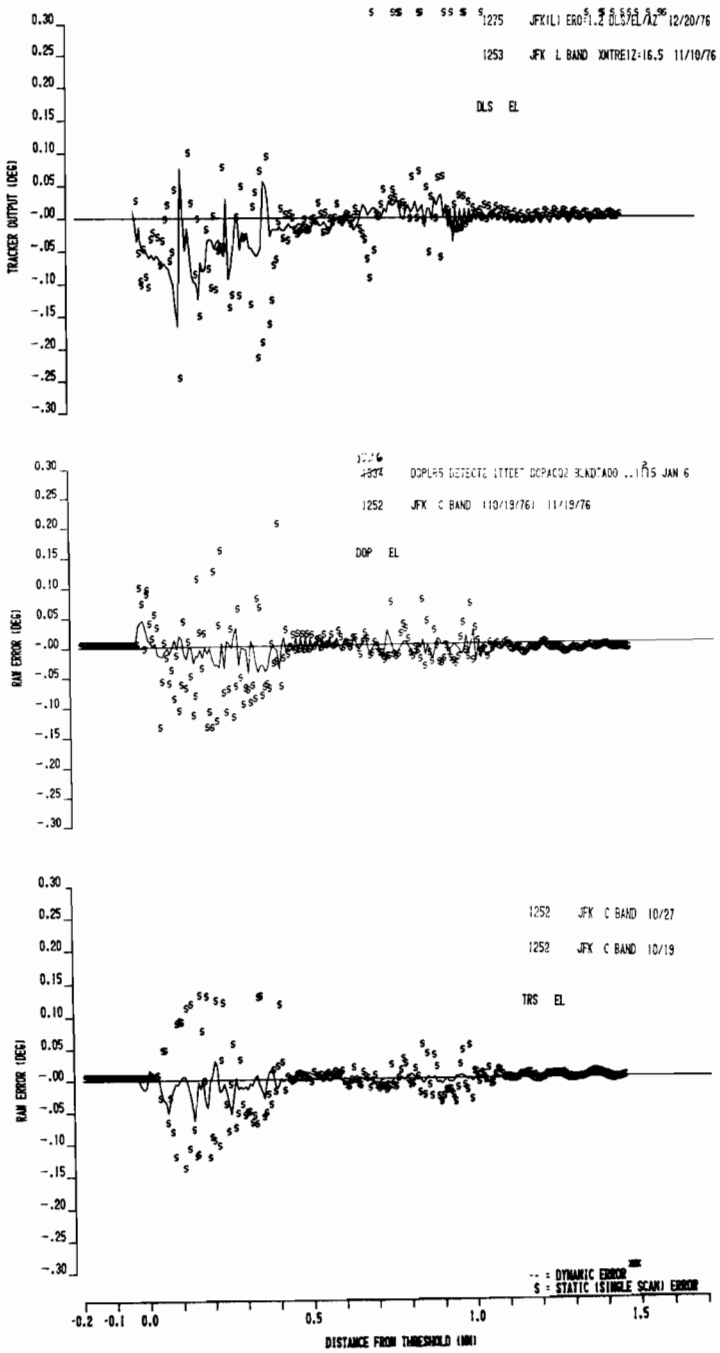

Fig. 2-60. Dynamic and single-scan elevation errors for scenario 1.

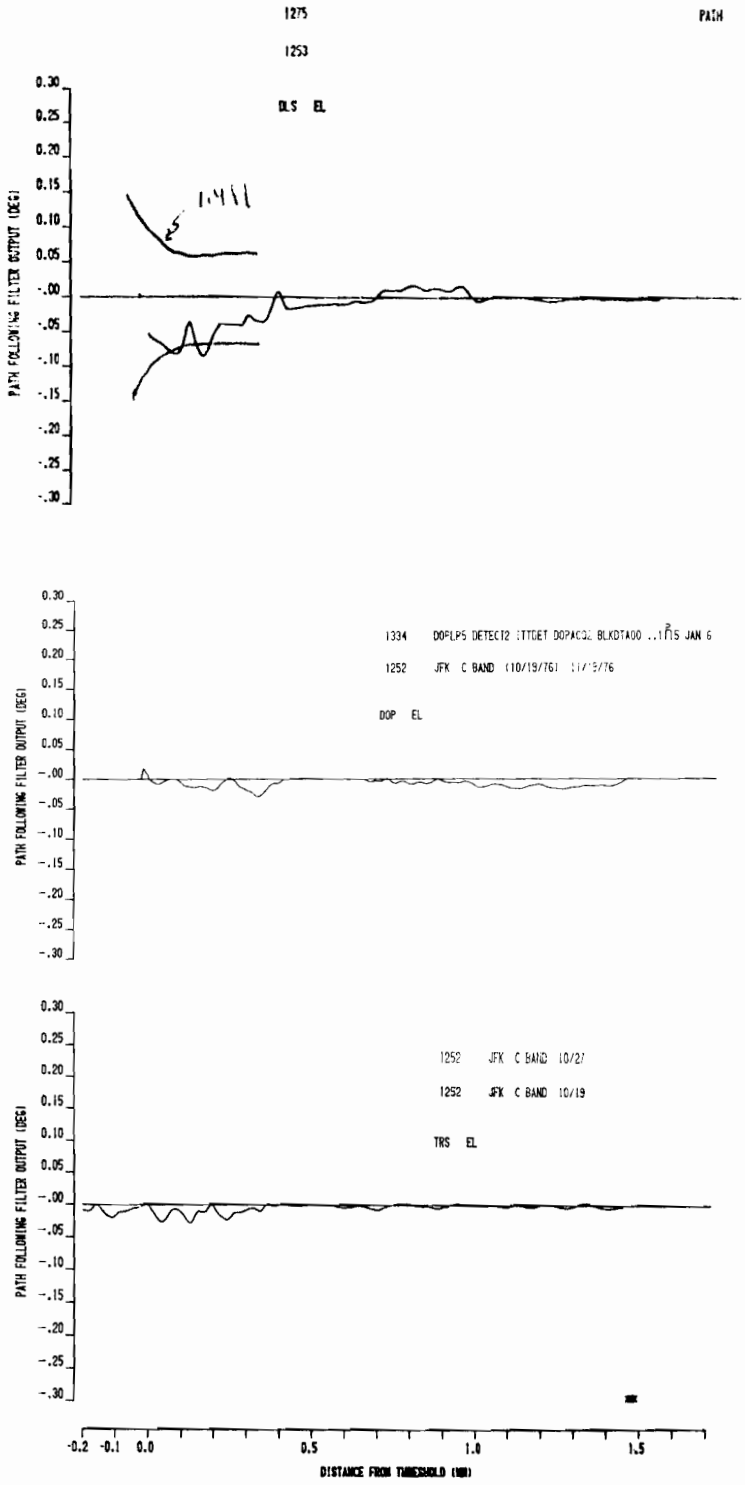

Fig. 2-61. Elevation path following filter output for scenario 1.

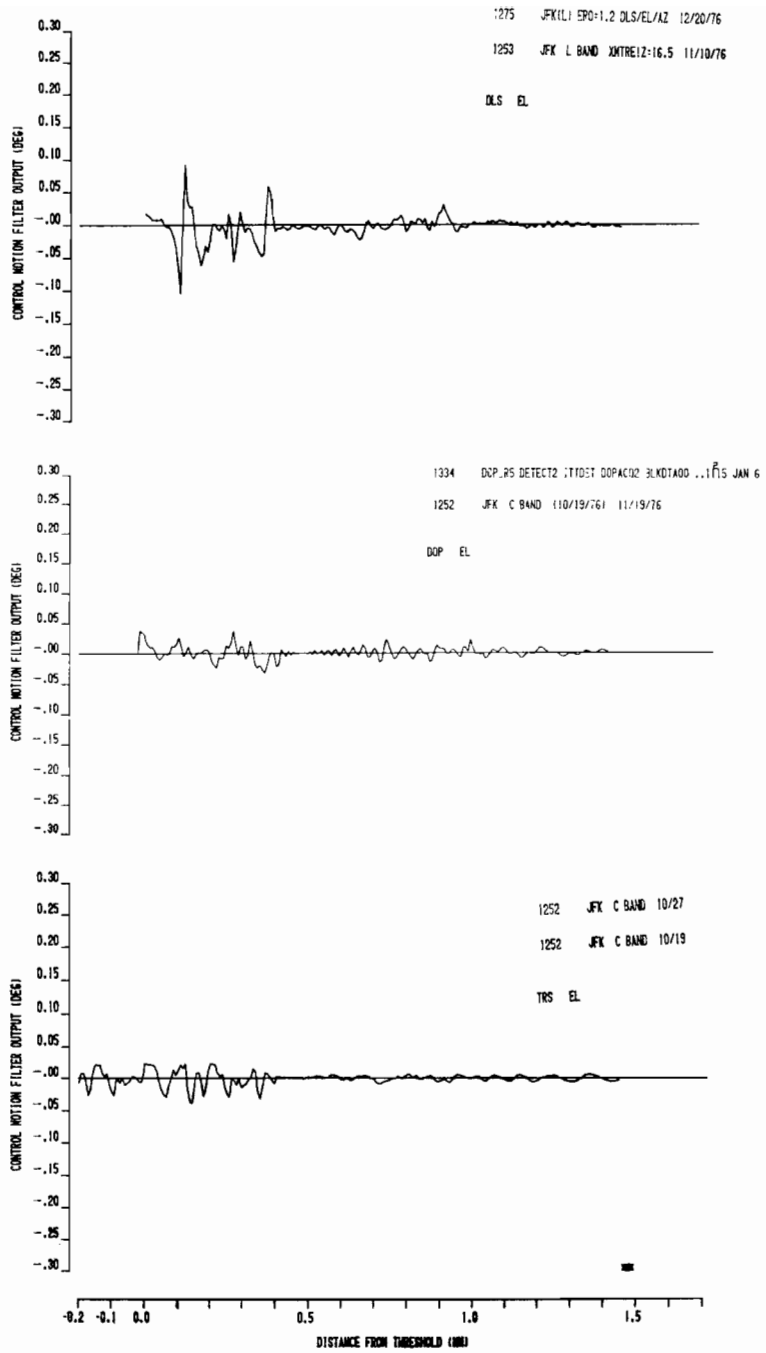

Fig. 2-62. Elevation control motion filter output for scenario 1.

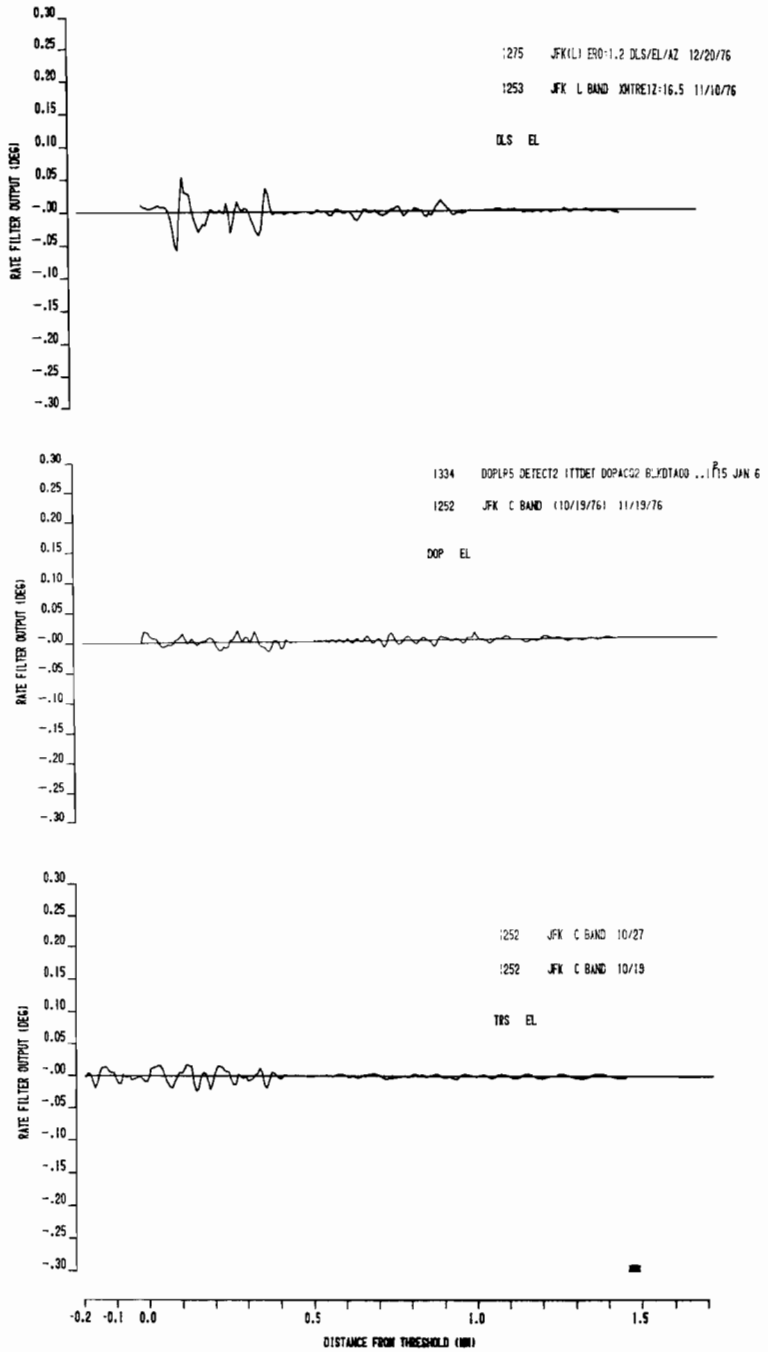

Fig. 2-63. Elevation rate filter ouput for scenario 1.

The flight control system filter outputs in Figs 2-61 to 2-63 show that the bulk of the elevation errors consist of "control motion" and "rate" noise as opposed to path displacement of the aircraft.

Changing the terrain dielectric constant to $\varepsilon/\varepsilon_o$ = 13 yielded virtually no change in the DMLS and TRSB errors and a small change in DLS error. This suggests that the DMLS and TRSB elevation errors here were not due to ground reflections, while the DLS elevation errors were slightly affected by the ground.

2. Results for Scenario 2

"Most capable" implementation results for scenario 2 with a terrain dielectric constant of 1.2 are shown in Figs. 2-64 to 2-70. For this scenario, the principal multipath threats are a series of large buildings (hangars) located abreast of runway midpoint. These building locations generated very little elevation multipath. However, they do generate a significant amount of out of beam azimuth multipath.

The low DLS azimuth error is due to the time delay discrimination against the building multipath. The DMLS error that arises near 0.4 nmi is due to scalloping of the reference signal. Simulation (see fig. 2-71) of the originally proposed DMLS system [7] showed sizable errors for this scenario due to reference scalloping effects [41]. The DMLS error magnitude shown in Figs. 2-64 and 2-66 is considerably lower than that reported initially, primarily due to the use of centerline emphasis and the revised scan format. The TRSB azimuth error reflects "sidelobe leak through."

Figs 2-72 and 2-73 show the azimuth errors with a "reduced capability" azimuth array. Increase in the DLS and TRSB errors due to higher sidelobe

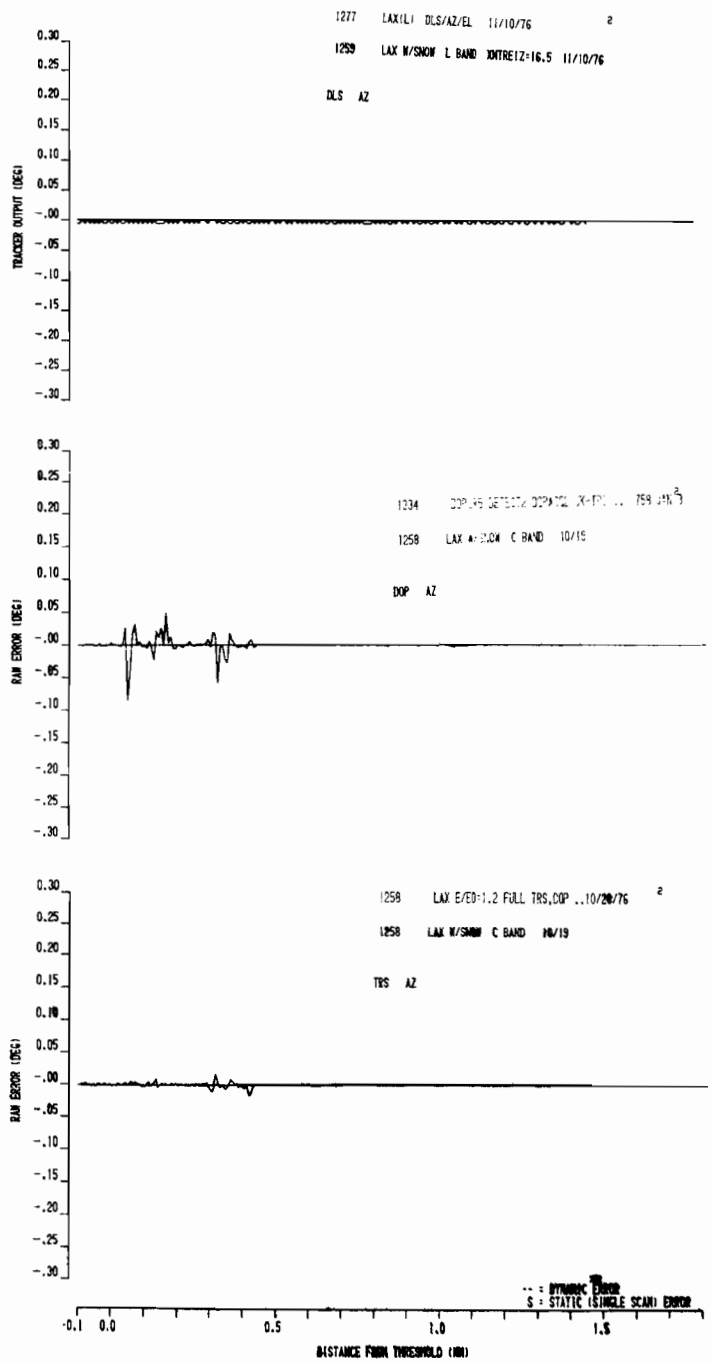

Fig. 2-64. Dynamic azimuth errors for scenario 2.

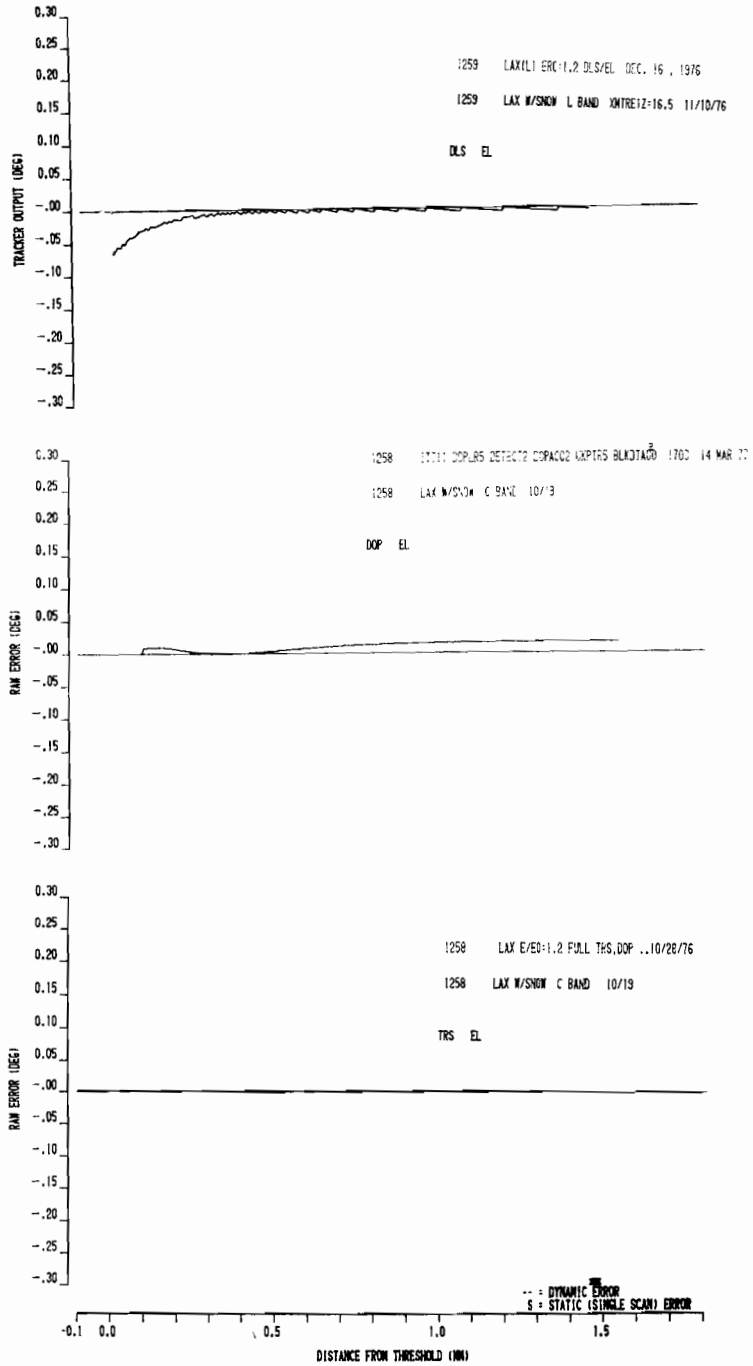

Fig. 2-65. Dynamic elevation errors for scenario 2.

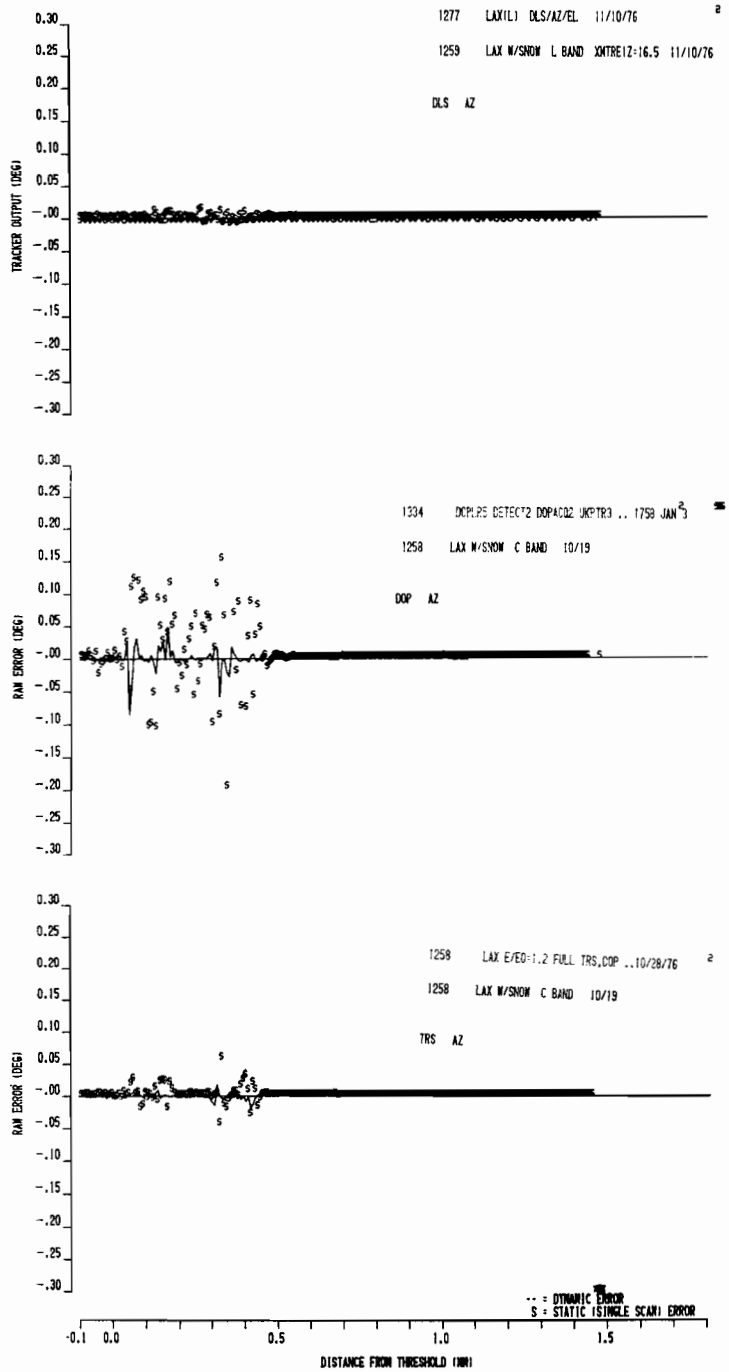

Fig. 2-66. Single-scan and dynamic elevation errors for scenario 2.

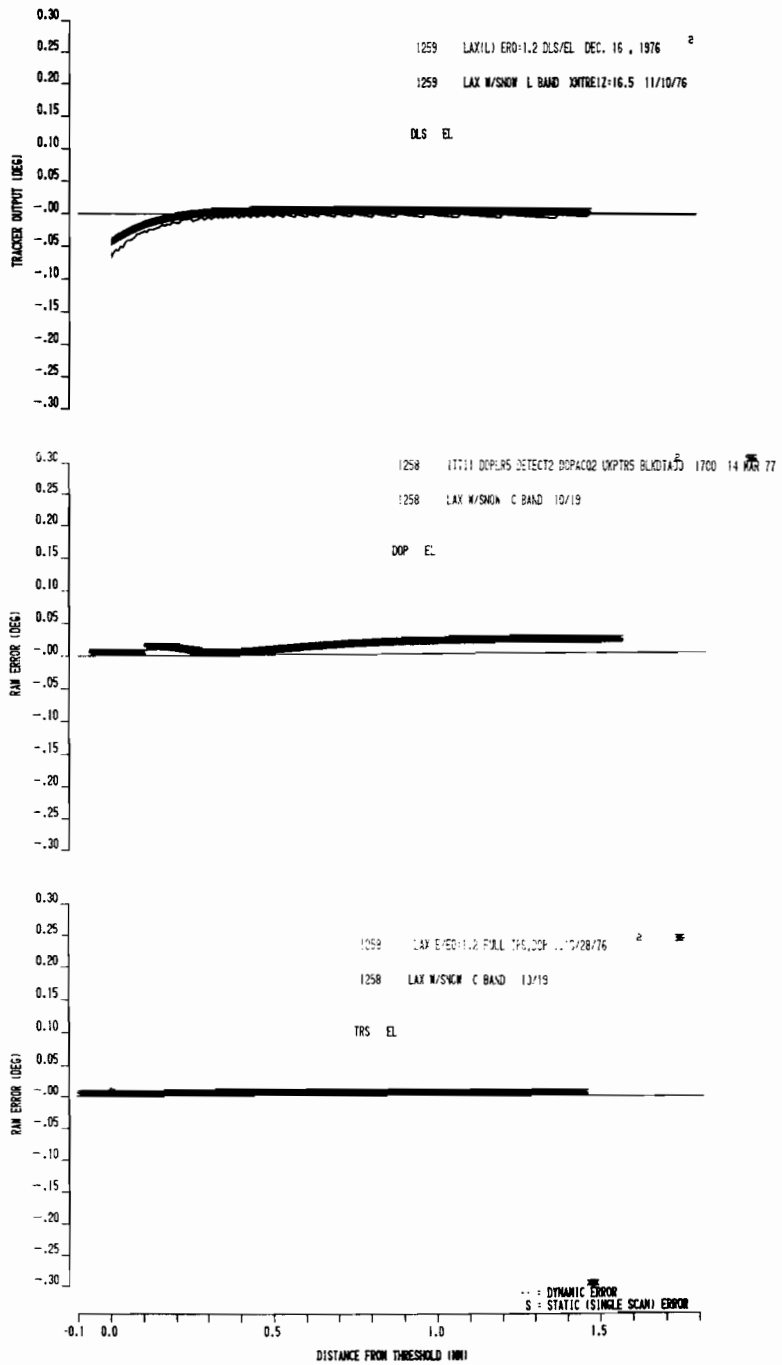

Fig. 2-67. Single-scan and dynamic elevation errors for scenario 2.

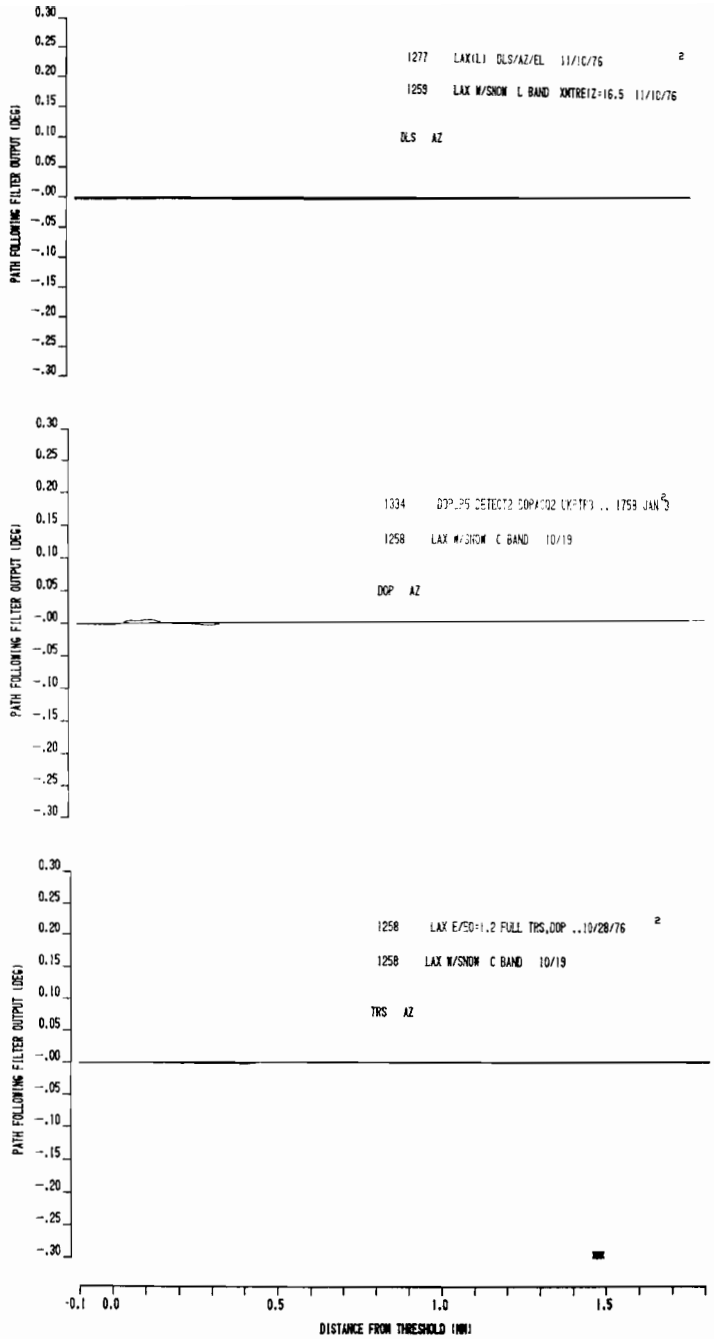

Fig. 2-68. Azimuth path following filter output for scenario 2.

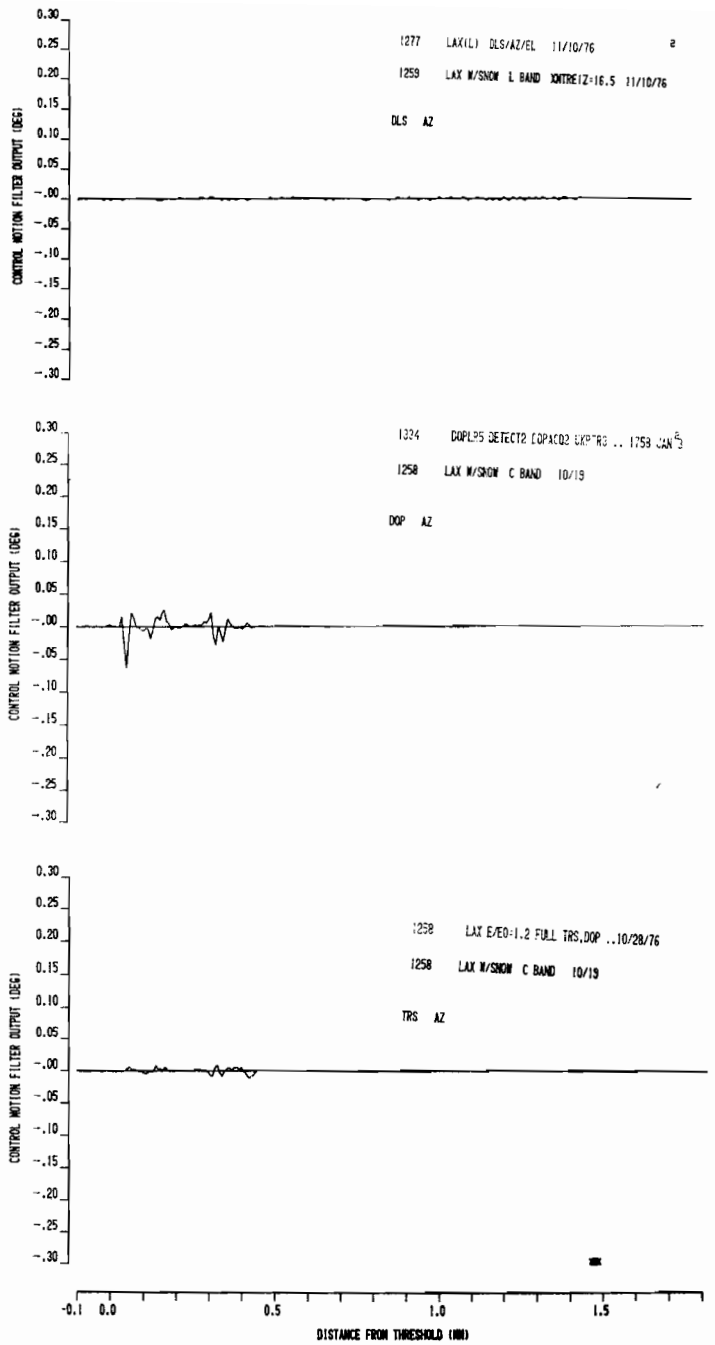

Fig. 2-69. Azimuth control motion filter output for scenario 2.

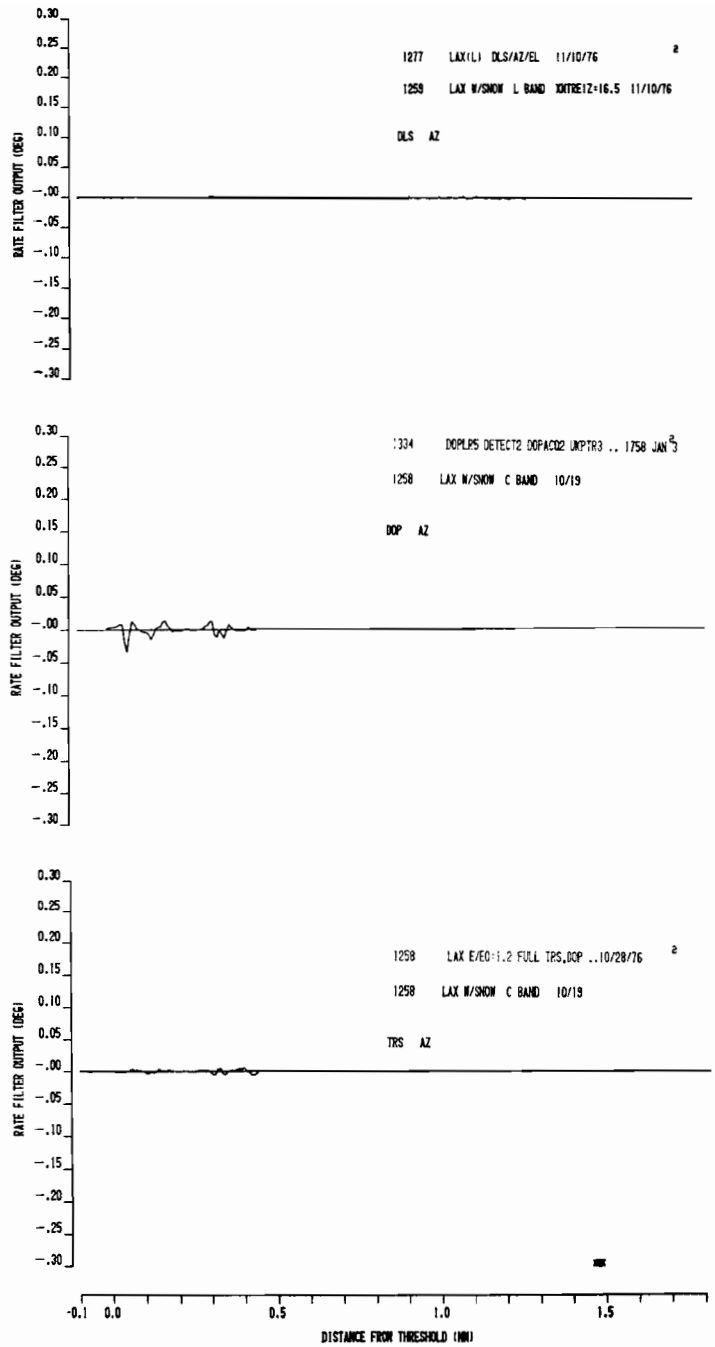

Fig. 2-70. Azimuth rate error filter output for scenario 2.

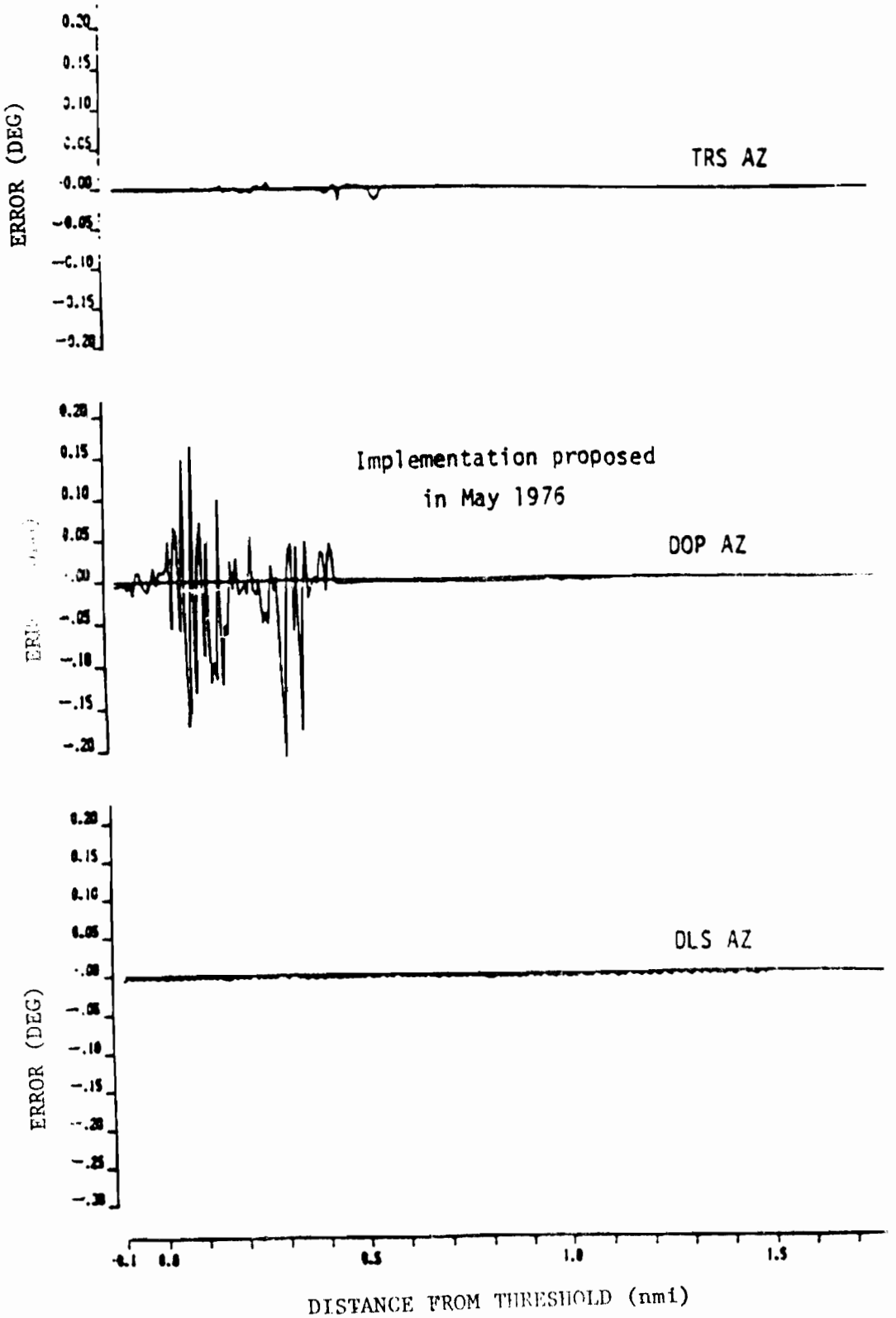

Fig. 2-71. Dynamic azimuth errors for scenario 2 with original implementations.

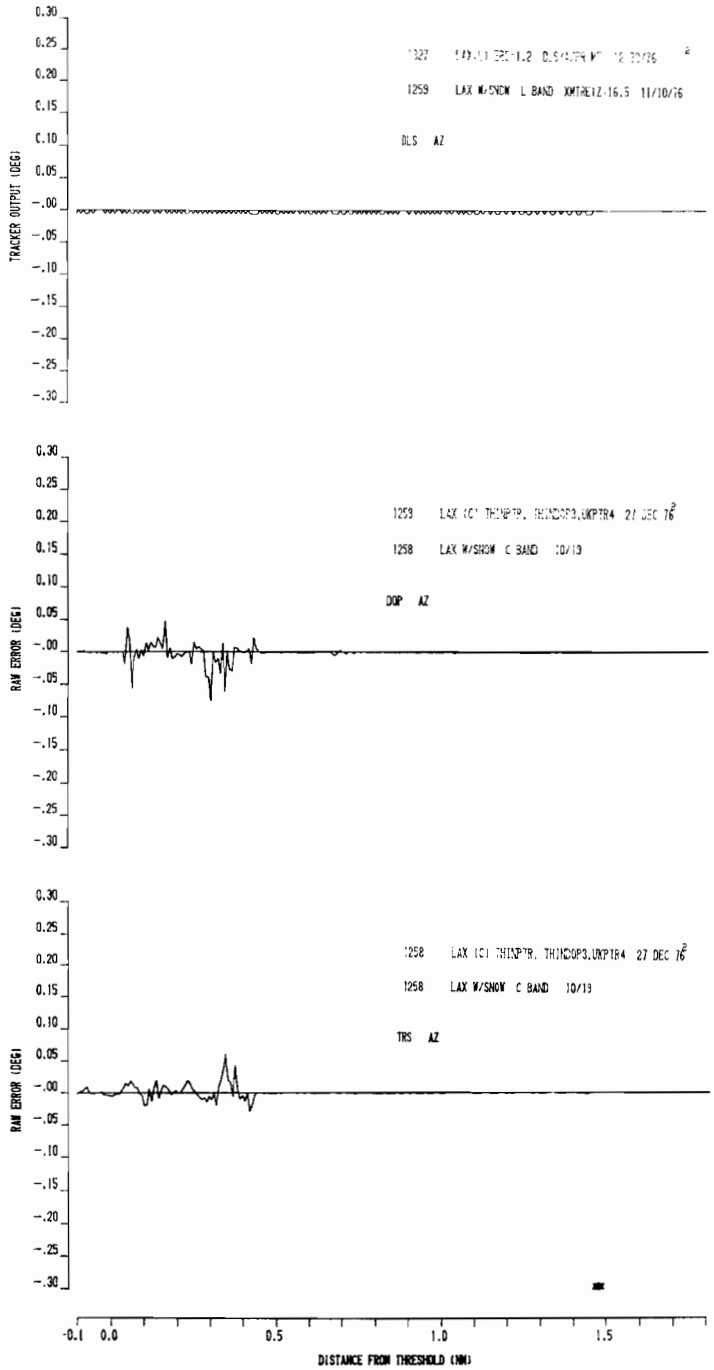

Fig. 2-72. Dynamic "reduced capability" azimuth errors for scenario 2.

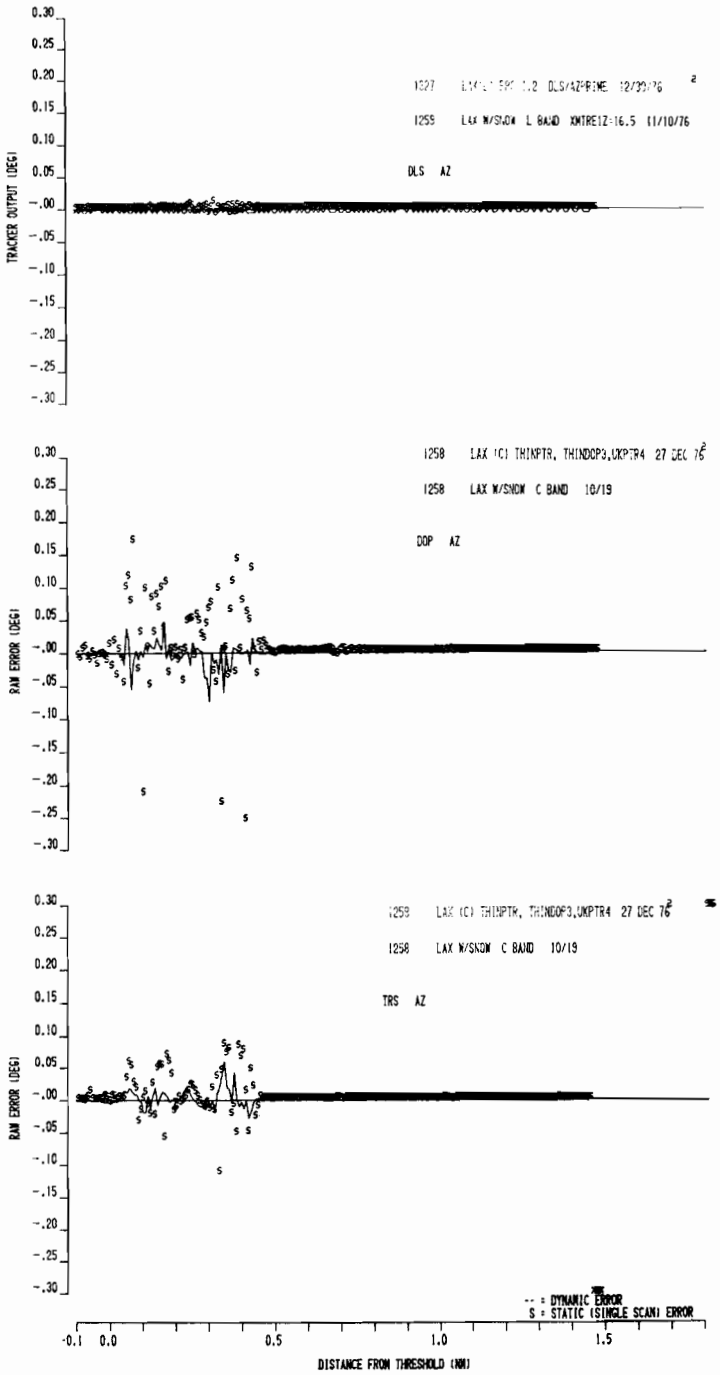

Fig. 2-73. Single-scan and dynamic "reduced capability" azimuth errors for scenario 2.

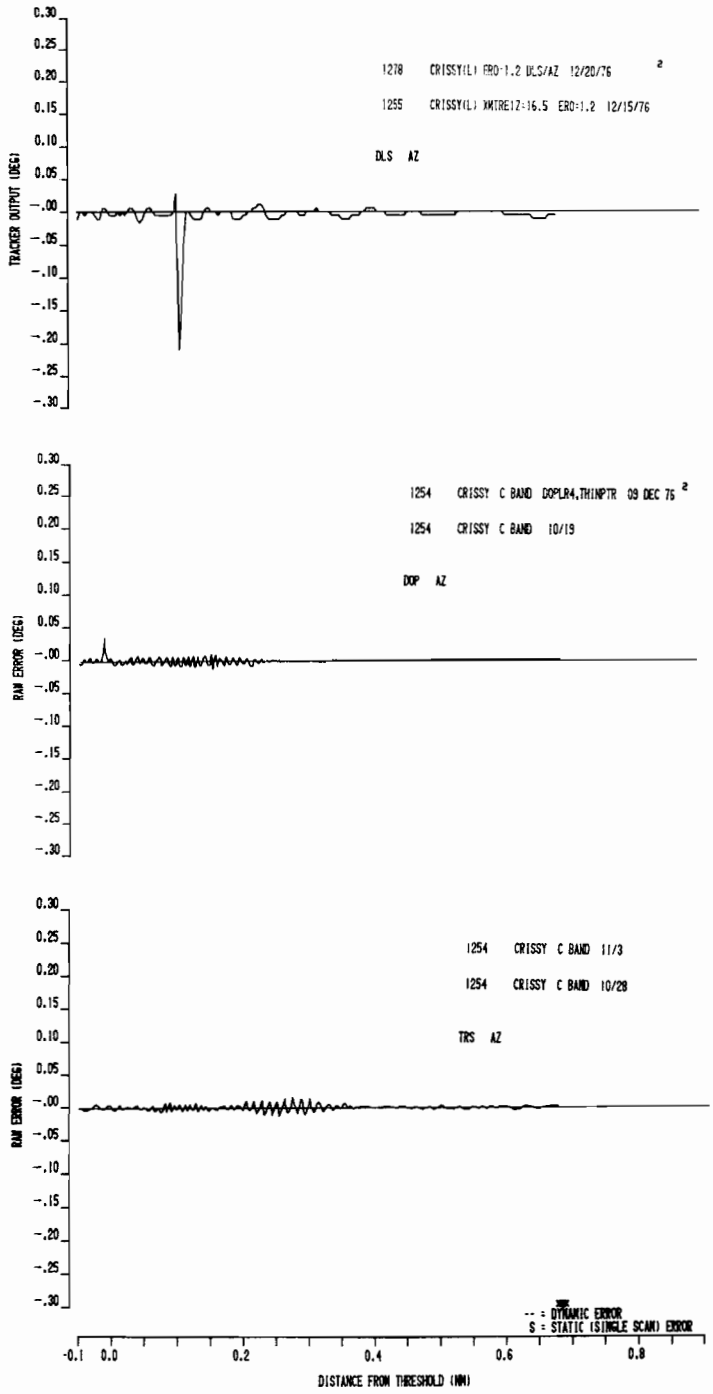

Fig. 2-74. Dynamic azimuth errors for scenario 3.

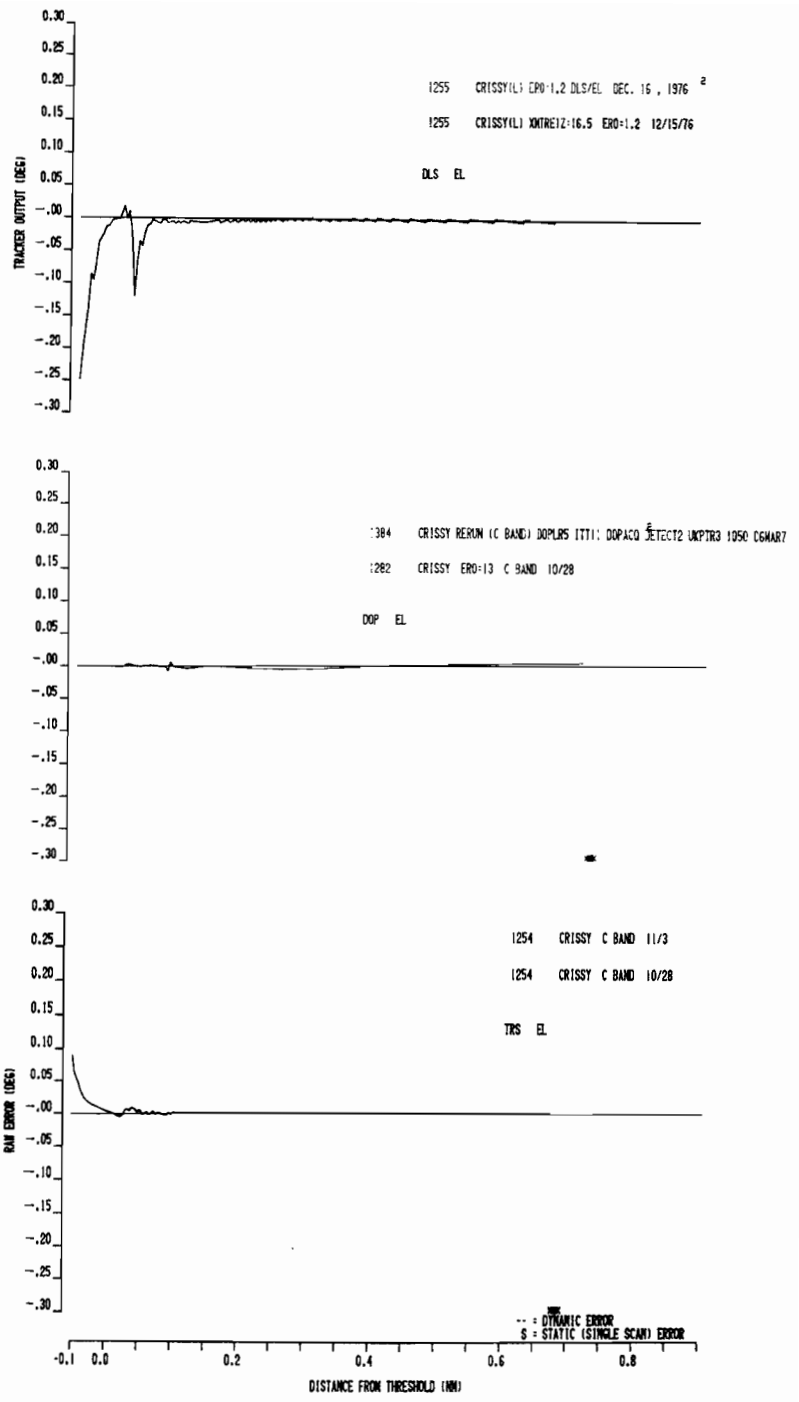

Fig. 2-75. Dynamic elevation errors for scenario 3.

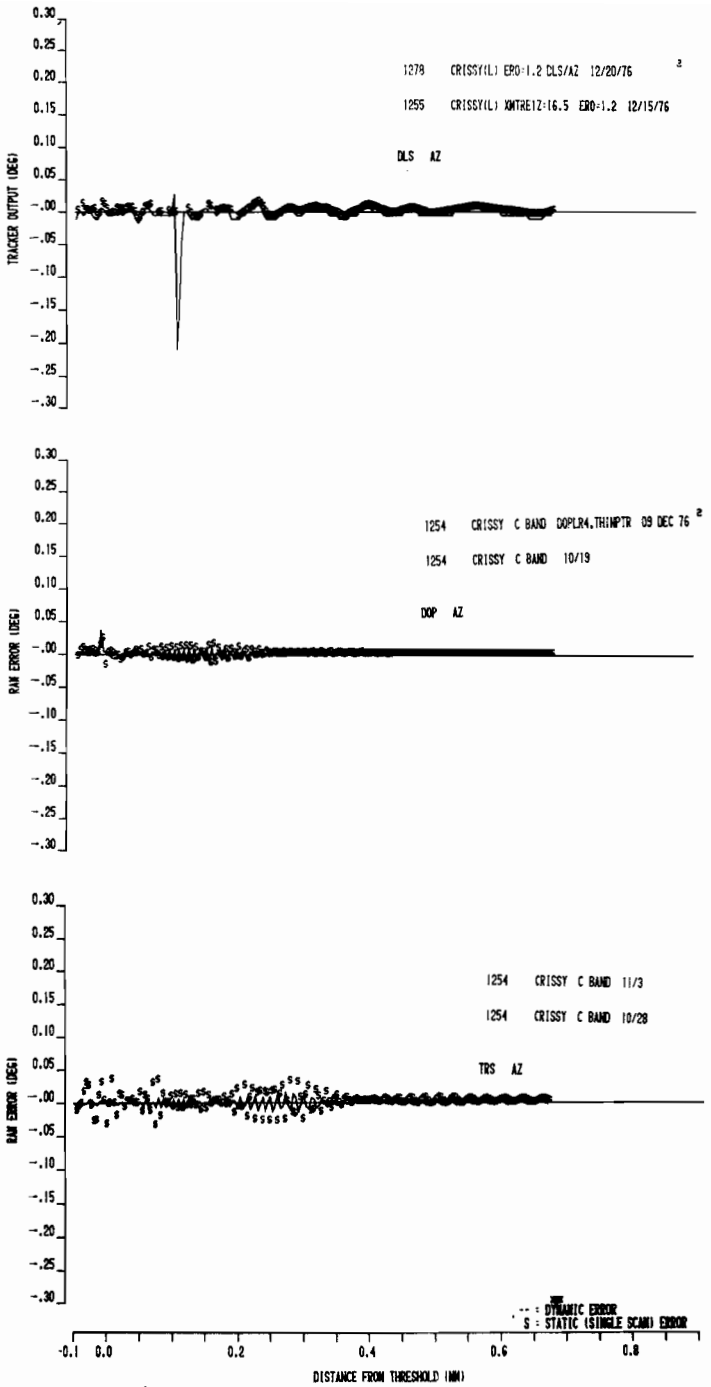

Fig. 2-76. Single-scan and dynamic azimuth errors for scenario 3.

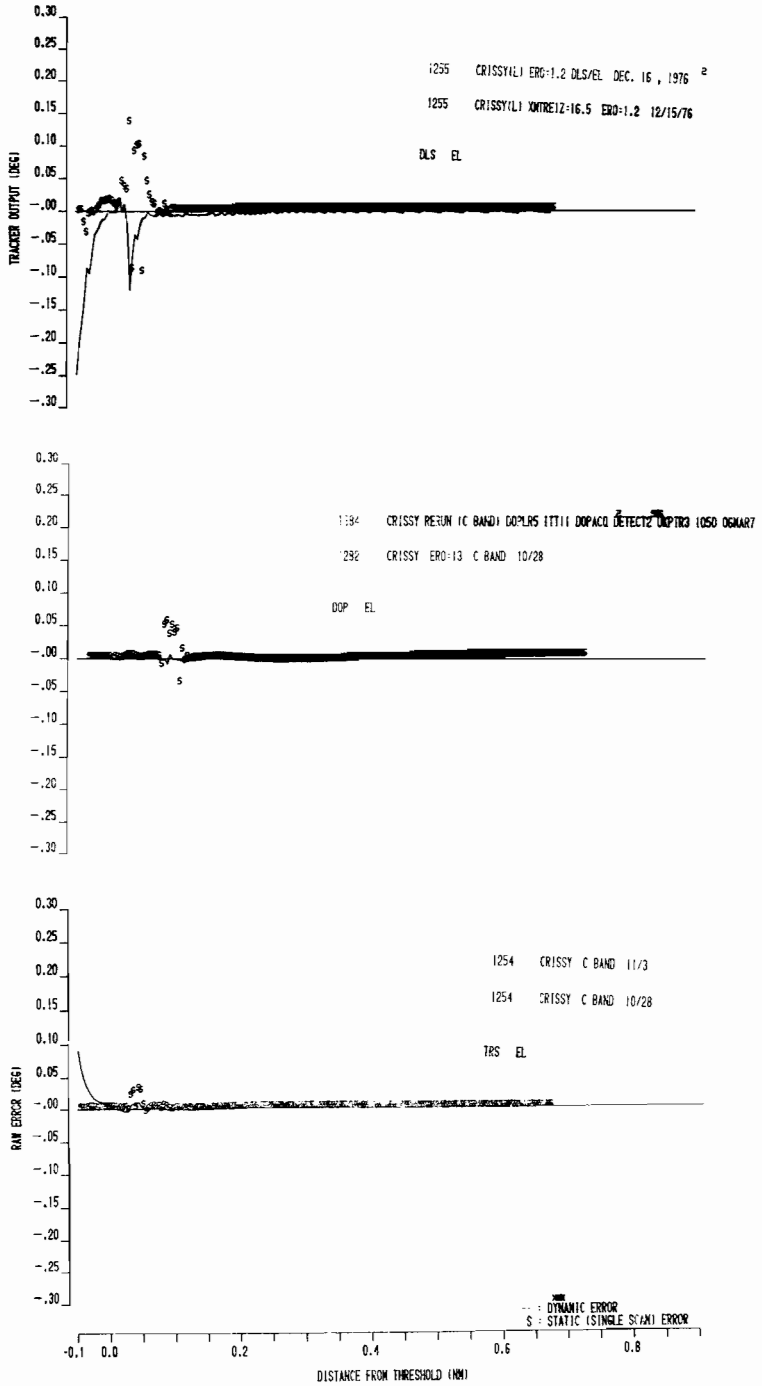

Fig. 2-77. Single-scan and dynamic elevation errors for scenario 3.

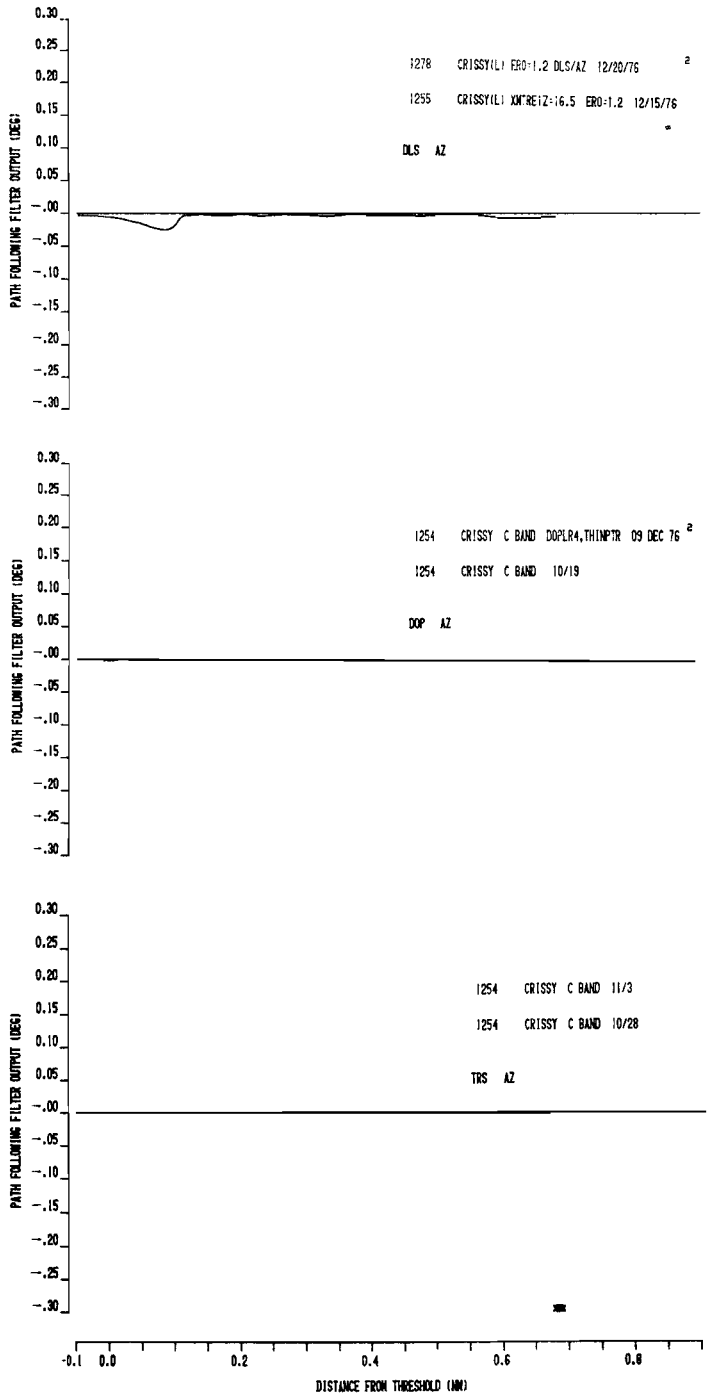

Fig. 2-78. Azimuth path following filter output for scenario 3.

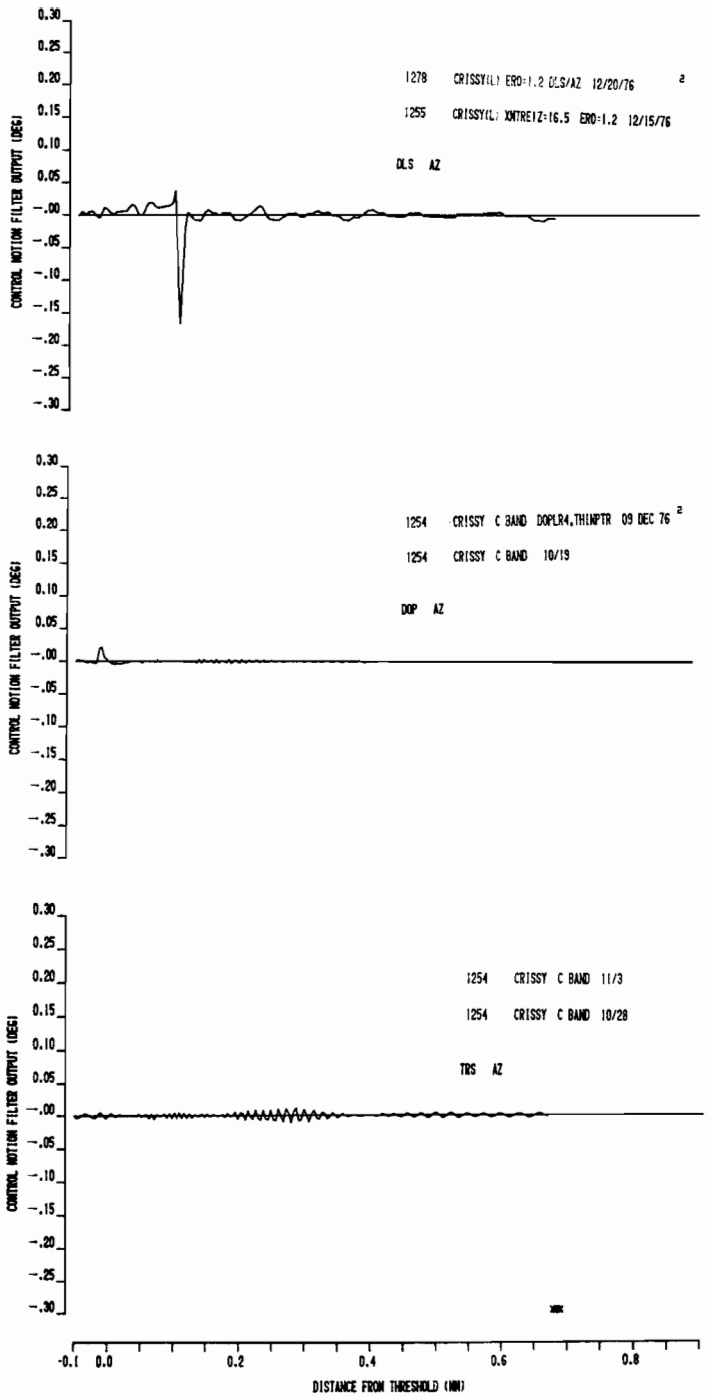

Fig. 2-79. Azimuth path following filter output for scenario 3.

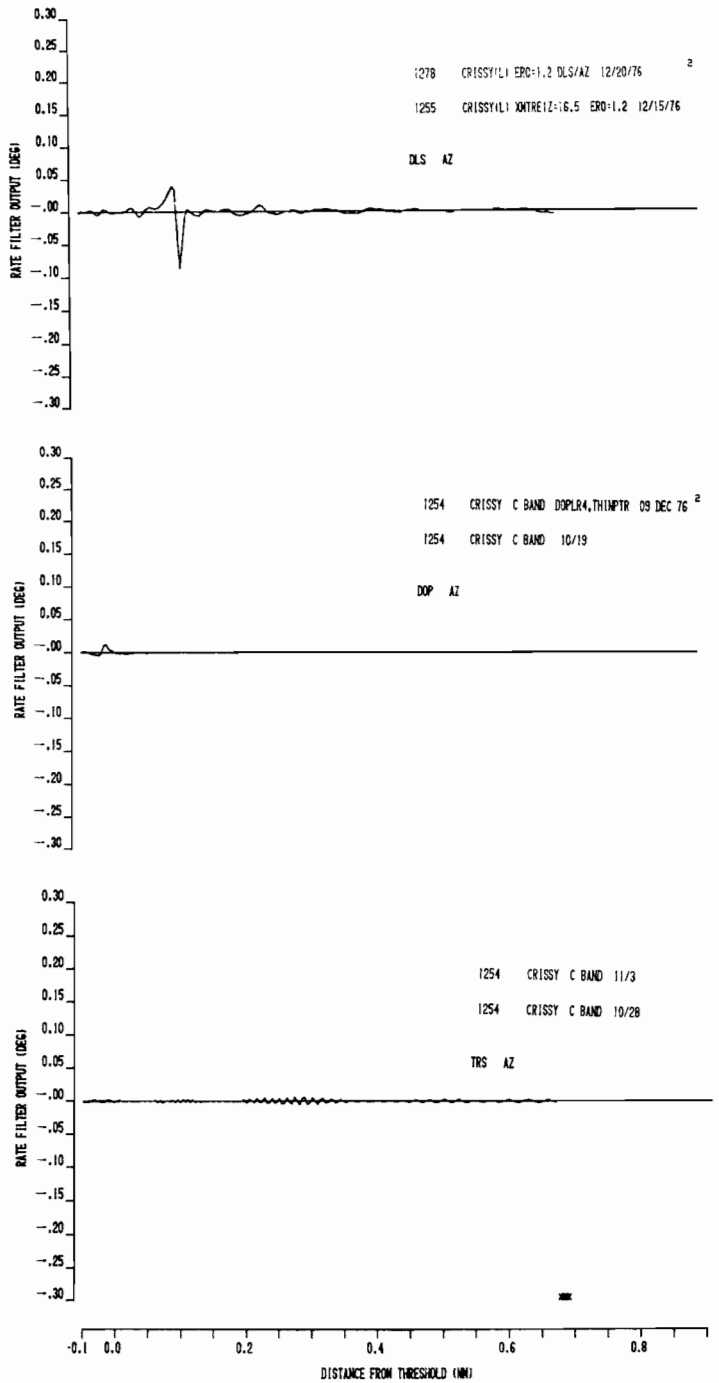

Fig. 2-80. Azimuth rate error filter output for scenario 3.

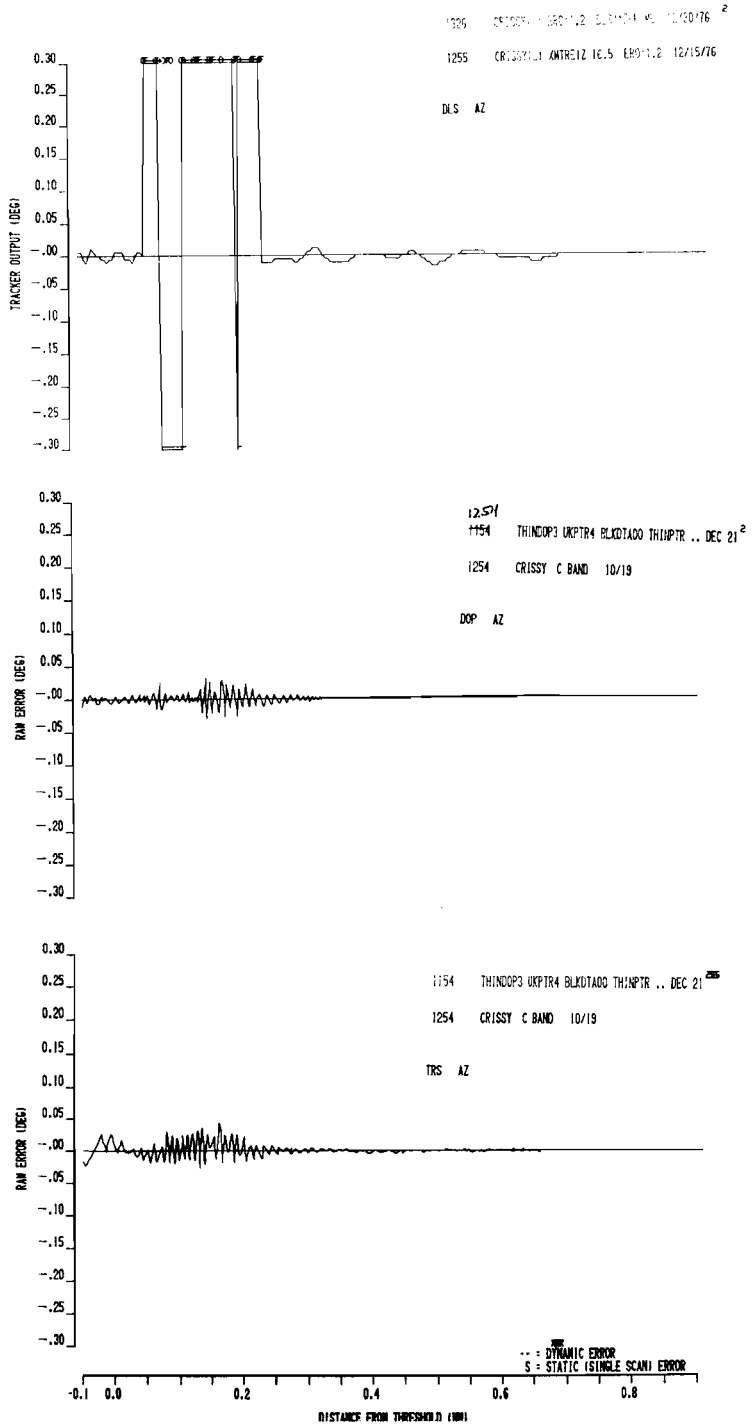

Fig. 2-81. Dynamic "reduced capability" aximuth errors for scenario 3.

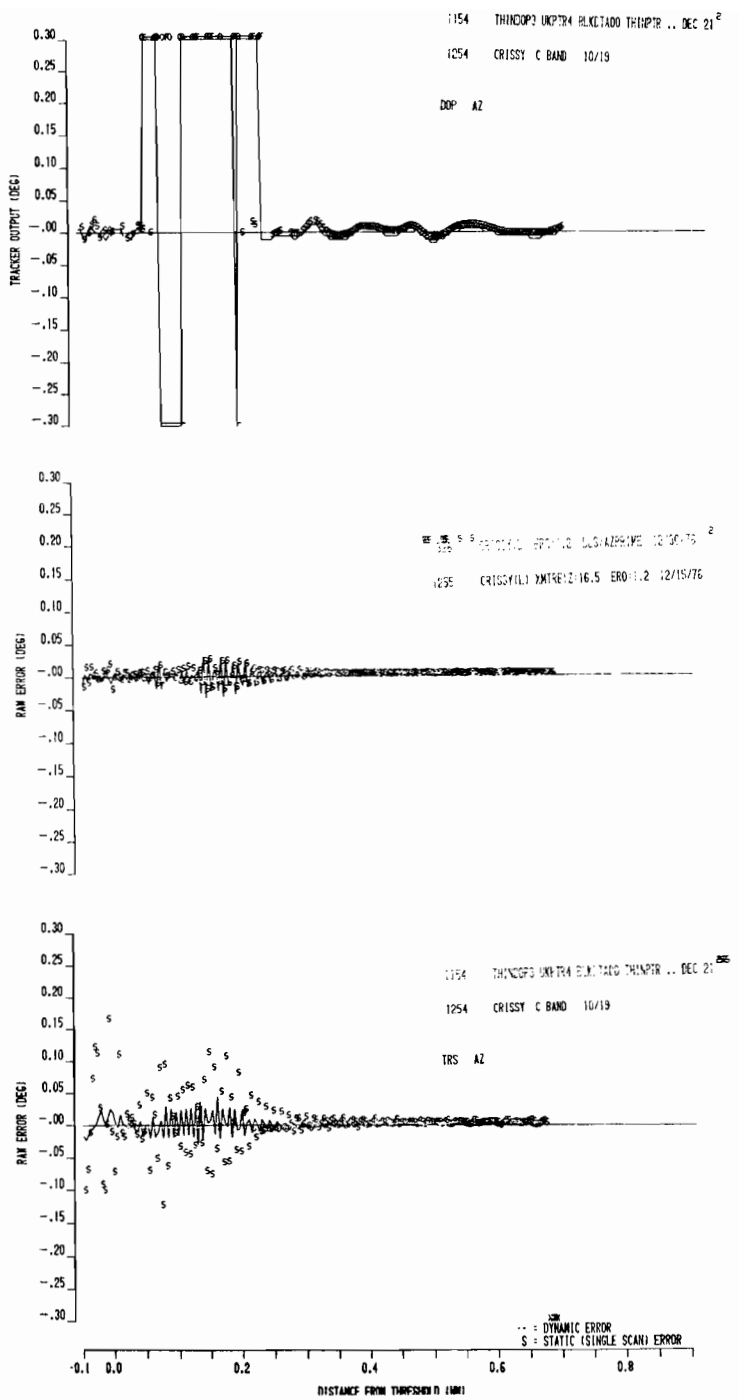

Fig. 2-82. Single-scan and dynamic "reduced capability" azimuth errors for scenario 3.

antennas is evident. The DMLS errors are reduced somewhat due to the use of a commutated reference antenna.

The elevation errors here arise primarily from ground reflections. Consequently, they have a very slow period. By contrast, the high scalloping frequencies of the azimuth multipath cause the errors to principally appear as "control motion" and "rate" noise.

3. Results for Scenario 3

The principal multipath threats here were the series of buildings beside the runway from near the transmitter to abreast of the elevation transmitter. These building locations generate relatively little elevation multipath; however, there is considerable out of beam azimuth multipath at a low scalloping rate over much of the approach.

Results for scenario 3 with a terrain dielectric constant of 1.2 are shown in Figs. 2-74 to 2-82. Figures 2-74 to 2-80 correspond to the "most capable" azimuth array implementation proposed. In Figs. 2-81 and 2-82, we see the corresponding azimuth errors with a "reduced capability" azimuth array. The TRS and DLS errors are significantly increased in Figs. 2-81 and 2-82 due to the higher array sidelobes. The DMLS errors in 2-81 are very similar to those in Fig. 2-74 since no multipath occurred at the angles where the DMLS commutated reference array has high sidelobes. Figs 2-83 and 2-84 show results for the "most capable" azimuth arrays in an "inhomogeneous" terrain in which the runway surface has a dielectric constant of 1.2 while the off runway terrain has a dielectric constant of 5.0.

The DLS azimuth spike near 0.2 nmi appears to represent the effect of a velocity term in the tracker algorithm. For several consecutive ground esti-

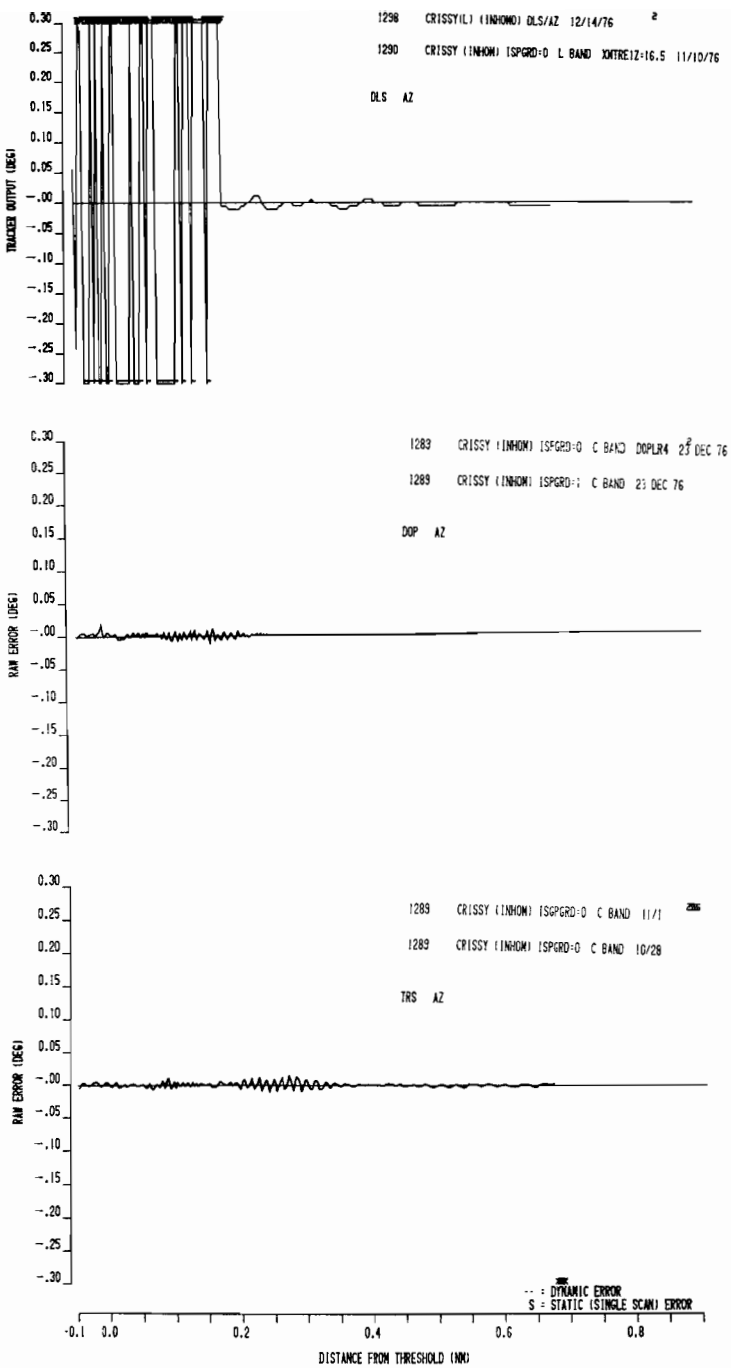

Fig. 2-83. Dynamic azimuth errors for scenario 3 with inhomogeneous terrain.

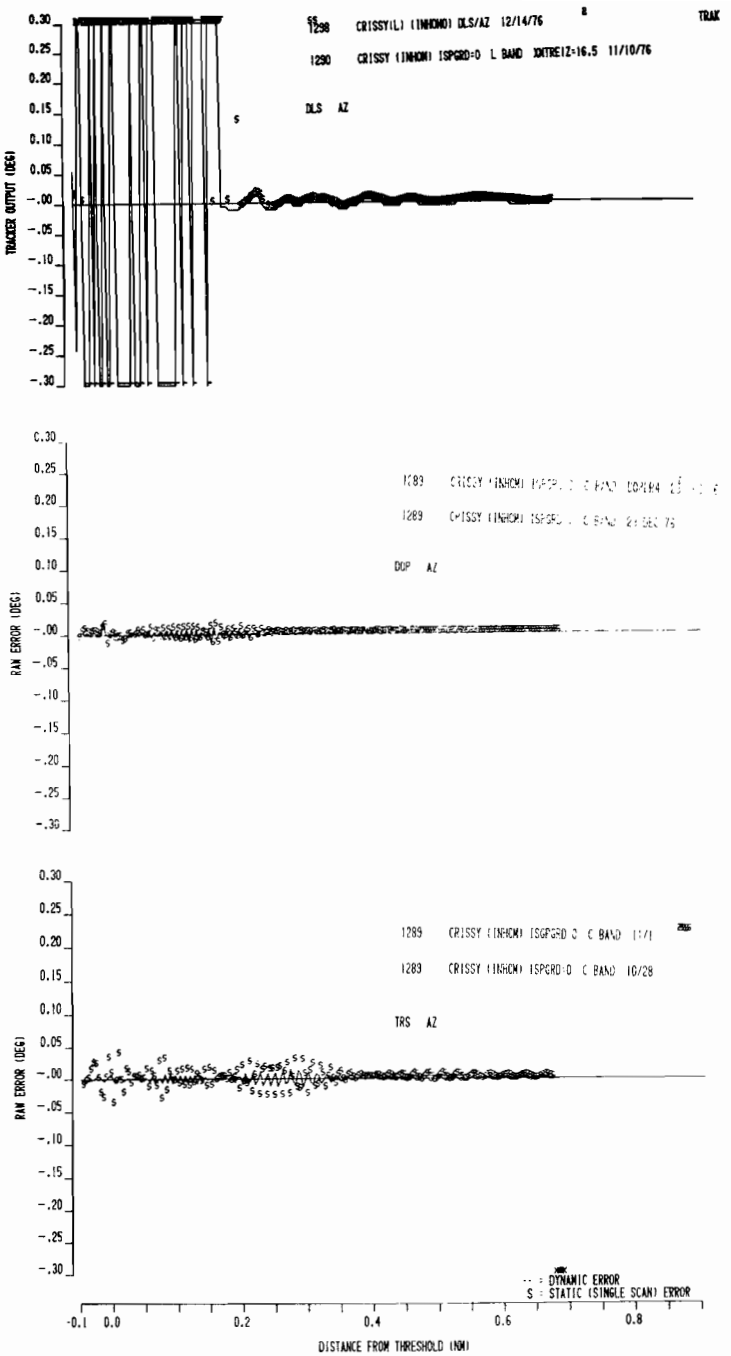

Fig. 2-84. Single-scan and dynamic azimuth errors for scenario 3 with inhomogeneous terrain.

mates, resolution breakdown occurs and updated tracker estimates are made using this velocity term. This causes the tracker estimate to drift until good input estimates are once again received. The very large DLS errors in Fig. 2-83 (20° to 40° peak) represent ambiguity resolution breakdown. Comparison of the tracker output with the single interrogation ground estimates shows that up to the time at which ambiguity breakdown occurred, the DLS errors were comparable to those of the other systems.

The DLS elevation error due to building multipath 0.1 nmi from the threshold does not arise to the same extent for the other systems due to the large separation angle (in elevation and azimuth). The DLS and TRSB elevation errors after threshold are not due to multipath, but rather, represent tracker lag due to very rapid change in conical elevation angle in that region.* Not only is the angular rate of change very high (> 1 deg/sec at the end), but there is also a substantial angular acceleration which cannot be closely followed by the second order tracking loops in the DLS and TRSB receivers. Since the elevation transmitter-to-receiver distance is small (≈ 200 feet at the flight path end), the height errors due to tracker lag is small (< 0.5 feet).

4. Results for Scenario 4

The results for scenario 4 with a terrain dielectric constant $\varepsilon/\varepsilon_o = 1.2$ are shown in Figs. 2-85 to 2-89. This scenario was derived from scenario 1 by moving the elevation transmitter across the runway so that it was on the

*To verify this, separate simulations of the DLS and TRSB trackers were conducted with a tracker input angle equal to direct signal angle. These yielded similar behavior as the aircraft neared the threshold.

opposite side of centerline from the principal building threats. The effect of this siting change was to increase the separation angle, azimuth and scalloping frequencies of the in beam elevation multipath.

For DMLS and TRSB, the errors are generally smaller than those of scenario 1 while the DLS errors are similar to those of scenario 1. Again, a principal factor in the larger DLS errors is believed to be the (electrically) smaller aperture.

5. Results for Scenario 5

Scenario 5 was broken into two parts: one in which multipath reflections from buildings are encountered and one in which building shadowing occurs. The two portions have a different receiver altitude. Figures 2-90 and 2-91 show the "most capable" azimuth implementation results* for the reflection portion with a terrain dielectric constant $\varepsilon/\varepsilon_o$, of 1.2. Figures 2-92 and 2-93 show the reflection portion azimuth errors using the "lesser capability" azimuth implementations while the results for the shadowing portion with $\varepsilon/\varepsilon_o$ = 1.2 are shown in Figs. 2-94 and 2-95.

First, we consider the building reflection portion results. The principal multipath threat here is out of beam azimuth multipath from two buildings near the azimuth transmitter. These yield substantial multipath over a considerable flight path region, similar to that in scenario 3. However, in this case, the receiver is not on centerline and the scalloping rates are much higher.

---

*Only azimuth results are shown since the elevation multipath in this case arose only from the ground.

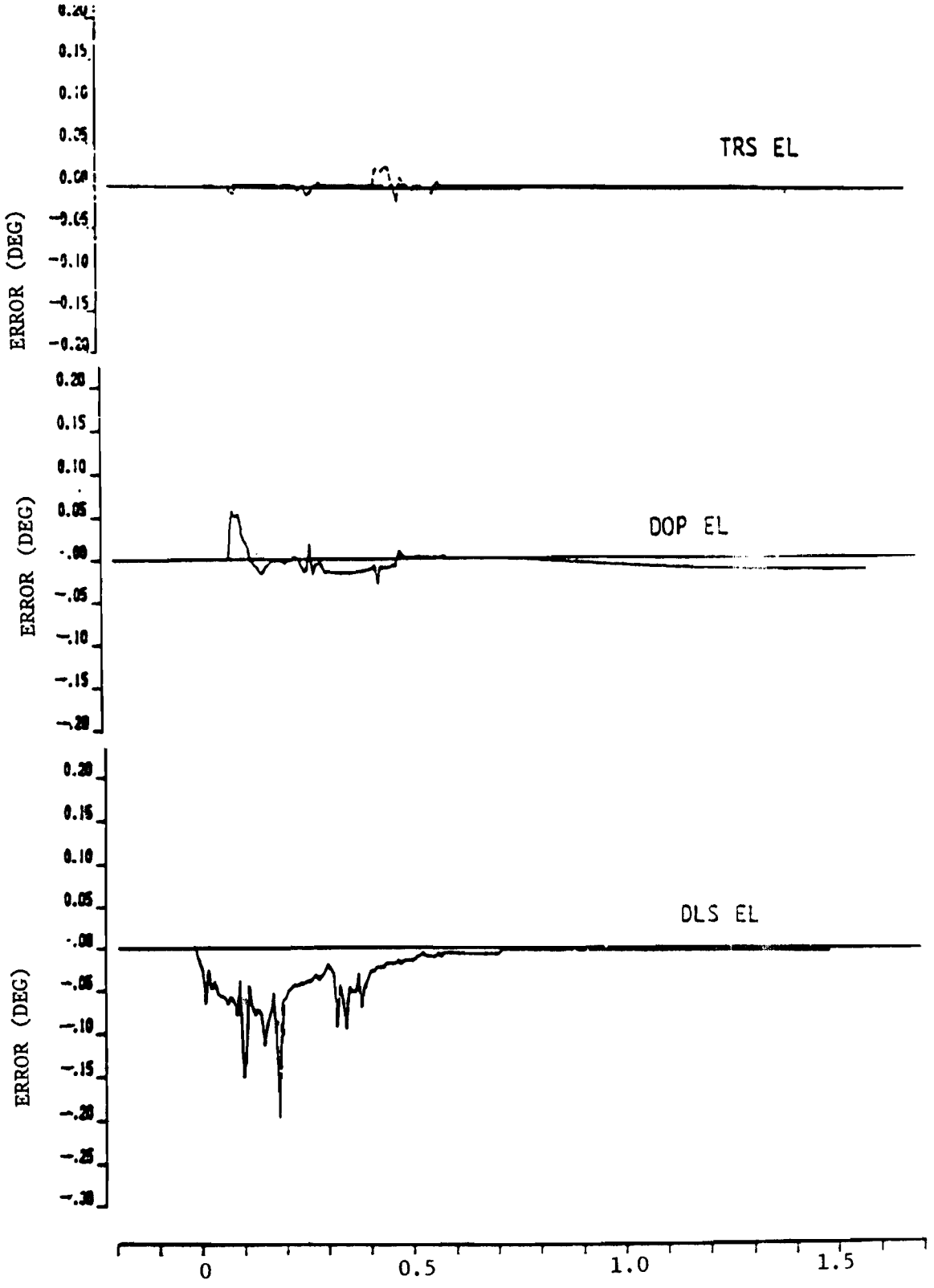

Fig. 2-85. Dynamic elevation errors for scenario 4.

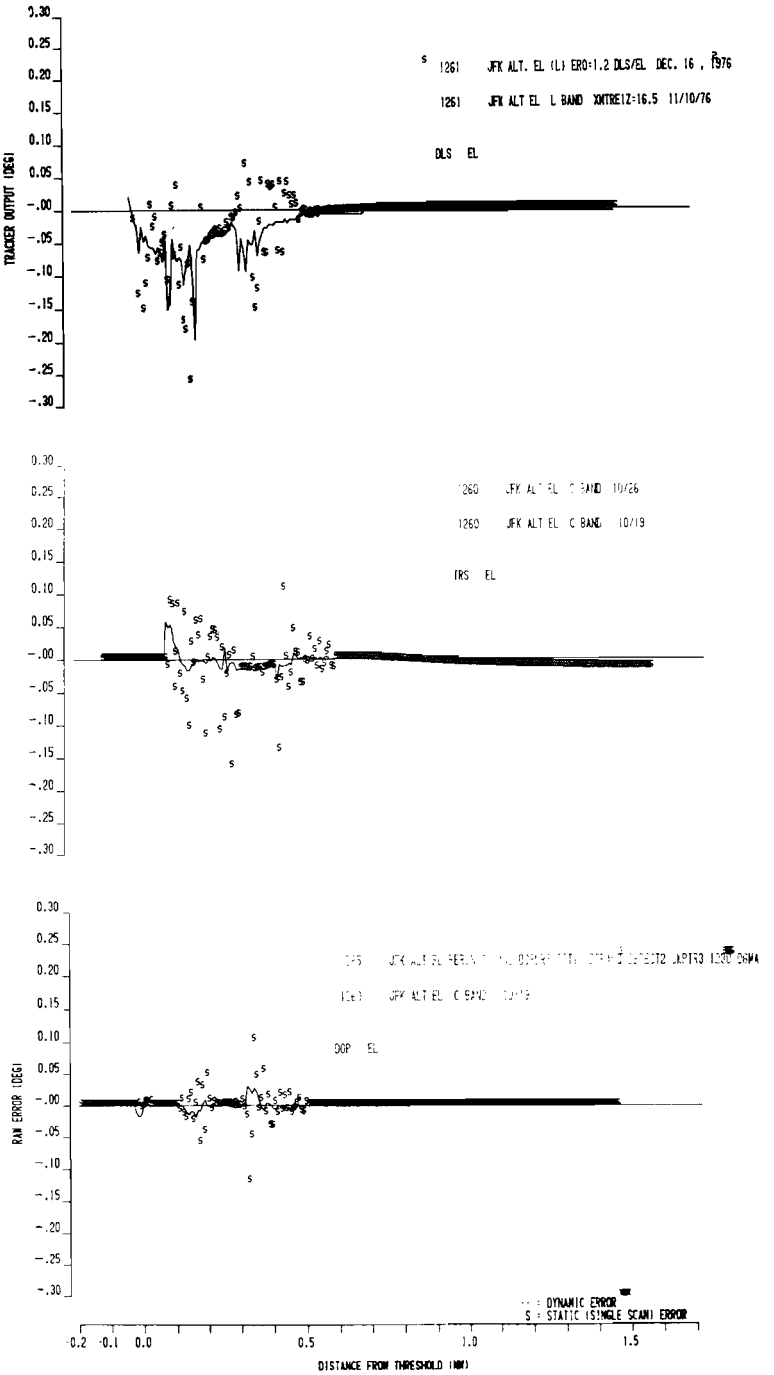

Fig. 2-86. Dynamic and single-scan elevation errors for scenario 4.

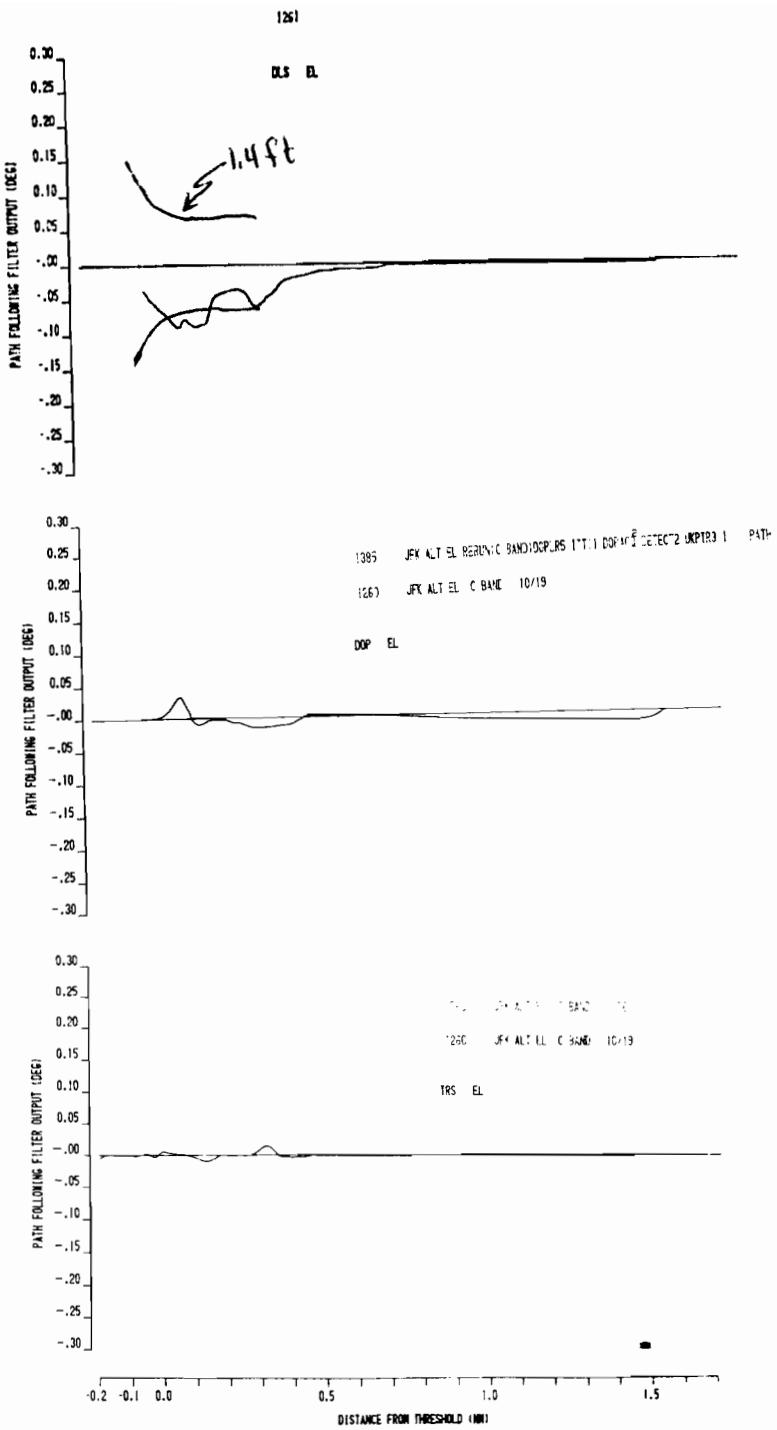

Fig. 2-87. Elevation path following filter output for scenario 4.

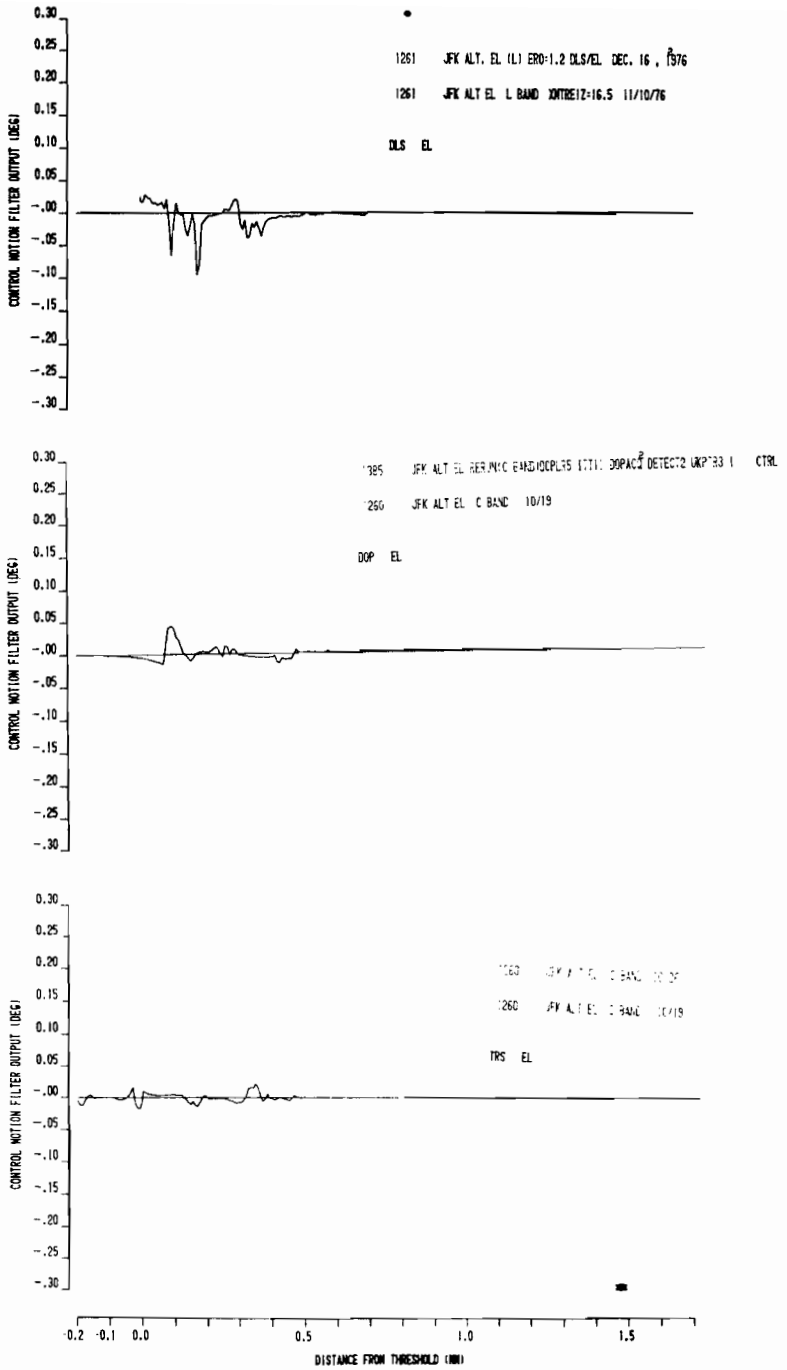

Fig. 2-88. Elevation control motion filter output for scenario 4.

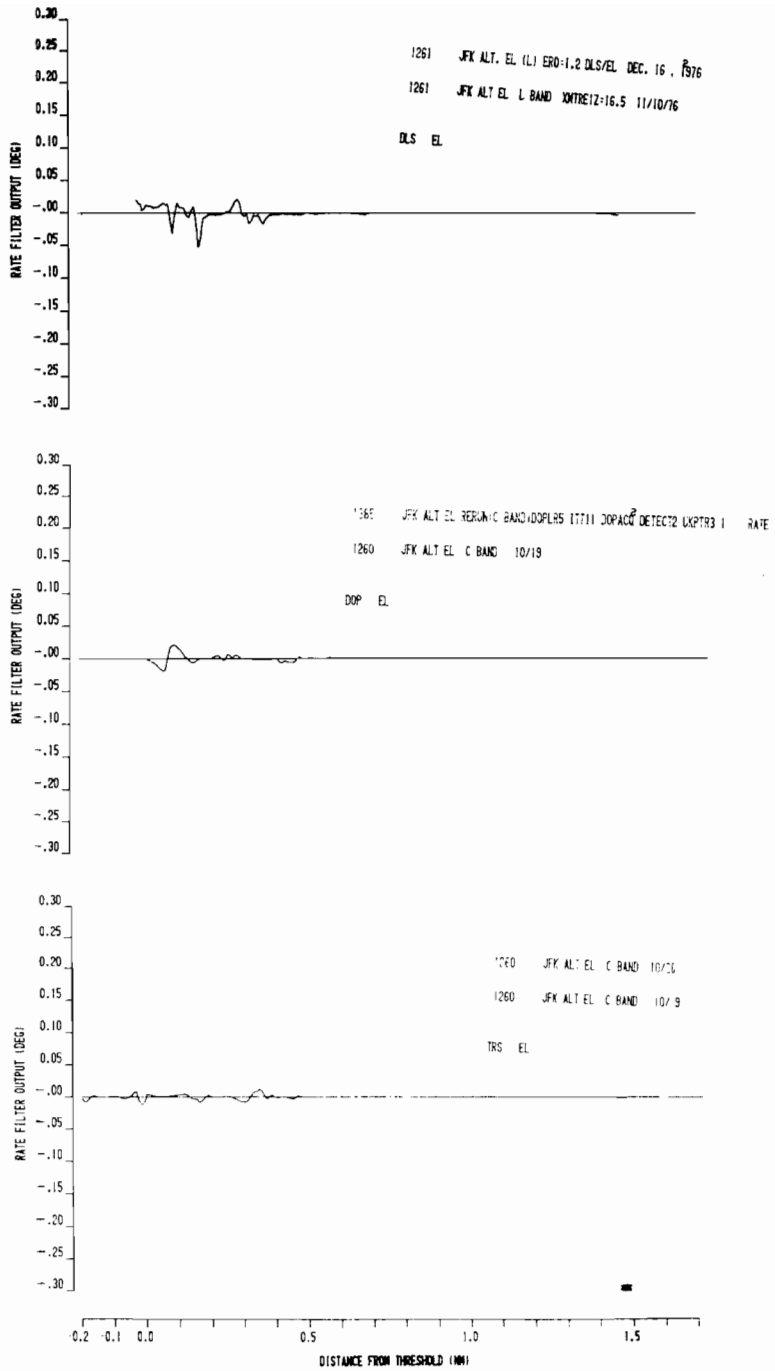

Fig. 2-89. Elevation rate error filter output for scenario 4.

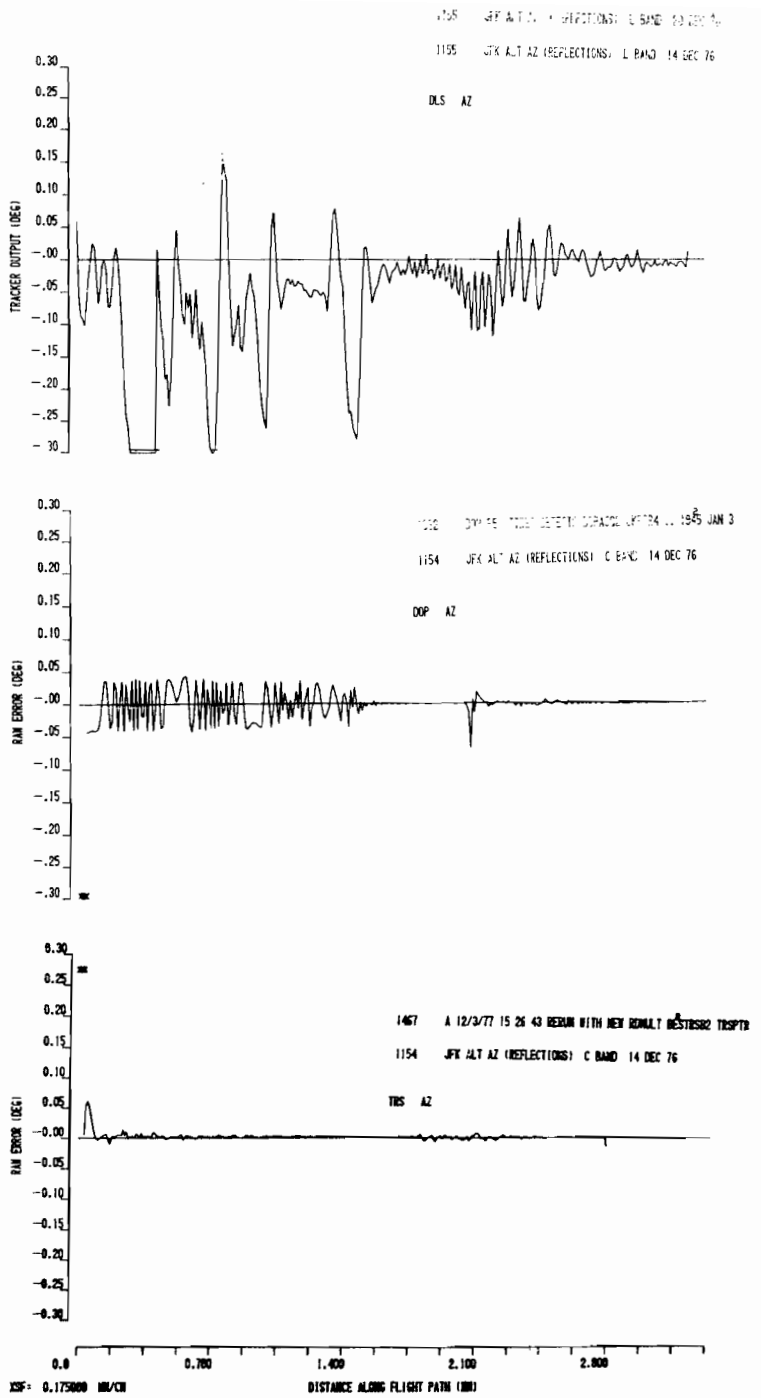

Fig. 2-90. Dynamic azimuth errors for scenario 5 (reflections).

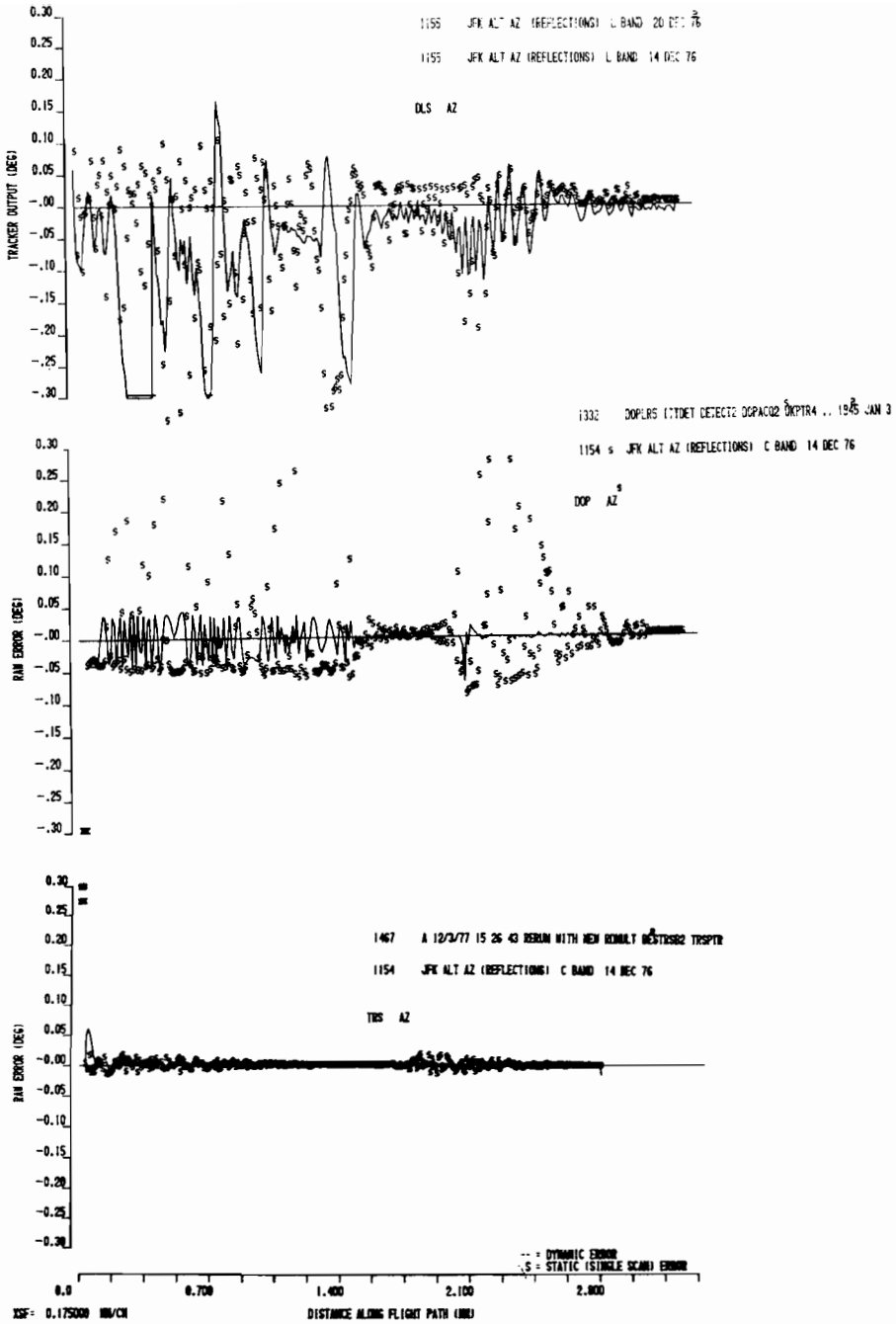

Fig. 2-91. Single-scan and dynamic azimuth errors for scenario 5 (reflections).

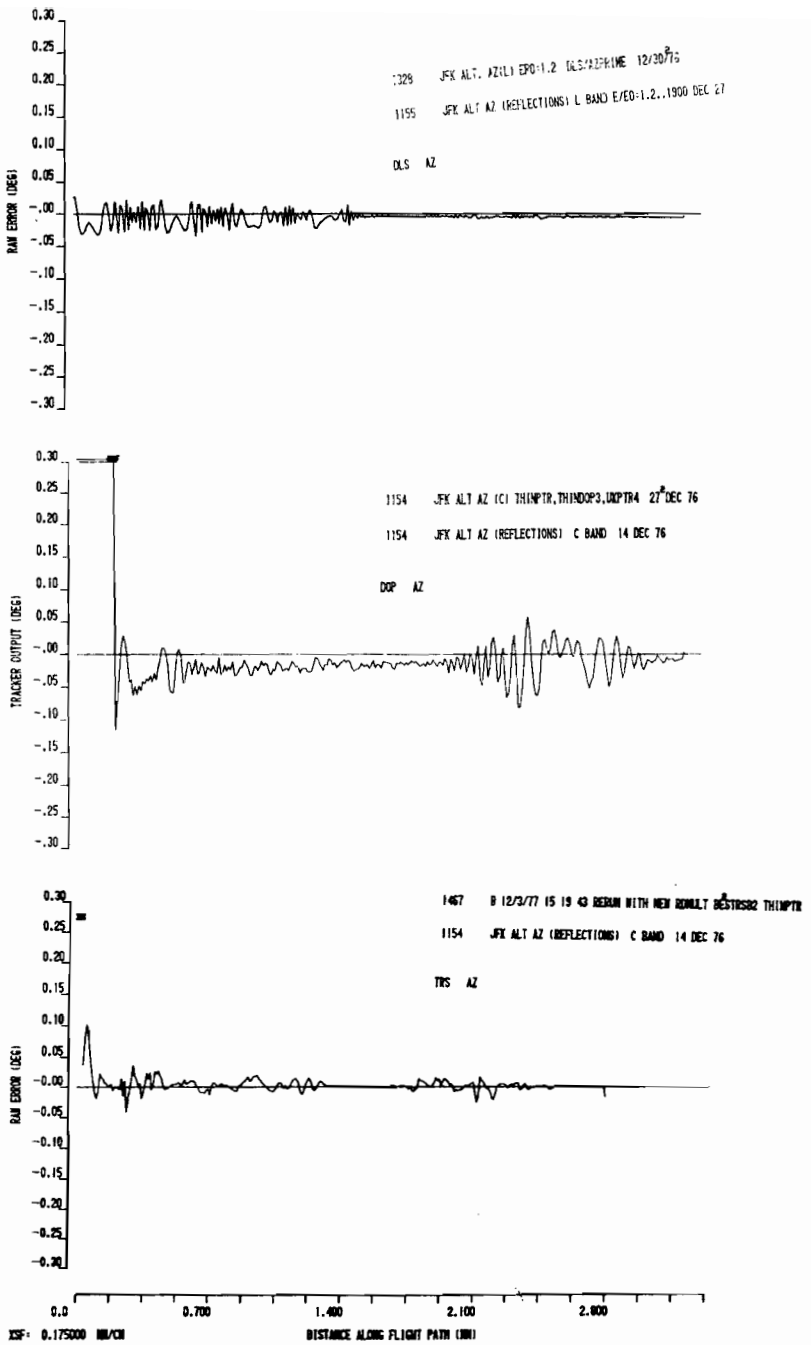

Fig. 2-92. Dynamic "reduced capabllity" azimuth errors for scenario 5 (reflections).

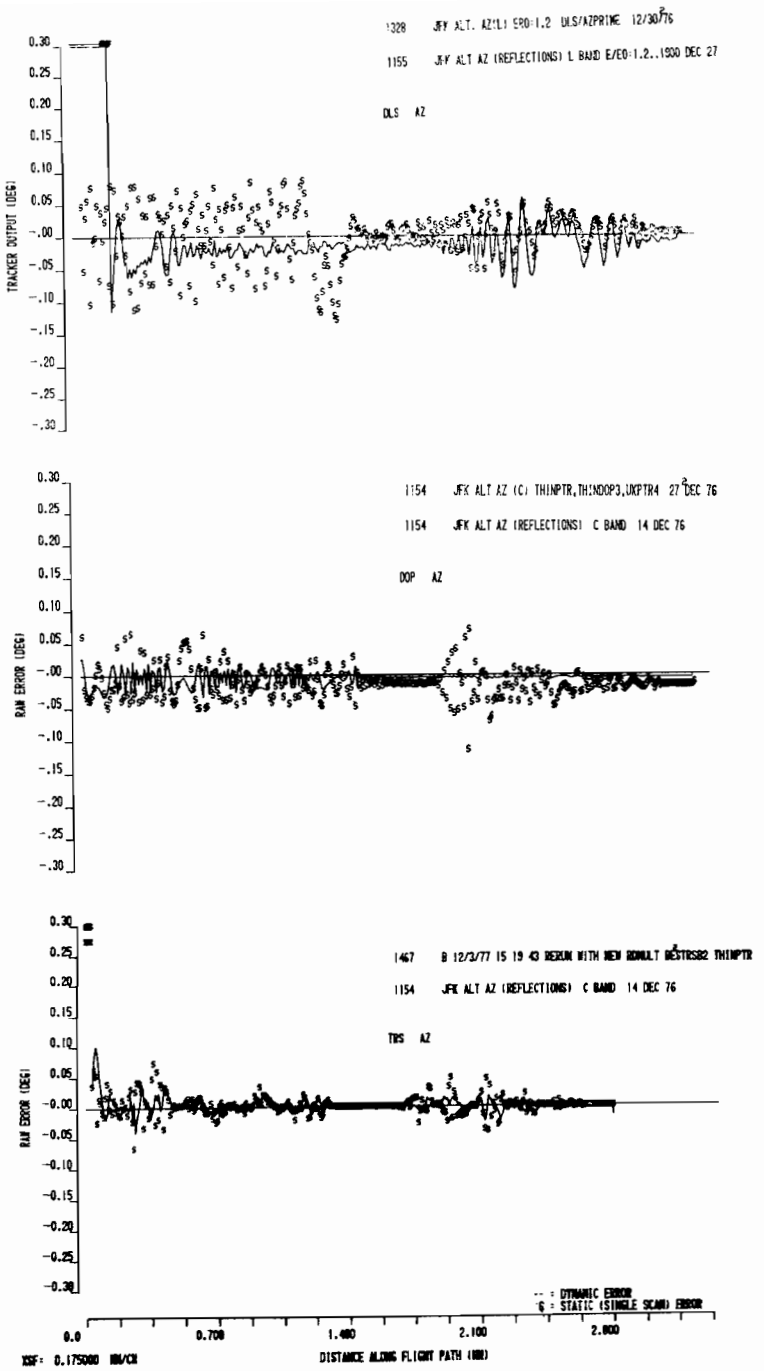

Fig. 2-93. Single-scan and dynamic "reduced capability" azimuth errors for scenario 5 (reflections).

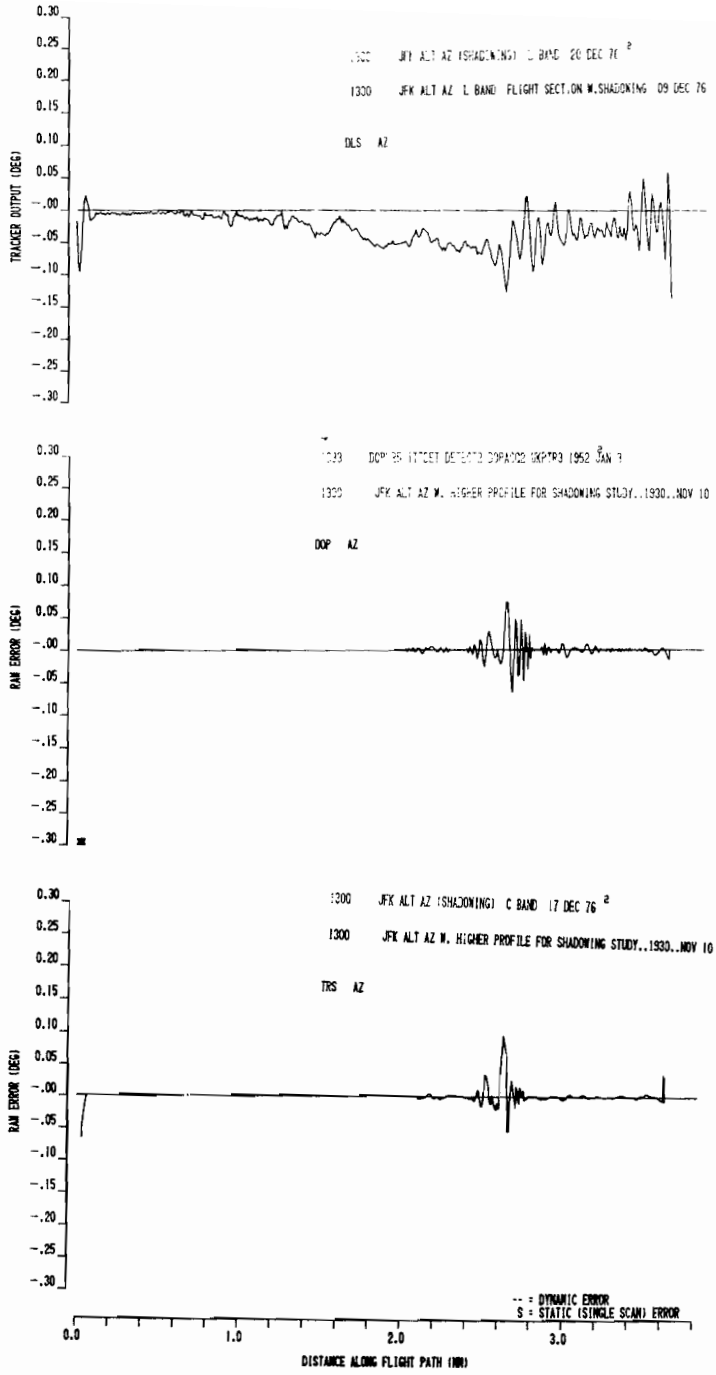

Fig. 2-94. Dynamic azimuth errors for scenario 5 (shadowing).

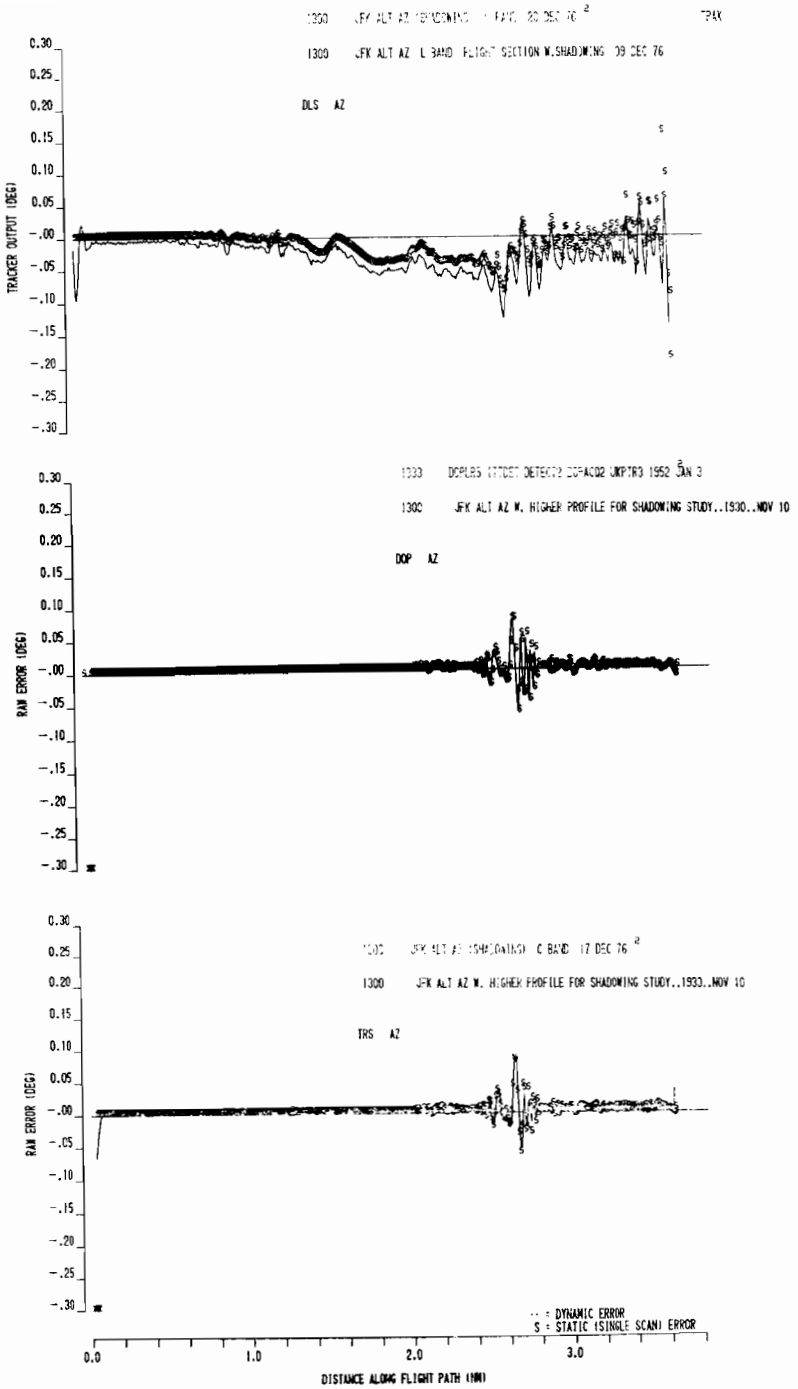

Fig. 2-95. Single-scan and dynamic azimuth errors for scenario 5 (shadowing).

The DLS errors are primarily due to ambiguity resolution breakdown. Also, in this case, the DLS data rate was 15 Hz so that there is less effective motion averaging and/or data editing in the airborne receiver. The DMLS error is due to reference scalloping effects, centerline reference emphasis not being effective in this particular case. The TRSB error represents sidelobe leak through.

In the shadowing portion, diffraction rays from the building edges are the principal multipath threat (the direct signal decrease due to shadowing does not itself directly yield an error). At L band, these rays are $\sqrt{5}$ stronger at a given direct signal - edge separation angle; this is felt to account for much of the error differences in Figs. 2-94 and 2-95 between the C and L band systems. The diffraction rays essentially have zero scalloping rate; consequently, differences between DMLS and TRSB here reflect differences in static error characteristics (e.g., error versus separation angle at fixed M/D level). Since the DMLS and TRS azimuth static error characteristics are quite similar, so are the shadowing errors in this case.

The short spike in the DLS and TRSB error traces at the start of the flight path are due to start up of the trackers in the middle of an orbital characterized by high angle rate of change. The single measurement errors (Fig. 2-95) show no error.

6. Results for Scenario 6

The results for scenario 6 are shown in Figs. 2-96 and 2-97. Scenario 6 is the elevation portion of scenario 1 with a flight path which has a lateral sinusoidal oscillation around the extended runway centerline. For scenario 6,

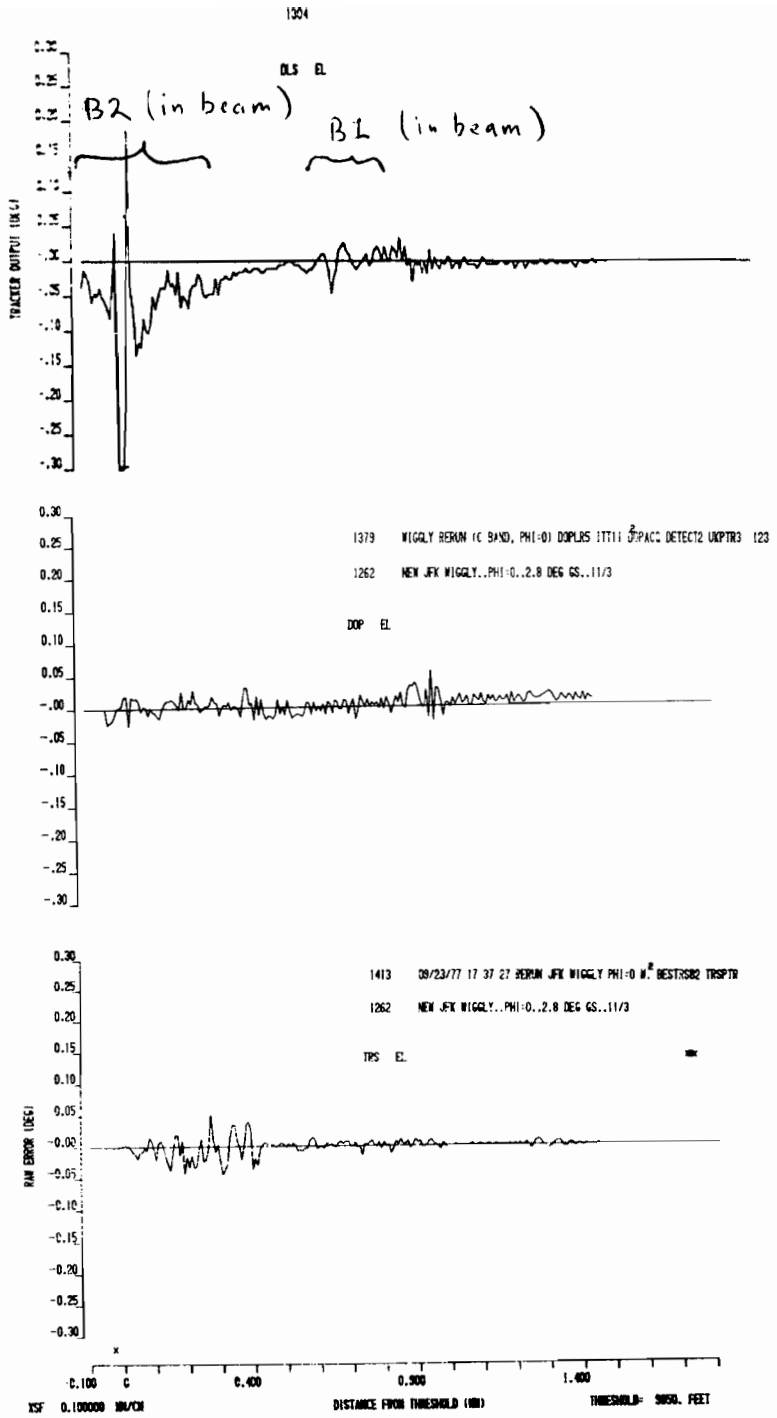

Fig. 2-96. Dynamic elevation errors for scenario 6.

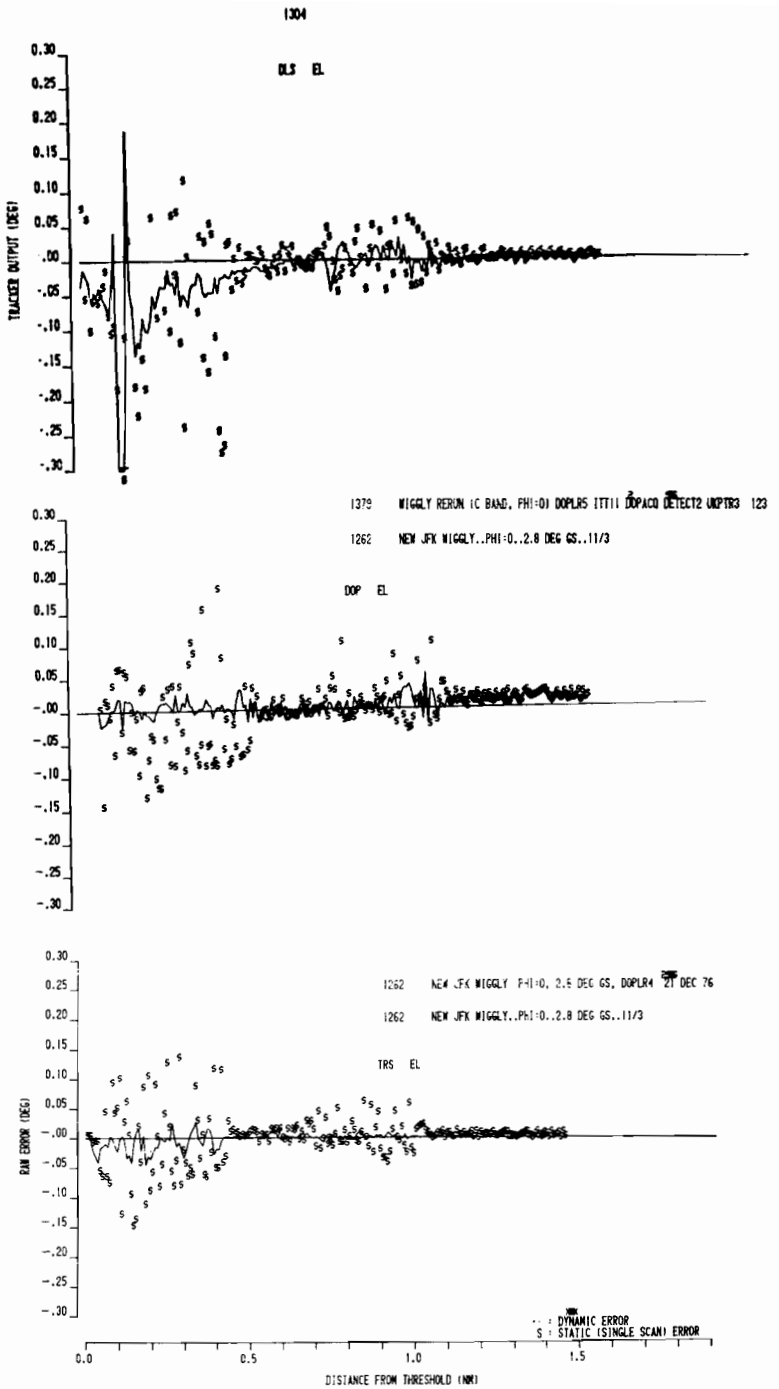

Fig. 2-97. Single-scan and dynamic elevation errors for scenario 6.

the starting phase of the sinusoid is 0°. This yields much the same multipath that occurred in scenario 1 except that the scalloping frequencies and relative rf phases are changed somewhat.

The error waveforms are somewhat changed, but their gross characteristic (e.g., region of peak errors and peak error magnitude) is quite similar to that of scenario 1 (compare, e.g., Fig. 2-96 to Figs. 2-58 and 2-60). The cause of the DLS elevation errors here is the same as that in scenario 1.

7. Results for Scenario 7

The results for scenario 7 are shown in Figs. 2-98 to 2-99. Scenario 7 is identical to scenario 6 except for the starting phase of the receiver sinusoidal lateral displacement (now 120°). The elevation multipath environment is basically that of scenarios 1 and 6.

Again, the error waveform details are different, but their gross characteristics are quite similar to those of scenarios 1 and 6.

8. Results for Scenario 8

The results for scenario 8 are shown in Figs. 2-100 to 2-101. Scenario 8 differs from scenarios 6 and 7 only in the starting phase of the receiver lateral displacement (now 240°). The elevation multipath environment is basically that of scenarios 1, 6 and 7.

Again the error waveform details are different, but the gross characteristics are quite similar to those of scenarios 1, 6 and 7.

9. Sensitivity of DMLS Azimuth Error in Scenario 2 to Elevation Pattern of the Azimuth Array

The elevation pattern used for the DLMS azimuth array in the simulations above was derived from a theoretical pattern* in the U.K. proposal. This pattern has a rolloff at the horizon which is substantially less than that of

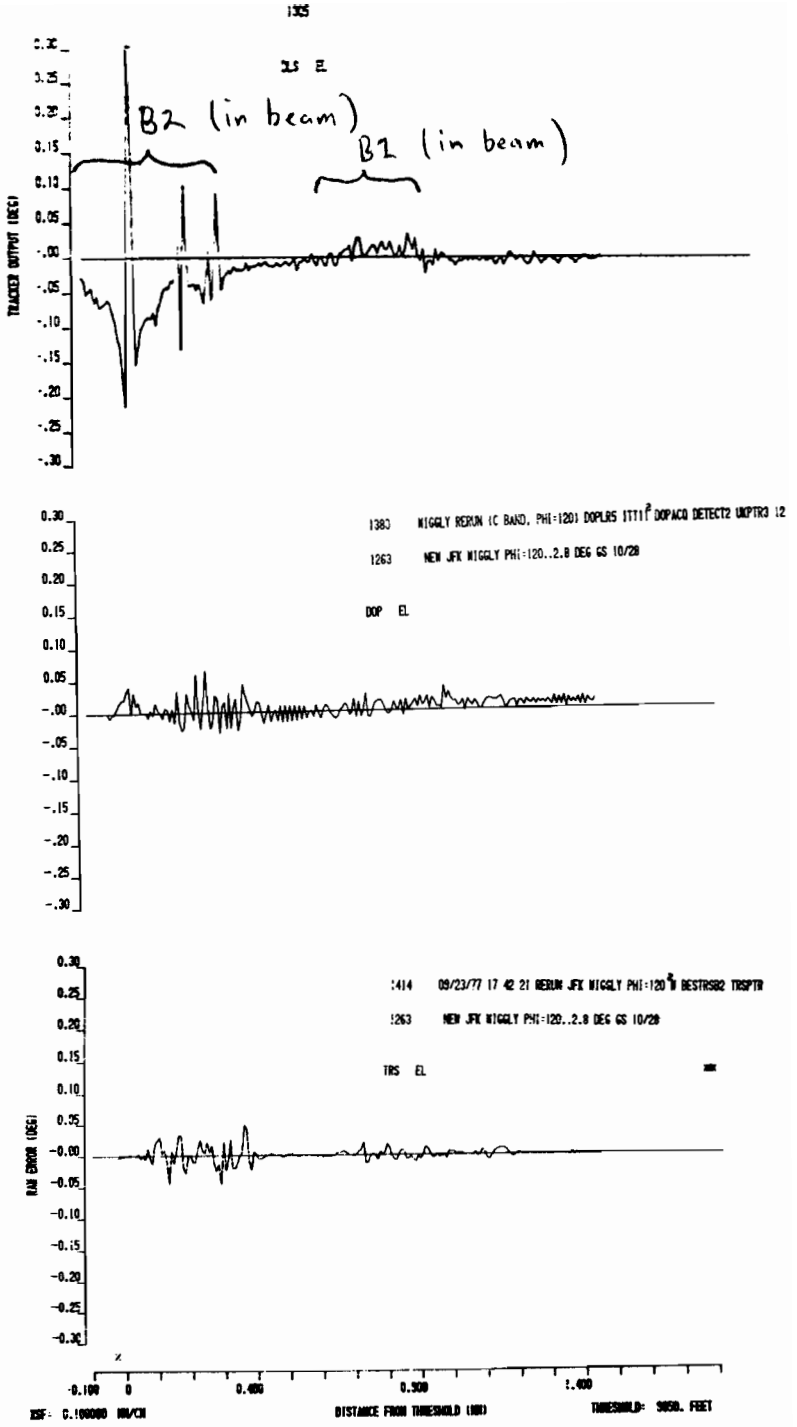

Fig. 2-98. Dynamic elevation errors for scenario 7.

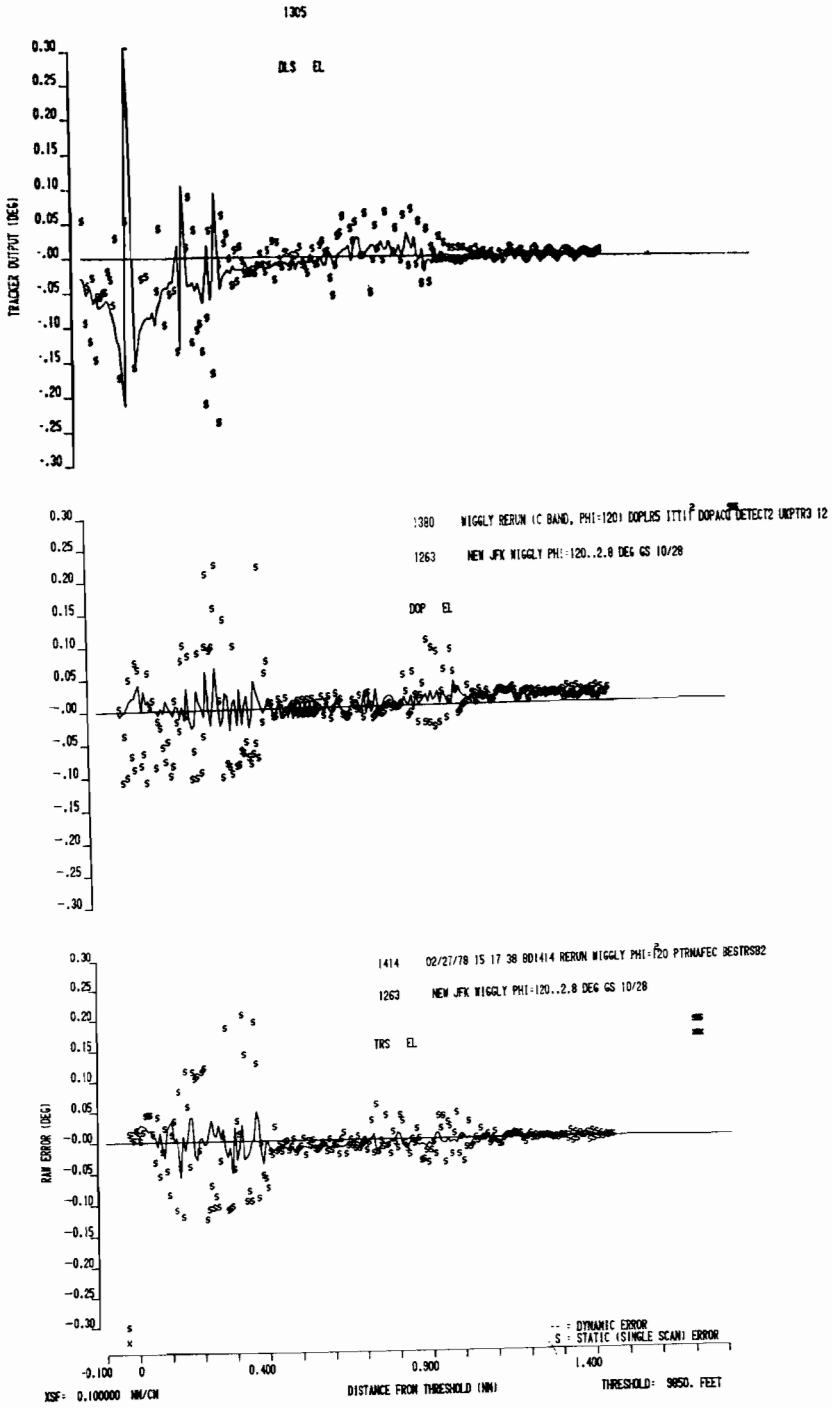

Fig. 2-99. Single-scan and dynamic elevation errors for scenario 7.

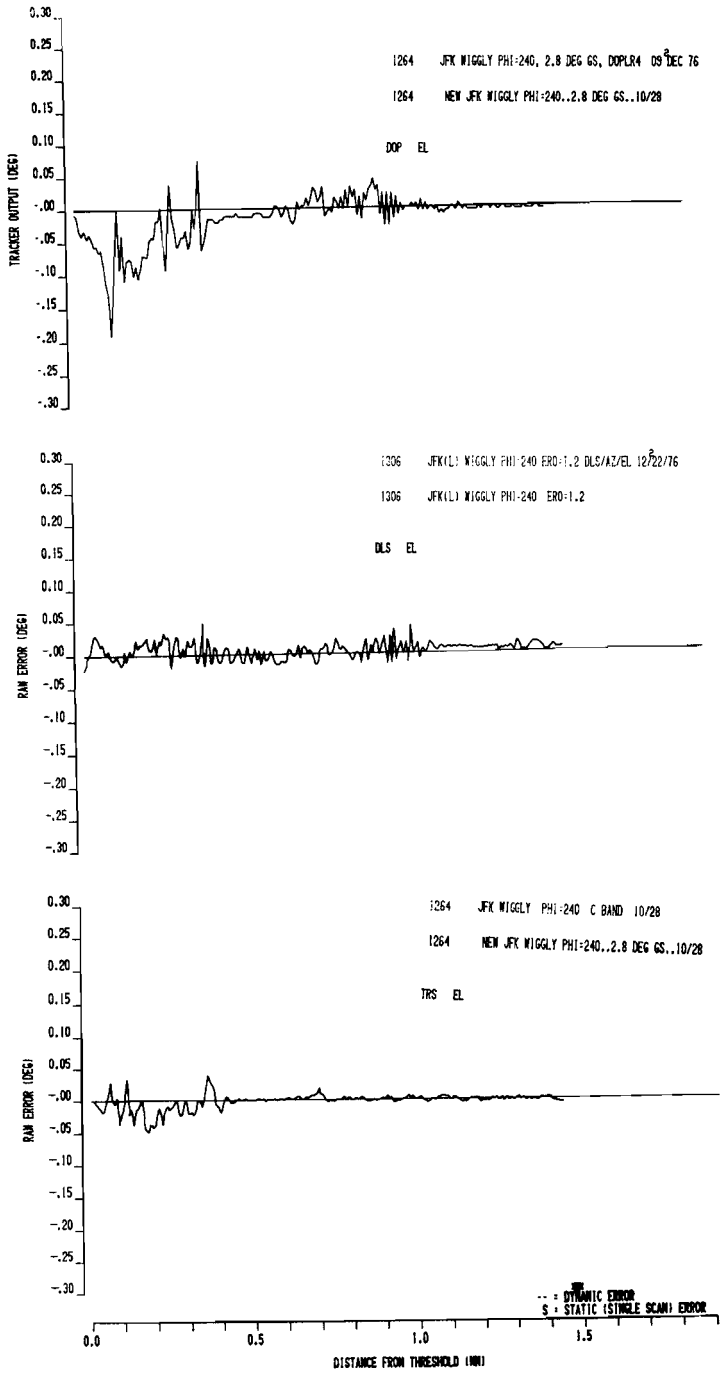

Fig. 2-100. Dynamic elevation errors for scenario 8.

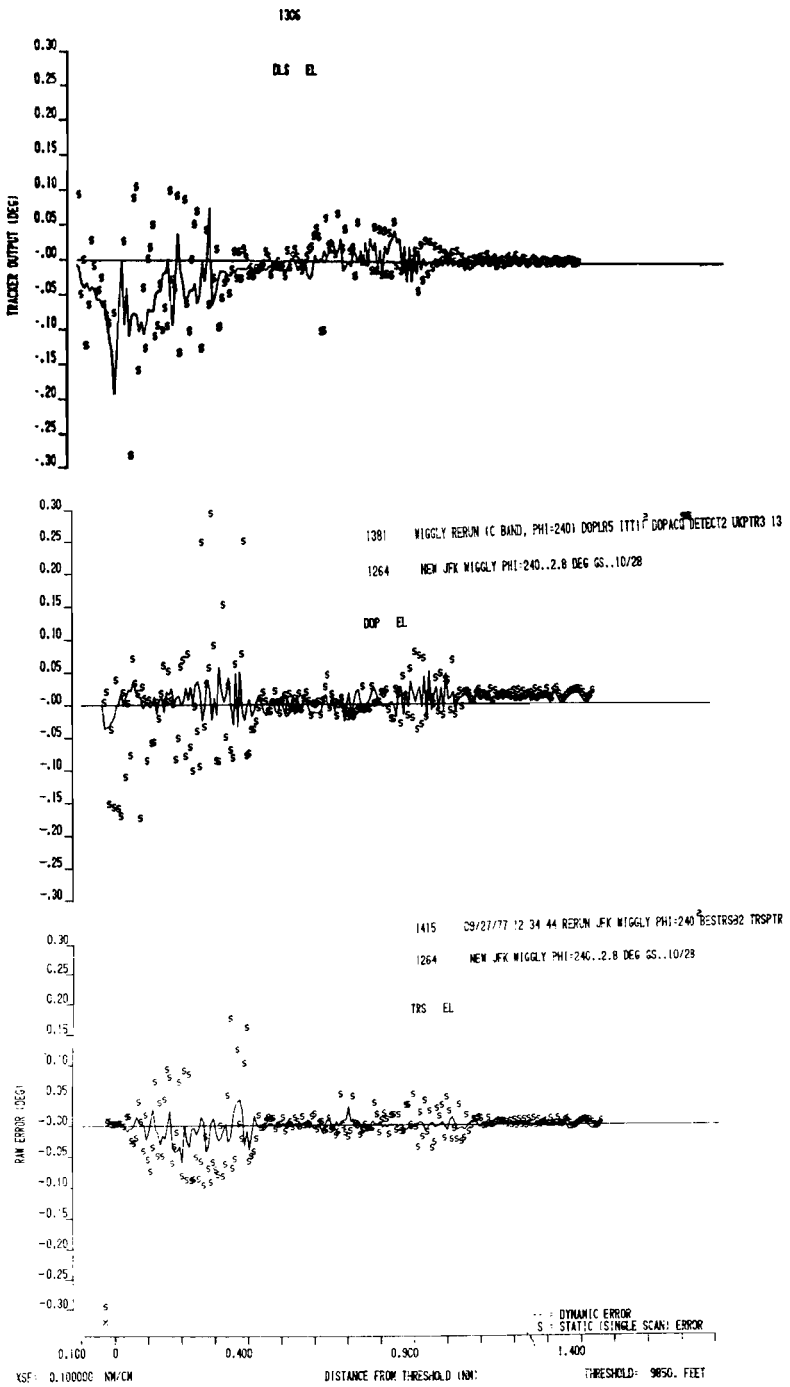

Fig. 2-101. Single-scan and dynamic elevation errors for scenario 8.

the corresponding TRSB pattern (which was derived from measured field patterns). This rolloff plays an important role in determining the extent to which various secondary paths involving ground bounces combine to yield an effective M/D ratio. Since the WG-A cost group assumed identical column radiators would be used for TRSB and DMLS, it seemed appropriate to simulate DMLS in at least one case using the elevation pattern of the TRSB azimuth array.

Scenario 2 with $\varepsilon/\varepsilon_o$ = 1.2 seemed an appropriate choice since (1) the elevation angles here are small enough to yield significant changes in multipath and (2) this scenario was the object of considerable controversy. Figures 2-102 and 2-103 compare the azimuth simulation results using the elevation pattern of the UK proposal to those using the TRSB elevation pattern. We see that the peak errors near 0.35 nmi are reduced approximately 30% whereas those near 0.05 nmi are little changed. This suggests that the M/D levels near 0.35 nmi were increased by fading on the direct signal due to the specular ground reflection whereas such fading was not present near 0.05 nmi.

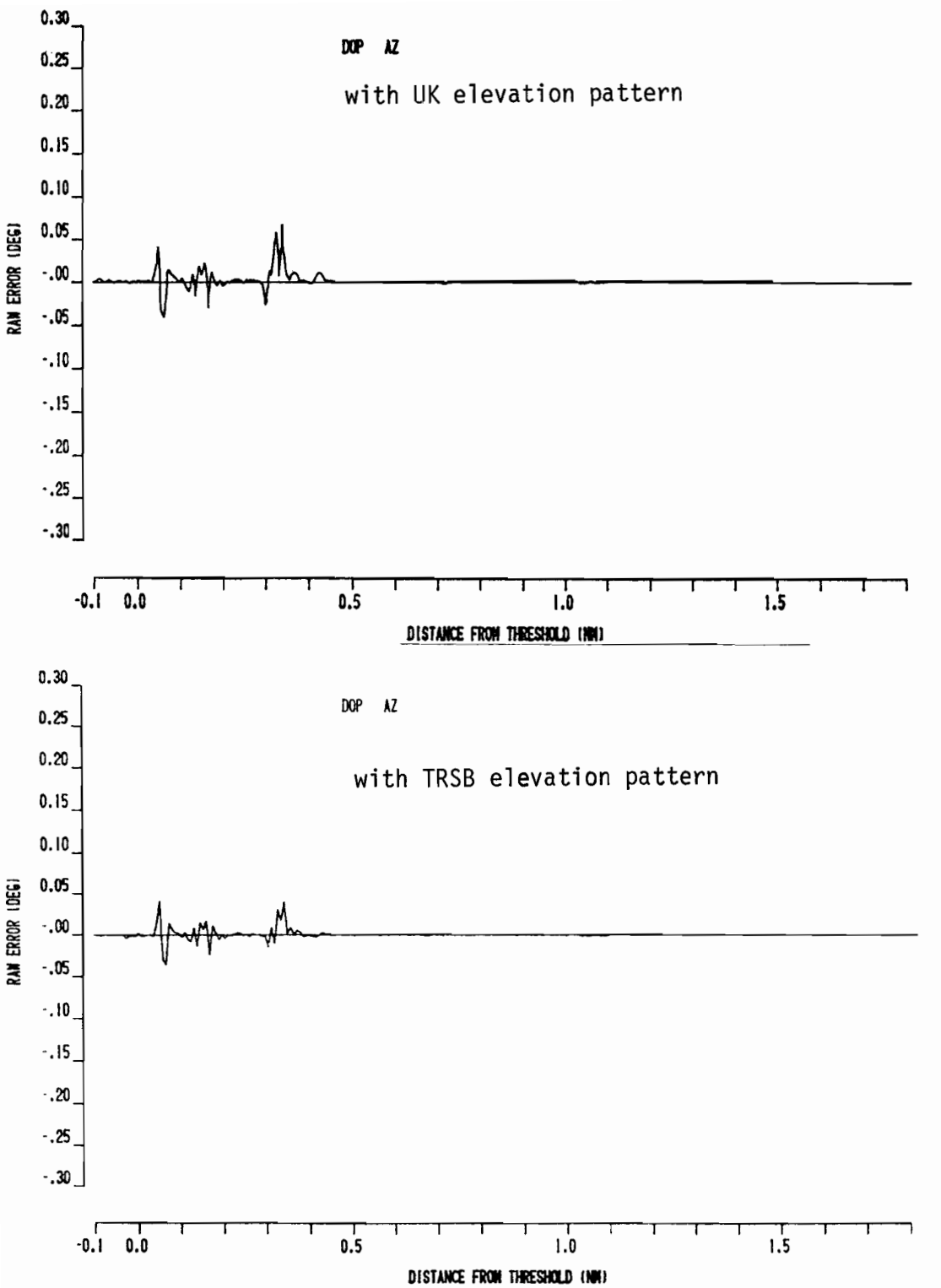

Fig. 2-102. Raw DMLS AZ error for scenario 2; $\varepsilon/\varepsilon_0 = 1.2$.

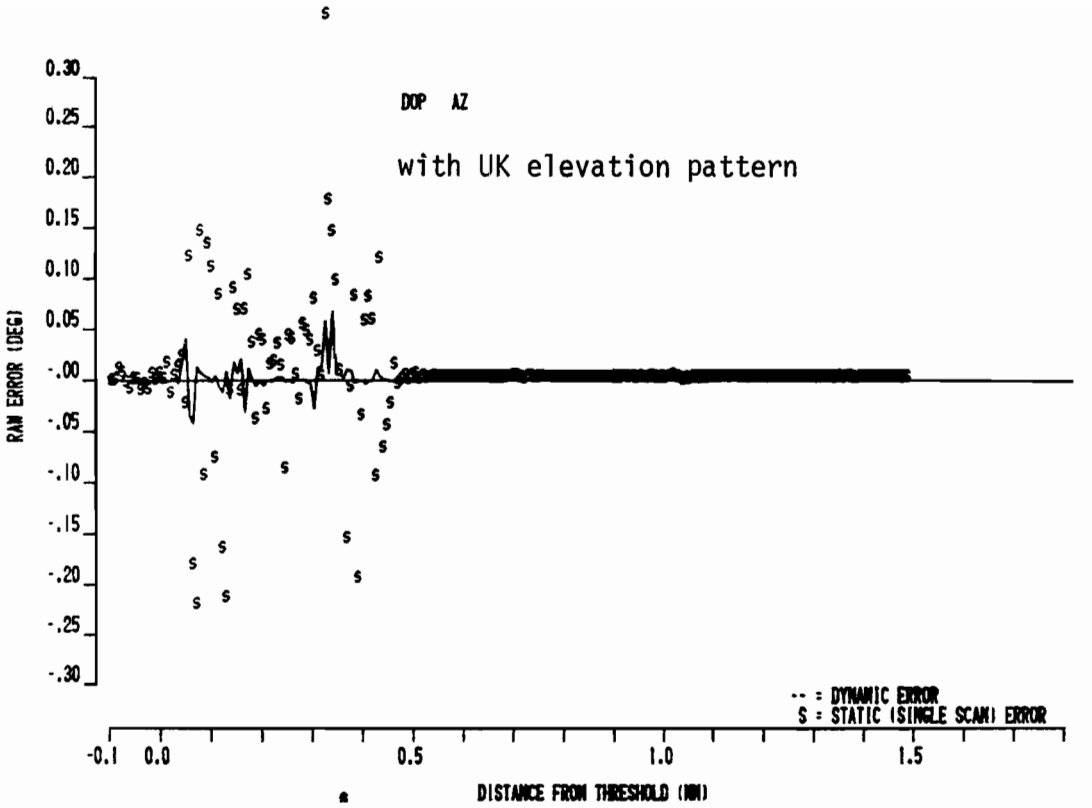

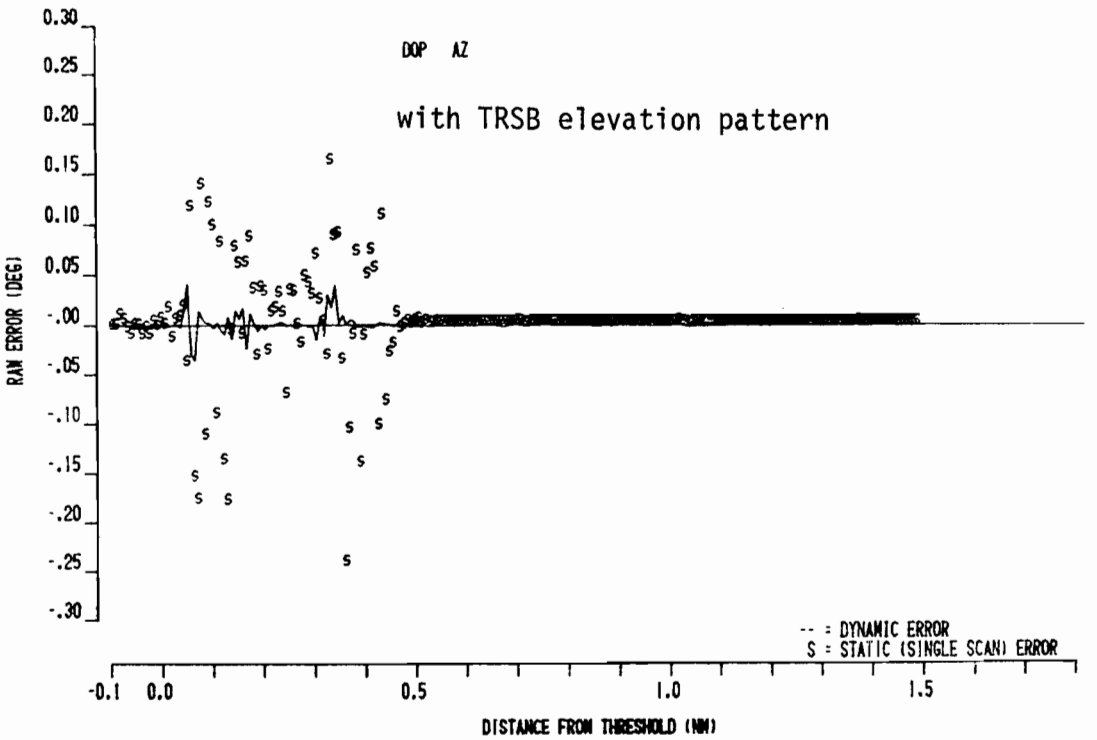

Fig. 2-103. Dynamic and single scan errors for scenario 2; $\varepsilon/\varepsilon_o$ = 1.2.

III. ADDITIONAL COMPARATIVE SCENARIOS SUGGESTED BY INDIVIDUAL AWOP MEMBERS

The "standard" AWOP comparative scenarios discussed in the previous chapter were developed by the panel to explore the sensitivity of the various systems to in-beam and out-of-beam multipath. However, due to the differences in system features such as antenna patterns, motion averaging, etc., a scenario that was stressful for one technique might not be stressful for the others. To explore the behavior of specific systems in stressful situations, various panel members suggested additional scenarios for simulation.

In this chapter, we present several of these additional scenarios which focus on reflection phenomena. The first pair of scenarios, due to T. Hagenberg [115] of the Netherlands, is intended to explore possible sensitivity of the TRSB system to building multipath. The second set of scenarios, presented by T. Bohr [116] of the Federal Republic of Germany (FRG), are intended to explore the sensitivity of CW systems (DMLS and TRSB) to terrain reflection multipath in a mountainous environment.

A. Hagenberg Building Reflection Multipath Scenarios

1. Considerations Used by T. Hagenberg in Developing the "TRSB Stressful" Scenarios

T. Hagenberg's memo VV-77-041 [115] characterizes the unfavorable multipath factors for TRSB as follows:

"The performance of TRSB might be critical, if the multipath meets some conditions:

A. The multipath preferably must be in-beam (in main beam or in side lobe) with a high level.

B. The scalloping frequency must be lower than 1 Hz or must be situated in a frequence grating lobe.

C. The multipath region of different reflectors preferably must coincide.

D. The duration of the multipath phenomenon must be sufficiently long.

ad A.

For the azimuth subsystem, in-beam multipath along centre line originates from ground reflections in the antenna main beam or from buildings in the antenna side lobes. The peak angle error caused by reflections in a side lobe is given by:

$$\varepsilon = \frac{M}{D}\,\frac{1}{2}\,\phi_o \qquad (3\text{-}1)$$

in which

$\frac{M}{D}$: the multipath to direct signal ratio.

Γ : the side lobe to main beam antenna gain ratio

ϕ_o: beamwidth of the antenna main beam.

ad B.

The scalloping frequency f_s is given by

$$f_s = \frac{v}{\lambda}\,(1 - \cos\beta) \qquad (3\text{-}2)$$

in which

v : speed component to ground antenna

λ : wave length of the signal transmitted

β : angle between the line segments ground antenna-aircraft and reflector-aircraft

ad C.

The geometry of the reflectors must be such that the multipath of these reflectors coincides with the (extended) runway centerline.

ad D.

The duration of the multipath phenomena is dependent on aircraft

groundspeed and the extension of the multipath region."

2. Multipath Scenarios As Described in Memo VV-77-041 by T. Hagenberg [115]

The airport scenarios are derived from the existing AWOP WG-A scenarios. The equipment siting, the flight profiles and the multipath scatter characteristics of the buildings, aircraft and ground will be the same as the original AWOP WG-A scenarios [66, 72]. The modifications incorporated meet the OCL criteria set in ICAO annex 14 [117].

(a) Scenario for elevation multipath

The new scenario for elevation multipath is based on AWOP WG-A scenario 1 (Kennedy Airport New York) with the following modifications (Fig. 3-1).

- From the existing geometry omit buildings 1, 2, 3, 4 and 5.
- Add two buildings with the following coordinates of the frontplane

  Building A: (9700, -900) (10700, -952) height 70 ft.

  Building B: (11300, 1250) (12140, 705) height 40 ft.

In figure 3-1 the location of the buildings A and B is shown and the region along the extended runway centerline where multipath can be expected. In this region the scalloping frequency will lie in a frequency grating lobe for an aircraft groundspeed of 130 kts.

(b) Scenario for azimuth multipath

The new scenario for azimuth multipath is based on AWOP WG-A scenario 1 (Los Angeles International Airport) with the following modifications (Fig. 3-2).

Three buildings are added to the existing geometry. The coordinates of the frontplates of the buildings are:

Building A: (1500, -1300) (2486, -1468) height 120 ft.

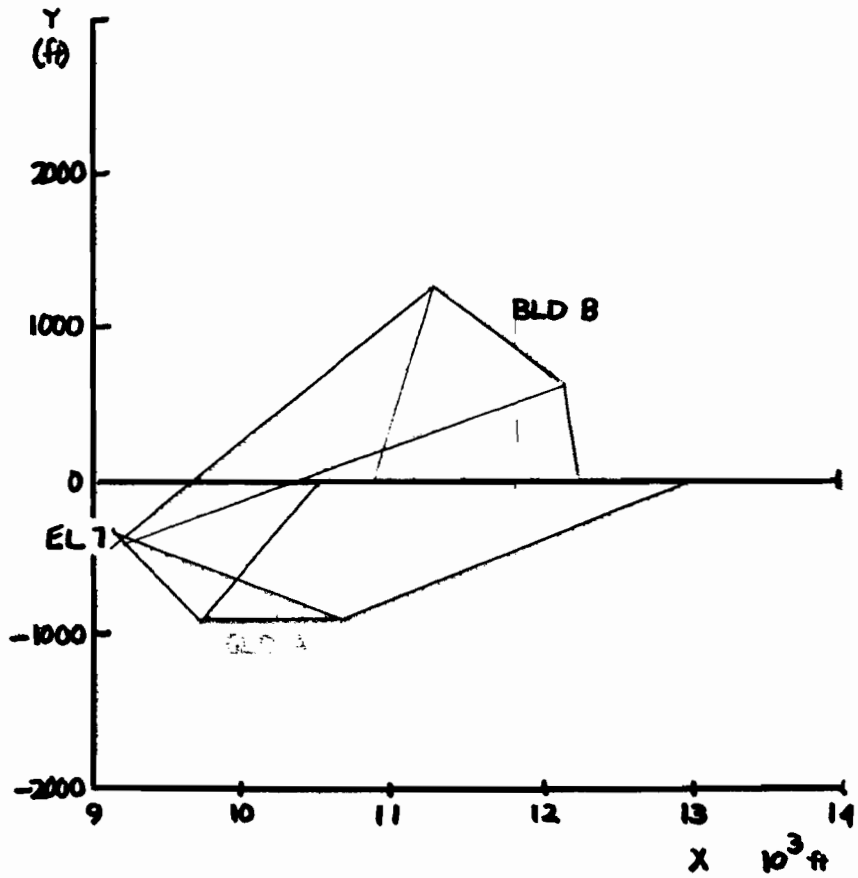

Fig. 3-1. Modification to AWOP WG-2 scenario 1 for elevation multipath (from [12]).

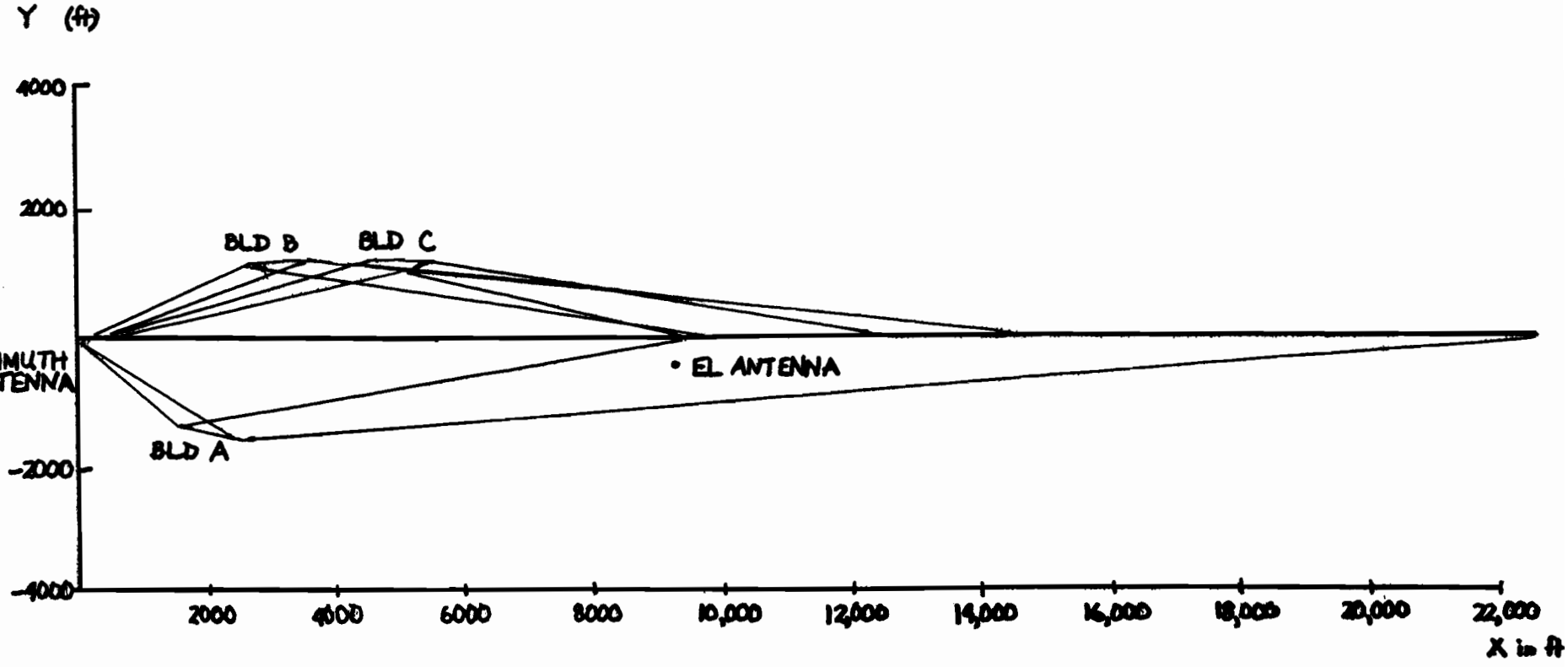

Fig. 3-2. Modifications to AWOP WG-2 scenario 2 for azimuth multipath (from [12]).

Building B: (2600, 1150) (3579, 1228) height 100 ft.

Building C: (4500, 1150) (5499, 1184) height 100 ft.

Incorporate longitudinally upsloping terrain with a slope of 0.8% from x = 5500 ft. up to x = 10,000 ft. The elevation of the original buildings and aircraft has to increase in accordance with the increased terrain elevation (due to the sloping terrain).

The location of the buildings A, B and C and the region along the extended runway centerline where the multipath can be expected is shown in figure 3-2.

In this region the multipath scalloping frequencies of the added buildings will lie in a frequency grating lobe for an aircraft groundspeed of 130 kts. The scalloping frequency of the ground reflections will be so low (<1 Hz) that motion averaging has no effect on performance improvement anymore.

3. Elevation Multipath Scenario Results

Simulations were made for five elevation scenarios based on the scenario 1 description above in section B. The building locations and flight paths were identical in all cases; however, several choices of building heights were considered as shown below.

Version	Building Heights
1	as described in Section B
2	meeting ICAO OCL criteria
3	as in 2 except heights of Hagenberg's building B and original building 3 were increased to 150 ft. and 64 ft. respectively

It is our understanding that ICAO annex 14 obstruction clearance criteria [117] for class A, B, and C runways calls for a clear zone with edges parallel to runway centerline and extending some 200 feet beyond each threshold. The edges parallel to the centerline are 500 feet away from centerline. To the side of the clear zone, there is a transitional region which slopes upward and outward at a slope of 1:7 as measured in a vertical plane perpendicular to runway centerline. Thus, the obstruction clearance height corresponding to a building which is at threshold at a distance y from centerline is to yield:

$$h_{OCL} = \begin{cases} \frac{1}{7} & (|y| - 500 \quad |y| > 500' \\ 0 & |y| < 500 \end{cases} \qquad (3\text{-}3)$$

Applying (1) to building A in section III we obtain h_{OCL} = 57 feet whereas the scenario description calls for a building height of 70 feet.

The multipath levels and errors due to Hagenberg's building A were essentially identical for all three versions. Hagenberg's building B did not yield significant multipath nor errors with versions 1 and 2 due to the aircraft flying above the specular region. Since the scalloping frequencies associated with the multipath from buildings B2 and B3 were much higher than that for building B1 and the scalloping frequencies in the AWOP scenarios, it seemed useful to explore the TRSB capability to resist high level in-beam multipath at such scalloping rates. Therefore, the heights of Hagenberg's building B and the original scenario's building 3 were increased substantially to insure the aircraft would not fly over the respective specular regions. Specifically, the height of Hagenberg's building B was increased to 150 ft. (110 ft. in violation of the ICAO OCL criteria!) while that of original

building 3 was increased to 64 ft.

Figure 3-3 shows the airport map while figure 3-4 shows the computed elevation multipath characteristics. We see that the Hagenberg objective of simultaneous high level in-beam multipath was achieved with the increased building heights.

Figures 3-5 and 3-6 show the computed TRSB and DMLS errors for this scenario. It was found that single scan errors are higher than those for scenario versions with lower building heights, but that dynamic errors are quite similar. This suggests that the multipath errors due to Hagenberg's building B were effectively eliminated by motion averaging for both systems.

The results for this scenario are in accordance with the analytical studies and bench test data presented in volume II of this report. Figures 3-7 and 3-8 show the static error versus separation angle curves for TRSB and DMLS. These plots show the in-beam region to be approximately ±1.7° around the direct signal. There is a relatively high DMLS sidelobe at -8° separation angle which results in the ground reflection sidelobe error just after threshold in the DMLS error plots.*

The elevation multipath from building B1, B2 and B3 is of high level and in-beam. To understand the resulting receiver errors, we must consider the system error characteristics in a dynamic environment (i.e., when the scalloping frequency is non-zero).

Figures 3-9 and 3-10 show the dynamic elevation in-beam multipath error versus scalloping frequency for TRSB and DMLS respectively. Also shown in these figures are the scalloping frequencies associated with the multipath

---

*The flight path flown had a 2.86° planar elevation angle. Hence, near threshold, the separation angle in conical coordinates became greater than 2 x 2.86° = 5.92°.

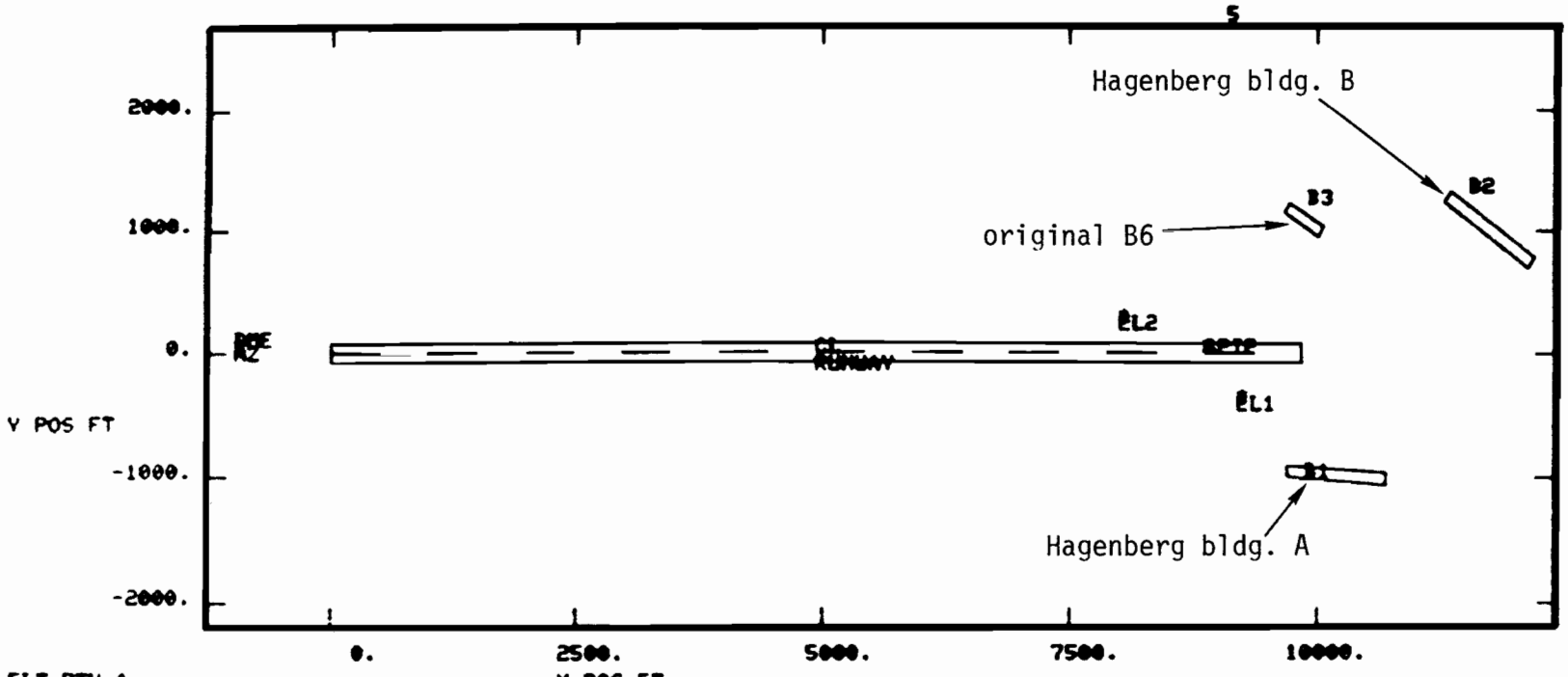

FLT PTH A

AZ SYSTEM

OBST	RANK	AMP	DIST	RDOP
G	1	0	10312.0	0.
B1	4	-43	7332.7	-114.
B2	2	-2	7025.3	-756.
B3	3	-5	8649.9	-653.
D	0	-80	0.0	0.

EL SYSTEM

OBST	RANK	AMP	DIST	RDOP
G	1	-1	9511.7	0.
B1	2	-3	7464.4	-140.
B2	3	-4	6761.9	-1060.
B3	4	-31	9186.9	-1102.
D	0	-80	0.0	0.

AMP = peak M/D ratio (in dB)

DIST = distance along flight path at point of peak M/D = 18850 - x

RDOP = scalloping frequency in Hz at point of peak M/D ratio.

Fig. 3-3. Airport map for scenario 1-E.

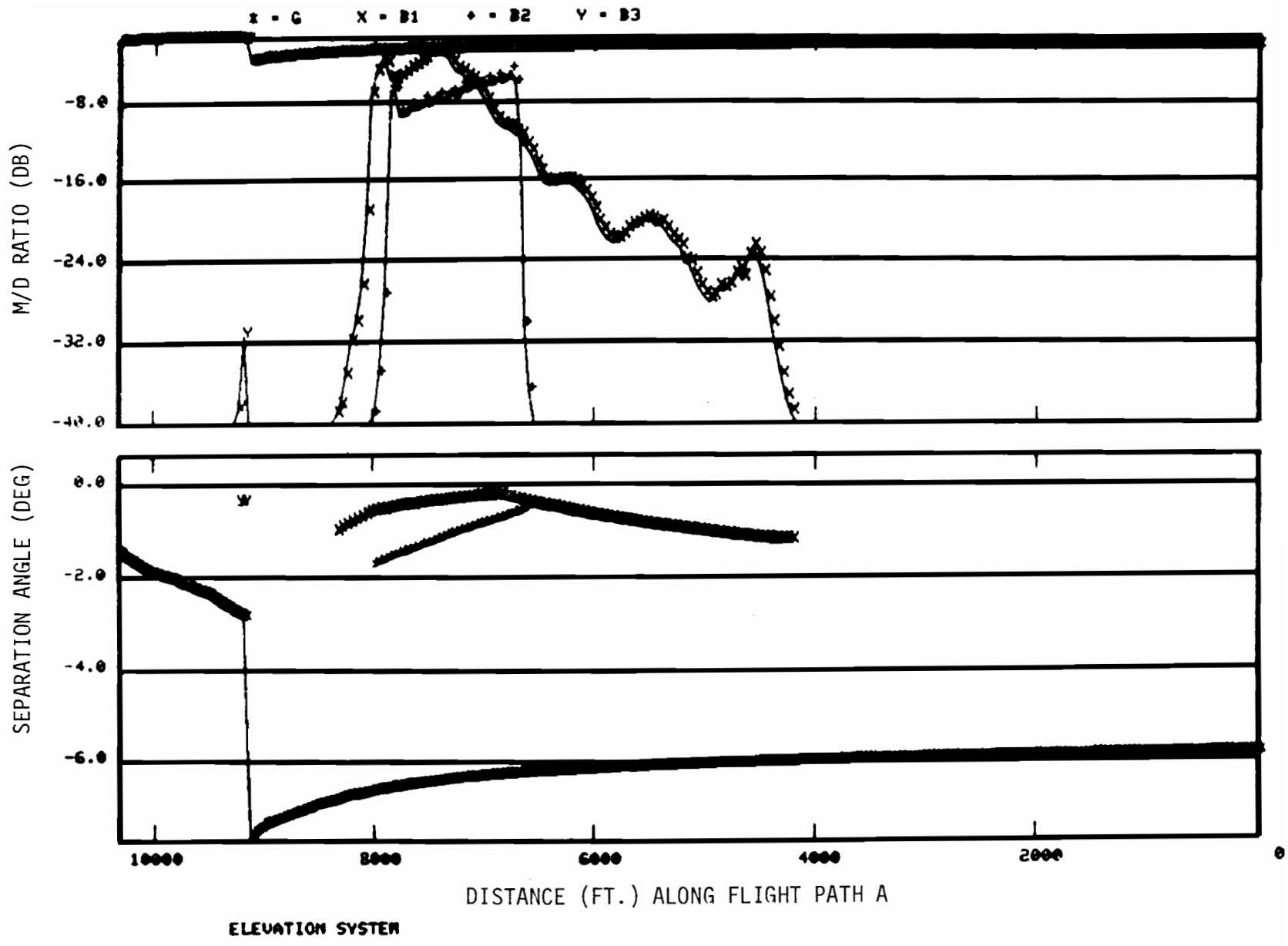

Fig. 3-4. Elevation multipath characteristics for scenario 1-E.

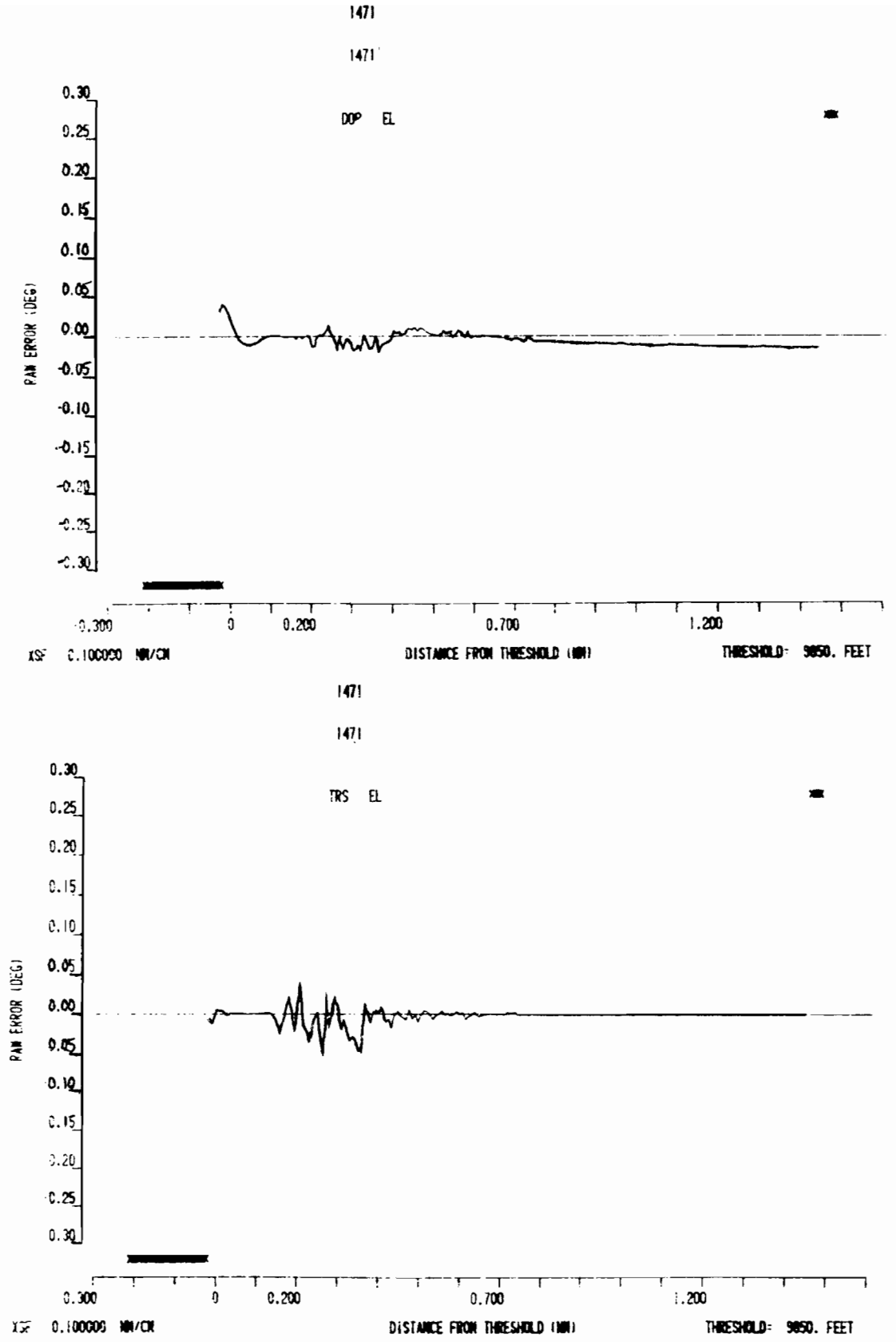

Fig. 3-5. Dynamic elevation errors for scenario 1-E.

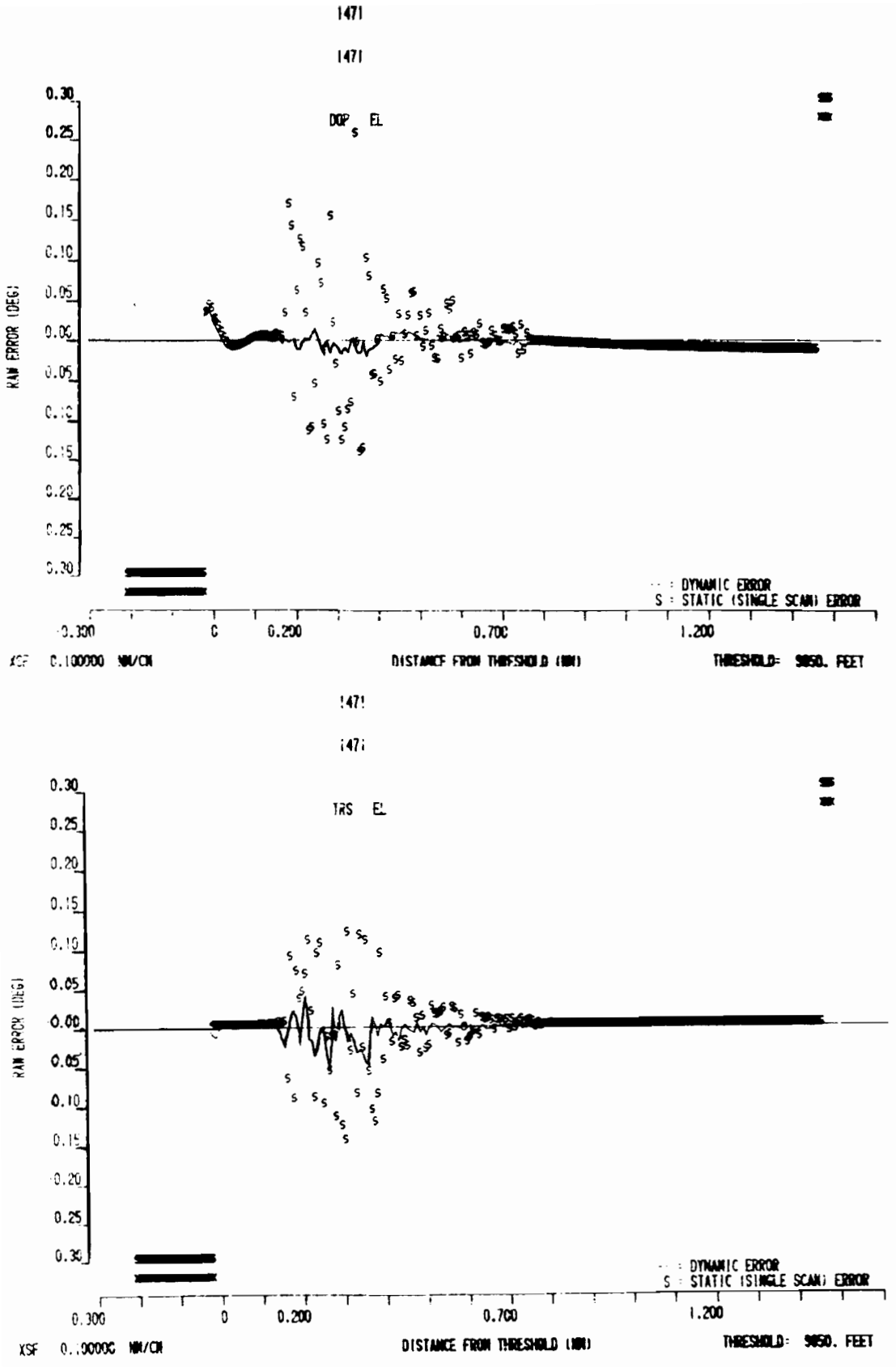

Fig. 3-6. Dynamic and single-scan elevation errors for scenario 1-E.

Bench Tests on Bendix Phase III Receiver P101

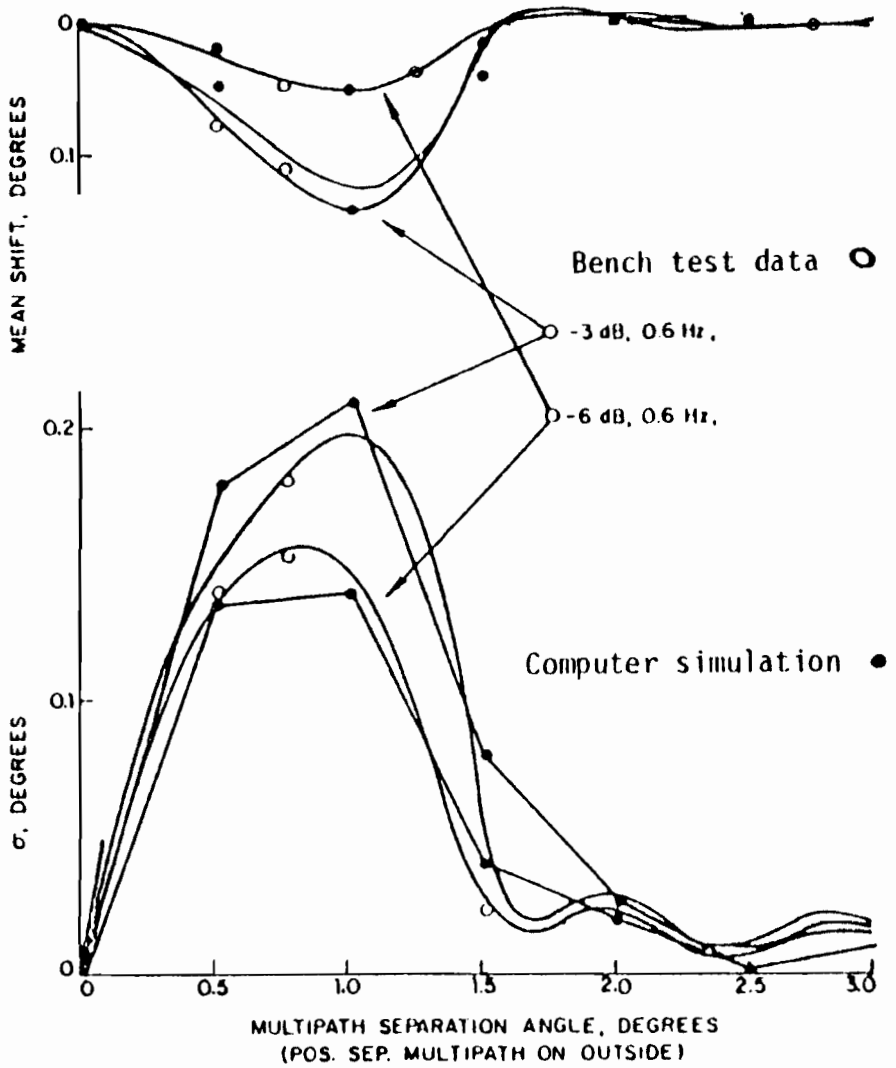

Fig. 3-7. Comparison of TRSB bench test data and computer model for inbeam multipath.

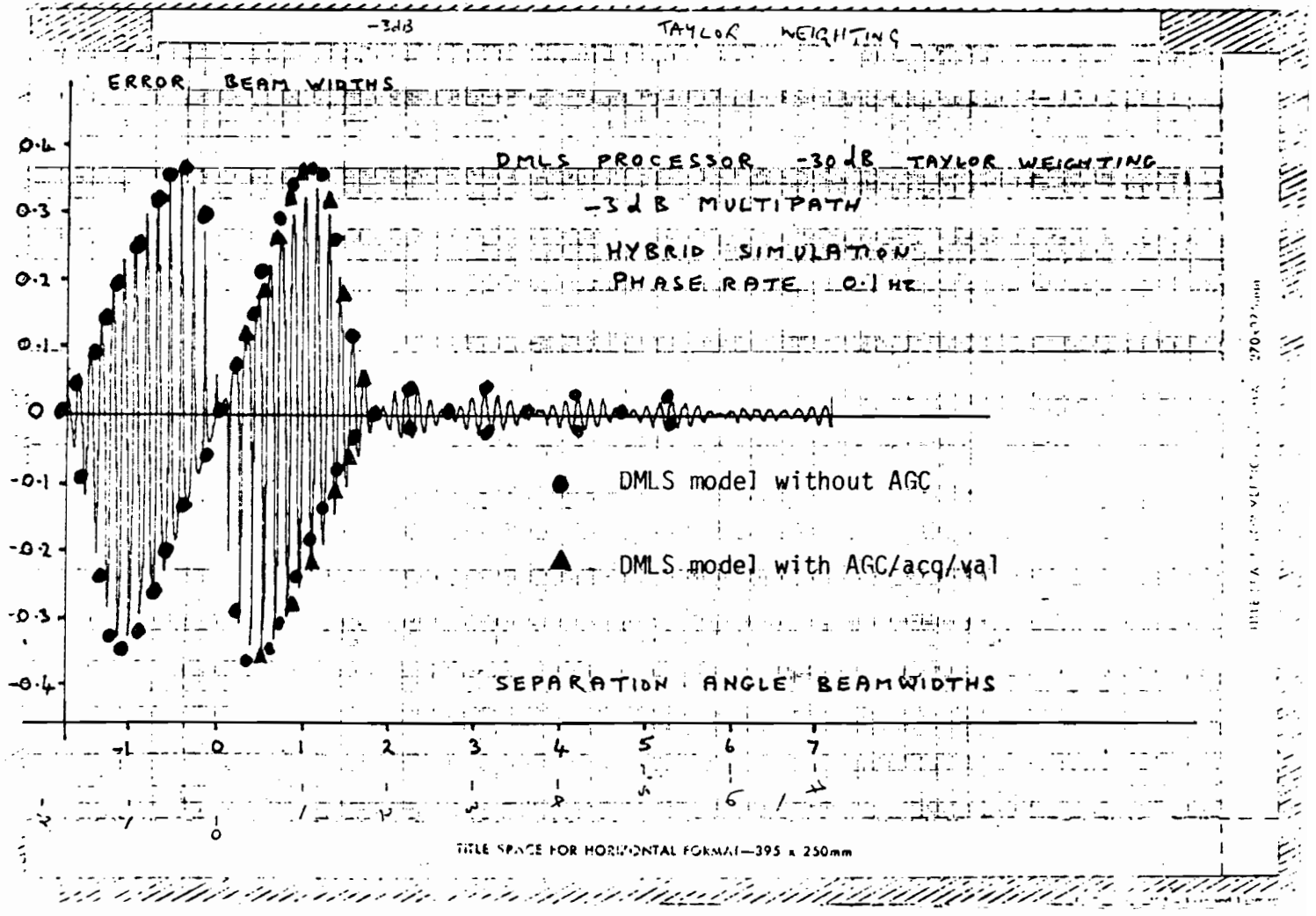

Fig. 3-8. Comparison of DMLS computer models with RAE hybrid bench simulator static data.

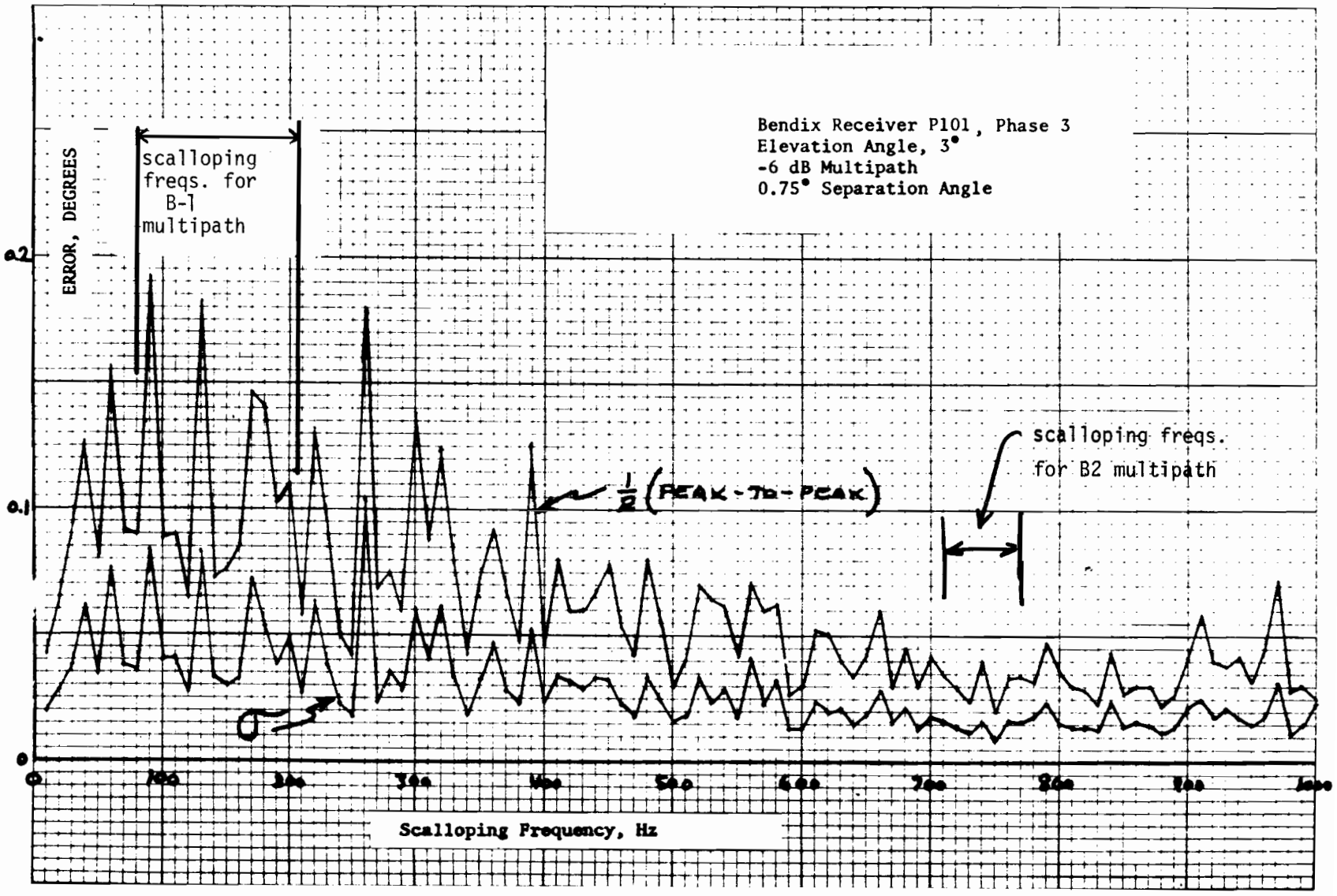

Fig. 3-9. Scalloping frequency results (from [93]).

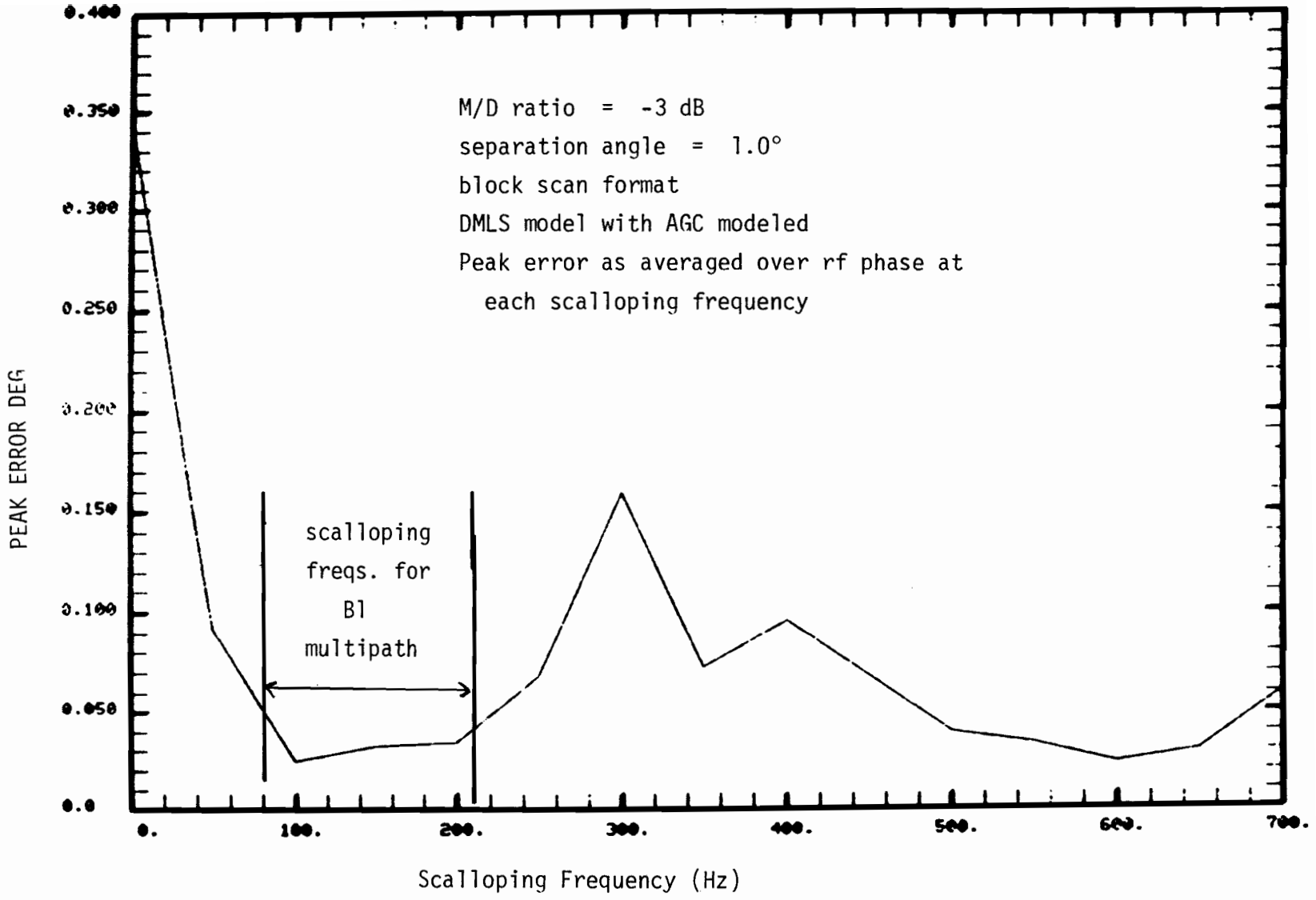

Fig. 3-10. Dynamic inbeam elevation error for DMLS.

from buildings B1 and B2. The general reduction in TRSB error at high scalloping frequencies (e.g., above 600 Hz) arises from the motion averaging between the to-and-fro scans of a single TRSB angle measurement.

The multipath from B1 encompasses several of the TRSB motion averaging "grating lobes" which occur at multiples of 40.5 Hz, [28], but lies between the DMLS motion averaging "grating lobes" at 0 - 15 Hz and 400 Hz. Since B1 was the dominant error source for the scenarios, it is not surprising that the DMLS errors due to multipath were generally lower than those of TRSB.

4. Azimuth Multipath Scenario Results

Simulations were made for several azimuth scenarios based on the scenario description in section 2. The flight path and building heights were the same in all cases; however, several building locations were considered as shown below:

Version	Buildings and runway Slope Locations
1	Section B text as applied to previous coordinate system of Chapter II.
2	From figure 2 in Hagenberg report [115].

The building location differences arise because the numerical values given in [115] for building locations were presumed to apply to the AWOP scenarios described in [72] in which the point (0, 0, 0) corresponds to the stop end of the runway. However, in figure 3-2, it appears that the point (0, 0, 0) is beneath the azimuth array which is the point (-1000, 0, 0). To ensure a full investigation of the effects, both possible locations were simulated. Both versions gave similar results; version 2 will be discussed here.

The original AWOP scenario based on Los Angeles included a humped runway, whereas the modified scenario has a runway which slopes upward towards threshold. The multipath from the rectangular plates used to model the runway sections was computed using the same algorithms [29] that are used to compute scattering from the plates used to model buildings, except that only the path transmitter-plate-receiver was considered [29]. This permitted the multipath from each runway section to be displayed in the multipath diagnostic plots and act as separate input to the receiver models.

There were a total of seven buildings and four aircraft in the original AWOP scenario. Program limitations at the time these scenarios were run permitted a total of 10 plates to be simulated, thus it was necessary to drop out two of the original buildings (B5 and B7) which did not yield significant multipath. The locations of the remaining buildings were unchanged; however, the heights of the building and aircraft bases were increased to be the same height as the nearest section of the runway in accordance with Hagenberg's memo. This yielded the following building base elevations:

Building or Aircraft in Present Simulation	Building or Aircraft Origin	Base Elevation*
B1	Previous B1	0
B2	Previous B2	0
B3	Previous B3	0
B4	Previous B6	13
B5	Previous B7	21
B6	Hagenberg bldg. A	0
B7	Hagenberg bldg. B	0
B8	Hagenberg bldg. C	0
A1	Previous A1	2.4
A2	Previous A2	10.4
A3	Previous A3	26.6
A4	Previous A4	27.2

*elevation = 0 ft. is terrain beneath azimuth array

The airport map for version 2 of the scenario is shown in figure 3-11 and the computed azimuth multipath diagnostics are shown in figure 3-12. Figures 3-13 and 3-14 show the computed TRSB and DMLS errors using the "most capable" filled array implementations. Figures 3-15 and 3-16 show the computed TRSB and DMLS errors using the "lesser capability" thinned array implementations.

The peak errors for version 2 of the scenario were very similar to those shown in figs. 3-13 to 3-16 except that the region of greatest errors was 0.40 nmi before the runway threshold. This displacement in error region is approximately twice the longitudal difference in the assumed location of Hagenberg's buildings A and B. Hagenberg's building C gave very low multipath levels in all cases because the aircraft flew above the specular reflection level.

The result for this scenario is generally in accordance with the bench

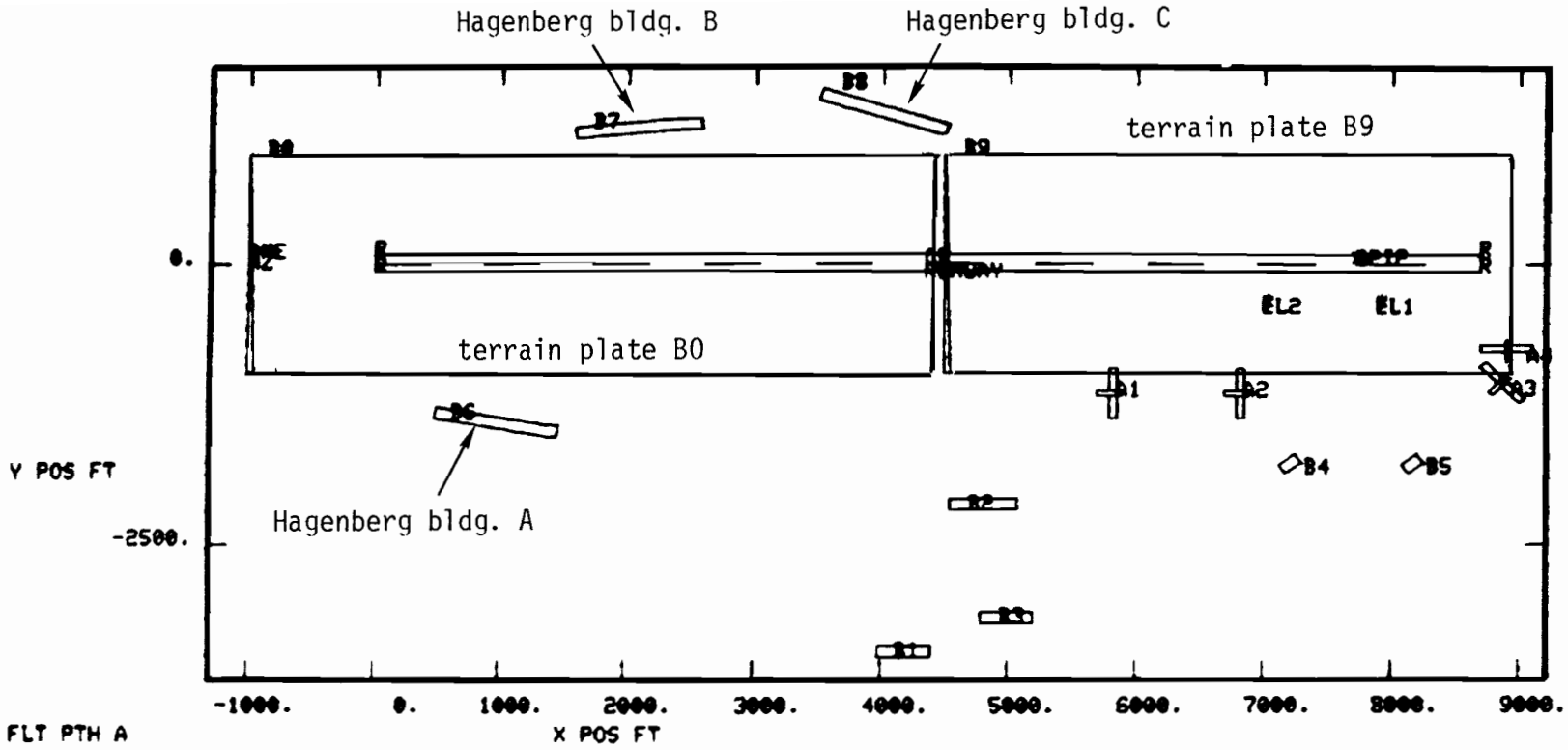

FLT PTH A

AZ SYSTEM

OBST	RANK	AMP	DIST	RDOP
G	15	-80	0.0	0.
B1	7	-3	7991.3	-173.
B2	4	-1	7376.6	-69.
B3	6	-2	7025.3	-130.
B4	12	-42	10010.1	-832.
B5	8	-4	9352.4	-978.
B6	3	-1	9132.8	-23.
B7	5	-1	8298.6	-17.
B8	13	-54	10010.1	-69.
B9	1	+1	8430.3	0.
B0	2	0	2766.3	0.
A1	11	-22	4873.9	-14.
A2	10	-21	9484.1	-225.
A3	9	-18	9132.8	-1301.
A4	14	-68	8957.2	-1333.
D	0	-80	0.0	0.

EL SYSTEM

OBST	RANK	AMP	DIST	RDOP
G	15	-80	0.0	0.
B1	11	-69	7508.3	-137.
B2	7	-63	7157.1	-62.
B3	9	-66	7376.6	-146.
B4	5	-59	8825.5	-263.
B5	4	-50	9703.6	-1167.
B6	10	-67	5927.7	-6.
B7	13	-69	7552.2	2.
B8	14	-70	9703.6	20.
B9	1	0	9659.7	-1.
B0	3	-39	0.0	0.
A1	8	-64	0.0	-4.
A2	6	-62	351.3	-6.
A3	2	-22	9176.7	-1186.
A4	12	-69	9001.1	-1284.
D	0	-80	0.0	0.

AMP = peak M/D ratio (in dB)

DIST = distance along flight path at point of peak M/D = 17500 - x

RDOP = scalloping frequency in Hz at point of peak M/D ratio

Fig. 3-11. Airport map for scenario 2-C.

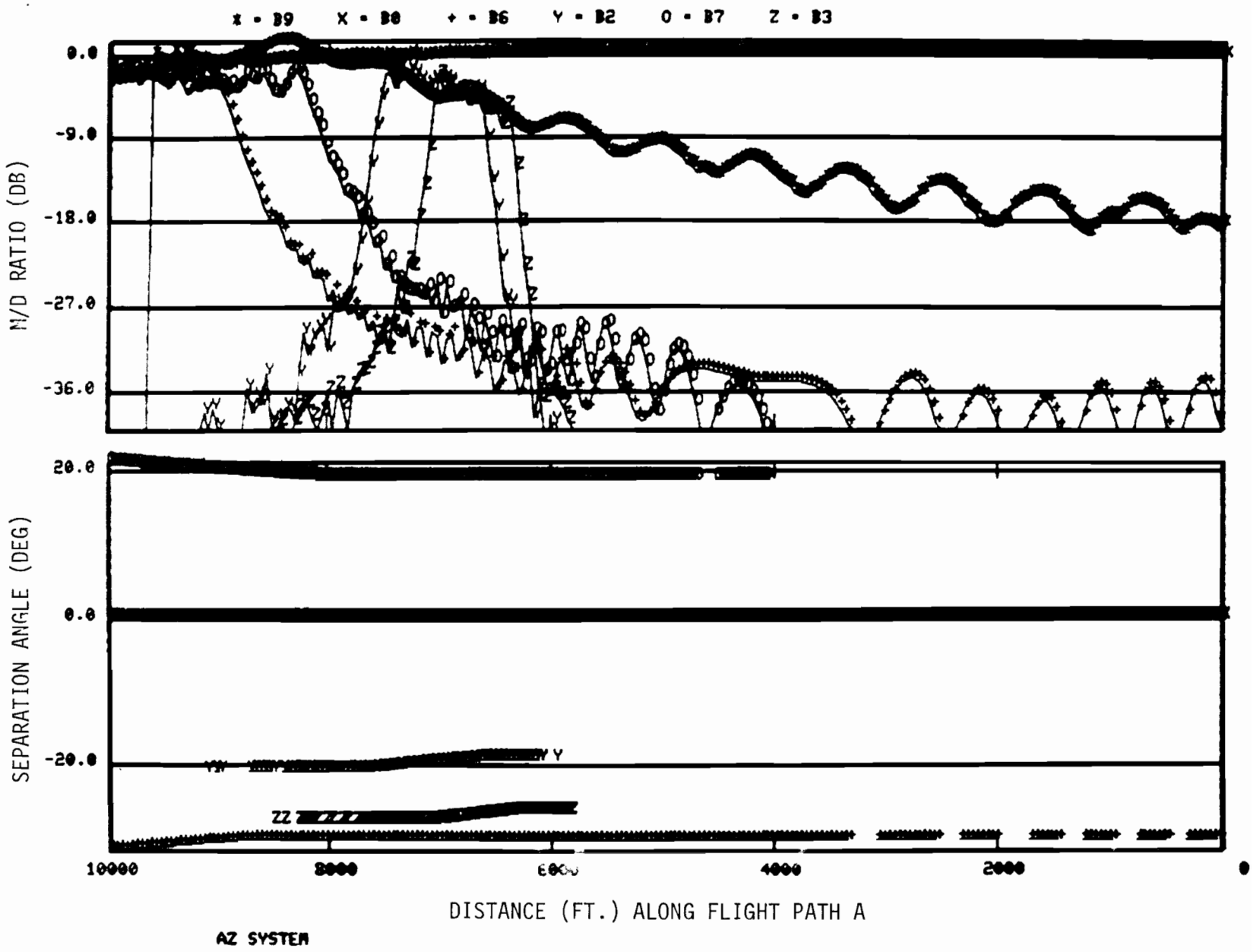

Fig. 3-12. Azimuth multipath characteristics for scenario 2-C.

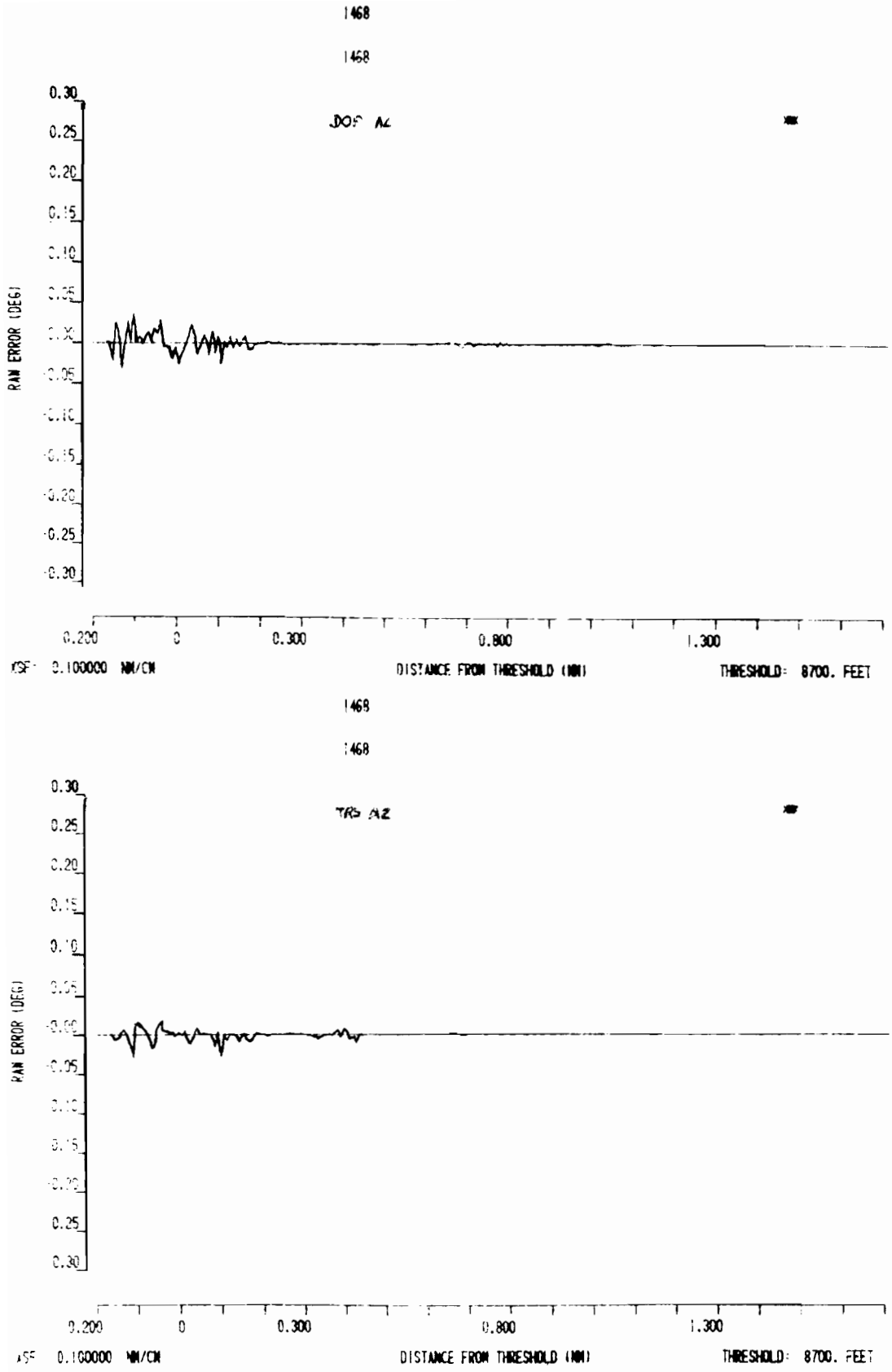

Fig. 3-13. Dynamic filled array azimuth errors for scenario 2-C.

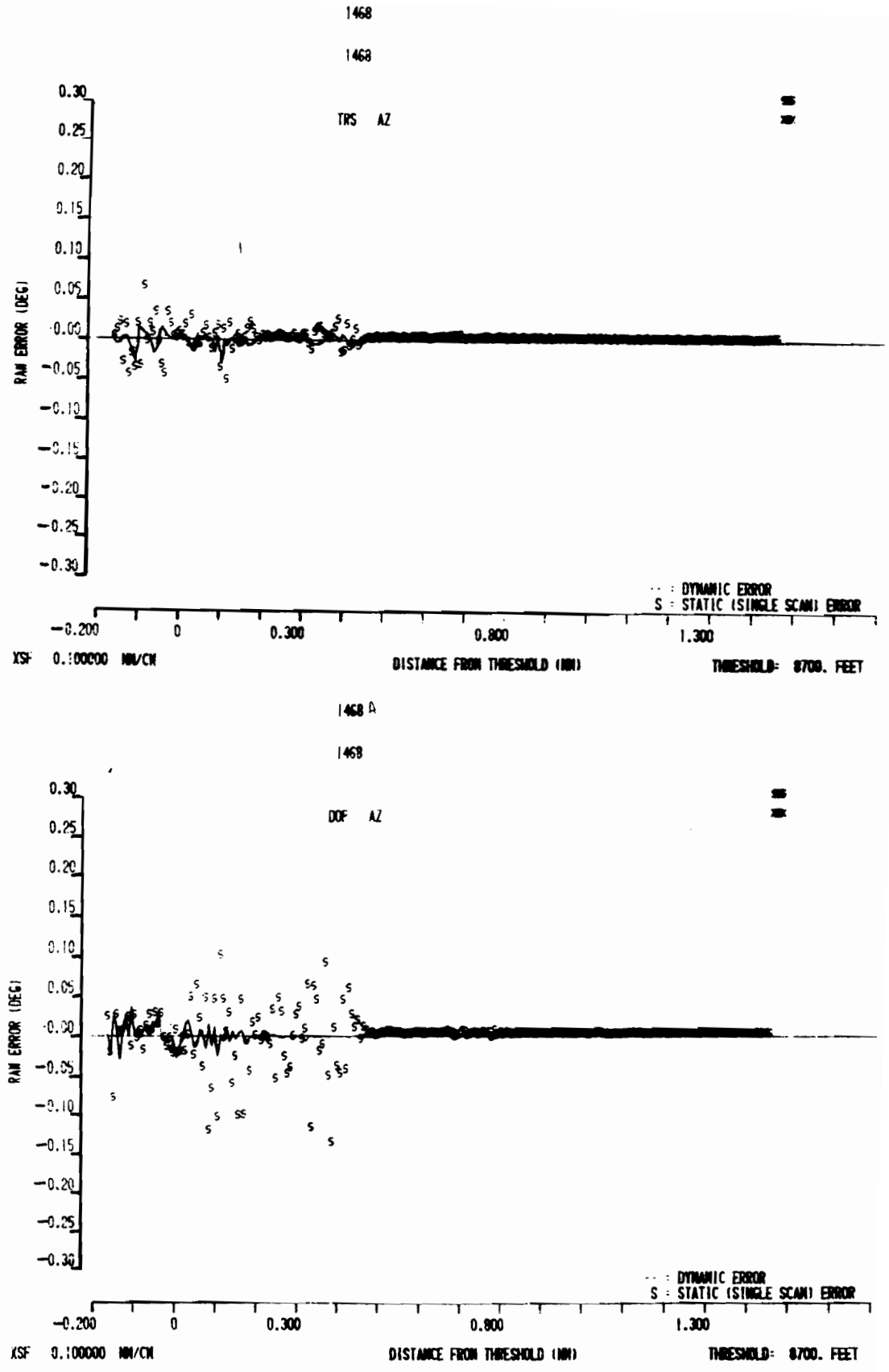

Fig. 3-14. Dynamic and single scan multipath errors for filled azimuth arrays in scenario 2-C.

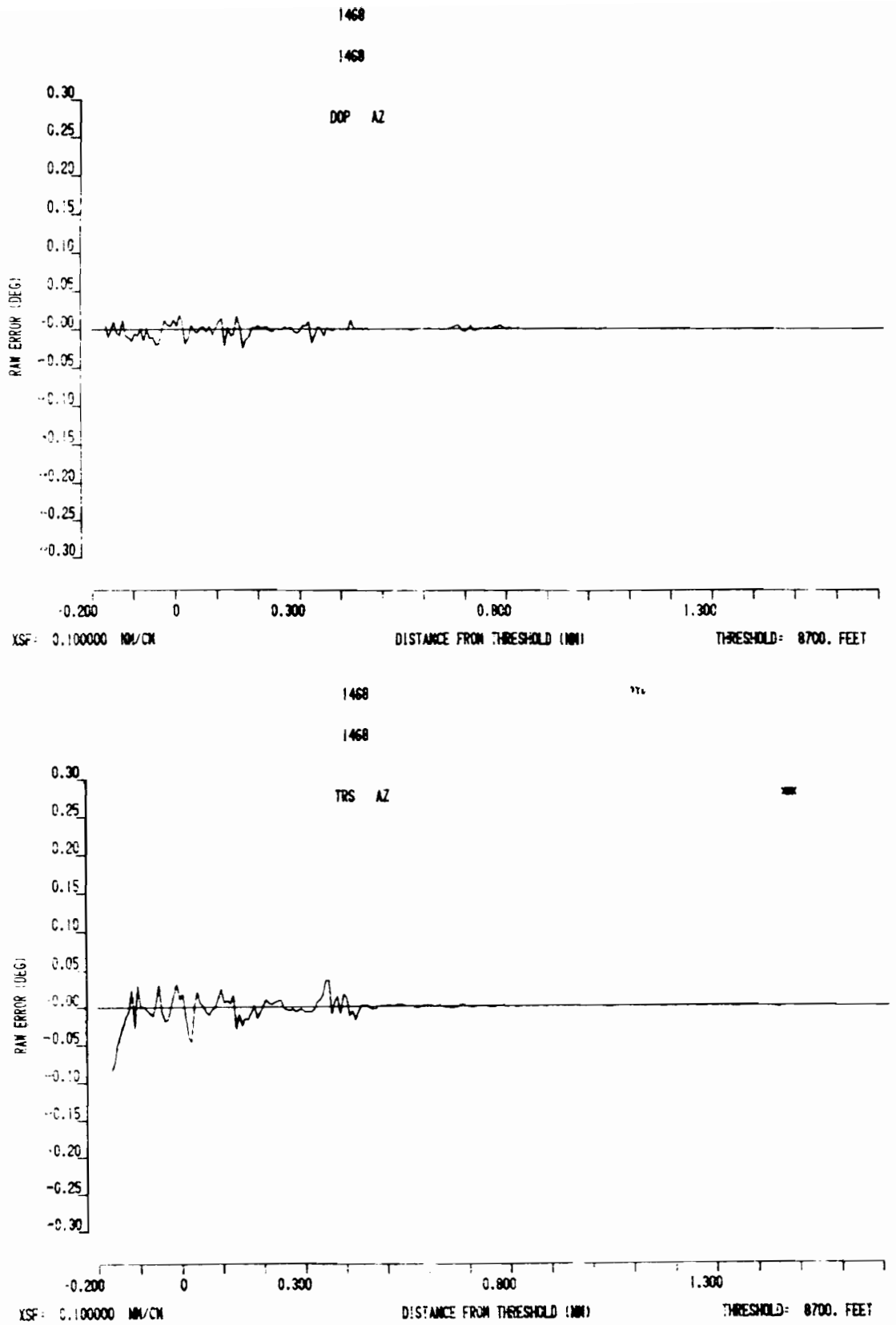

Fig. 3-15. Dynamic thinned array azimuth error for scenario 2-C.

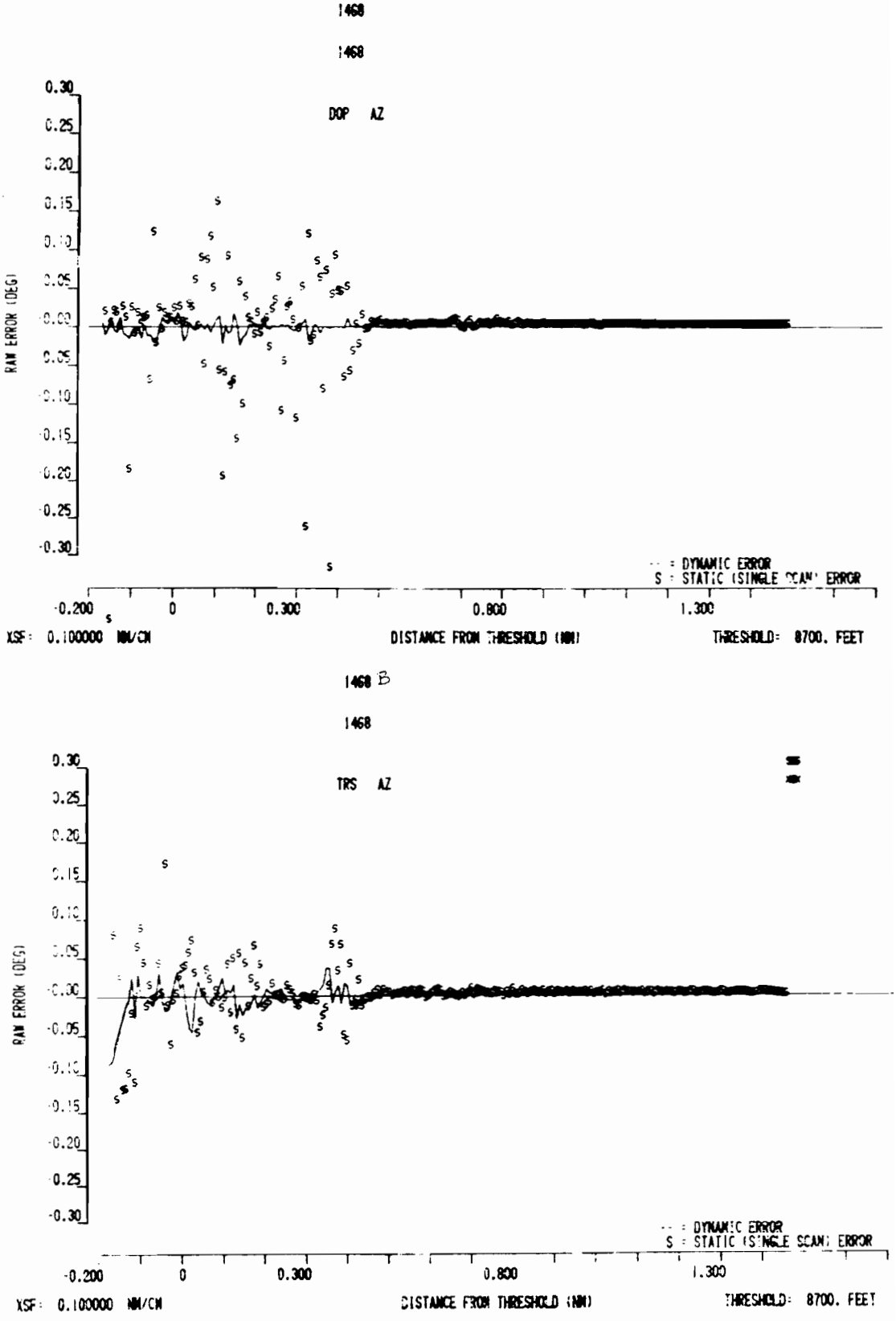

Fig. 3-16. Dynamic and single-scan thinned array azimuth errors for scenario 2-C.

test data and system theory discussed in volume II of this report. Figures 3-17 and 3-18 show the static error versus separation angle curves for the models of filled TRSB and DMLS arrays while figures 3-19 and 3-20 are the corresponding plots for the thinned TRSB and DMLS array models. We see that both filled arrays have low sidelobes at the angles of concern for the azimuth scenarios of this section. Hence, we expect the sidelobe errors for these arrays to be small.

However the TRSB density tapered array has high sidelobes in the angular region of the Hagenberg buildings, whereas no buildings were located in the high sidelobe region of the DMLS thinned array. Hence, it is to be expected that the TRSB thinned array would exhibit much larger errors for those scenarios than either filled array or the DMLS thinned array.

The static error versus separation angle curves together with the azimuth multipath diagnostic data (figure 3-12) give a reasonably good estimate of the TRSB and DMLS single scan errors during the initial portion of the flight path (when the scalloping rates are low). The reflections from the ground are seen to be in-beam, but at zero separation angle, which yields zero error. The other scattering objects are all out-of-beam so that the dominant error sources are sidelobe and reference scalloping effects. To understand the motion averaging differences as well as the error behavior nearer threshold, one must consider the system dynamic azimuth multipath error characteristics.

Figure 3-21 shows the TRSB dynamic azimuth error versus scalloping frequency for the TRSB thinned array with multipath located at a high sidelobe position. Also indicated are the scalloping frequencies or some of the principal multipath sources. We see that the multipath from Hagenberg's building A (= B6 in the figures of this section) overlaps the motion averaging "grating lobe" at 26 Hz. This is believed to account for the large TRSB density ta-

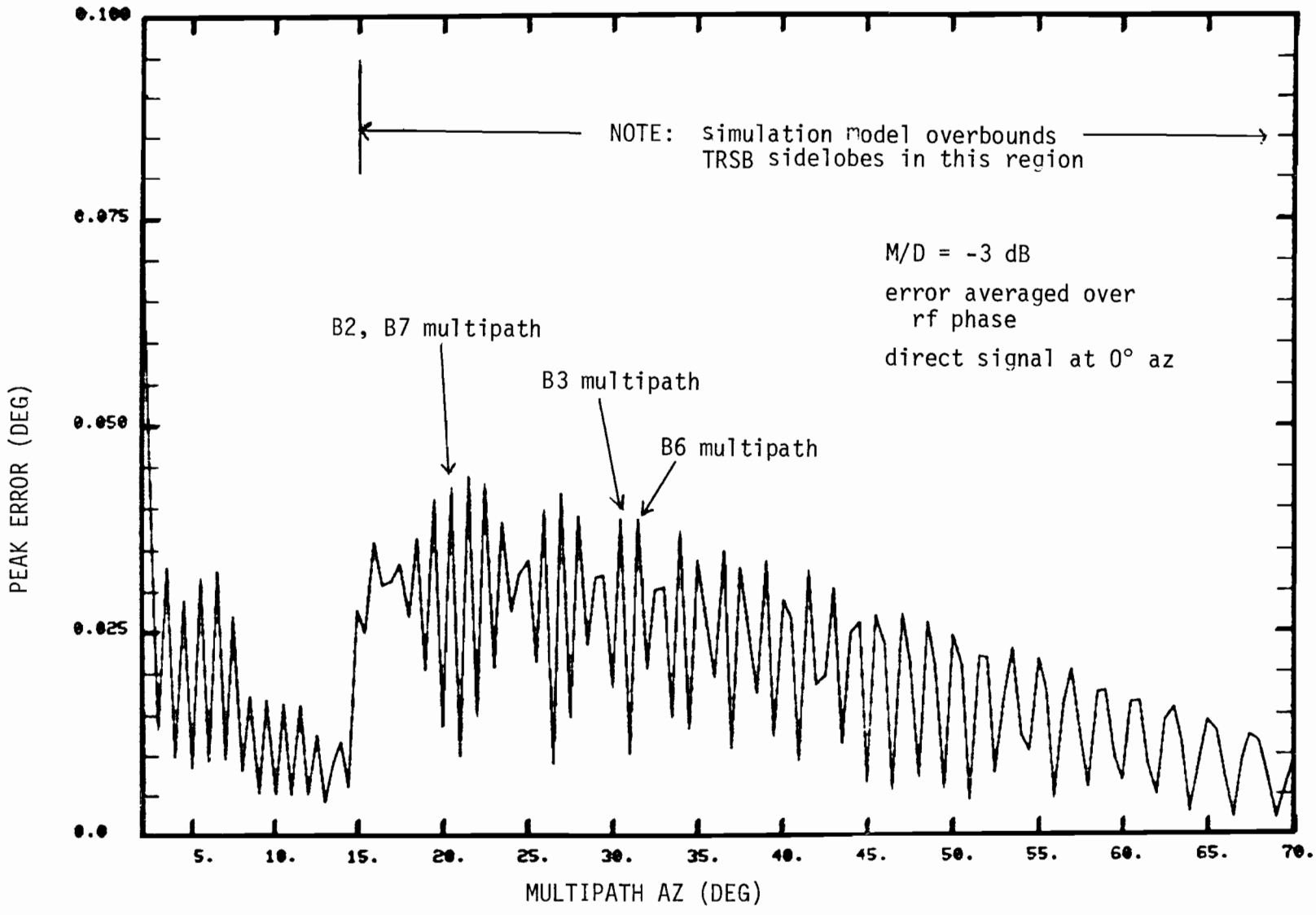

Fig. 3-17. Static azimuth error vs separation angle for model of TRSB filled azimuth array.

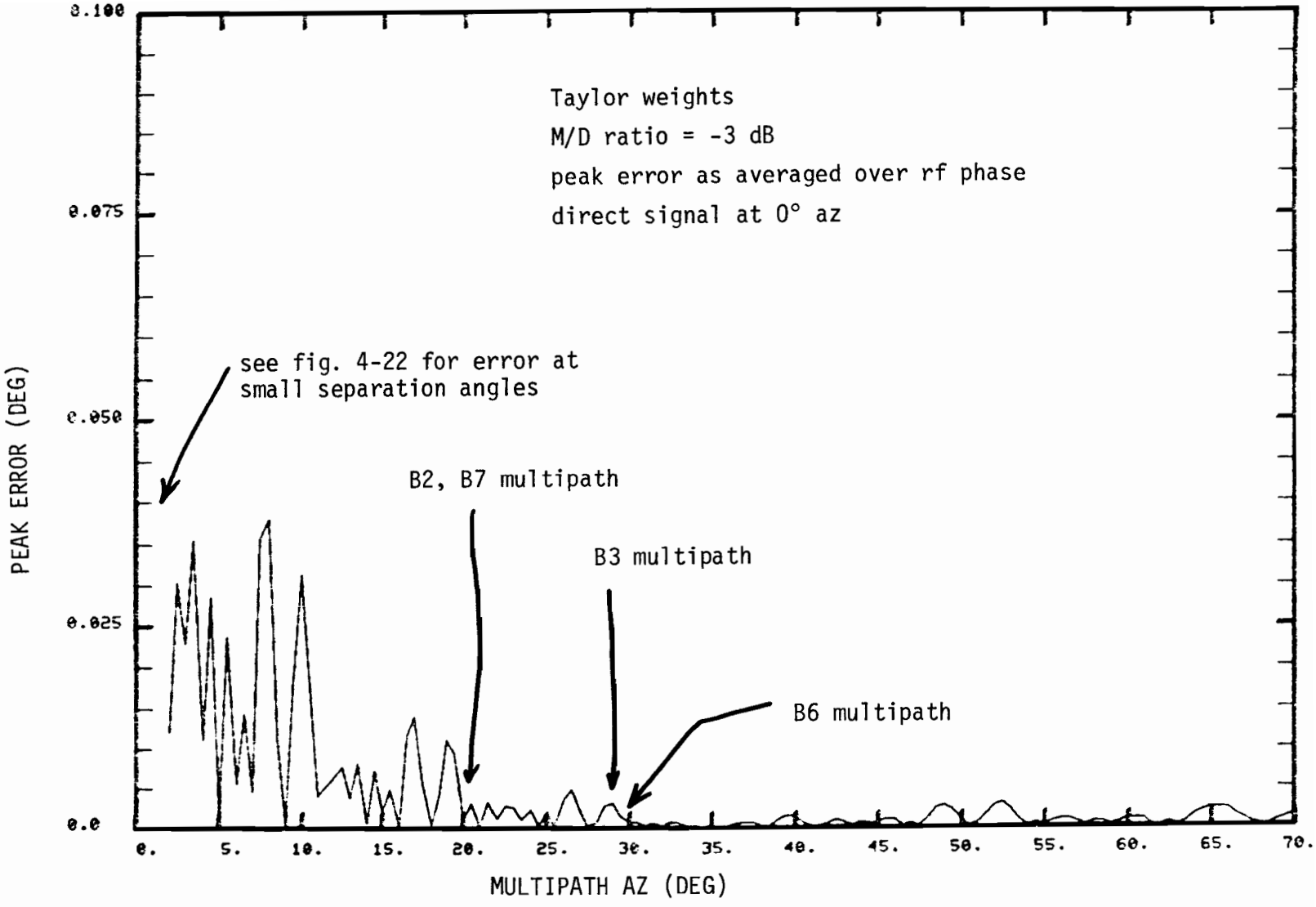

Fig. 3-18. DMLS model static azimuth error vs separation angle.

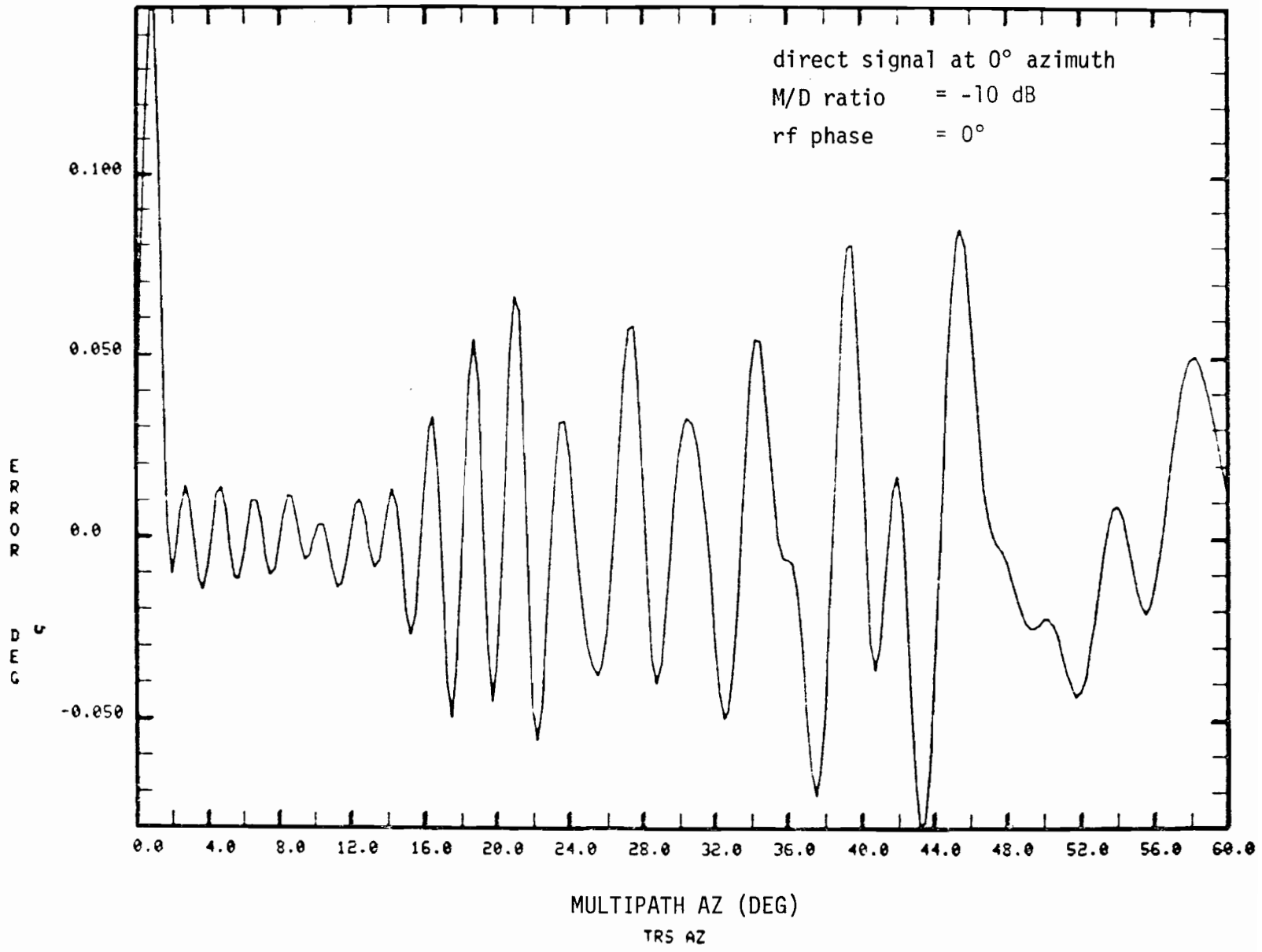

Fig. 3-19. Thinned AZ array model error vs separation angle (from ref. [14]).

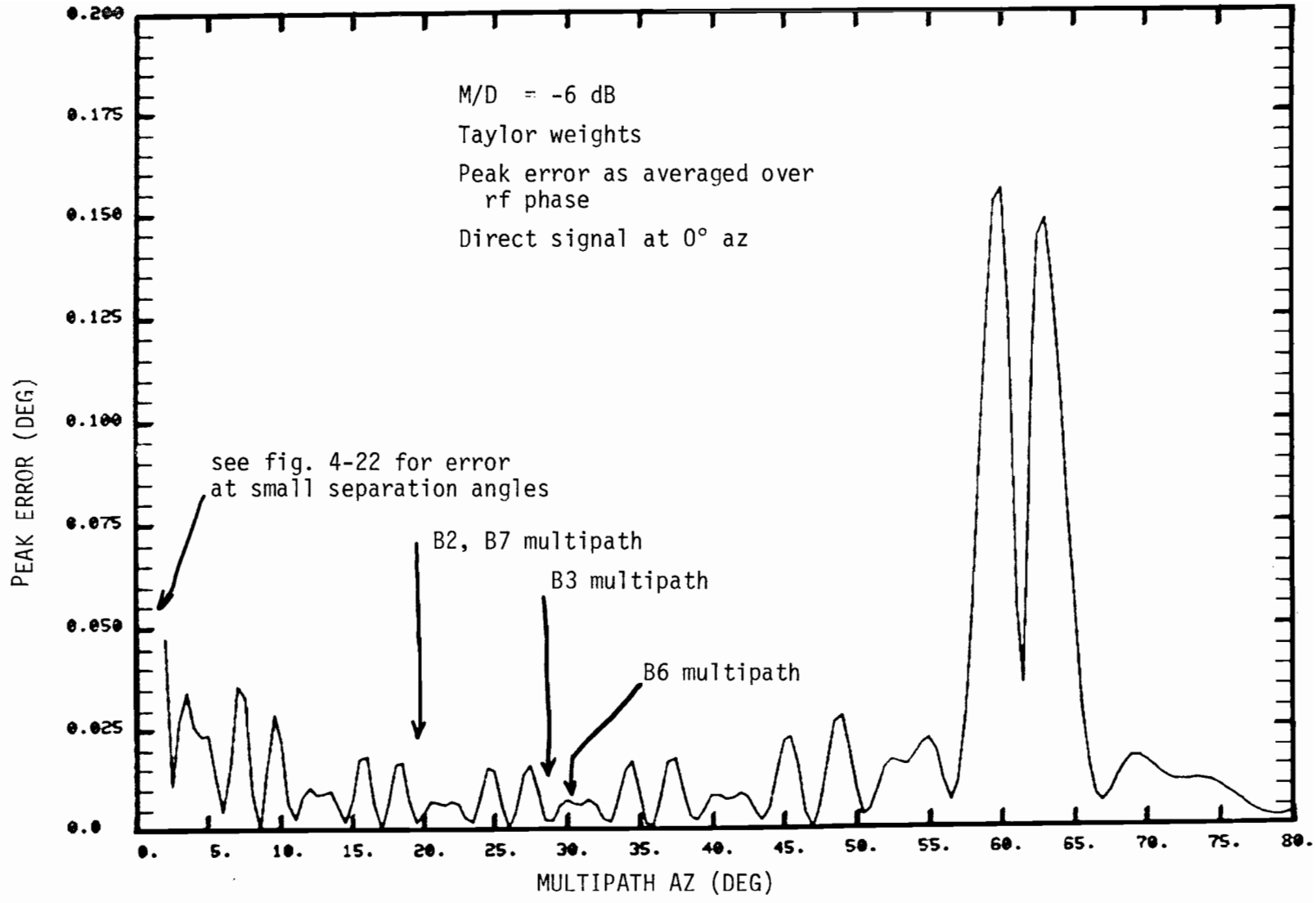

Fig. 3-20. Static error vs separation angle for model of DMLS thinned azimuth array.

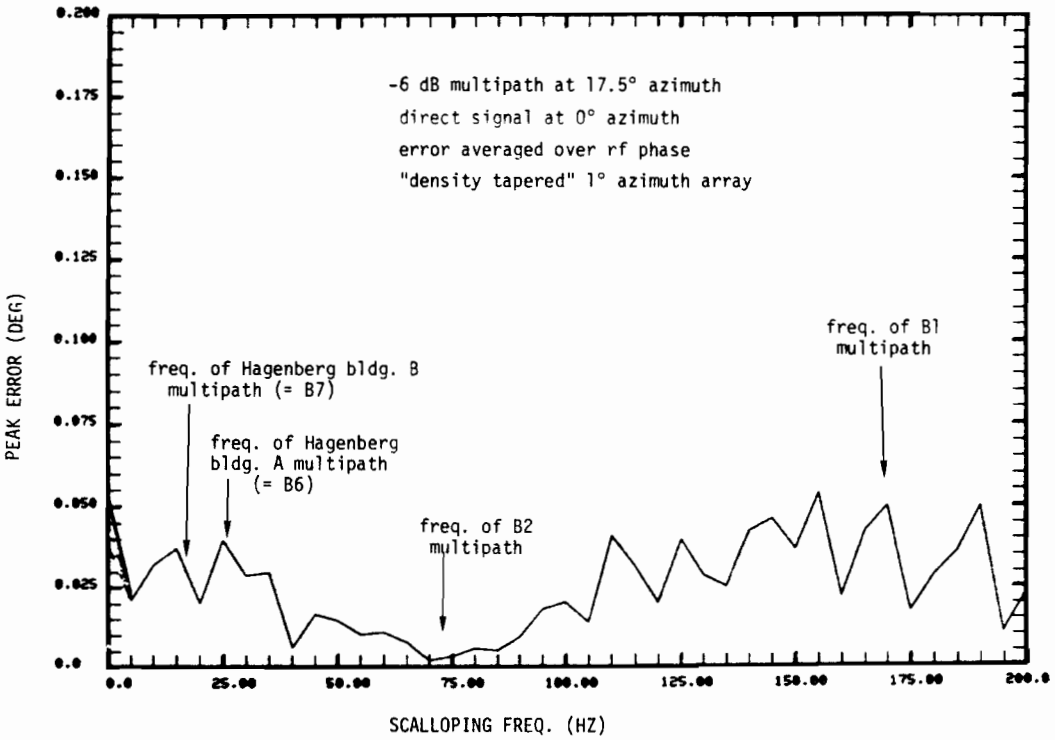

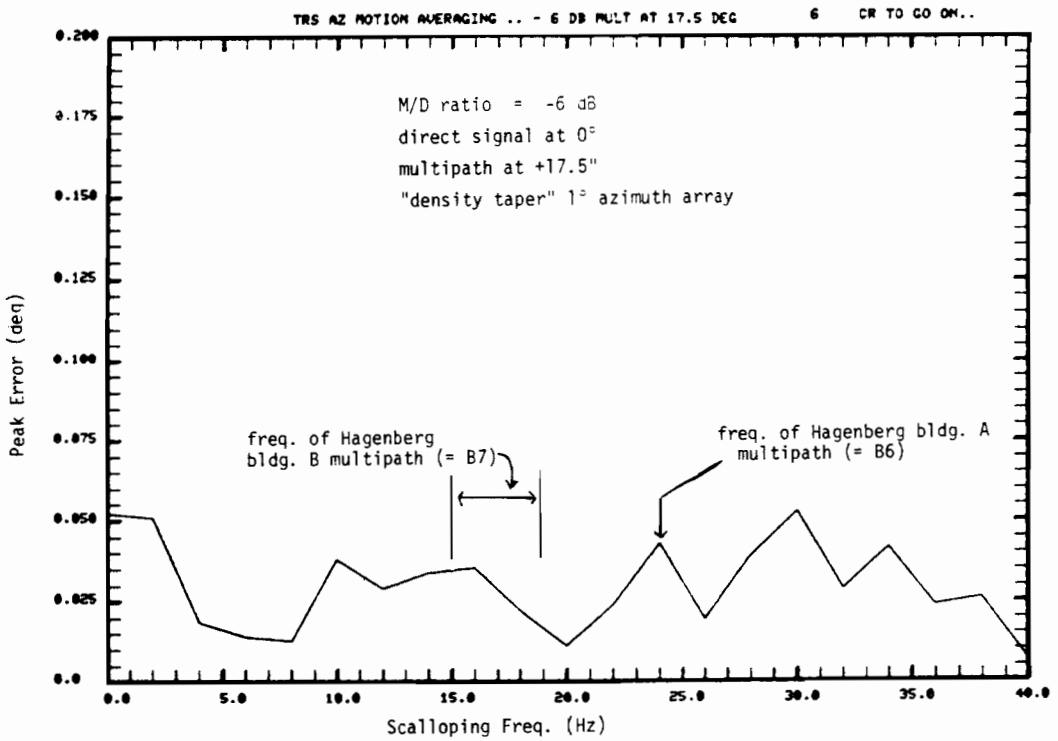

Fig. 3-21. TRSB azimuth motion averaging of sidelobe multipath.

pered array error "spike" which arose near the threshold.

The DMLS error at low scalloping rates (e.g., below 30 Hz) in these scenarios is primarily due to sidelobe errors. Figure 3-22 shows the DMLS Taylor weighted correlator sidelobe error behavior at low scalloping rates. At higher scalloping frequencies, reference scalloping errors become the dominant DMLS multipath error source. Figure 3-23 compares the DMLS filled array reference scalloping error data from RAE bench tests with computer simulation results. Nonlinear aspects of the DMLS angle processor algorithms yield the reference scalloping error below 300 Hz, consequently it is hard to make a precise quantitative estimate of the error due to overlapping multipath signals from figure 3-23. We surmise that the larger DMLS errors result from the B1 multipath near 200 Hz scalloping frequency combining with deeper fades due to multipath from buildings B2 and B6.

Whereas the DMLS filled array reference scalloping error due to out-of-beam multipath is a very weak function of the multipath angle, the DMLS commutated array scalloping error is much more dependent on the multipath azimuth as shown in figure 3-24. This difference in azimuth angle dependence is believed responsible for the lower reference scalloping errors which arose for the commutated reference array.

B. Specular Reflections from Mountainous Terrain

The multipath performance of MLS systems in mountainous areas has been of considerable interest since it has been quite difficult, if not impossible, to provide ILS service in such regions. None of the MLS implementations* pro-

*Field tests with Ku band scanning beam systems [21] had shown good performance at such sites. Subsequent TRSB and DMLS tests in mountainous terrain gave good results [63].

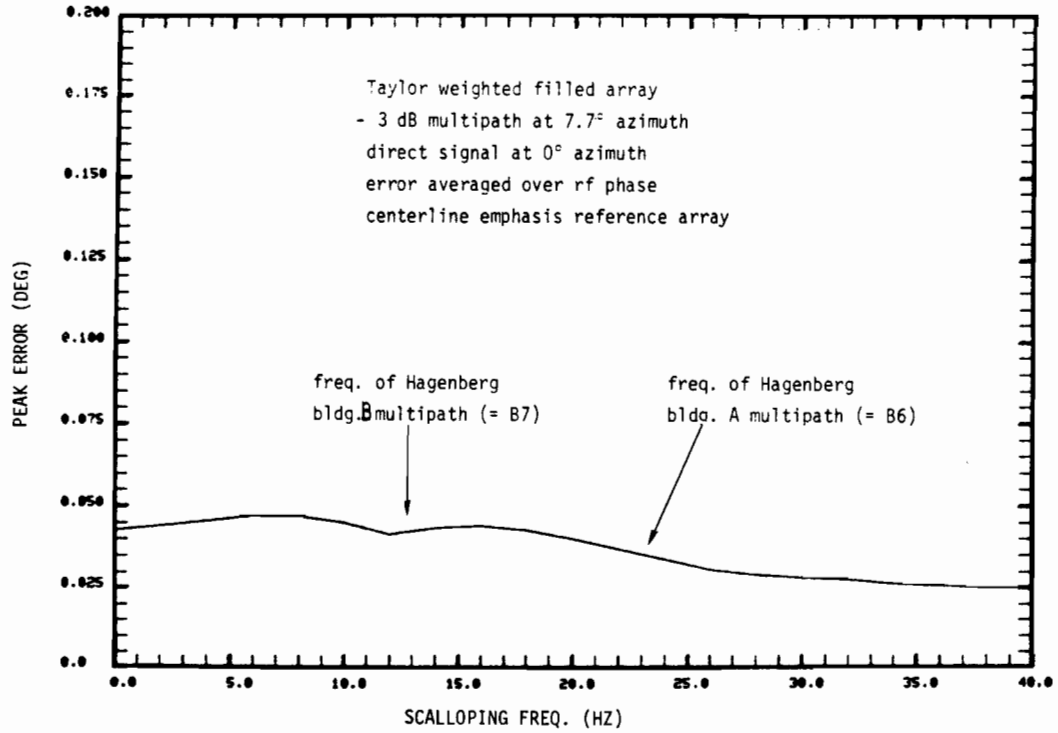

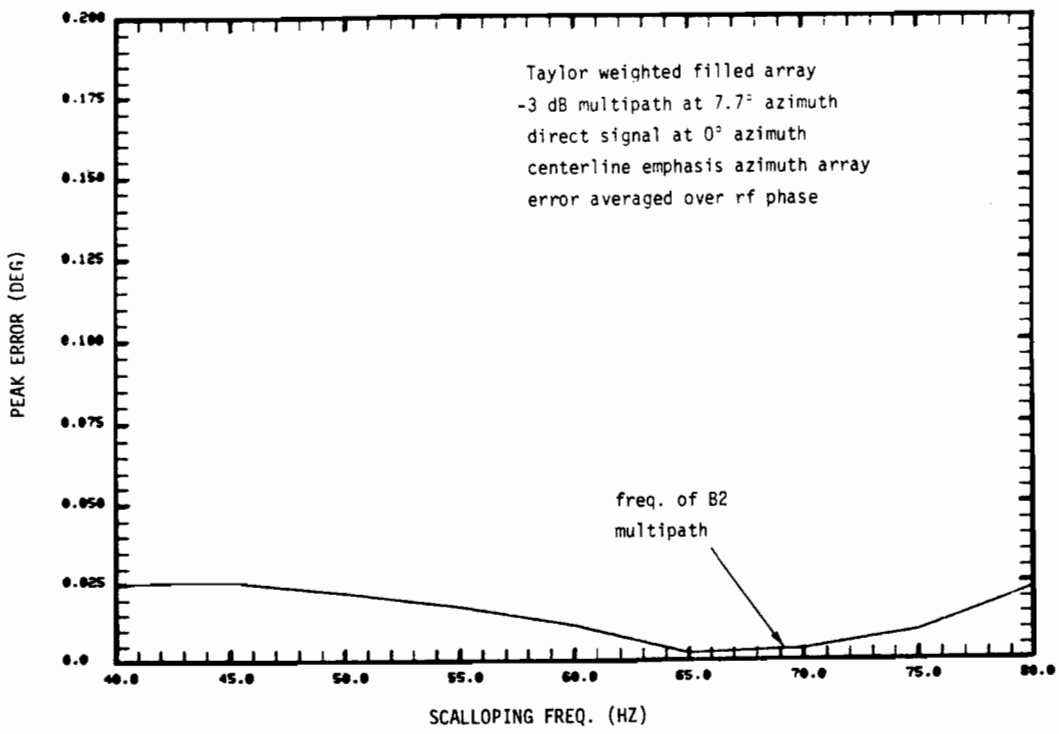

Fig. 3-22. DMLS azimuth averaging of sidelobe multipath for 54λ array.

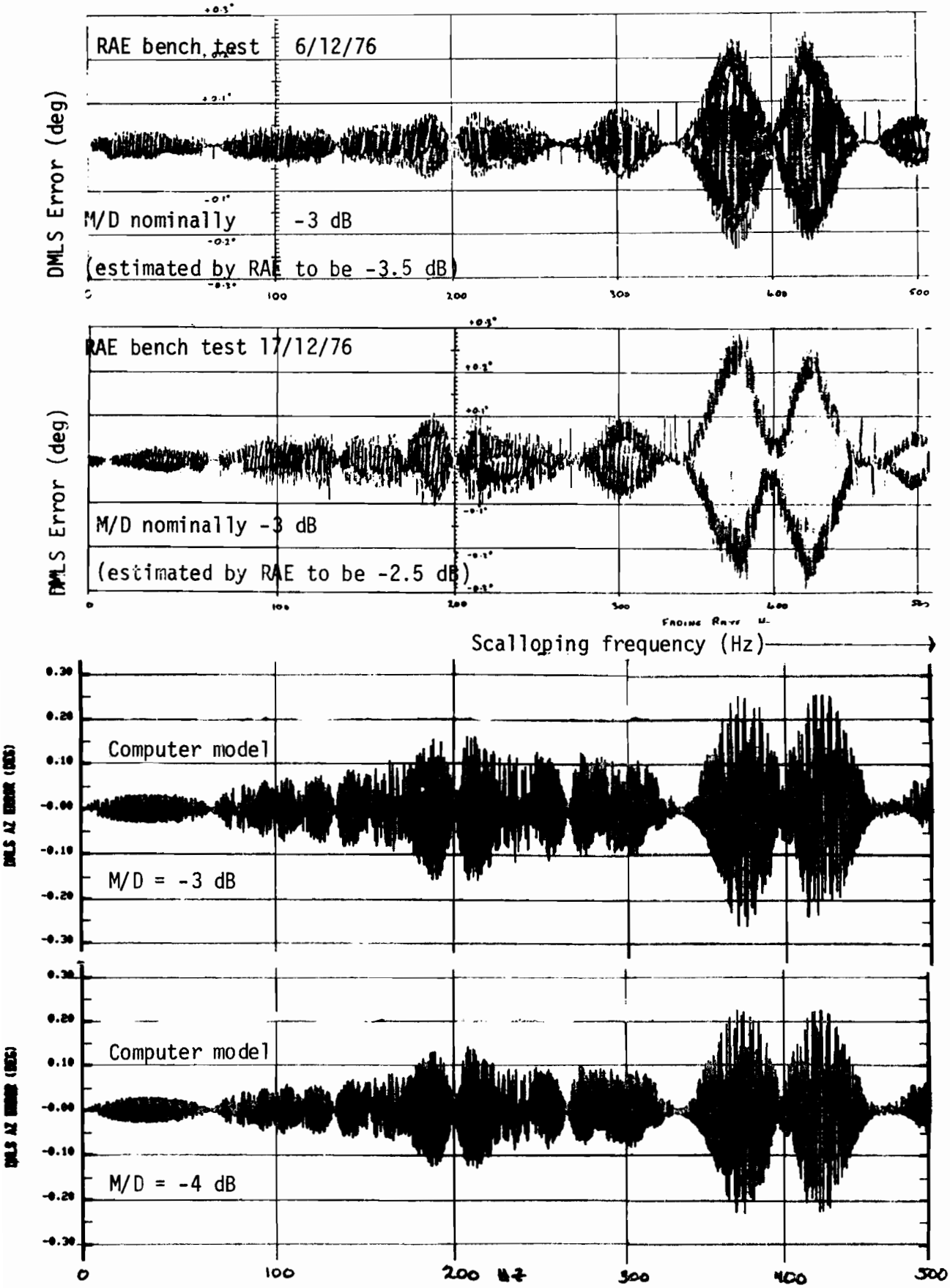

Fig. 3-23. Comparison of computer model with Doppler receiver bench test data for out-of-beam azimuth multipath.

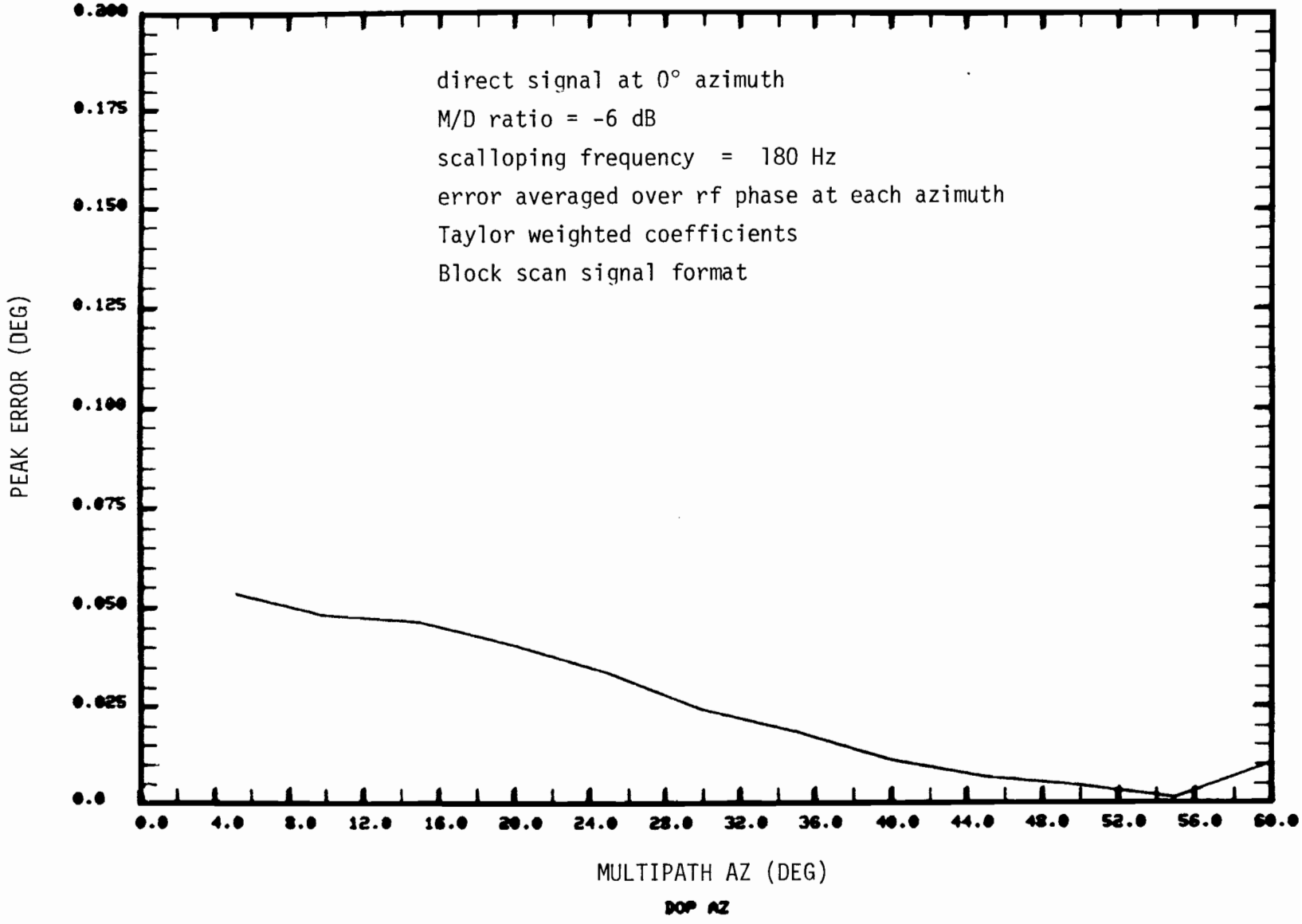

Fig. 3-24. DMLS commutated reference scalloping error vs multipath azimuth.

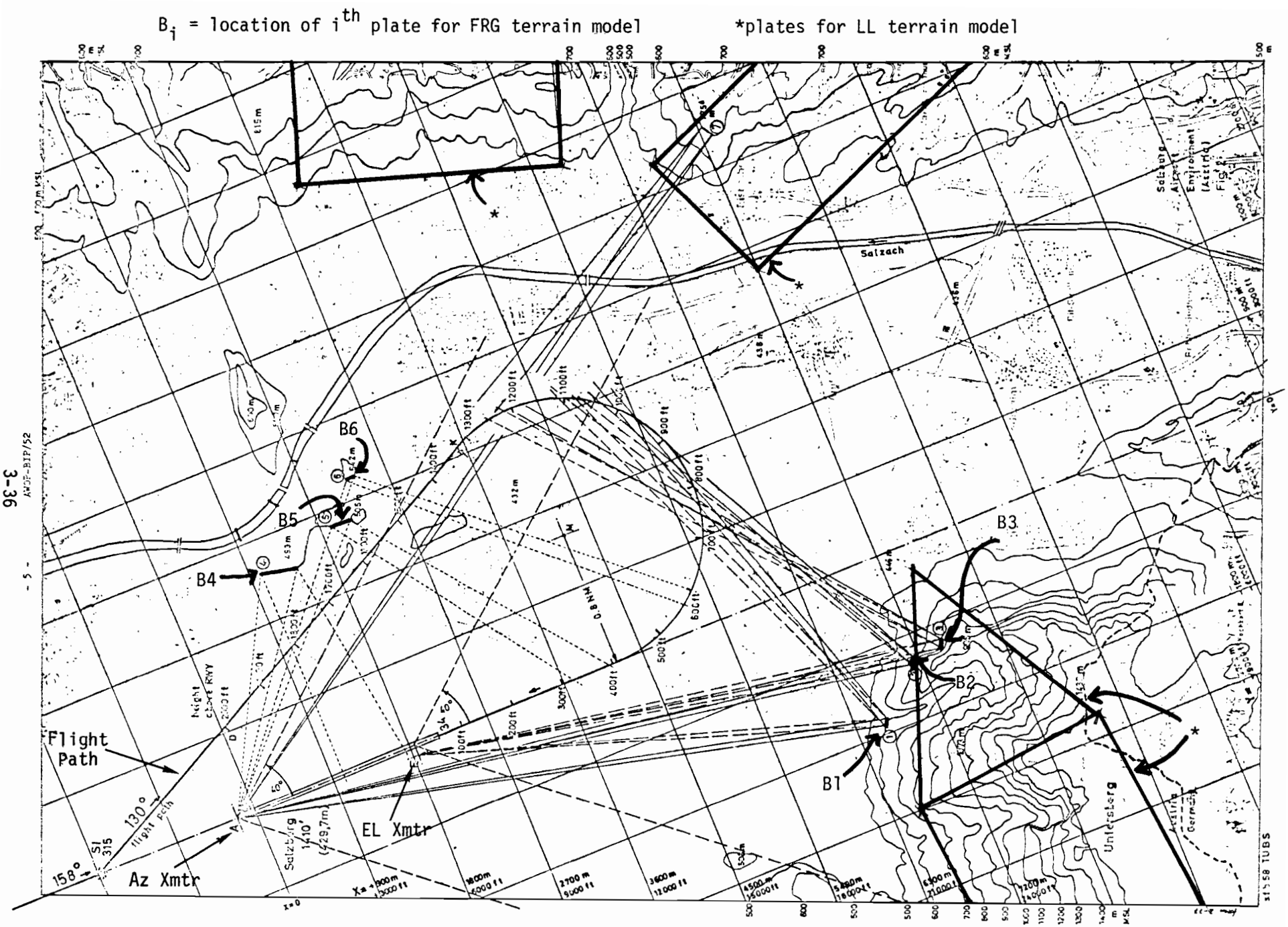

Fig. 3-25. Salzburg area map showing flight path and locations of reflecting surfaces.

posed to ICAO had been tested at such sites during the WG-A assessment. At the London meeting of AWOP WG-A, it was proposed that comparative computer simulations be made for the ICAO MLS proposals in a representative mountainous scenario [119].

A standard VFR approach to the Salzburg, Austria airport was simulated for two terrain models:

(1) a Lincoln Laboratory generated model in which the mountains are represented as flat snow covered rectangular or triangular plates whose orientation corresponds to published map contours [120].

(2) an FRG generated model in which the terrain of concern was represented by a number of flat vertical rectangles simulating vertical cliffs [116].

Model (1) yielded no significant multipath for either the AZ or the EL function. This lack of multipath occurred because the terrain plate slopes were not steep enough to yield specular reflections for the assumed transmitter-receiver-mountain geometries.

The same is true of model (2) for reasonable roughness and verticality assumptions. Under an "exaggerated worst case" condition in which the cliffs are assumed to be perfectly vertical smooth metallic surfaces, significant multipath was encountered.

1. Terrain Models

Model 1

Figure 3-25 (taken from [116]) shows the approach superimposed on a contour map of the airport vicinity. In an initial simulation, five sloping surfaces were modeled as triangular or rectangular plates on tilted ground. These are partially sketched in Fig. 3-25 and are shown in plane view in Fig.

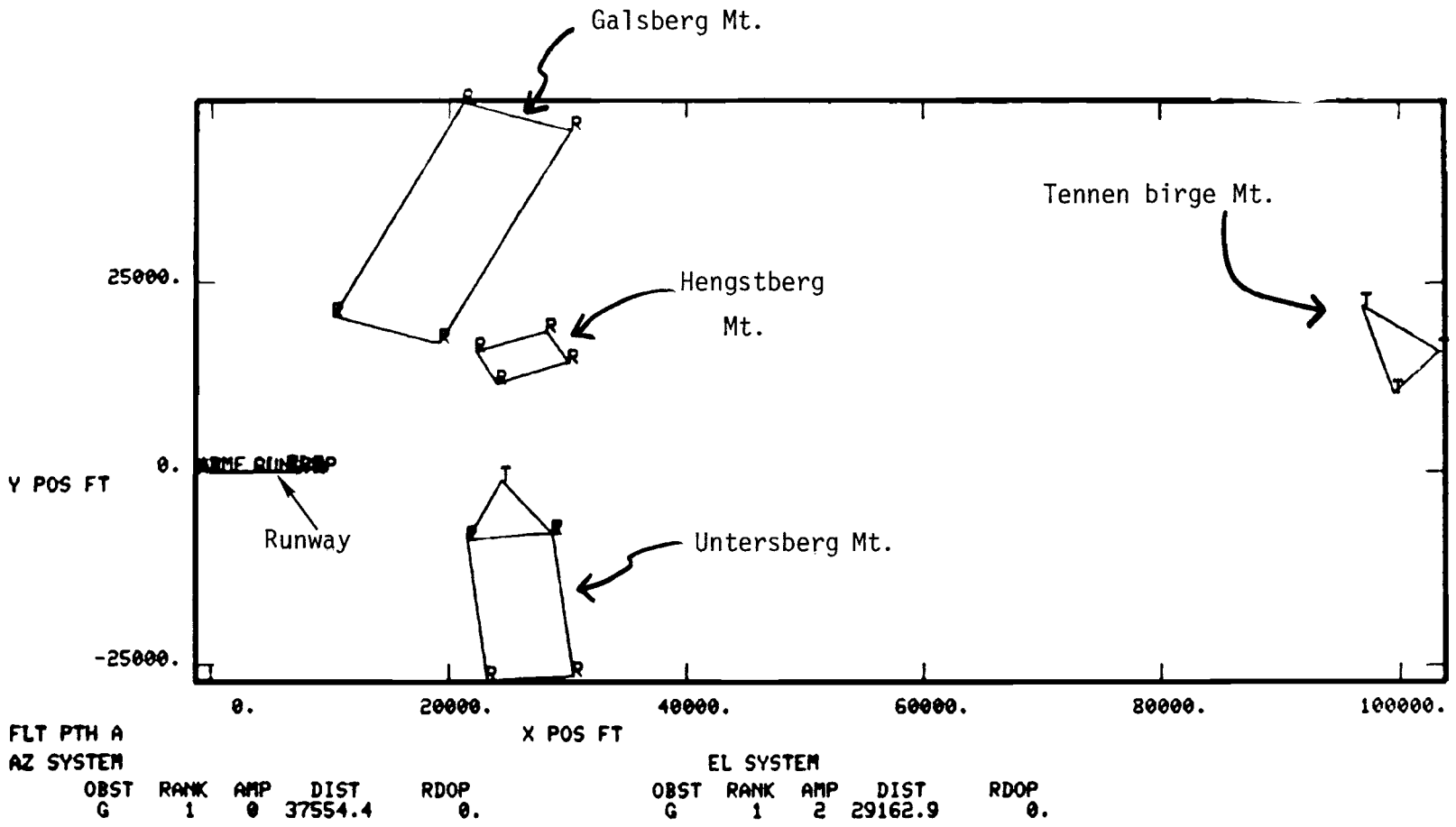

AMP = -peak M/D ratio (dB)
DIST = distance along flight path at point where peak M/D occurred
RDOP = scalloping frequency (Hz) at point of maximum M/D

Fig. 3-26. Computer-generated airport map; tilted ground scenario.

3-26. The flight path was essentially that of the FRG paper [116].

Model 2

Model 2 is based almost entirely upon data given in an FRG AWOP/6 paper [116]. Seven vertical walls representing reflecting surfaces either in the mountains to the south of the city or structures within the city itself were modeled (see Fig. 3-25 and the computer-generated map in Fig.3-27). Multipath computations were made with several different assumptions regarding the surface characteristics:

(a) Smooth rock surface with an 85° slope

(b) Smooth rock surface with a 90° slope (perfectly vertical)

(c) Perfectly vertical rock with a 1 ft rms roughness

(d) (worst case) Perfectly vertical smooth metal

2. Multipath Computation Results

In all cases, the flight path shown in Fig. 3-25 was flown at a ground speed of 150 knots.

(a) Terrain Model 1

The results of the C band simulation for the tilted ground scenario are shown in Fig. 3-28. No AZ or EL multipath component other than the ground reflection ever exceeded -40 dB along the entire flight path.* It was subsequently determined that the tilted elements were not oriented for specular

*In these and similar plots, the level and separation angle of the six largest specular components relative to the direct signal are plotted. If less than six components are shown, the remaining components had levels less than -40 dB. The M/D levels shown do not take into account ground antenna patterns nor various secondary paths involving the ground - thus, they should not be interpreted as a precise quantitative estimate of the M/D levels that would be measured at the airborne receiver.

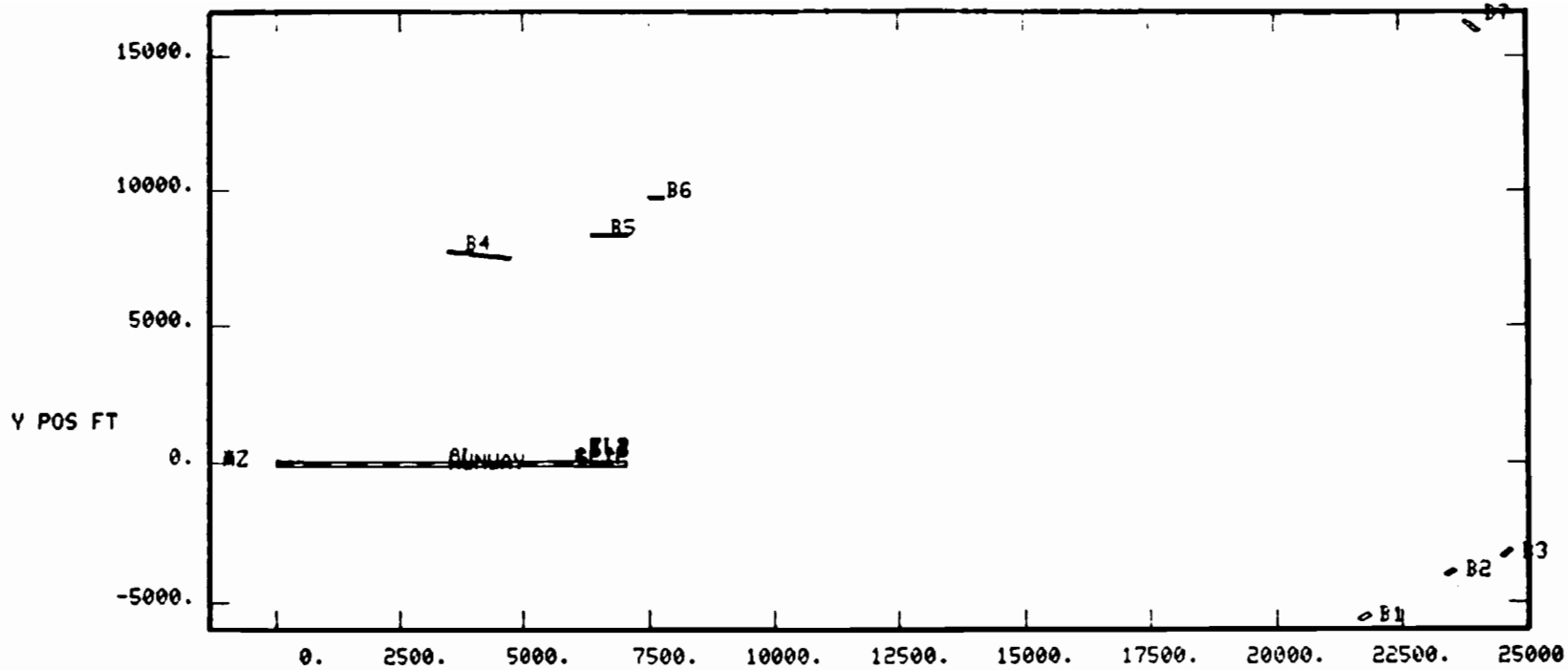

• FLT PTH A

AZ SYSTEM

OBST	RANK	AMP	DIST	RDOP
G	1	0	44142.6	0.
B1	4	2	30670.2	635.
B2	5	2	28693.7	1139.
B3	6	3	29758.0	708.
B4	8	45	44126.2	-894.
B5	3	1	37791.2	-491.
B6	2	0	33609.6	-868.
B7	7	6	21142.4	2382.

EL SYSTEM

OBST	RANK	AMP	DIST	RDOP
G	1	2	35890.2	0.
B1	2	5	32494.7	-172.
B2	3	6	23017.6	1542.
B3	4	7	21801.3	1617.
B4	7	41	1013.6	120.
B5	6	39	44142.6	-1119.
B6	5	37	40578.6	-915.
B7	8	50	19303.4	2349.

AMP = - peak M/D ratio (dB)
DIST = distance along flight path at point where peak M/D occurred (ft)
RDOP = scalloping frequency (Hz) at point of maximum M/D

Fig. 3-27. Computer-generated airport map; smooth metal vertical surface scenario.

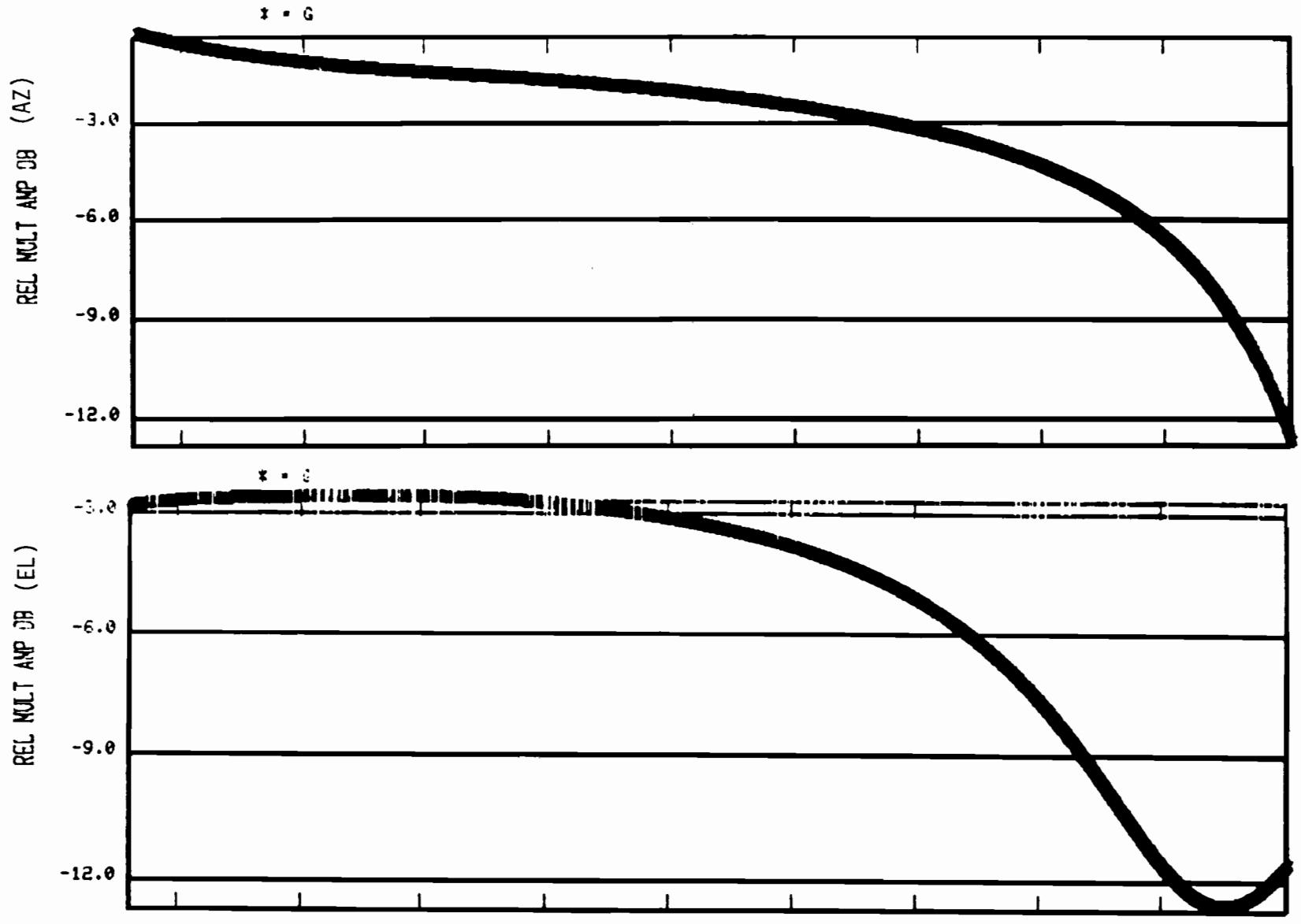

Fig. 3-28. AZ and EL C-band multipath amplitudes for tilted ground scenario.

reflection with respect to the flight path.

This may be explained as follows (Fig. 3-29). If the aircraft is between the transmitter (XMTR) and the mountain (as in position 1), the inclination α must exceed 45° for there to be specular multipath. To place in context the likelihood of encountering such slopes, we might note that the steepest ski slopes are usually < 40°. Contours on the Salzberg map suggest a maximum slope of 41° on the mountain sides facing the runway, so it is not surprising that very low multipath levels were encountered. Had the aircraft been above or slightly beyond the mountains, there would be a possibility of specular reflection from tilted plates. However, the M/D levels would be reduced by depolarization, the vertical pattern of the azimuth array, and the gain of the airborne antenna (especially top-mounted antennas).

In view of the very low M/D levels found for this terrain model, no system simulations were carried out inasmuch as bench tests and analysis have shown that such levels do not cause significant errors.

b. Terrain Model 2

(i) tilted smooth rock "cliffs"

Figures 3-30 and 3-31 show the computed multipath characteristics for a smooth rock (concrete) surface with at 5° tilt away from normal (i.e., an 85° slope). In AZ, specular reflections from B2 are encountered on both passages of the aircraft through the specular zone, but their amplitudes are low ($\leq$ -19 dB).

(ii) rough vertical rock "cliffs"

Figures 3-32 and 3-33 correspond to the case in which the rock walls are

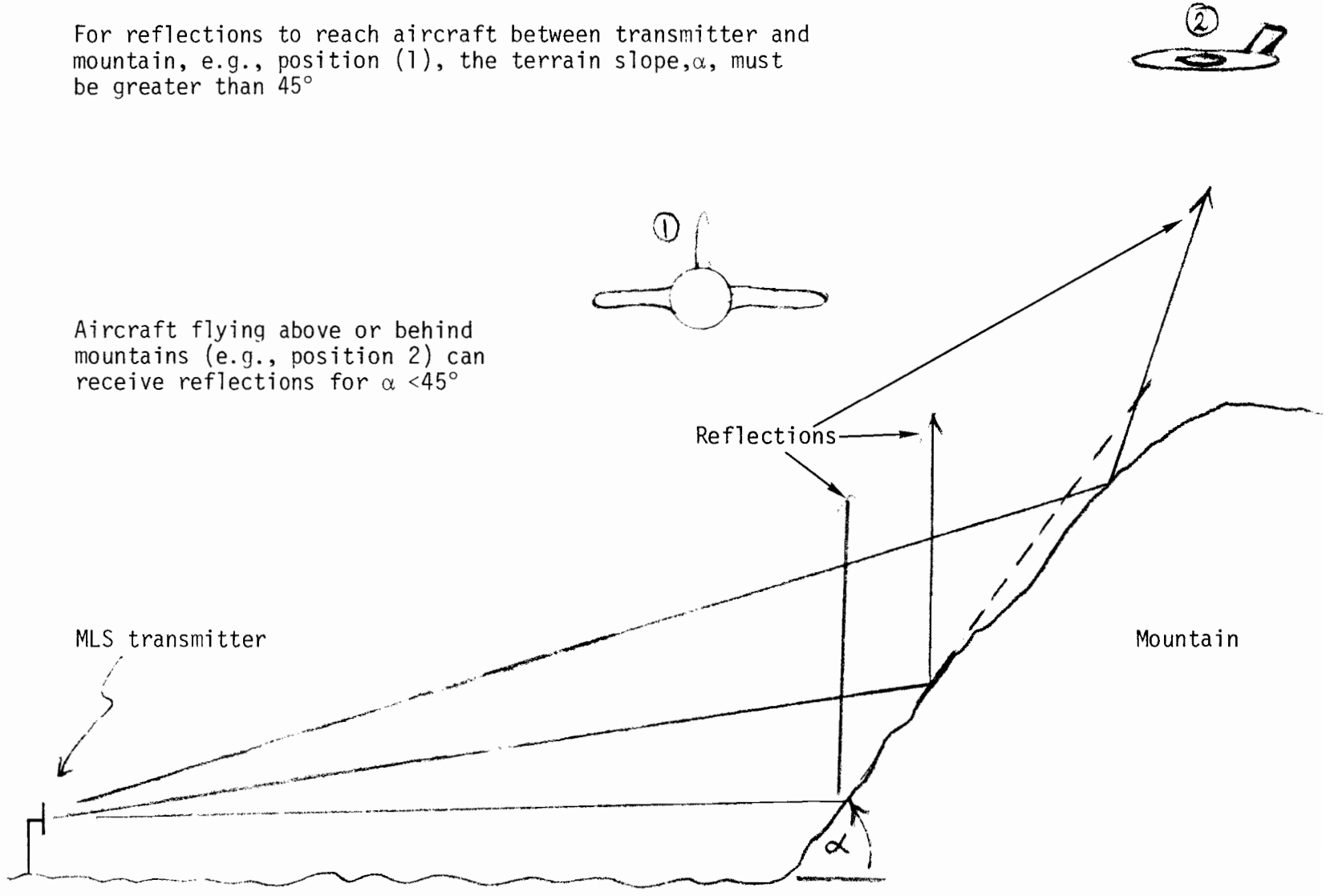

Fig. 3-29. Geometry for reflections from mountainous terrain.

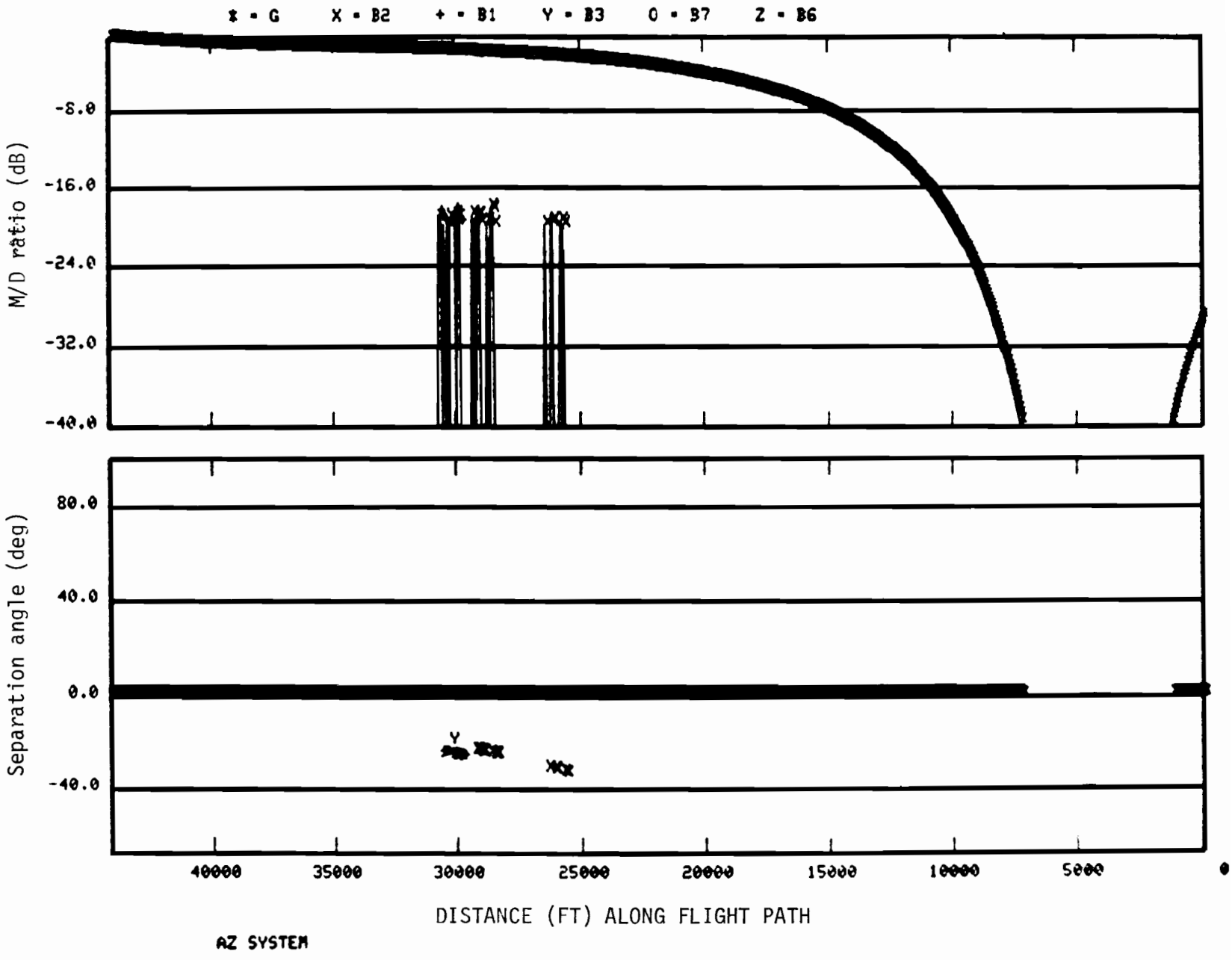

Fig. 3-30. Azimuth multipath characteristics for smooth rock surface with 85° slope

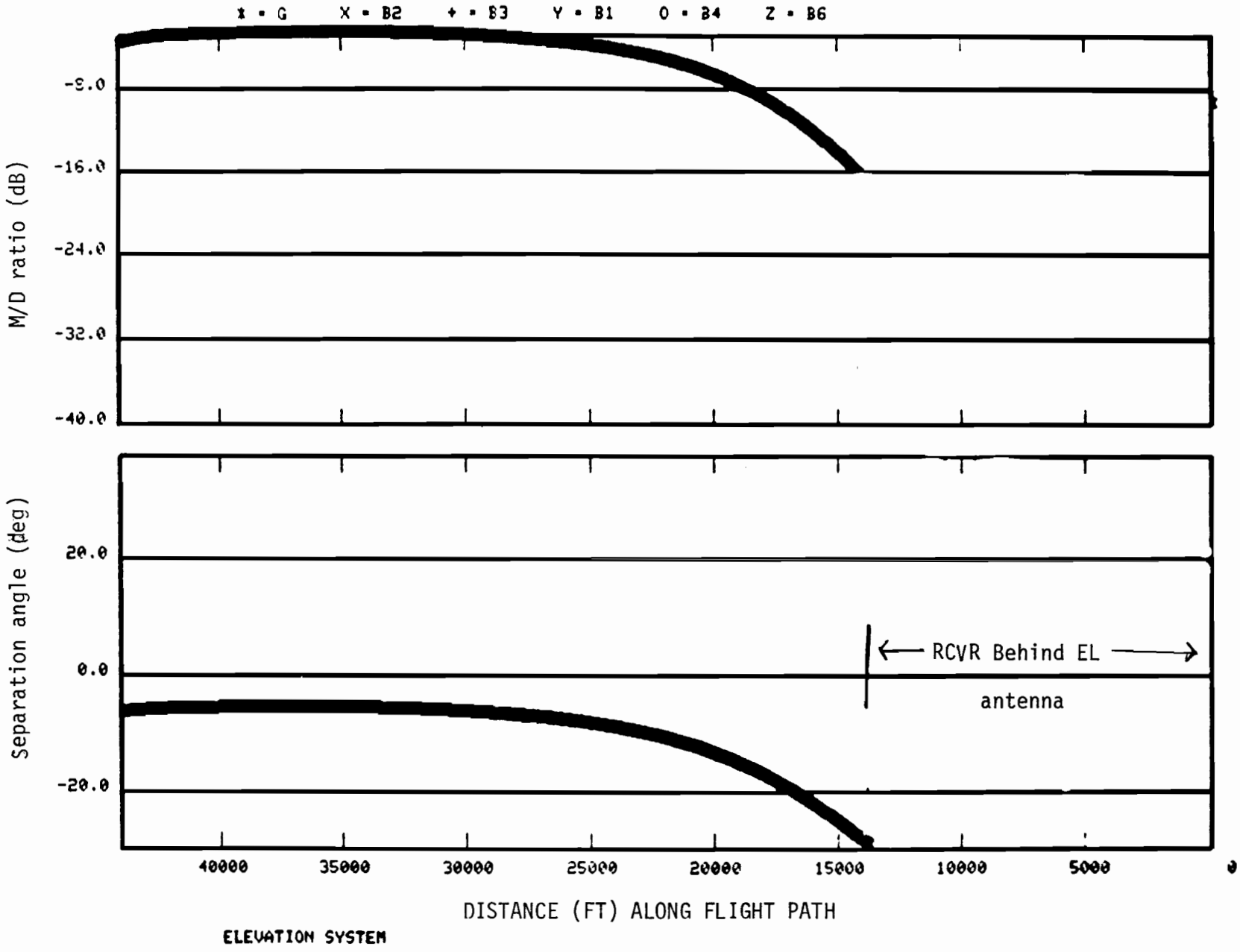

Fig. 3-31. Elevation multipath characteristics for smooth rock surface with 85° slope

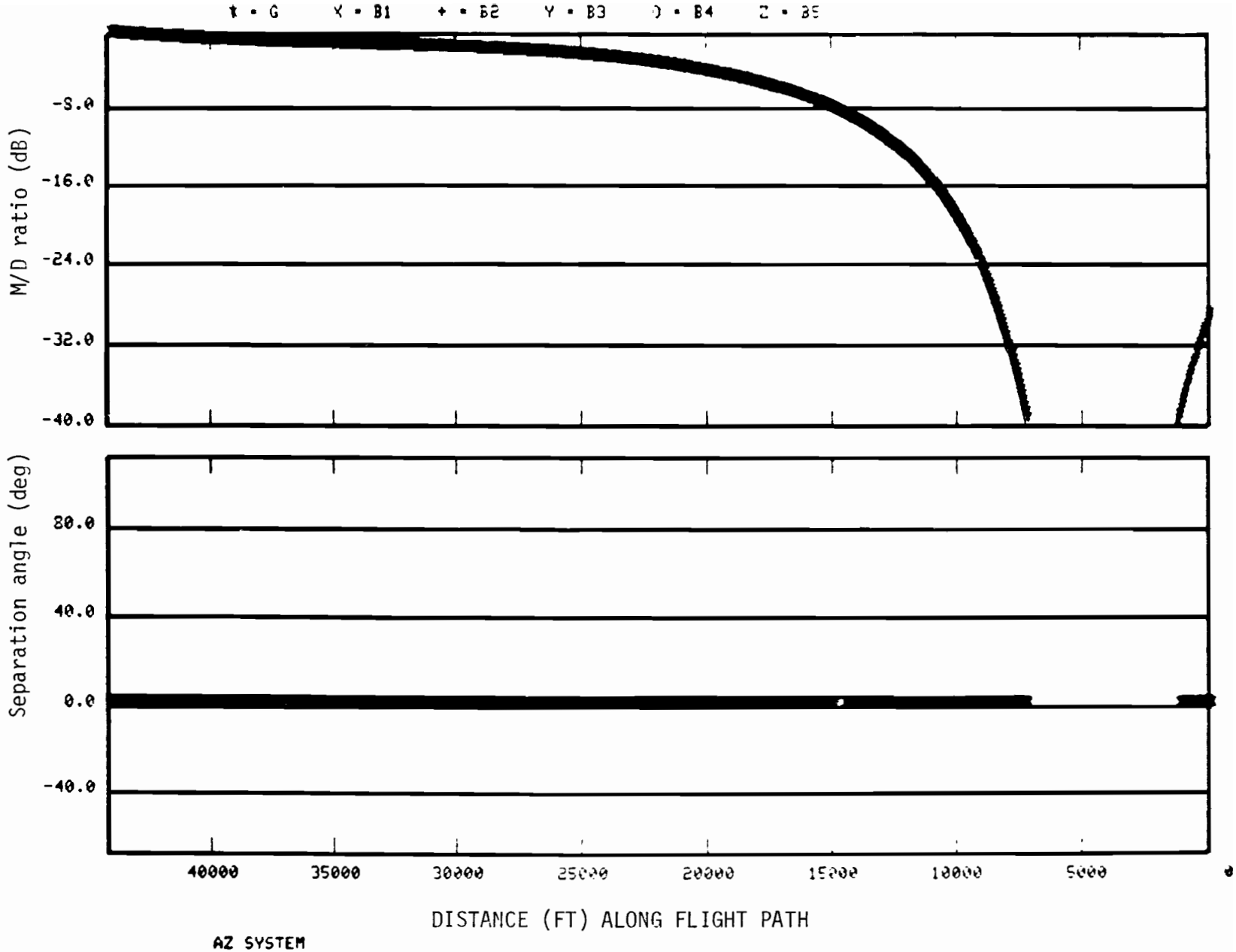

Fig. 3-32. Azimuth multipath characteristics for vertical rock surface with 1 foot rms roughness

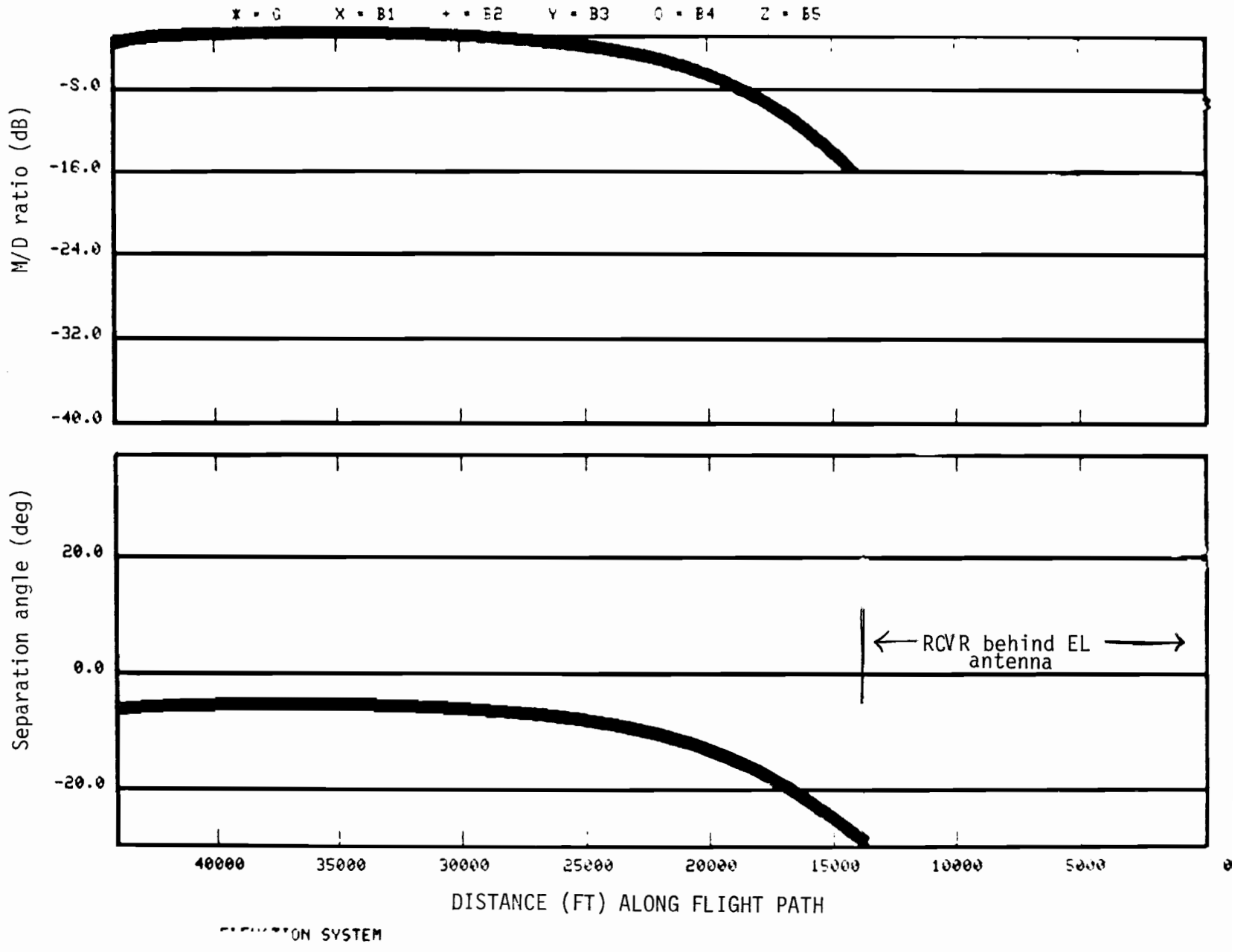

Fig. 3-33. Elevation multipath characteristics for vertical rock surface with 1 foot rms roughness

vertical (no tilt) and have 1 ft rms roughness. In this case, no C band specular multipath greater than -40 dB is found, other than ground reflection. In this case, it is possible that a diffuse reflection from the surface might be greater than -40 dB (see Appendix D of reference [53]). However,

(i) the current [29] multipath model does not consider diffuse reflections from building surface

and

(ii) there is no measured data available on C band scattering from vertical walls with a "randomly rough" surface

(iii) smooth vertical rock "cliffs"

By reducing the roughness to zero in the above scenario, specular reflections from a number of surfaces are found in both AZ and EL (Figs. 3-34 and 3-35). Similar reflections are found in the worst case scenario described below and their analysis is given there.

(iv) smooth vertical metal "cliffs"

In the worst case runs (smooth vertical metal reflectors), significant C-band multipath was found in both AZ and EL (Figs. 12 and 13). As is indicated by the geometry in Fig. 3-24, the aircraft encounters specular reflections twice from some of the surfaces on the curved path. In AZ, peak amplitudes range from -6 dB to 0 dB; the separation angles lie betwen 20° and 40° and are therefore out-of-beam (Fig. 3-36).

Fewer specular reflections are found in EL, and the peaks are slightly lower (-7 dB to -2 dB). In this case, the separation angles are near the in-beam region (Fig. 3-37).

The multipath levels and time delay diagnostic for the L-band DME multipath are shown in Fig. 3-38. The levels are identical to those which an L-band azimuth system (e.g., DLS) would encounter. Because of the large

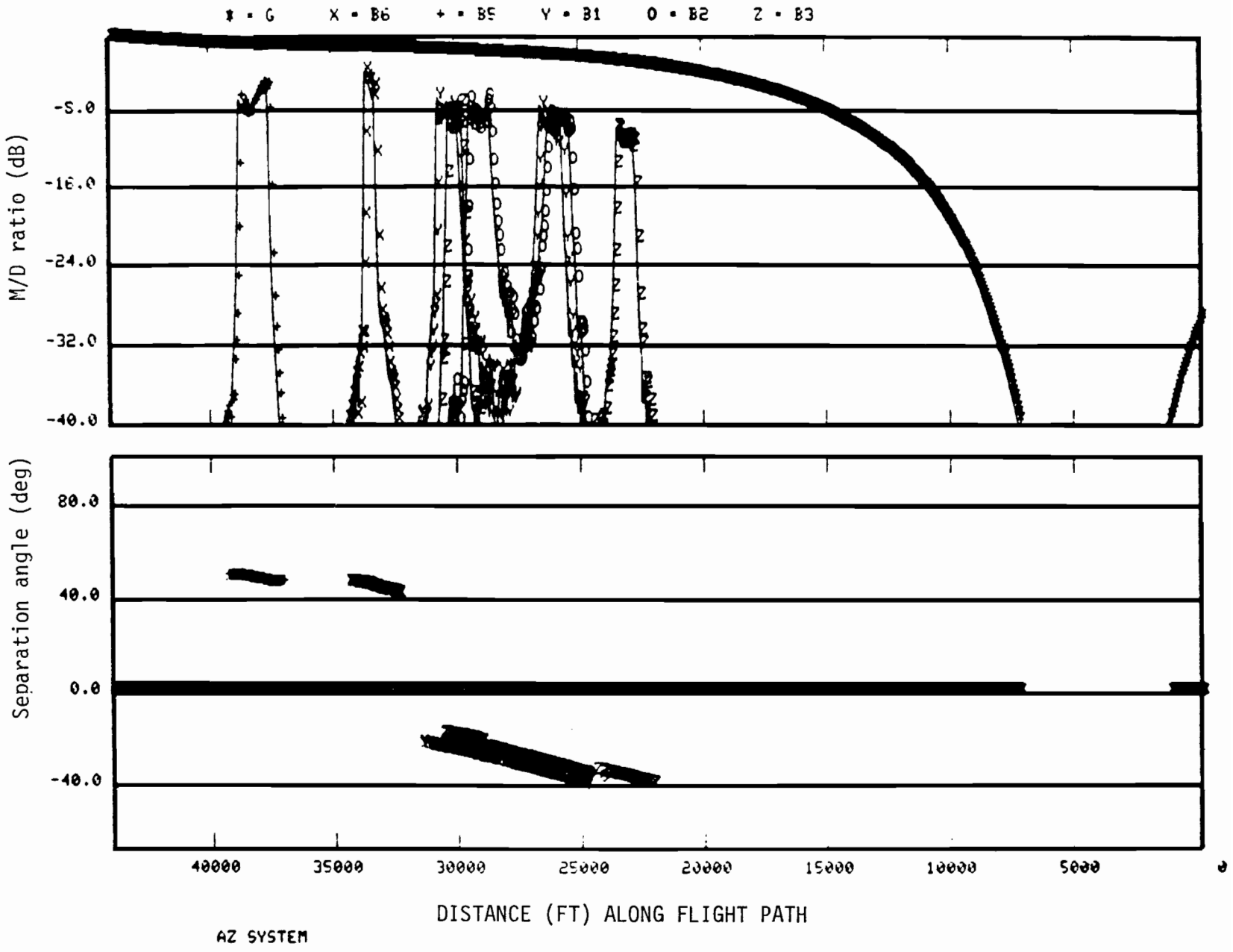

Fig. 3-34. Azimuth characteristics for smooth vertical rock surface model.

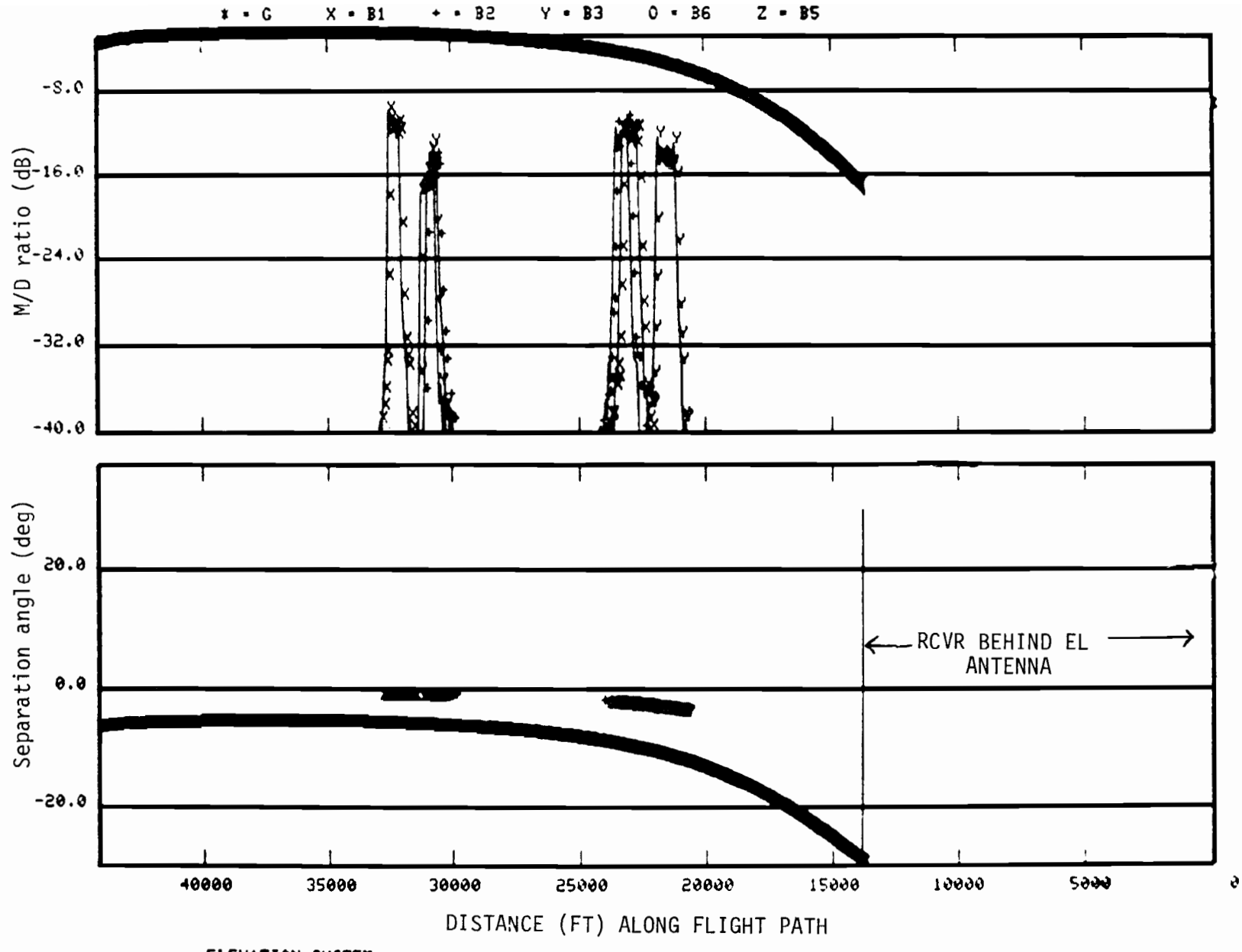

Fig. 3-35. Elevation multipath characteristics for smooth vertical rock surface model.

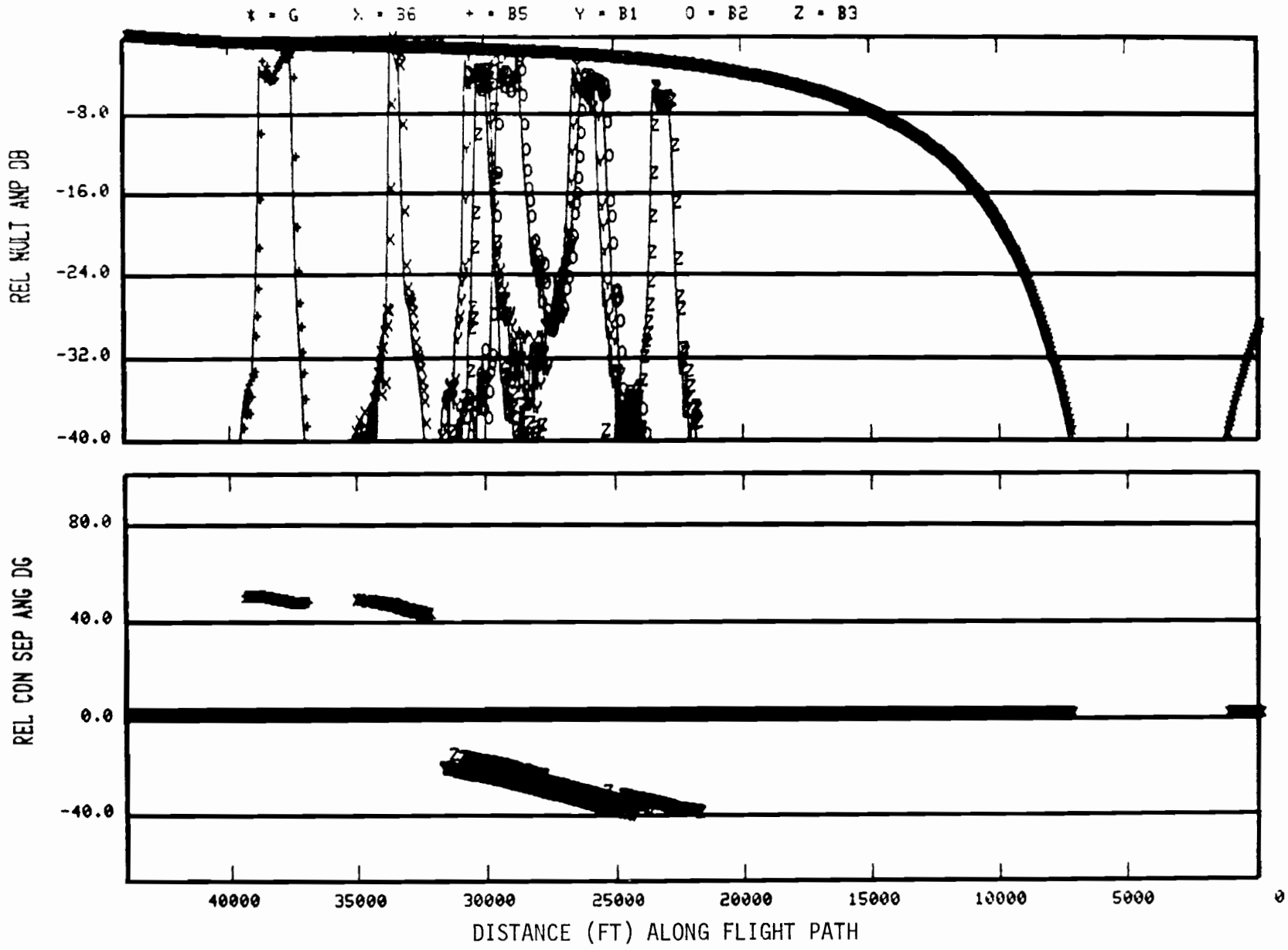

Fig. 3-36. AZ C-band multipath amplitudes and separation angles for vertical metal surface scenario (rms roughness = 0 ft).

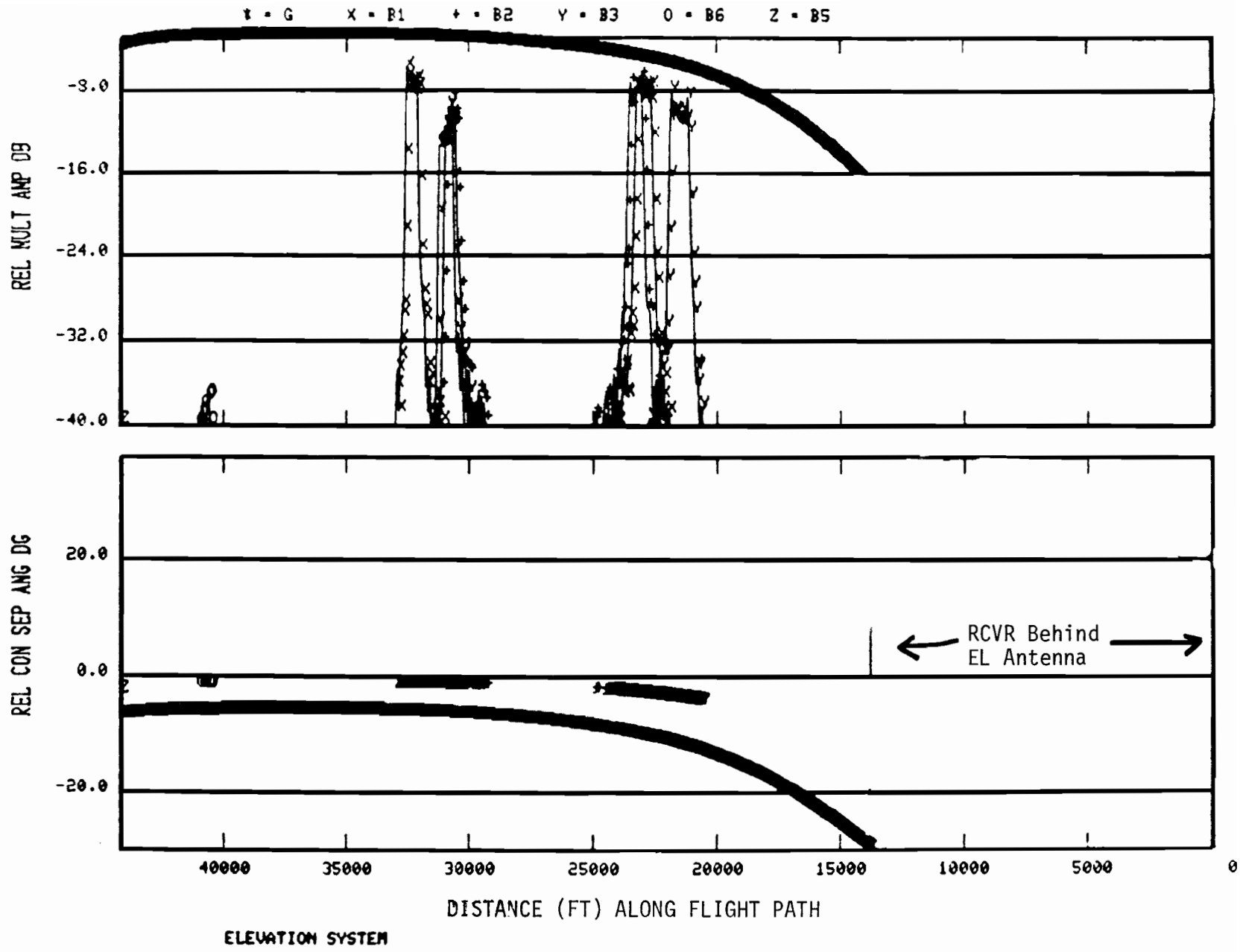

Fig. 3-37. EL C-band multipath amplitudes and separation angles for vertical metal surface scenario (rms roughness = 0 ft).

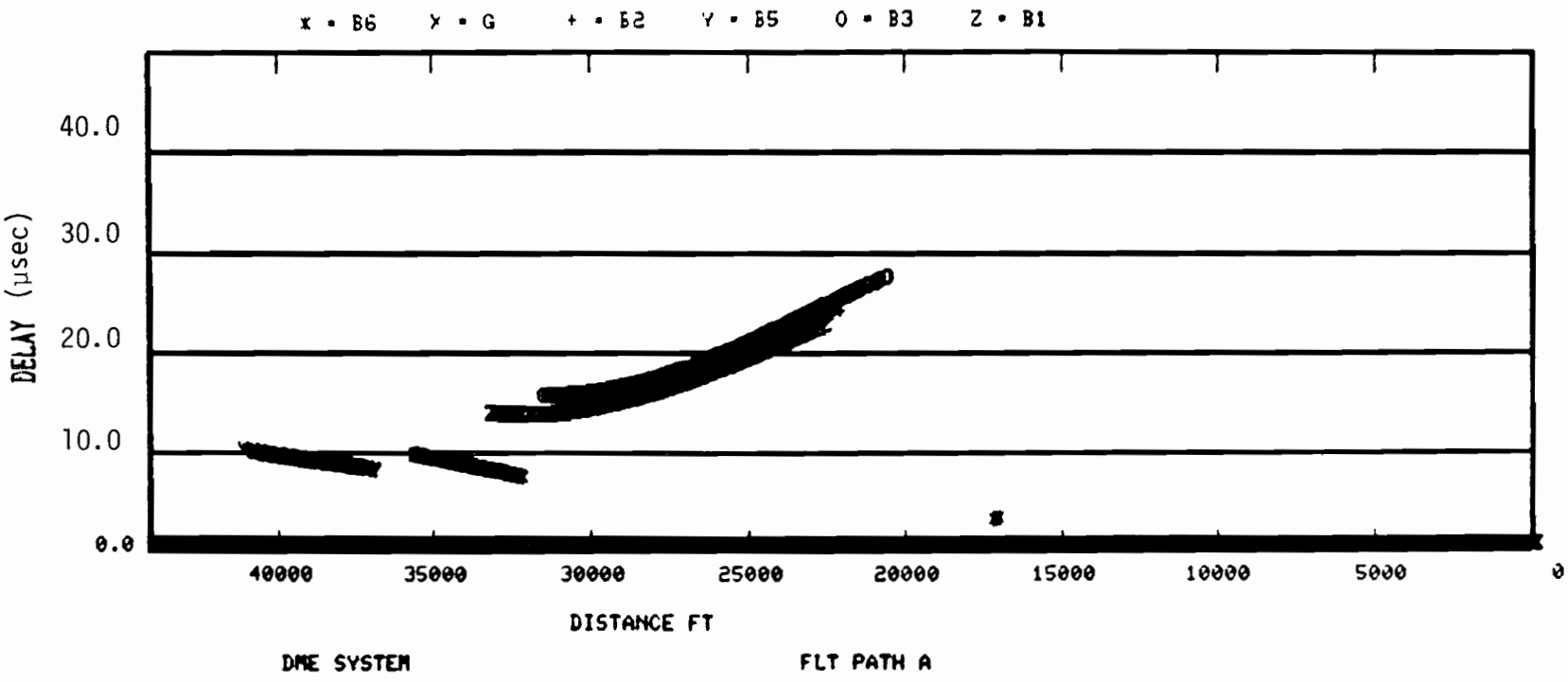

Fig. 3-38. AZ multipath time delays for vertical surface scenario (rms roughness = 0 ft).

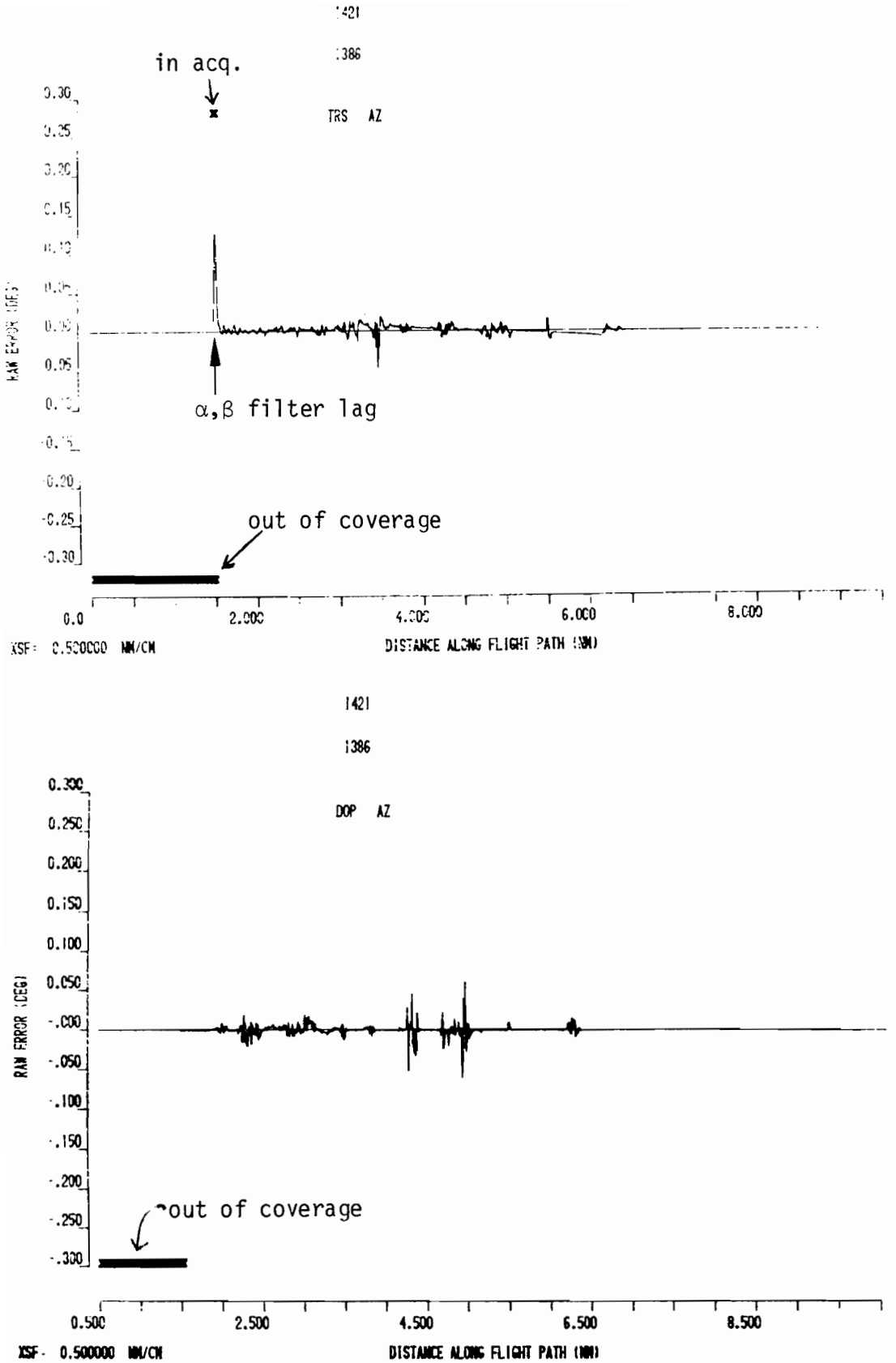

Fig. 3-39. TRSB and DMLS raw dynamic azimuth errors for vertical flat metal scenario

differential path lengths, no multipath component has delay less than 7.5 μsec. In the elevation case, the geometry shows the minimum delay to be even greater. These delays are large enough that DLS time delay discrimination would prevent the corresponding multipath components from causing angle errors.

3. C-band System Simulation Results

The DMLS and TRSB systems were simulated for the smooth vertical metal surfaces scenarios only and the results are shown in Figs. 3-39 to 3-42. The system models used were those described in volume II of this report. The coverage limits for the run were ±60°, not the ICAO suggested ±40°. Since the azimuth and elevation sites are located at different points on the airport surface, the azimuth coverage is entered some 2.5 nmi before entering elevation coverage.

a. TRSB Results

In azimuth (see Figs. 3-39 and 3-40) and elevation (see Figs. 3-41 and 3-42), the TRSB receiver acquired and validated the guidance signal within 1 second upon entering coverage. The transient in the dynamic azimuth data on entering coverage arises from the $\alpha - \beta$ tracking filter start-up procedure wherein the filter takes a while to converge to the high angular rate of change. Although the error that arises is probably not operationally significant, it may be advisable to utilize an alternate filter initialization procedure (e.g., to obtain a non-recursive estimate of the angle rate of change over the initial acquisition period and then initialize the $\alpha - \beta$ recursive filter with this initial estimate).

Lag in the $\alpha - \beta$ filter angle rate tracking during turns yields the low frequency ramp errors. The shorter duration TRSB azimuth errors represent

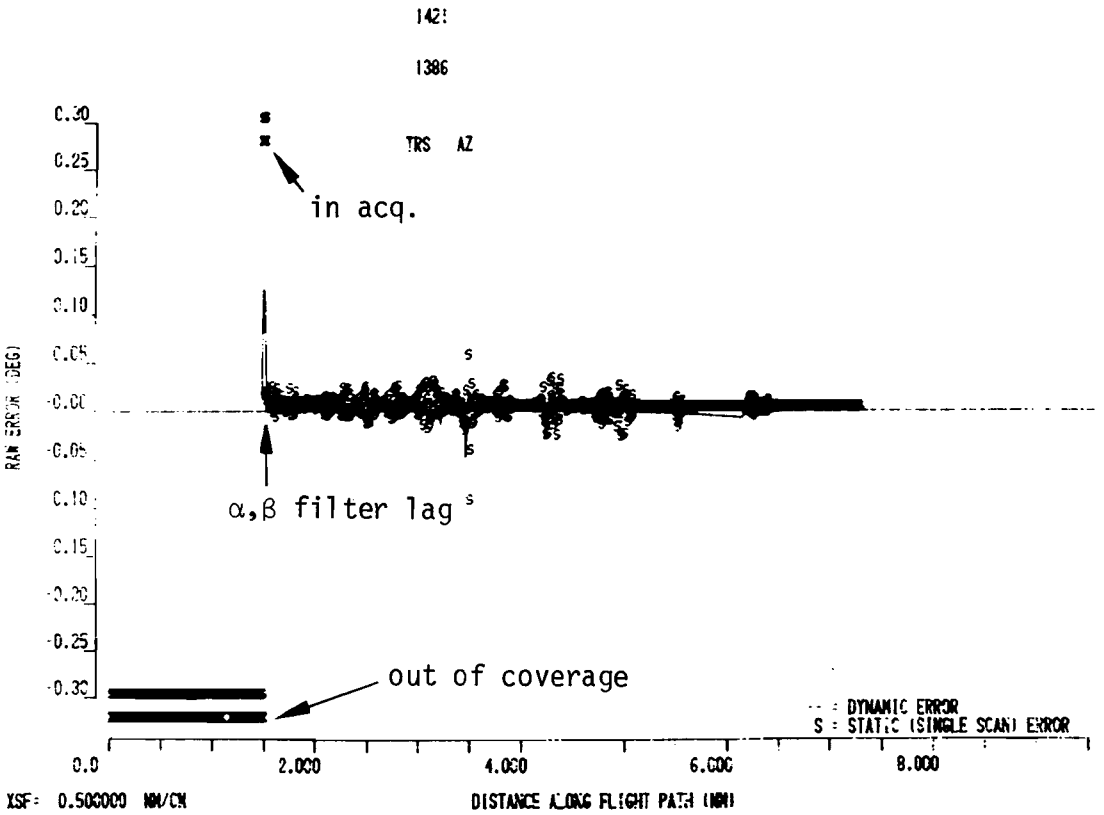

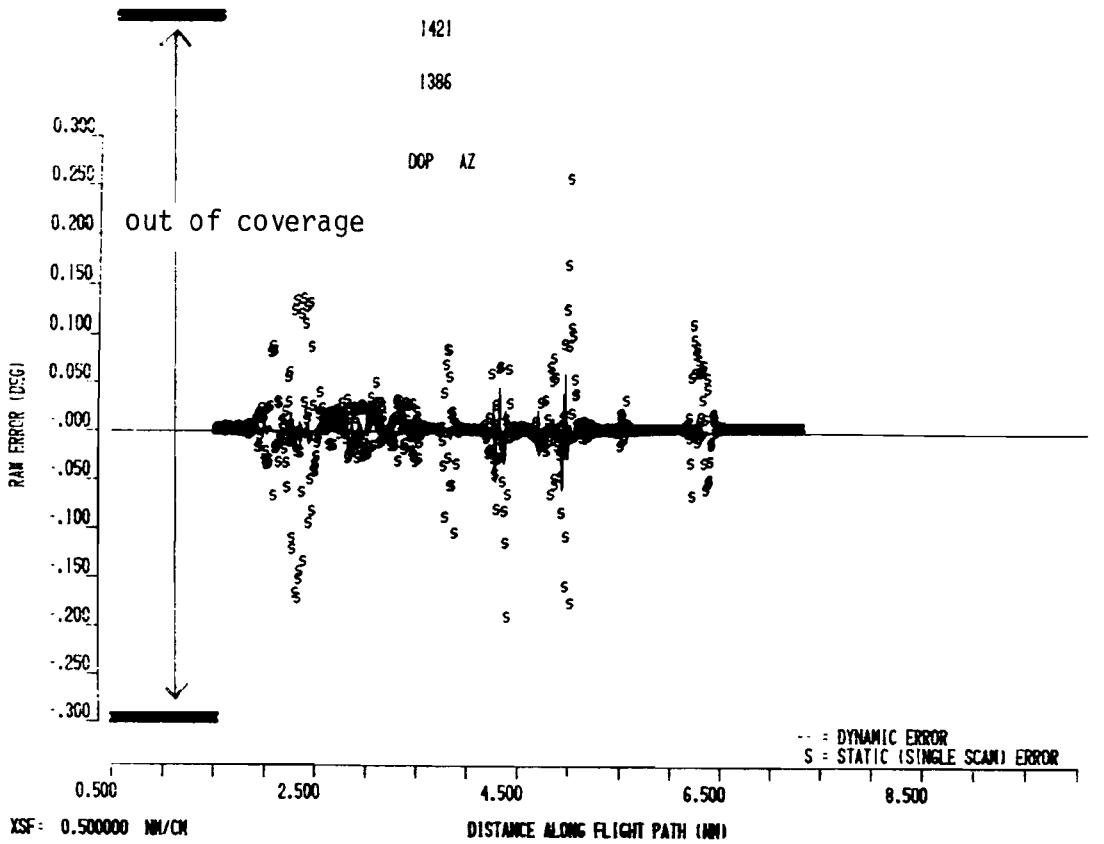

Fig. 3-40. TRSB and DMLS raw dynamic and single scan azimuth errors for vertical flat metal scenario

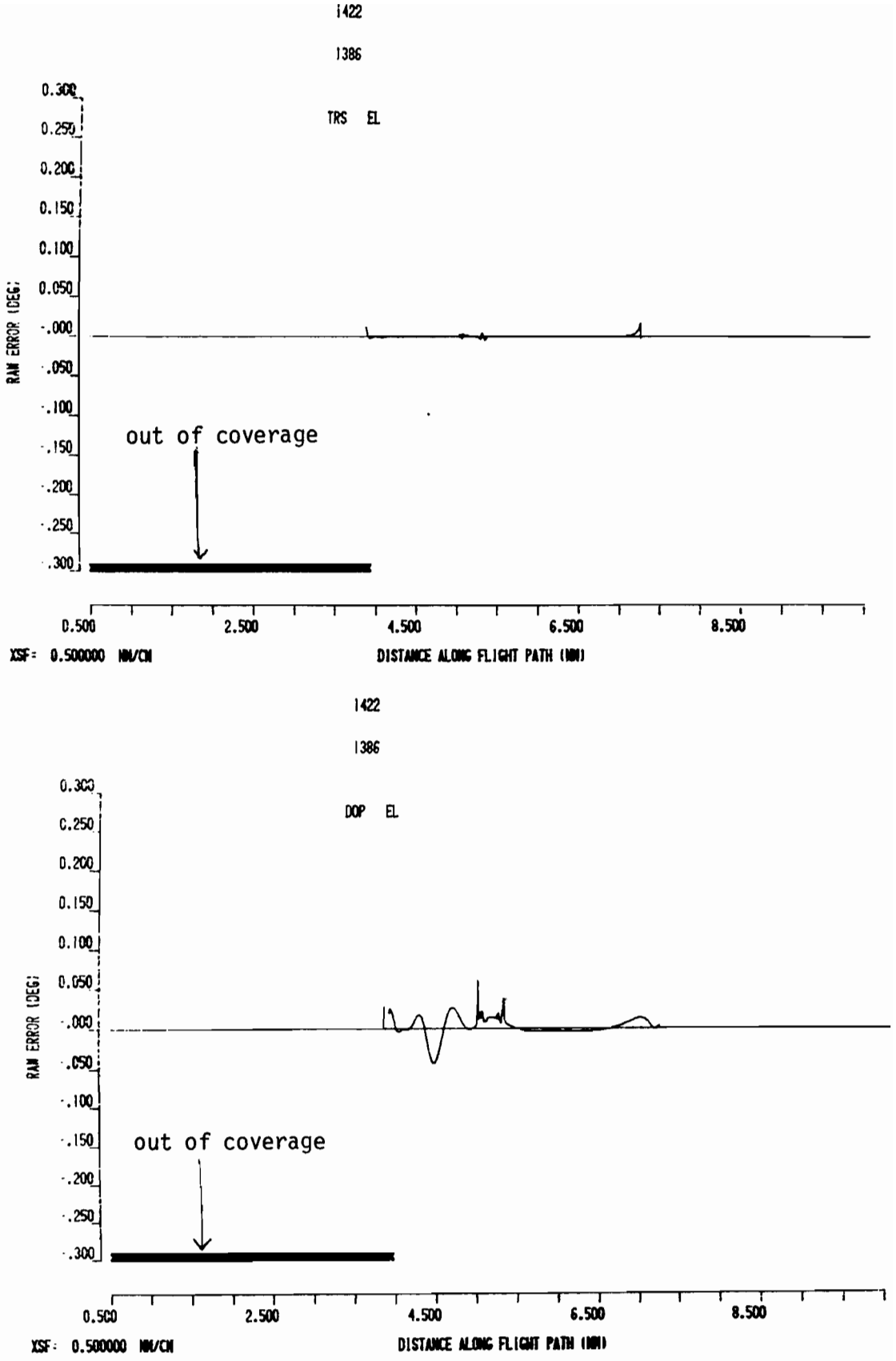

Fig. 3-41. TRSB and DMLS raw dynamic elevation errors for vertical flat metal scenario

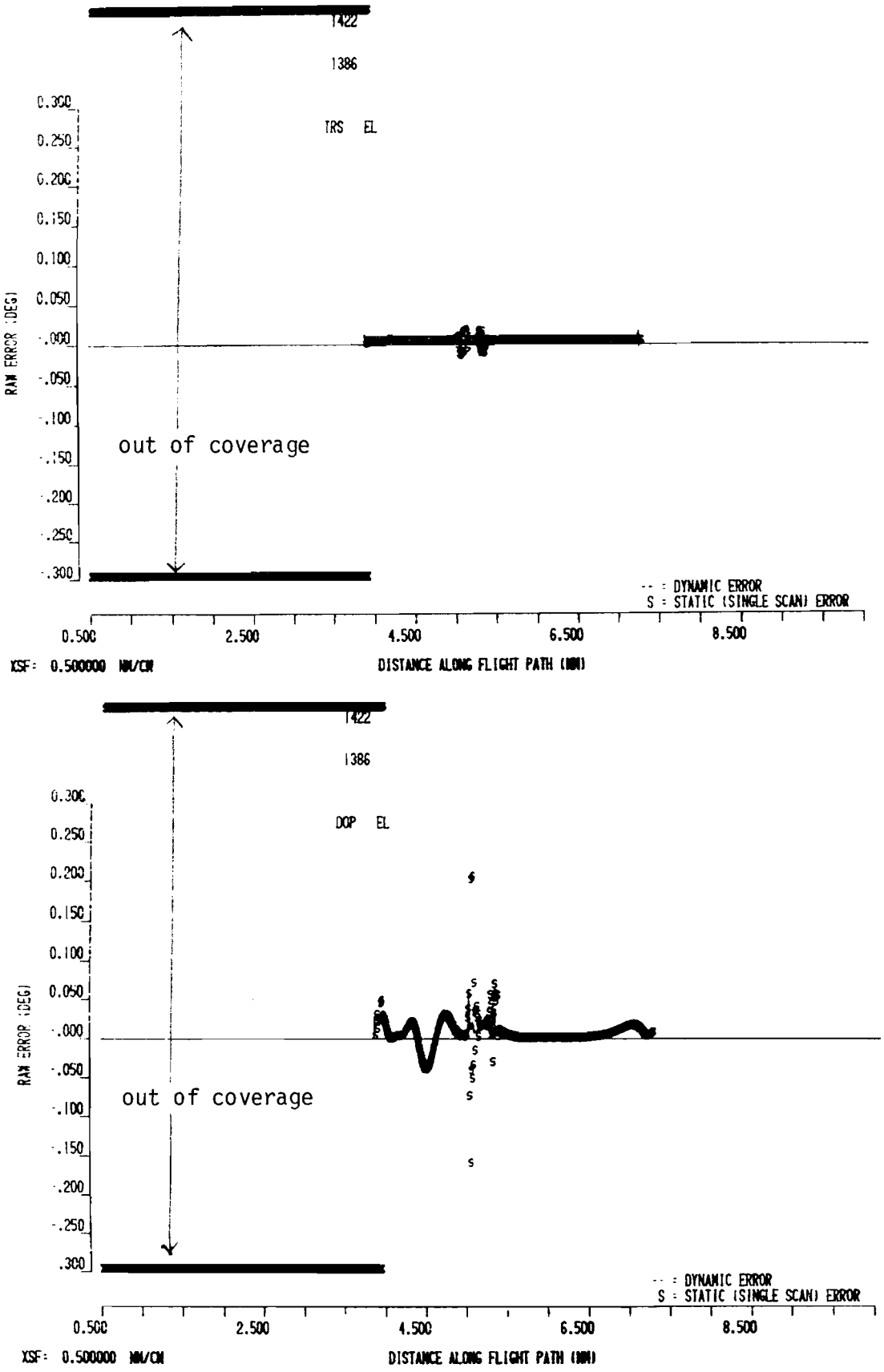

Fig. 3-42. TRSB and DMLS raw dynamic and single scan elevation errors for vertical flat metal scenario

sidelobe errors which have been reduced by motion averaging (compare the single scan and dynamic errors in Fig. 3-40). The elevation TRSB errors represent in-beam elevation multipath which has been reduced by motion averaging. The elevation multipath is nearly out-of-beam due to the longer path traveled by the multipath; hence the static errors are small.

b. DMLS results

The DMLS receiver acquired and validated the azimuth signal within 1 second, but took 2 seconds to acquire and validate the elevation signal due to difficulties in homing under a condition of a high angular rate of change. The DMLS azimuth errors arise principally from dynamic motion effects since the static errors are small for the angle ranges of interest (see Fig. 3-43). The errors near 4.3 nmi along the flight path are due to multipath with a scalloping frequency near +200 Hz from B1. The errors near 5.0 nmi represent a mixture of reference scalloping errors and AGC-induced sidelobe errors (B2 yields multipath near 1200 Hz, which is a multiple of the azimuth scan rate). Figure 3-42 shows that reference scalloping effects from the various scatterers yielded significant single scan errors; however, these were effectively reduced in most cases by the 12 scan averaging.

The error near 6.5 nmi represents a reference scalloping error due to multipath with a scalloping frequency of 491 Hz. Had the final approach segment been flown at 116 knots ground speed as opposed to 150 knots ground speed, the peak error at this point would have been on the order of 0.2° for the flat metal scenario and 0.1° for the flat vertical rock scenario.

The low frequency errors seen in the DMLS elevation data are due to high sidelobes in the current Taylor weight digital correlator algorithm. Figure 3-44 shows a plot of peak DMLS error as a function of multipath angle for a

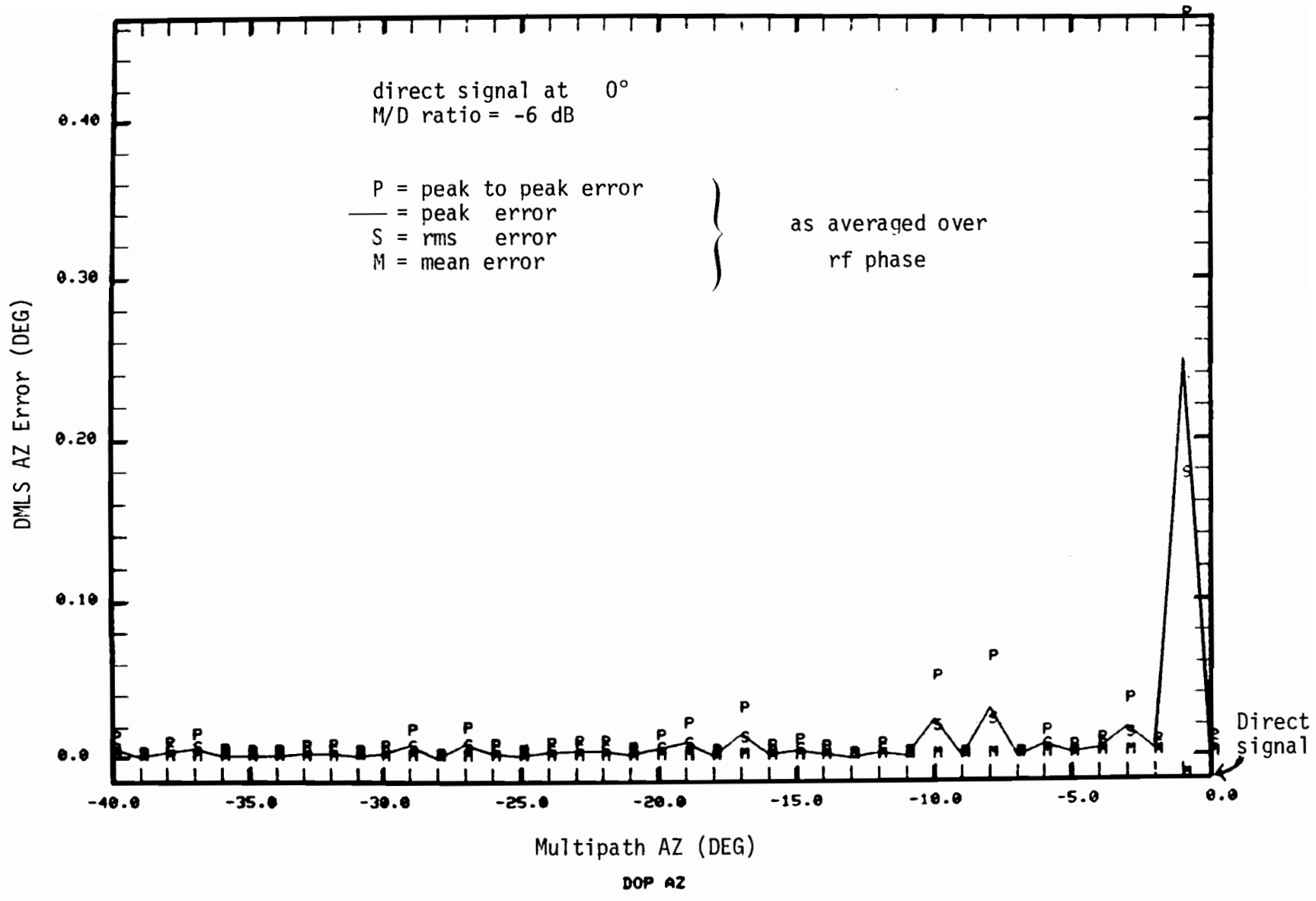

Fig. 3-43. DMLS AZ static error vs separation angle.

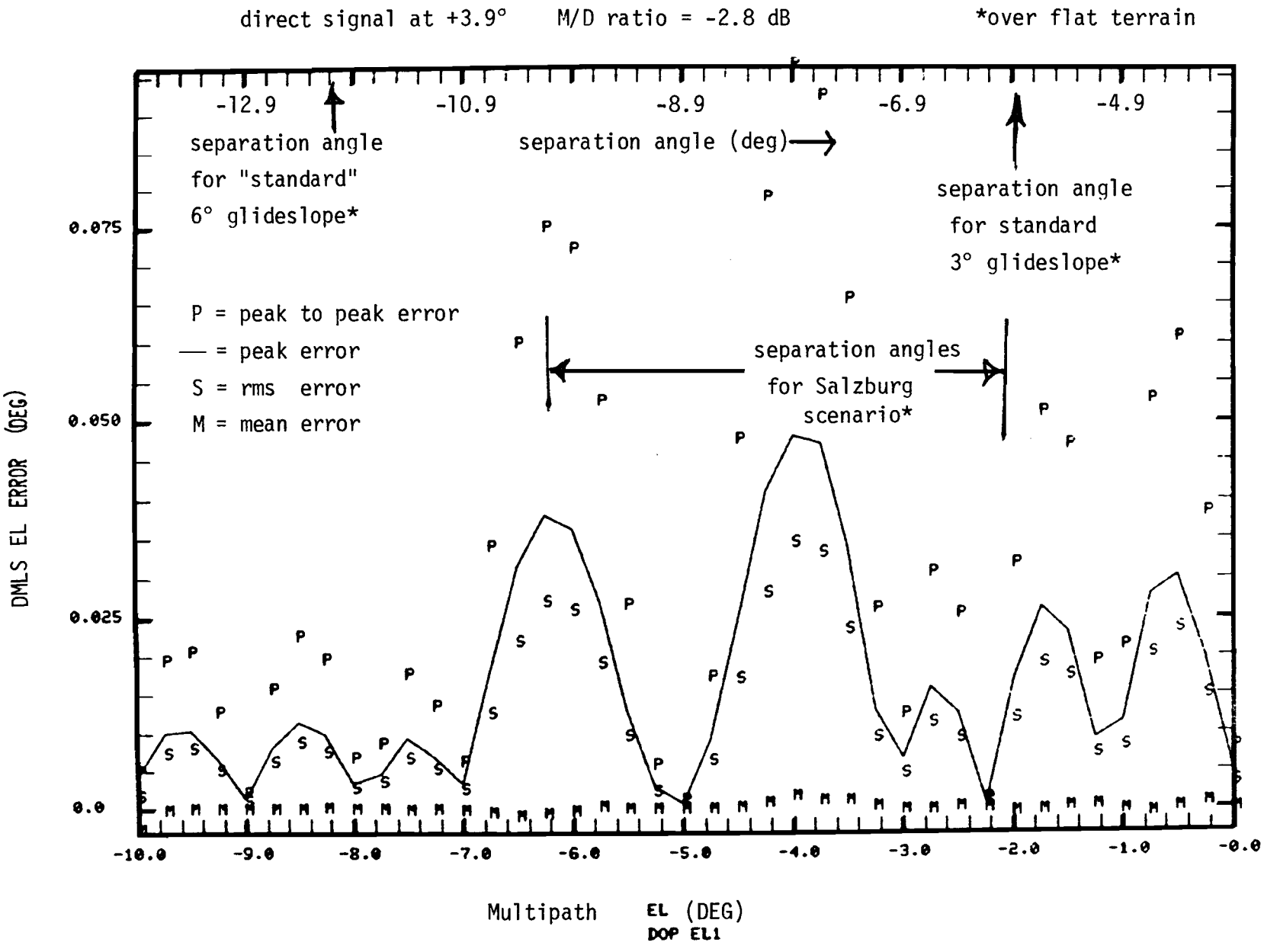

Fig. 3-44. DMLS EL static error vs. multipath angle

direct signal at +3.9 degrees and an M/D ratio of -2.5 dB (≈ ground reflection level at the time of largest errors). Also shown in the figure are the separation angles for this scenario and for a standard radial approach along 3° and 6° glideslopes over flat terrain. As a consequence of the flight profile geometry, the separation angles pass through the region of high sidelobes here, whereas they would not do so on "standard" approaches. The higher frequency DMLS errors arise from a combination of reference and array scalloping effects associated with the reflections from plates B1, B2, and B3. Plate B3 is particularly significant because its multipath is near a multiple of the DMLS elevation scan rate. In such cases, normal motion averaging improvement benefits are not obtained.

As was the case in the other AWOP simulation scenarios, omnidirectional azimuth and elevation patterns were assumed for the on-board antenna. For some portions of the approach (e.g., the initial 130° leg where the direct signal arrives aft of the aircraft and the reflection from B7 arrives to the fore), this assumption could underestimate the received M/D (multipath/direct) ratios, and hence the errors as well. Alternatively, aircraft equipped with switched front-back antennas could discriminate against multipath even more effectively than the simulation indicates. In considering the sensitivity of the results to the aircraft antenna assumption, it is well to recall that signficant multipath errors were found only in the "worst case" scenarios in which the reflected levels are unrealistically large.

We must re-emphasize that the airport model used here may be a very crude approximation of the actual Salzburg environment. No data was available to permit modeling of fine details of the immediate airport environment (e.g., terrain, runway contours, reflecting and/or shadowing buildings, etc.). Moreover, no detailed data was available regarding the degree of vegetation

cover on the mountain slopes nor the actual terrain slope fine structure (e.g, the terrain contour maps [120] do not indicate the presence of the vertical cliffs postulated by the FRG).

4. Extrapolation of Results to Other Mountainous Situations

The insights gained from this particular scenario suggest that situations in which the flight profile lies between the mountains and the runway should not yield significant multipath errors for any of the proposed MLS systems. In particular, we have seen that even small deviations from verticality can yield very low specular levels.

Two other types of flight profile can occur which could yield larger errors:

(a) flight paths passing beside a hill or mountain (e.g., as down a valley)

(b) flight paths which pass over the top of a hill or mountain.

In both cases, especially in case (a), geometric considerations suggest that rough terrain (e.g., diffuse) reflections are likely to be the greatest threat. Unfortunately, there is not currently available sufficient experimental data regarding rough terrain reflection characteristics to adequately validate the propagation model for such scattering [121].

Scanning beam tests at Ku band using AIL equipment were conducted at French and Norwegian mountainous sites such as cases (a) and (b) above. A paper by AIL indicates that good performance was obtained at these sites. Theroetical considerations suggest that Ku band would yield lower specular reflection levels over rough and/or vegetated terrain than would be the case at C or L band.

Both of the mountainous situations discussed above would be more likely

to yield substantial DLS errors than was the case for the Salzburg scenarios considered here. This is because the multipath time delays would generally be much shorter than in the Salzburg scenarios. Additionally, the larger wavelength of the DLS system is expected to yield greater specular reflection levels for rough and/or vegetated terrain than would be the case at C band.

Another factor in DLS performance which was not simulated here, but may be worthy of future study, is the decoding problems generated by multipath of long delays such as arose here. This could take two forms:

(1) downlink garbling of the ground station identity

(2) coherent uplink angle code garbling

IV. STUDIES OF COMPARATIVE PERFORMANCE WITH SHADOWING BY AIRCRAFT

A. Introduction

At the November 1976 meeting of WG-A in London, considerable controversy arose over the comparative resistance of DMLS and TRSB to azimuth shadowing by intervening (i.e., taxiing or overflying) aircraft [126 - 129]. Subsequent to that meeting, a variety of analytical studies of the shadowing phenomena were conducted as well as field tests. This chapter summarizes the various results which bear on this issue.

In the next section, we present a conceptual background for representing shadowing phenomena with the two systems. The viewpoint taken is that shadowing can be thought of as a multipath problem in which various diffraction rays (from the obstacle center or edges) act much like specular reflections. This permitted us to investigate the phenomena using the same framework that was successfully used by the AWOP WG-A performance subgroup to study low angle elevation performance.

The "new" feature here is that the most severe shadowing problems arise when there is more than one inbeam multipath component present. The hybrid-bench simulators at RAE (UK) and CALSPAN (US) were limited to a single multipath component; thus, computer simulations were done to quantify the respective system responses to multiple inbeam multipath signals. Results for these are shown in Section C.

Some useful information can be obtained from the various field test results. The results for DLS, DMLS, and TRSB systems in the AWOP WG-A tests

are compared in Section D. Also presented in Section D are summary results for the Doppler and Scanning Beam contractor tests in the U.S. Phase II program.

The field test data proved difficult to compare directly due to differences in shadowing geometry, shadowing aircraft size, etc. Consequently, a number of comparative simulations were carried out. The results of these are shown in Section E. Section F summarizes the results of the various investigations.

B. Conceptual Framework

1. Shadowing Environment

The philosophical framework proposed here is that shadowing is analogous to specular reflections from the ground and buildings. Although this approach has been used in the quantitative studies to date, some of its consequences may be surprising. The basic idea is simple:

1. the received signal can be written

$$r(t) = fs(t) + shad(t) \tag{4-1}$$

where fs(t) is the received signal in the absence of shadowing,

$$shad(t) = \text{signal generated by shadow} \approx -a(t) \tag{4-2}$$

a(t) = signal generated by diffraction through an aperture which has the projected shape of the shadowing object

2. fs(t) can be represented by a direct signal ray

3. a(t) can be represented by a set of diffracted rays which have all the characteristics of specular reflections.

Mathematical models based on this viewpoint have been shown to agree with field data in MLS [29, Volumes I and II of this report] and ILS studies [3]. Theoretically, this general approach has its roots in the geometric theory of diffraction [126, 130]. Capon [29] gives an explicit description of the diffracted ray angles and amplitudes for rectangles (as well as some theoretical refinements not covered in the brief treatment here)*. Two cases are worth noting:

1. diffraction by a high wide rectangle when line of sight (LOS) is not blocked as in Fig. 4-1. Here, the diffracted ray from the near edge is of greatest concern. Its amplitude relative to the unshadowed direct signal is given by [11, 29]:

$$\rho \approx \begin{cases} \frac{1}{2} - \Delta y/R_f \sqrt{2} & \Delta y < R_f \\ R_f/2\pi\Delta y & \Delta y > R_f \end{cases} \qquad (4\text{-}3)$$

where R_f is the Fresnel zone radius.

Since $\Delta y > 0$ if the LOS is not blocked, $\rho < 0.5$, i.e., the equivalent M/D ratio is always less than -6 dB.

---

*The discussion here is based on the initial MLS shadowing model described in [29] as opposed to the refined model discussed in Volume I of this report. These two statements differ only in the number of diffracted rays associated with certain situations (e.g., shadowing obstacle in near field of an array or $\Delta y < R_f$ for a large blocking obstacle).

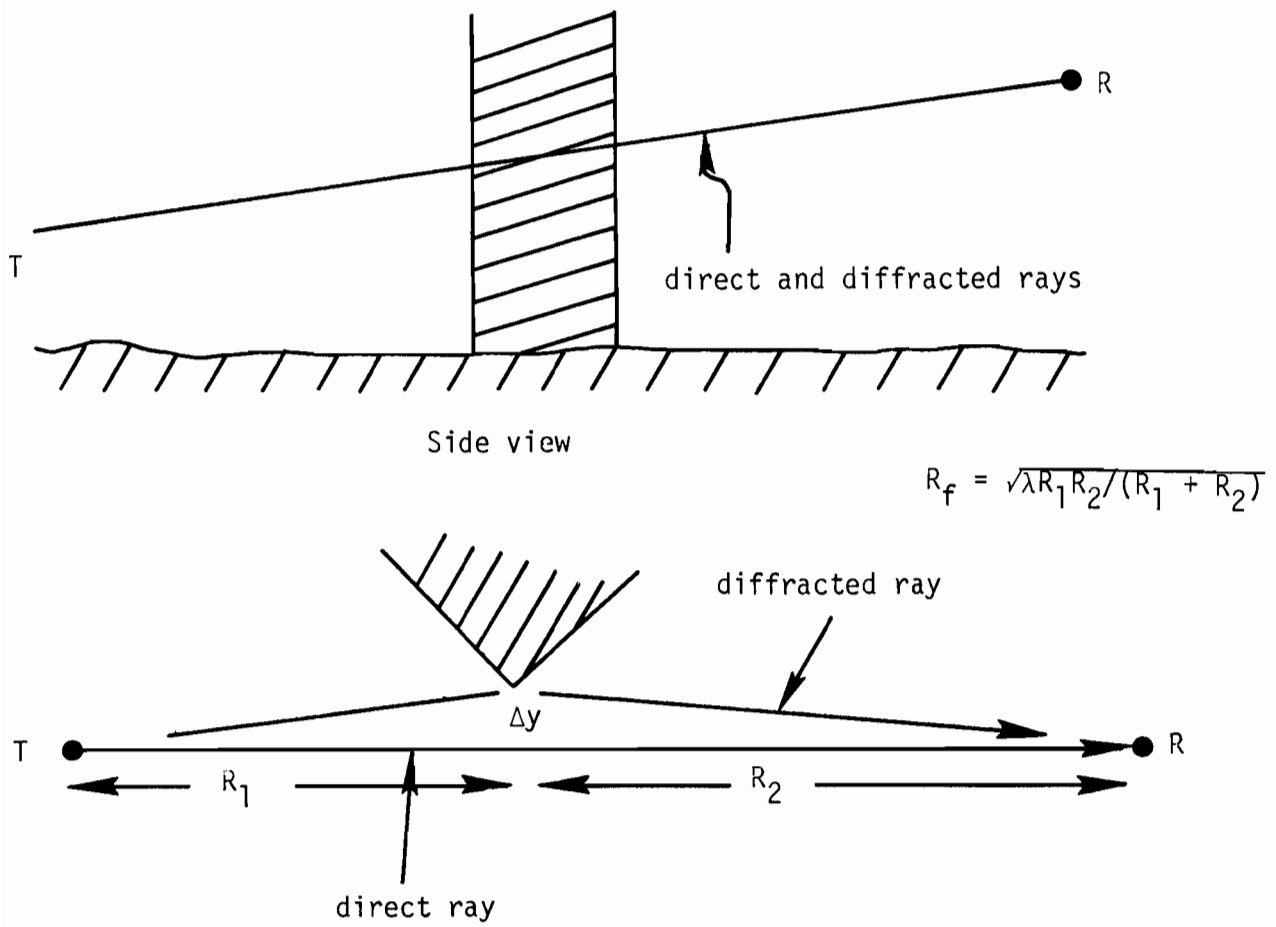

Fig. 4-1. Diffraction by a large obstacle when the LOS is not blocked.

2. diffraction by a large rectangle which blocks the LOS. Now, there are direct signal coded rays which pass over and under** the object as well as side edge rays. The side edge ray amplitudes are given by (4-3) with Δy as shown in Fig. 4-2. The top and bottom ray amplitudes are approximated by (4-1) with Δy replaced by the Δz_i from Fig. 4-2. If $\Delta y_i < \Delta z_1$ and Δz_2, then the effective M/D can be > 1.0. Such cases are clearly challenging for an MLS.

More complicated shapes such as aircraft can be treated as a set of nonoverlapping rectangles with (4-2) becoming a sum over the signals diffracted through the various rectangles.

One of the rather surprising consequences of the above framework is that the shadowing environment is identical for DMLS and TRSB unless the ray amplitudes were to vary "substantially" over a single scan duration. Here, "substantially" means Δy or Δz is changing a sizable fraction of R_f. This does not occur in realistic cases:

Example 1: aircraft taxiing off runway at 15 mph at a distance of 1000 feet. Here $R_f = \sqrt{(.197)\ (1000)} =$ 14 ft. The aircraft moves:

(a) 0.16 feet during a TRSB to-fro scan and 0.002 feet during the time the main beam is scanning by the TRSB receiver

(b) 0.76 feet over a DMLS frame (12 scans) and 0.06 feet during a single DMLS scan

---

**It is suggested in [128] that rays beneath a fuselage are not important due to the rolloff in elevation pattern of azimuth arrays. This, however, is not quite the case, since the elevation angle subtended by fuselages is often small. For example, the fuselage of a VC-10 1500 feet from the azimuth transmitter subtends an angle of 0.46°. A "typical" pattern rolloff of 6 dB/degree attenuates the bottom ray by 2.8 dB. The 1971 paper of J. Benjamin and Reich [132] notes the importance of rays passing beneath the fuselage in interpreting the RAE shadowing field data.

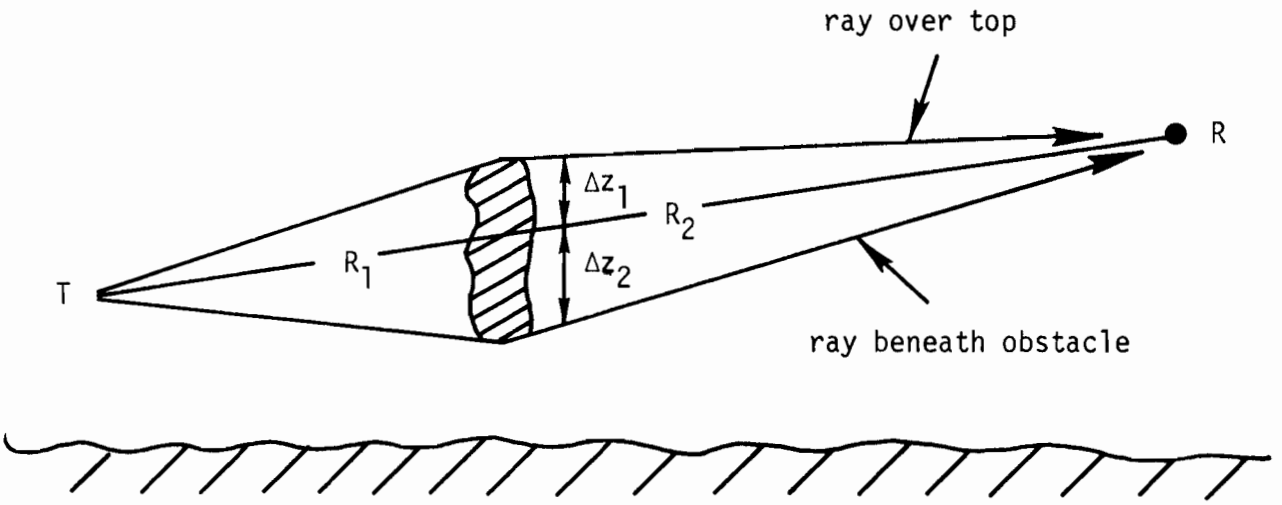

Side view

$$R_f = \sqrt{\lambda R_1 R_2 / (R_1 + R_2)}$$

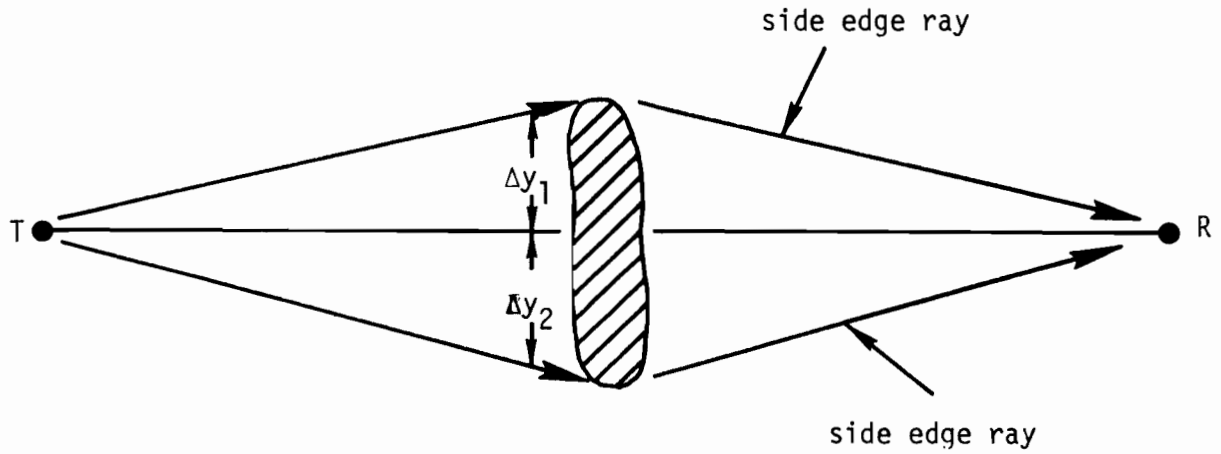

View from top

Fig. 4-2. Diffraction by a large obstacle which blocks the LOS.

Example 2: aircraft taking off over azimuth site at 160 knots at a distance of 1000 feet at an angle of 6°. The receiver is at an elevation angle of 1° with respect to the azimuth site. The projected shape moves upward:

(a) 0.2 feet during a TRSB to-fro scan and 0.003 feet during the time the main beam scans by the TRSB receiver

(b) 0.96 feet over a DMLS frame (12 scans) and 0.08 feet during a single DMLS scan.

In both examples, we see that the aircraft movement is a small fraction of R_f.

Consequently, the errors do not arise from variations of shadowing loss due to movement of the taxiing or overflying aircraft, but rather from the distortion in the radiated field caused by the shadowing object. We stress this point because people with a communications background often have the notion that the angular errors arise entirely from a reduction in received signal amplitude during the measurement period.

The fact is that shadowing causes problems in two ways:

1. signals from a single element (e.g., a function ID antenna) are reduced in amplitude such that there might not be adequte SNR.

2. the shadowing of the signal from distributed apertures (e.g., line arrays) changes as a function of position on the aperture so as to cause angle errors when the antenna is scanned.

This second phenomena is what we represent by the edge ray formulation.

The principal new factor introduced by aircraft shadowing is the likelihood that more than one in-beam multipath signal may be present at a given instant of time. For example, the rays diffracted around the sides of a taxiing (or overflying) aircraft which is on runway centerline may both be

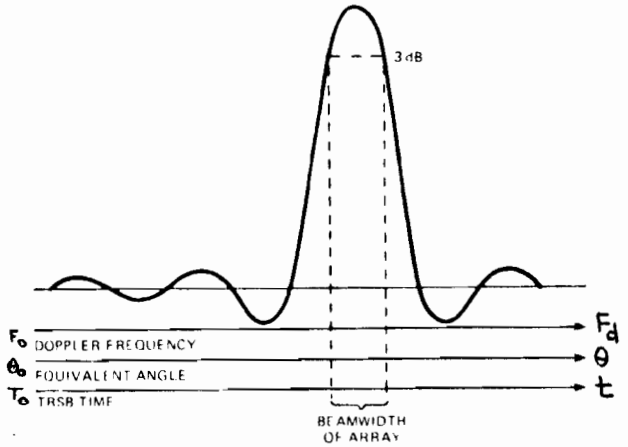

Received commutated spectrum. (from Barratt (1976) [18])

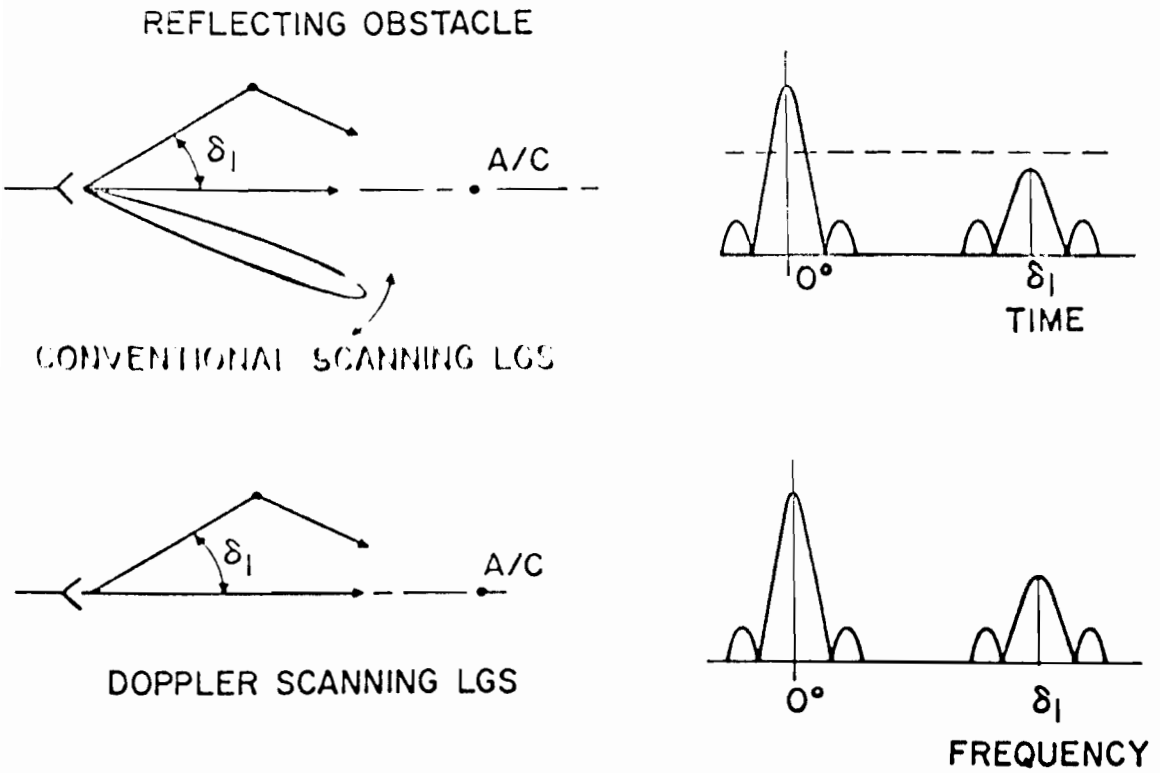

Multipath Geometry and Received Signals for Doppler and Conventional Scanning LGS (from Redlein and Masek (1971) [11])

Fig. 4-3. Equivalence of TRSB time envelope and static DMLS spectrum.

inbeam (e.g., the sides of a B747 at 1000 feet are at ±0.6°). By contrast, the AWOP multipath scenarios of Chapter II generally had, at most, a single in-beam multipath signal at a given point along the flight path.

2. Direction Finding for DMLS and TRSB

The objective of this section is to set forth a common framework for understanding DMLS and TRSB direction finding in a static environment*. The arguments here also are simple:

1. the received DMLS spectrum on a scan is equivalent to the received TRSB time envelope on a scan

2. both systems attempt to track the peak of the appropriate envelope: spectrum envelope in the case of DMLS and time envelope for TRSB,

3. the current implementations of peak tracking are different, but interchangeable. For example, the DMLS sum/difference tracker is analogous to the split gate tracker used in Australia for TRSB [16].

The equivalence of TRSB time envelopes and DMLS spectrum have long been recognized [131, 133]. Figure 4-3 illustrates the equivalence for a direct signal plus a single multipath signal. For the general case of N multipath components, it can be shown that:**

---

*In a dynamic multipath environment (i.e., appreciable scalloping frequencies), the equivalence argued here disappears, as will be discussed in the next chapter.

*We ignore here TRSB phase shifter noise and DMLS AGC effects; both of these yield second-order modifications to (4-4) and (4-5).

1. The DMLS spectrum is

$$R(\omega) = \sum a_i \, e^{j\phi_i} \, S[(\omega-\omega_i)T_s]$$

$$\text{with } (\omega-\omega i)T_s = \frac{v_s}{\lambda} (\sin\theta - \sin\theta_i)T_s \qquad (4\text{-}4)$$

$$S(u) = \int_{-.5}^{.5} a(x) \, e^{jux} \, dx$$

2. while the TRSB envelope is

$$r(t) = \left| \sum a_i \, e^{j\theta_i} \, S\left[\frac{L}{\lambda} (\sin \dot{\theta}t - \sin\theta_i)\right] \right| \qquad (4\text{-}5)$$

where v_s is the DMLS scan velocity and T_s the DMLS scan duration and

> a(x) = aperture weight -- applied as a time weight at receiver for DMLS and as driving coefficients for TRSB.

For equal aperture sizes, vT = L so that $|R(\omega)| = r(t)$.

The importance of the above equivalence is that any distortions which occur in the received TRSB envelope also occur to the same degree in the received DMLS spectrum! Thus, there is no reason to believe a priori that the DMLS use of amplitude as a function of frequency will be markedly different from the TRSB use of amplitude as a function of time, although differences

could arise from the fact that the DMLS has access to the phase information in $R(\omega)$.

We now want to show that the DMLS processor using the sum/difference tracking loop is quite similar to the TRSB split gate trackers in a static multipath environment. The DMLS tracker derives an error signal $\mathrm{Im}(\Delta/\Sigma)$ on each scan and uses this error signal to change the correlation frequency until a zero error signal is achieved (see Volume II Chapters 3 and 4). This generally* corresponds to $\Delta = 0$. If we assume $a(v) = 1.0$, then we have the condition

$$\Delta = \int D(\omega)\ S(\omega - u)\ du = 0 \qquad (4\text{-}6)$$

where $D(\omega)$ = the transfer function corresponding to the difference time weight coefficients. A typical $D(\omega)$ is shown in Fig. 4-4.

If we approximate $D(\omega)$ by a square wave as shown in Fig. 4-4, then the solution to (4-6) can be interpreted as a point at which equal masses lie under the $S(\omega)$ on each side of the tracker position.** Similarly, a TRSB split gate tracker achieves equilibrium when equal time envelope masses lie on each side of the tracker position. Such an equilibrium point may not neces-

---

*More precisely, the component of Δ which is in quadrature with the Σ must be zero. The worst case error condition corresponds to a multipath relative phase of 0° or 180° with respect to the direct signal, in which case Δ=0 for equilibrium.

**The rigorous interpretation is that equal masses lie under the two sides of a weighted $S(\omega)$ curve.

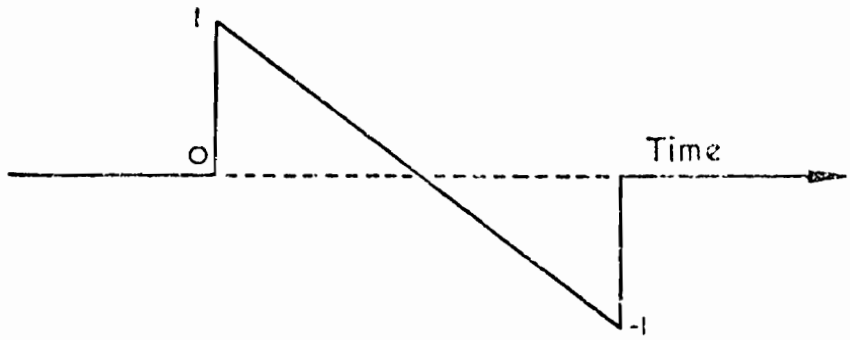

Taper function for difference pattern.

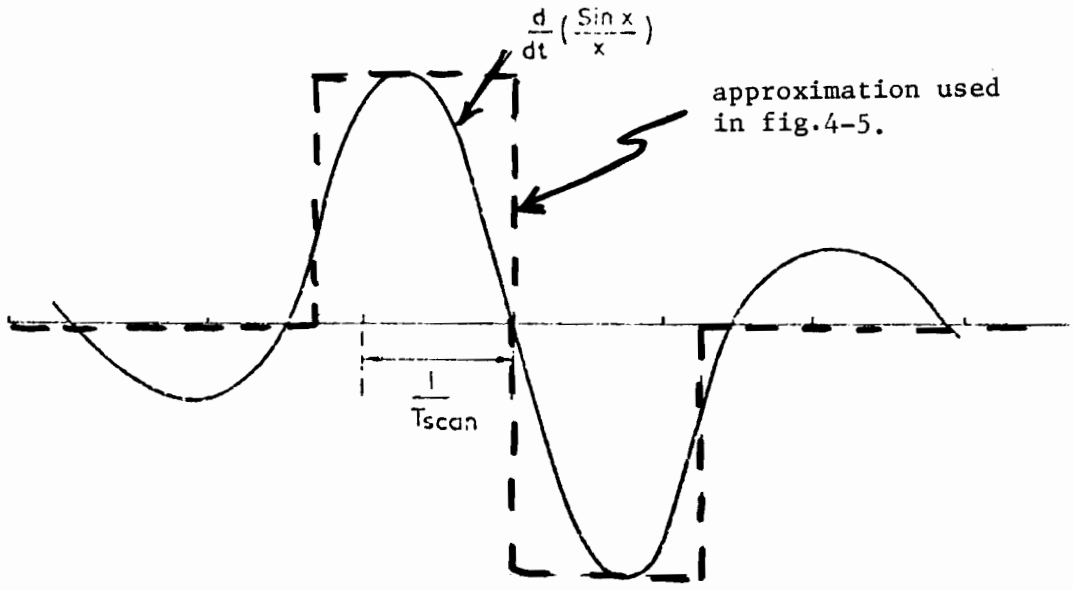

Fig. 4-4. Transfer function of DMLS difference correlation.

be stable, i.e., one must determine whether the tracker returns to the null position when perturbed slightly away from it.

Figures 4-5 and 4-6 provide a graphical illustration of peak finding by the two methods: thresholding and split-gate tracking. The key questions to be addressed are the:

1. differences between thresholding and split-gate tracking
2. utility of the "phase information" utilized in forming $\mathrm{Im}(\Delta/\Sigma)$

These topics are addressed in the next three sections.

C. Static Error Characteristics for DMLS and TRSB With Two Multipath Components

In this section, we present the results of computer simulations in which two multipath signals are present in addition to the direct signal. The objective is to give some insight into the errors that arise when the LOS is blocked by a tail fin or fuselage.

The current hybrid simulators at RAE (UK) and CALSPAN (US) cannot inject two multipath signals into the respective receivers - thus, it is not possible to compare these computer results with bench simulator data. However, the comparisons made between the DMLS and TRSB simulation models and single multipath component bench simulator data in Volume II of this report showed good agreement.

It is quite hopeless to show all the possible combinations for two multipath components. Thus, we will, for the most part, confine attention to the case of multipath signals symmetrically separated from the direct signal. In

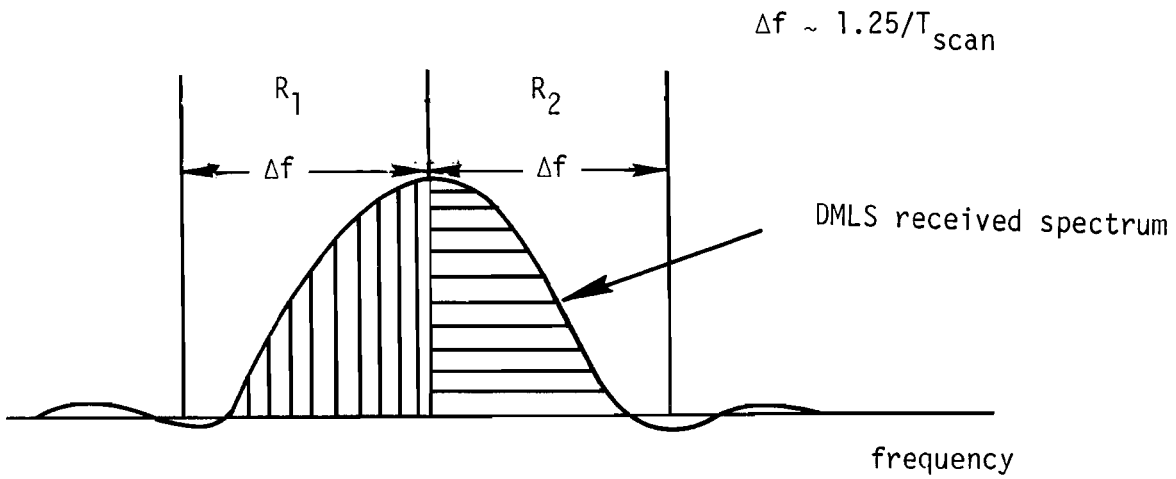

f_c = tracker estimate of spectrum peak location
= frequency such that area under R_1 = area under R_2

Fig. 4-5. Proposed DMLS peak centroid estimation.

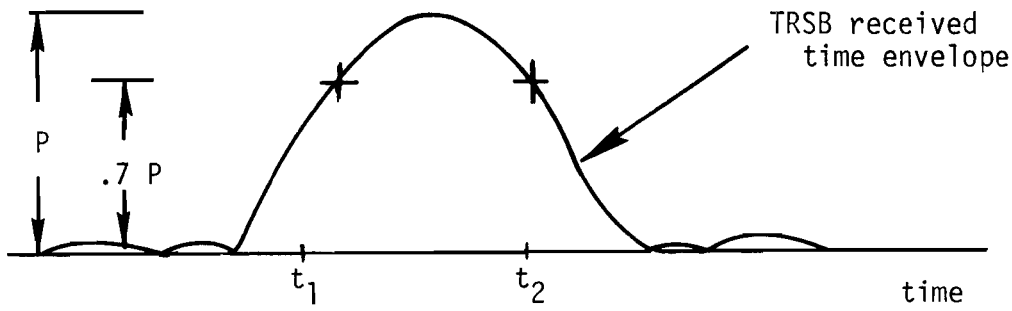

$$t_c = \frac{1}{2}(t_1 + t_2)$$

= estimate of peak location

Fig. 4-6. Peak centroid estimation in proposed TRSB implementation.

a number of cases, we will show the corresponding time/frequency envelope to give some insight into a particular error phenomena.

The computer program used to drive the respective system models treats as its independent variable one of the multipath characteristics for the first multipath signal. It is convenient to use the rf phase of that multipath signal relative to the direct signal as the independent variable.

One problem that arises with two multipath signal tests is that of past inputs.** With single multipath signals, there is generally only one stable equilibrium point for a tracker; thus, the previous inputs will generally not effect the error for a given multipath input. However, with two (large) multipath signals, there can be more than one stable equilibrium point, in which case the history of past inputs can substantially change the error. To minimize such effects, the input sequences have been chosen to

(a) yield a single stable point for both systems at the start of a sequence of rf phase changes,

and

(b) be the same for both systems.

Another aspect which can modify the results is the acquisition/validation tests. For example, the TRSB thresholding processor has dwell gate validation tests which have no direct counterpart in the current DMLS implementation. Similarly, the DMLS correlator comparison of tracked signal level with the results of the Ord bin search process is not quite equivalent to the TRSB checks due to the width of the DMLS search bins (6°). To understand the "basic" error phenomena, tests were also run in some cases with this logic

---

**Some discussion of this topic also appears in the UK studies [126].

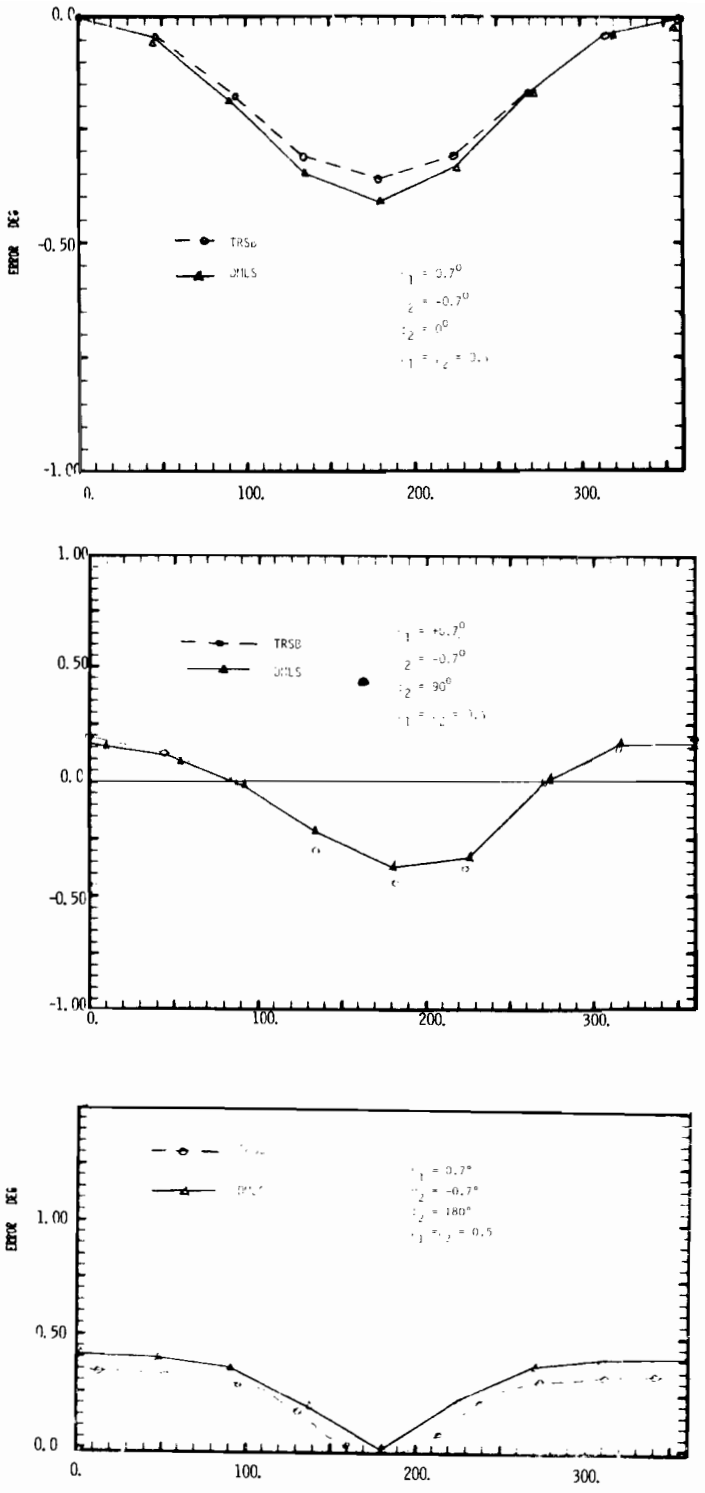

ϕ_1 = rf phase of multipath signal 1

Fig. 4-7. Comparison of errors for two -6 dB multipath signals at $\pm$ 0.7° separation angle.

disabled so that a more direct comparison of thresholding versus null tracker performance could be made.

The principal focus in the simulation tests was the case of two multipath signals at ±0.7° separation angle. Such angle might correspond to:

1. a narrow body jet fuselage parallel to centerline 500 feet from azimuth transmitter, or a similarly oriented wide body jet 1000 feet from the azimuth transmitter.

2. the average width of a large narrow body jet (B707) tail perpendicular to centerline (as in turnoff) some 550 feet from the azimuth transmitter; or the average width of a similarly oriented B747 some 1100 feet from the azimuth transmitter.

In Fig. 4-7, we compare the system errors when both multipath signal levels are -6 dB. The error behavior here is quite similar. Zero error arises when both multipath relative phases are 0°, 90°, or 180° because the received envelope has a single large peak and is symmetrical about the direct signal.

In Fig. 4-8, we compare the system errors when both multipath signal levels are -3 dB. Zero error again arises when both multipath relative phases are 0° or 90°; however there is a large error when both multipath relative phases are 180°. The reason for this is obvious from Fig. 4-9; the received envelope has its largest peaks at ±1.0° due to cancellation at the direct signal angle. Since both systems attempt to find the peak of the respective envelopes, it is not surprising that they both make a large error.

In the UK analytical investigation of shadowing [126], it was suggested that in this situation, TRSB would make a large error, but that DMLS would not due to symmetry. The argument presented in [126] for no DMLS error is

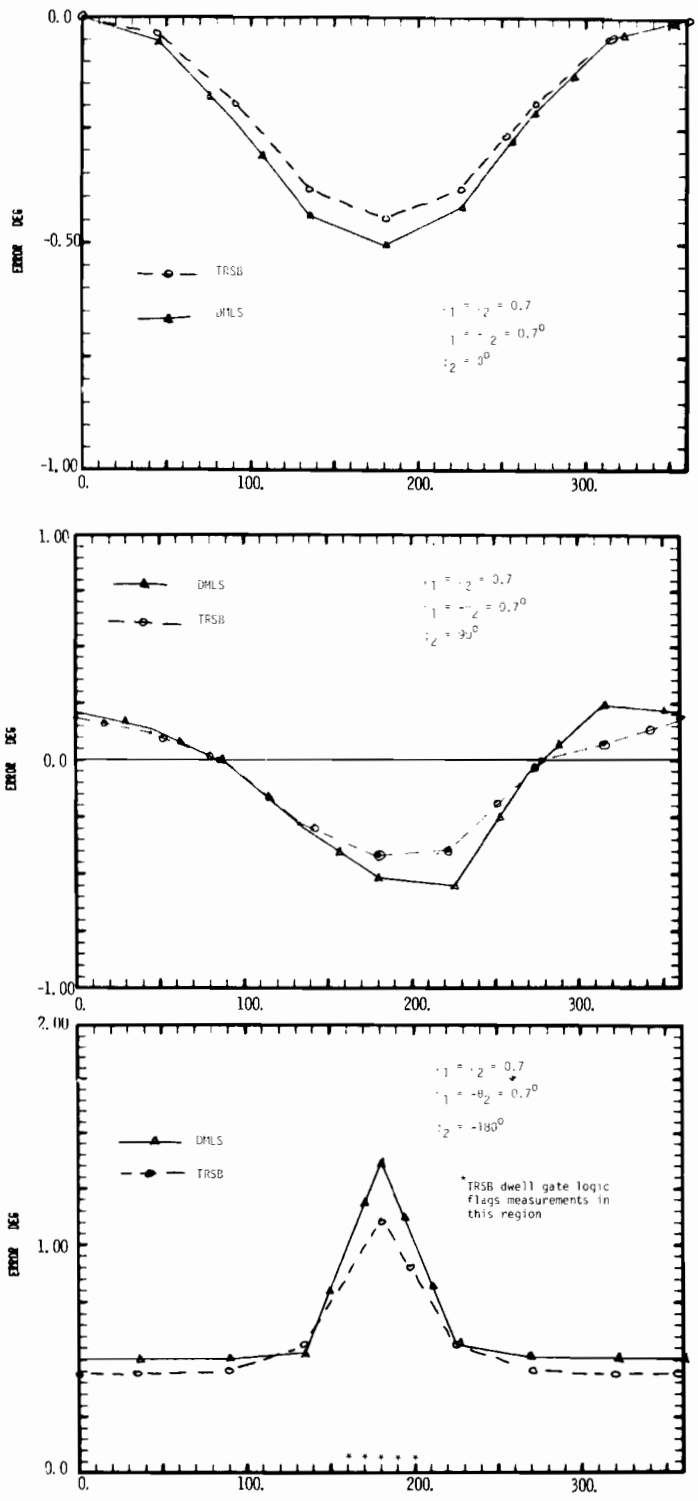

ϕ_1 = rf phase of multipath signal 1

Fig. 4-8. Comparison of errors for multipath signals at $\pm$ 0.7° separation angle with -3 dB M/D.

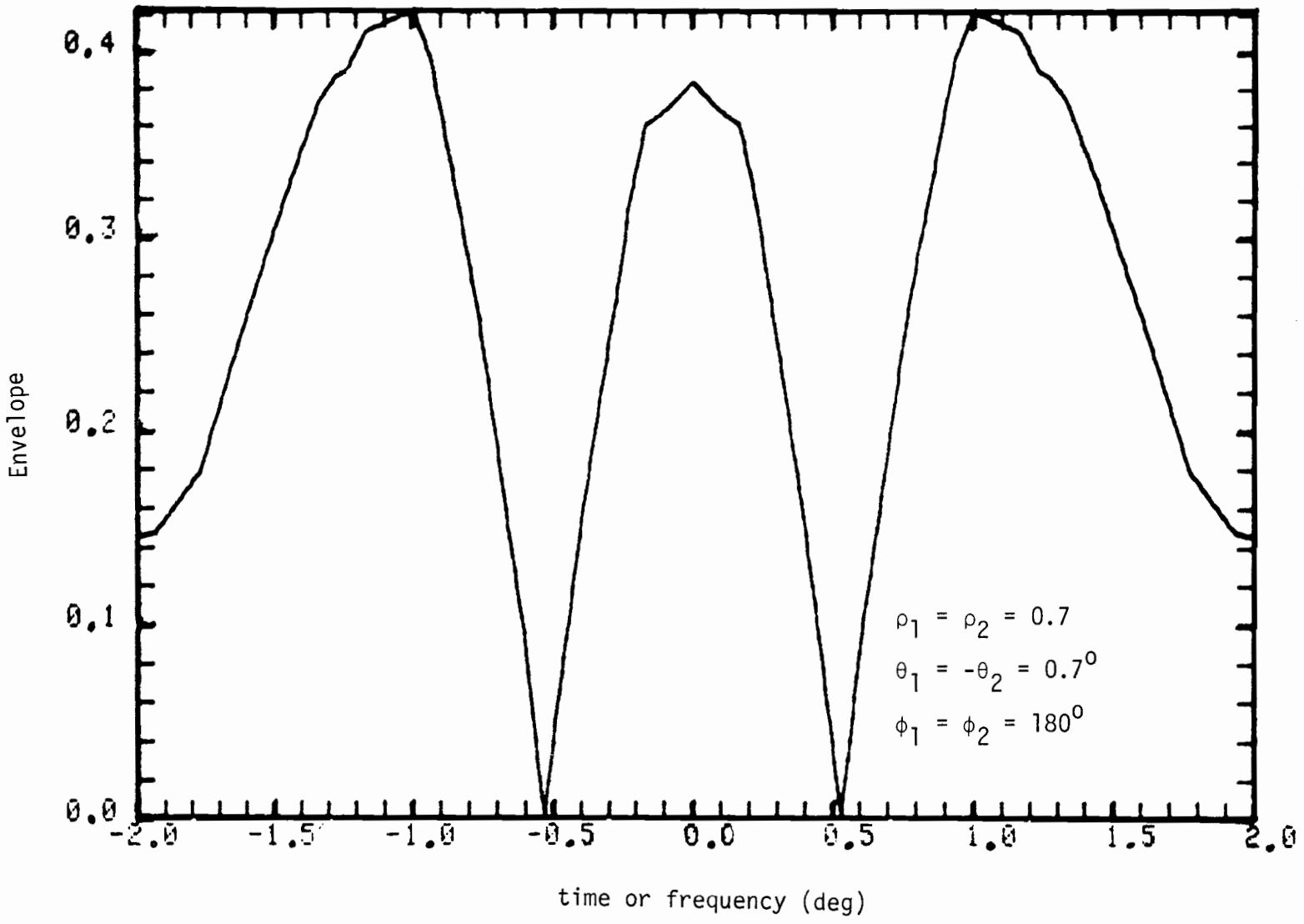

Fig. 4-9. Envelope for -3 dB M/D multipath signals at $\pm$ 0.7^o separation angle with multipath phases 180^o out of phase with direct signal

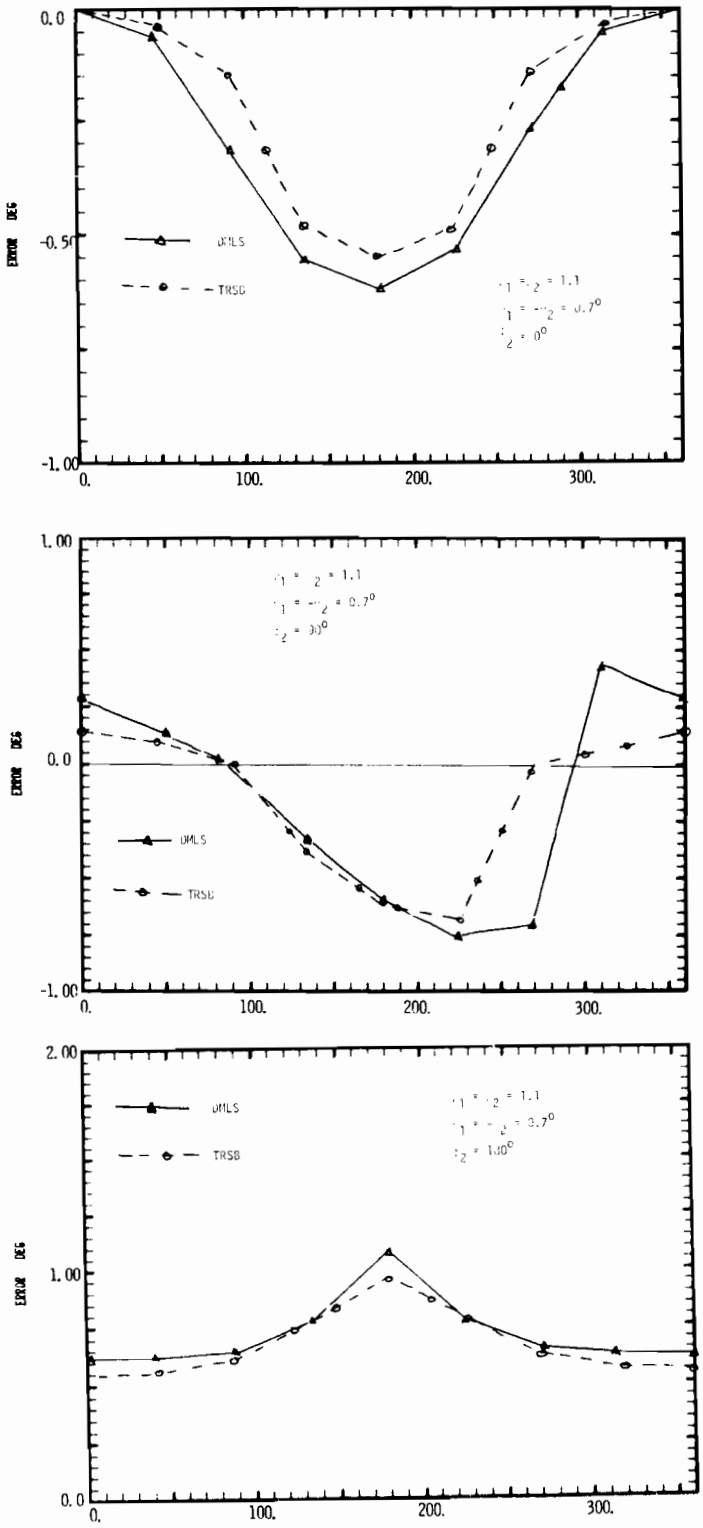

ϕ_1 = rf phase of multipath signal 1 wrt direct signal

Fig. 4-10. Comparison of errors for multipath signals at $\pm$ 0.7° separation angle with +1 dB M/D ratio.

obscure; our interpretation is that the error that would result = sum of the errors for each multipath signal alone = 0 by symmetry. This argument is equally applicable to TRSB -- and erroneous in either case. We have found that in certain anti-phase cases, where the M/D > -3 dB, one or both systems may stay in a no error condition provided exact symmetry holds and the receiver acquisition/validation logic is disabled. However, changing amplitudes or phases slightly (e.g., a 20° phase change) yields a large error.

Figure 4-10 compares the errors when both multipath signals are ±1 dB. The error behavior here is quite similar to that in Fig. 4-8, and for much the same reasons. Figure 4-11 shows the received envelope in the out of phase condition. We see that there is virtually no peak left at the direct signal angle.

The two component simulations of this section show some differences in error magnitude at certain multipath parameter combinations; however, the overall error characteristics and peak error are very similar. Both techniques yield zero error for symmetrical multipath situations where the multipath phase is not near 180°. When the multipath phases are near 180° with equal amplitude signals, the residual direct signal peak typically was so small that neither peak location technique could succeed it.

D. Comparison of DLS, DMLS, and TRSB Shadowing Field Test Results

In this section, we attempt to compare the published shadowing field test results for DLS, Doppler, and scanning beam systems. The available data base consists of the WG-A tests and the data from the US Phase II contractor

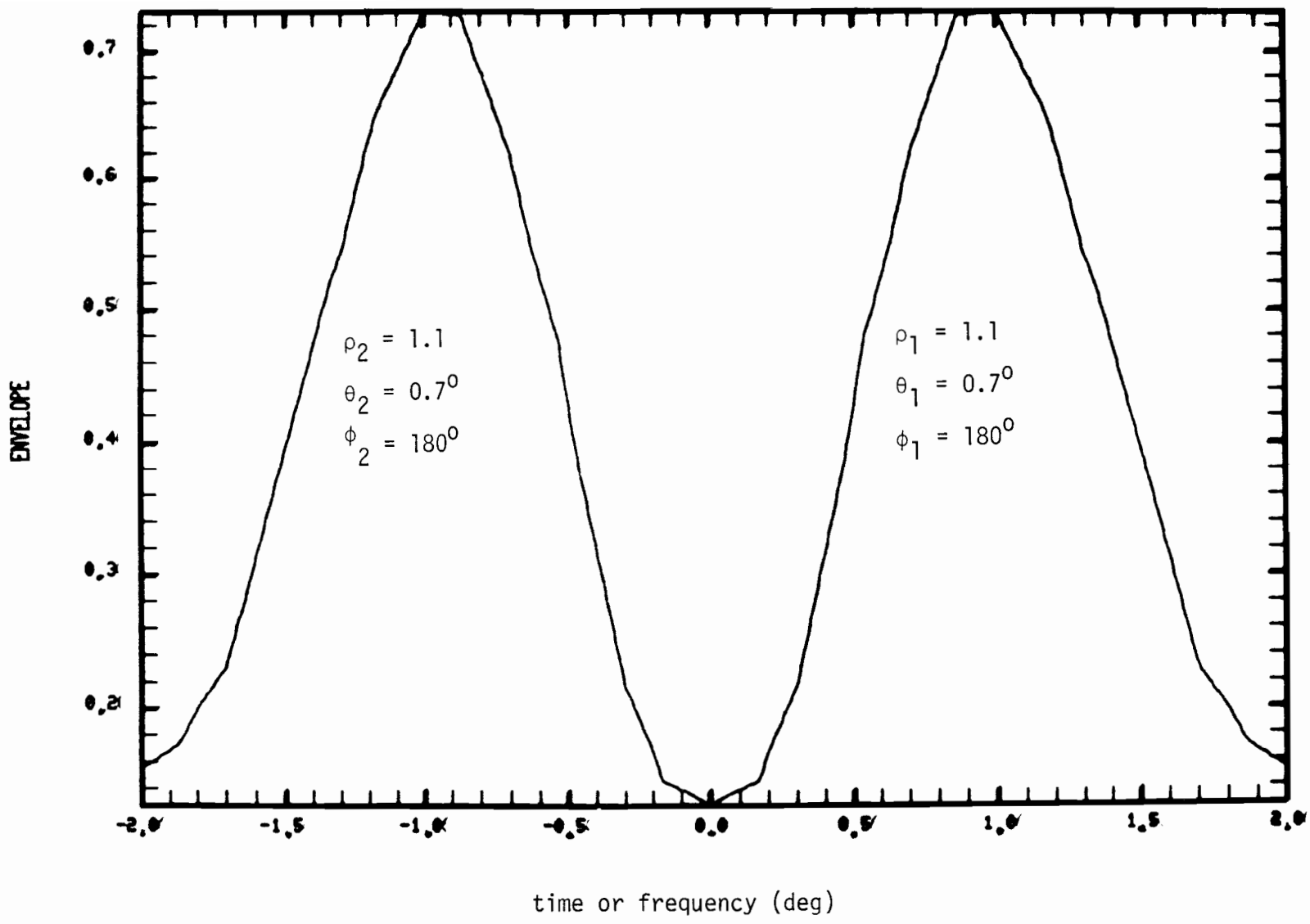

Fig. 4-11. Received envelopes for two -1 dB M/D multipath signals at $\pm$ 0.7° separation angle and anti phase condition

tests. Such a comparison necessarily must include assessment of differences in the experimental conditions and test equipment.

1. AWOP WG-A Tests

a. Experimental Conditions/Test Equipment

In Fig. 4-12, we compare the runway geometries in the DMLS and TRSB shadowing tests performed for the AWOP assessment. The DMLS site and the TRSB February 1977 test site are fairly similar as far as transmitter-to-runway end distance is concerned, whereas the original TRSB azimuth test site was much further back from the runway. This factor is important for comparing the taxiing aircraft test data. Also important in comparing taxiing test data are the runway profiles shown in Fig. 4-13.

Figures 4-14 and 4-15 compare the aircraft used for shadowing in the FRG, UK, and US field tests for which full test condition and tracker data is available. We see that the BAC-111 used for the UK tests is similar in size to the CV-580 used for the October 1976 TRSB tests, but substantially smaller than the CV-880 used for the 1977 TRSB tests. Consequently, the TRSB CV-880 data is probably more closely related to the UK B707 and VC-10 data for which there are only raw MLS plots.

The final factor concerns the ground and airborne equipment. The most striking difference here was ground system aperture where the DMLS aperture was 120λ, whereas the TRSB aperture was 60λ. The shadowing data discussion in [7] suggests that the errors are proportional to beamwidth, in which case the DMLS errors with a 120λ aperture should be doubled to yield errors for the

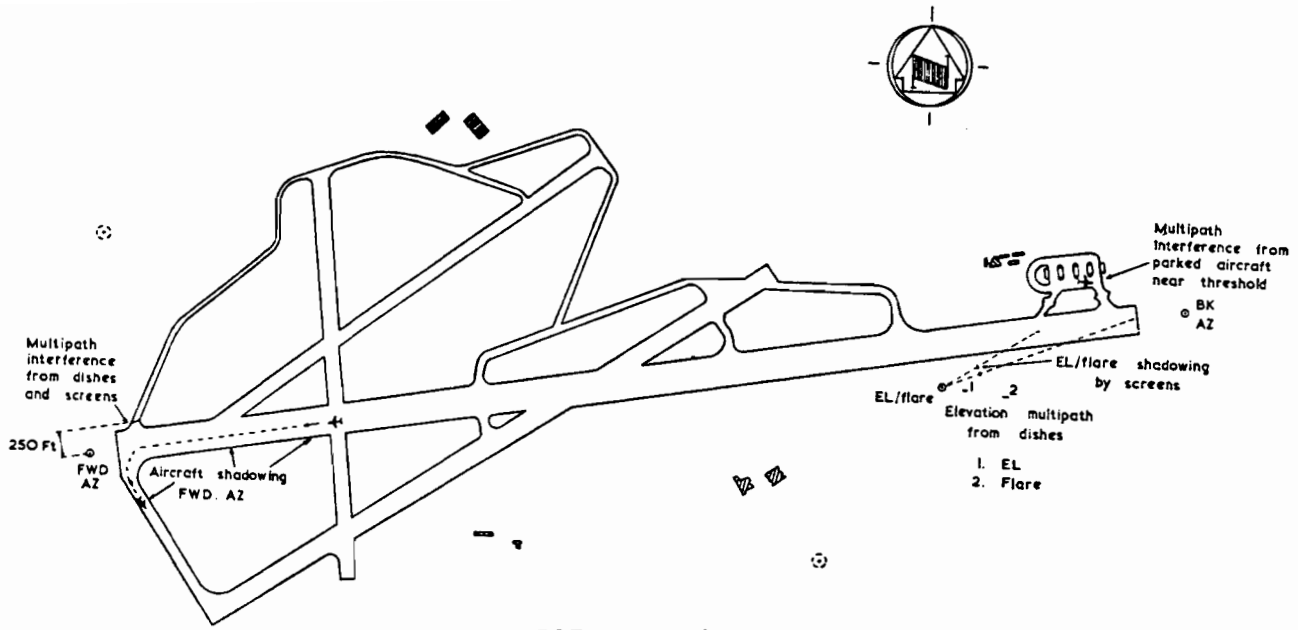

RAE test site

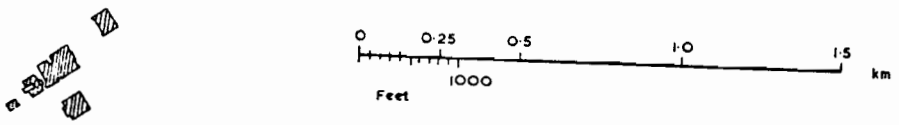

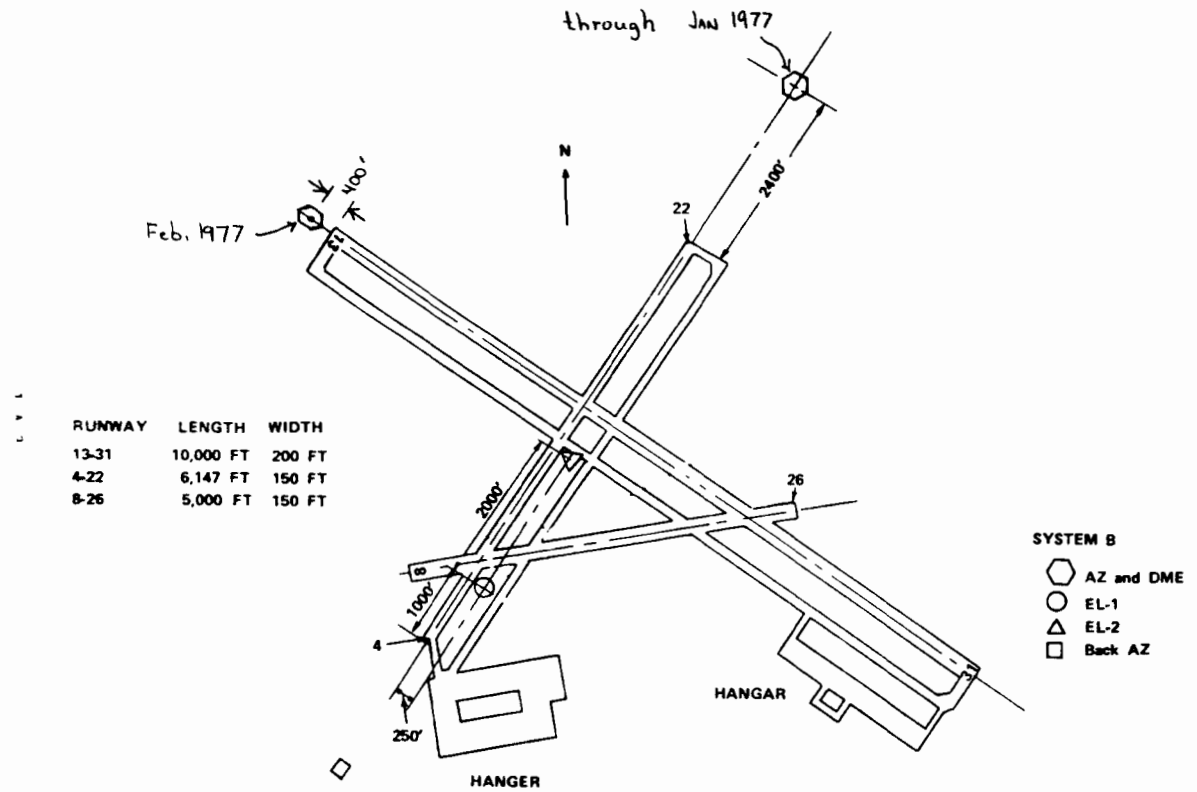

NAFEC MLS test site locations

Fig. 4-12. Comparison of shadowing test sites.

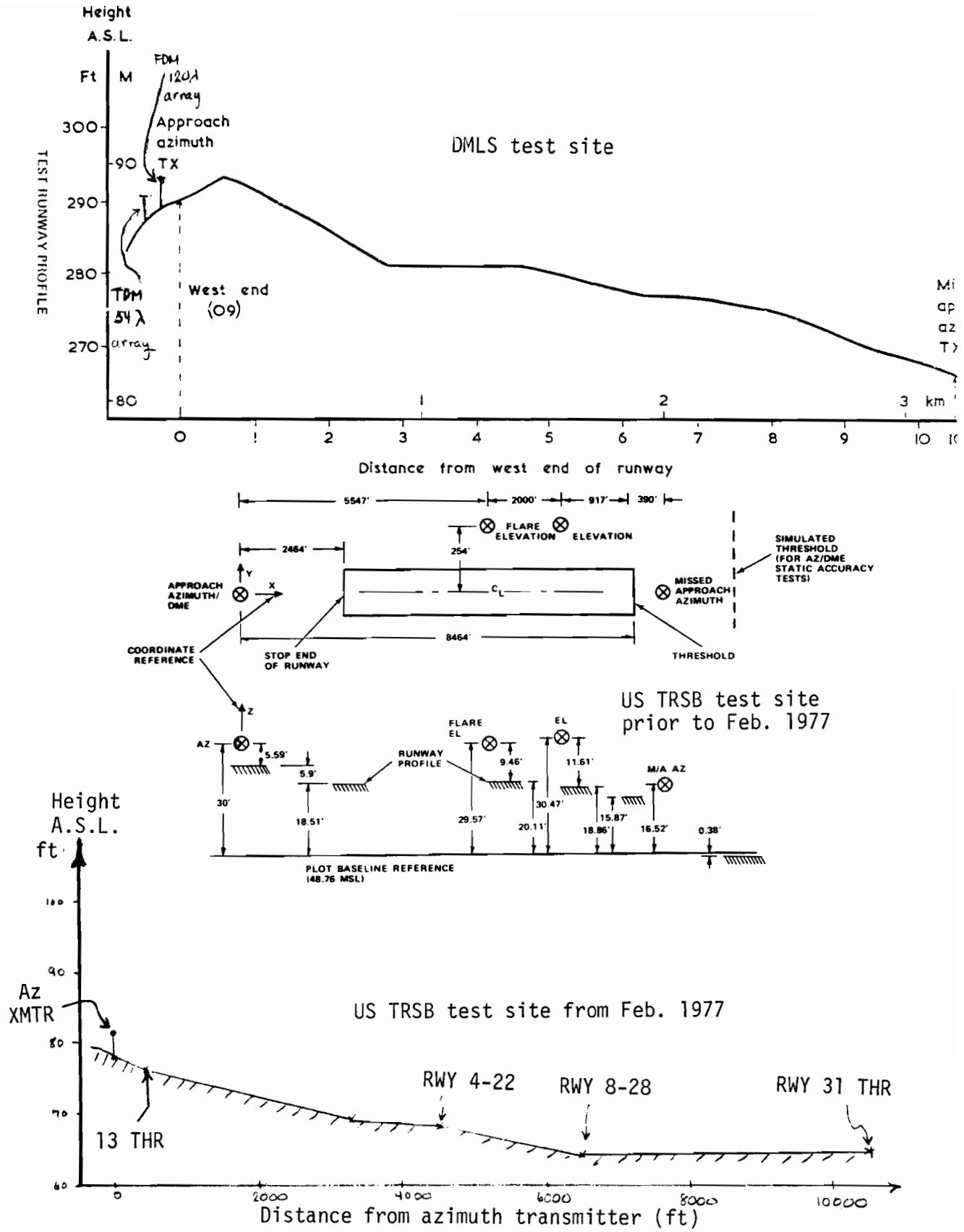

Fig. 4-13. Comparison of runway profiles.

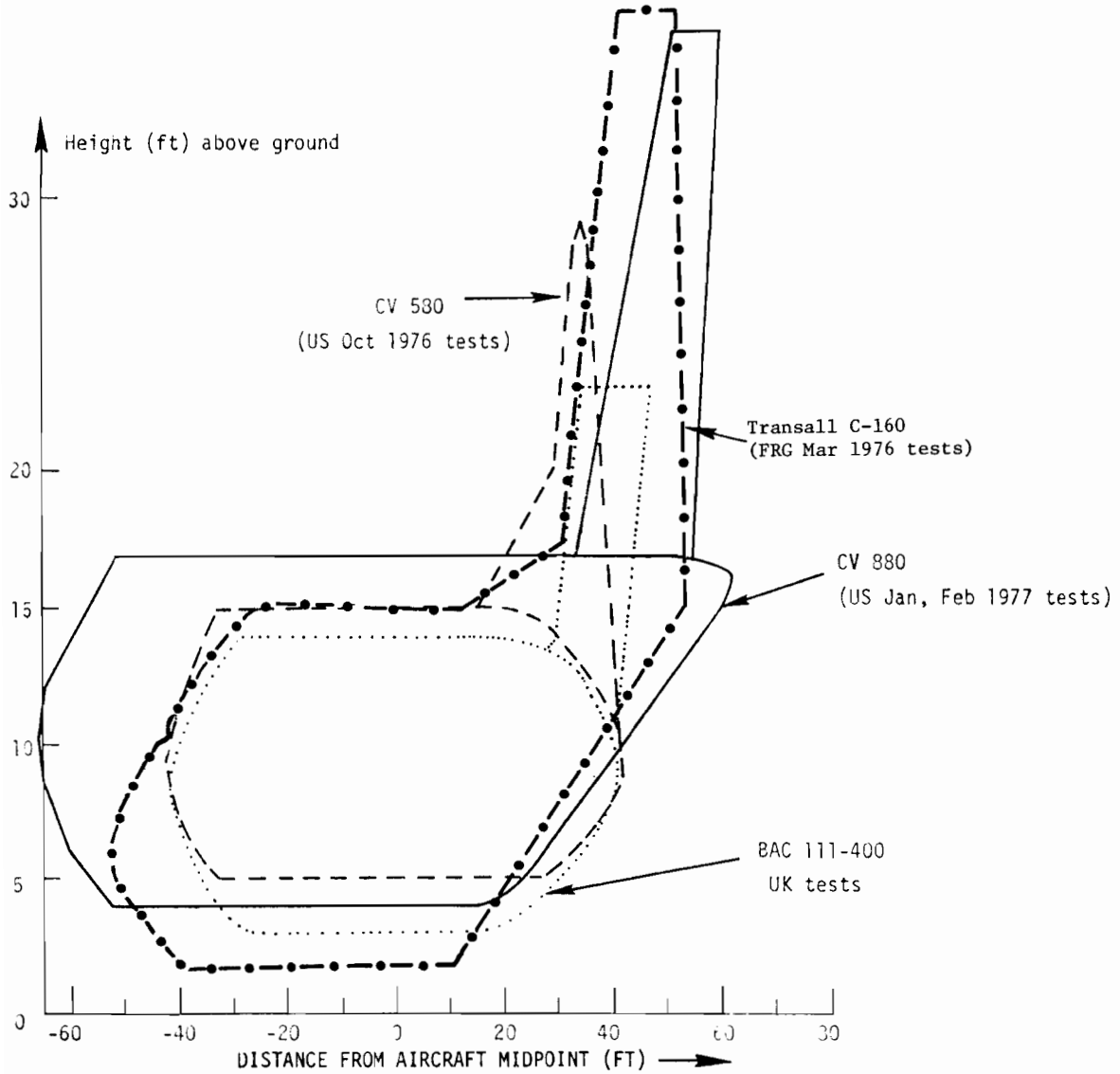

Fig. 4-14. Comparison of shadowing aircraft side profiles.

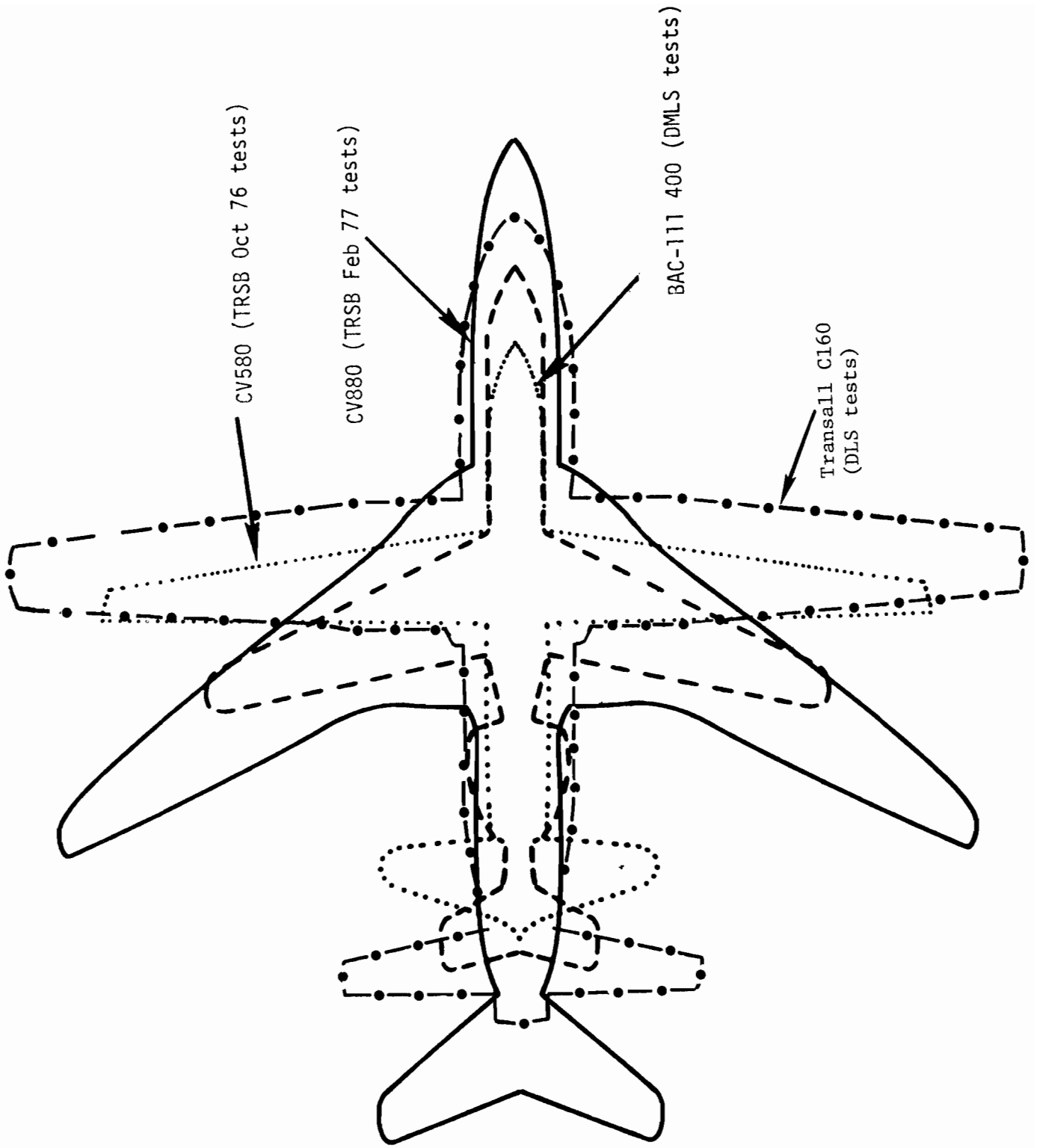

Fig. 4-15. Comparison of shadowing aircraft top profiles.

proposed 54λ implementation. However, at small separation angles, the DMLS (and TRSB) single component errors are independent of beamwidth (see Volume II of this report). A similar relationship can be shown with multiple components. Consequently, it is not clear how the array length difference should be handled.

From the discussion of shadowing multipath characteristics, it should be clear that TDM vs FDM signal formats would yield similar shadowing errors. The UK field test airborne receiver was a sine/cosine tracker. It is not clear how shadowing errors with that processor relate to those with the correlation processor--single multipath signal tests suggest the two are quite similar.

b. Overflight Test Results

In Table 4-1, we compare the DLS, DMLS, and TRSB test results for overflying aicraft. Lines have been drawn between the various flight results to indicate those cases which might be comparable. It is difficult, however, to draw strict comparisons, since there is insufficient data to ascertain where the same degree of blockage took place.

In the case of the US January 1977 TRSB tests, the overflying aircraft and receiving aircraft were tracked simultaneously so that the direct physical evidence of blockage could be established. Additionally, airborne recordings of the TRSB (wideband) video were made so that fade levels could be determined. Some UK data did have signal level plots from which fade depth can be ascertained; in those cases, the fade depths were comparable to those

TABLE 4-1

DMLS APPROACH AZIMUTH OVERFLIGHT INTERFERENCE

TEST AIRCRAFT	INTERFERING AIRCRAFT	FLIGHT /RUN	DATE	RANGE OF TEST A/C FROM THRESHOLD	HEIGHT	MLS MAX PK TO PK ERROR	MLS DURATION	ILS MAX PK TO PK ERROR	ILS DURATION
				nm	feet	degree	sec	degree	sec
Andover	BAC1-11	AA34/6	30.10.75	2·2	660	0·05	18		
Andover	BAC1-11	AA34/8	30.10.75	1·9	550	0·06	5		
Andover	BAC1-11	AA34/3	30.10.75	2·4	720	0·07	1		
BAC1-11	Comet IV	AB08/4	4.75	1·0		0·04	1		
BAC1-11	Comet IV	AB08/6	4.75	1·0		0·07	4		
BAC1-11	Comet IV	AB08/8	4.75	0·7		0·05	4		
BAC1-11	Comet IV	AB08/10	4.75	1·0		0·10	5		
HS748	VC10	B.5.8.9	11.73	1·2		0·21	4	1·27	6
HS748	B707	B.5.8.10	11.73	0·3		<0·047	1	>2·35	8
HS748	VC10	B.5.8.11	11.73	0·75		0·14	0·2	2·12	11
HS748	VC10	B.5.8.12	11.73	0·2		0·21	2·0	>2·35	9
HS748	VC10	B.5.8.13	11.73	1·2		0·07	4·0	1·32	10
HS748	B707	B.5.8.14	11.73	1·2		0·23	2·0	2·0	7
HS748	B707	B.5.8.15	11.73	0·3		<0·047	—	1·29	15
HS748	B707	B.5.8.16	11.73	—		<0·047	—	>2·35	10
HS748	B747	B.5.8.17	11.73	1·7		0·12	2	1·29	11
HS748	B747	B.5.8.18	11.73	—		<0·047	—	1·15	9
HS748	B707	B.5.8.19	11.73	1·5		<0·08	10	0·5	30

DLS APPROACH AZIMUTH OVERFLIGHT INTERFERENCE

Test Aircraft	Interfering Aircraft	Flight or Time	Date	Range of Test A/C from Threshold (nmi)	Height (ft)	Max Error Peak to Peak (deg)	MLS Duration (sec)
DO-28 Skyservant	C-160 Transall	14:27	3/26/76	3.41	700	0.13	≈ 4

TRSB APPROACH AZIMUTH OVERFLIGHT INTERFERENCE

Test Aircraft	Interfering Aircraft	Flight or Time	Date	Range of Test A/C from Threshold (nmi)	Height (ft)	MLS Max Error Peak to Peak (deg)	MLS Duration (sec)
DC-6	CV-580	17/12-1	10/21/76	0.5	200	.15	4
"	"	17/12-2	"	-0.2	20	.06	3
"	"	17/12-3	"	-0.3	8	.05	2
DC-6	CV-880	1355	1/6/76	0.2	180	0.04	2 sec
"	"	1416	"	0.3	220	0.04	2 sec
"	"	1427	"	0.15	200	0.14	1 sec
DC-6	"	1400	2/8/77	0.5	170	0.15	2
"	"	1411	"	0.7	192	0.08	1.5
"	"	1422	"	0.2	173	0.10	3

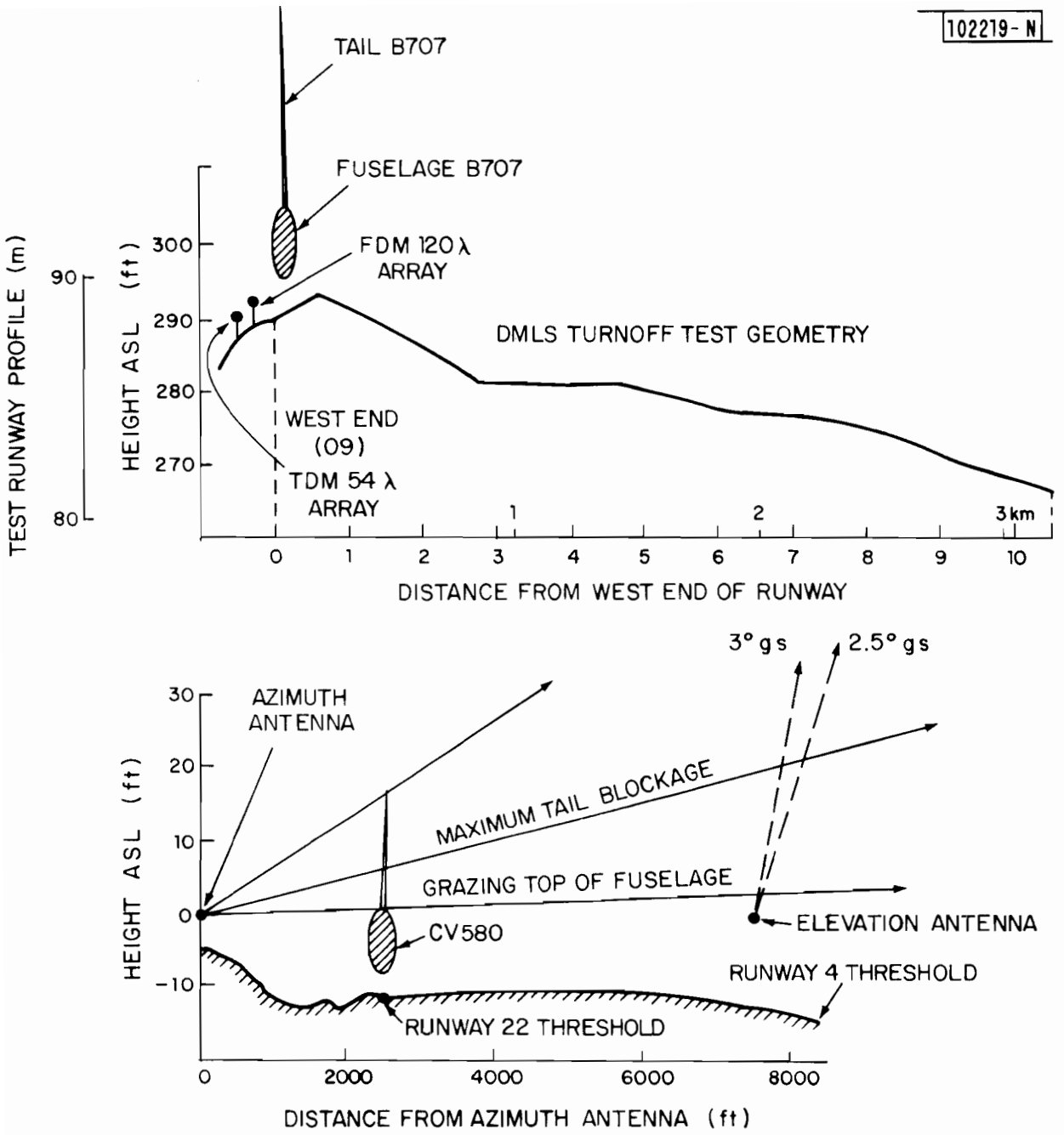

Fig. 4-16. Comparison of turnoff test geometries.

for TRSB.

c. Taxiing Aircraft Tests

It had been hoped a priori that this data would be fairly comparable since the shadowing aircraft locations are well known. However, there was a considerable difference in the shadowing geometry for the various sites.

Figure 4-16 compares the RAE site with the site used for the US TRSB October 1976 tests. We see that the principal shadowing threat for the UK tests is the fuselage, whereas the tail fin would be the principal threat at the US test site. For a receiver nearing the threshold, there would be considerable propagation beneath the taxiing aircraft fuselage at the UK site and very little at the US site. The greater distance from the azimuth transmitter would yield lower M/D levels for the US site, but a greater "in-beam" region.

Figure 4-17 compares the test site for the February 1977 US tests with the UK test site. We see that the two sites are comparable distances from the taxiing aicraft, but have rather different heights with respect to the fuselage underside. For example, for a receiver nearing threshold, the DMLS azimuth antenna has a nearly unobstructed LOS to the aircraft, whereas the TRSB LOS is blocked. Conversely, at greater heights, the TRSB azimuth antenna would have an LOS over the fuselage, whereas the DMLS LOS was blocked.

Another potential difference is the precise way in which the aircraft turned off the runway since this seems to generate the largest errors. In the US tests, it was noted that the largest error occurred in cases where the aircraft rotated to put the tail fin on the opposite side of the runway from the exit before taxiing off.

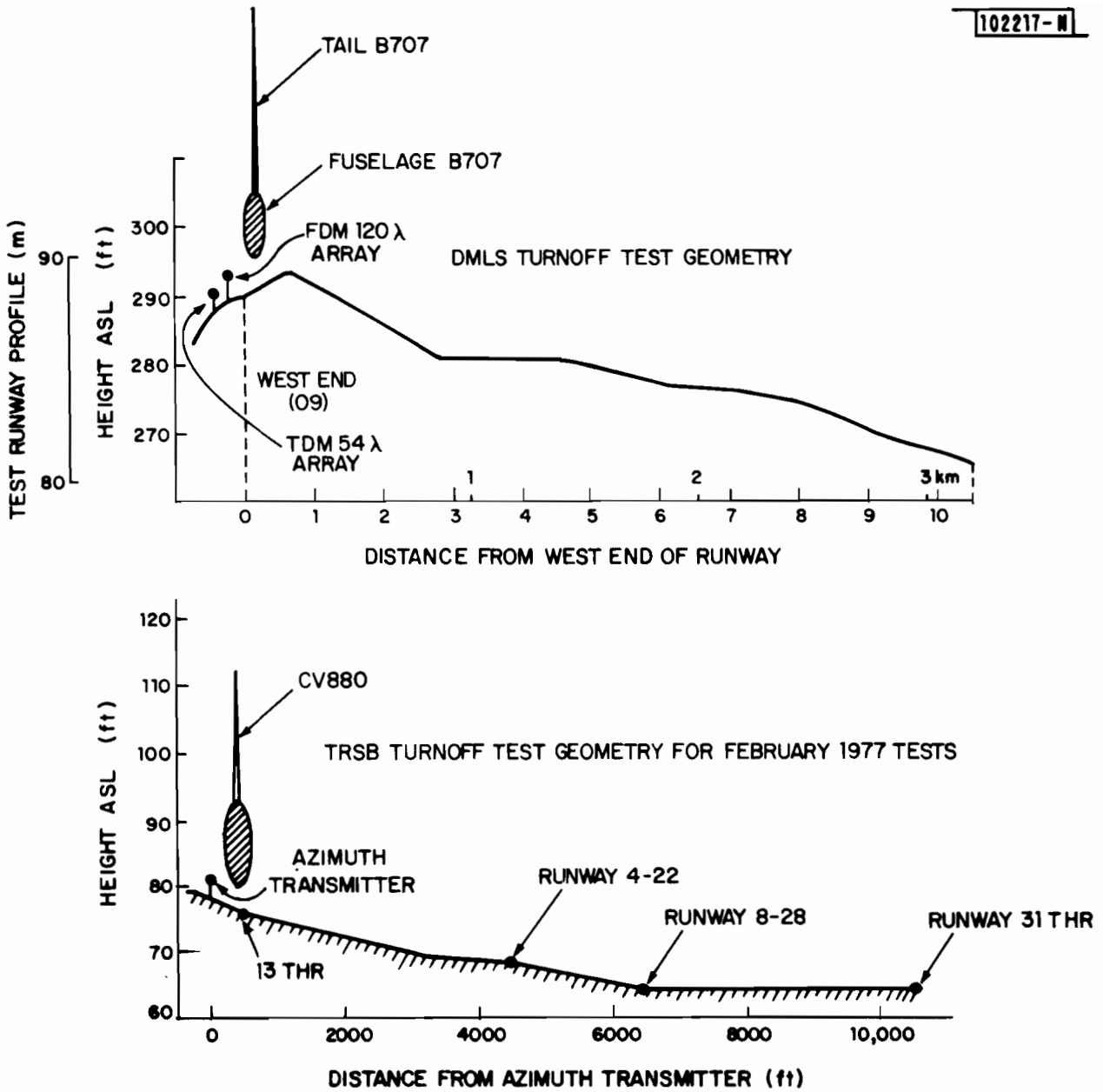

Fig. 4-17. Comparison of taxi/turnoff test geometries.

Table 4-2 summarizes the various test results. Again, lines have been drawn to denote results which may be comparable.

2. US Phase II Tests of Doppler and Scanning Beam

Several of the UK shadowing papers [126, 127] called attention to the scanning beam shadowing test data from the US Phase II tests. Thus, it is appropriate to compare that scanning beam data with the Doppler scan data from the same tests. The US Phase II azimuth shadowing tests involving two Doppler scan (Hazeltine and ITT/Gilfillan) and two scanning beam (Bendix and Texas Instruments) utilized a C-124 aircraft parked in front of the azimuth array. At three of the four sites, this distance was 800 feet, whereas the fourth site was that shown in Fig. 4-12, in which the minimum distance was 2400 feet.

Both static pole tests and flight tests were to be conducted. All four contractors submitted pole test data, but only three (Bendix, Hazeltine, and Texas Instruments) submitted flight test data.

In Table 4-3, we compare the static pole test data for the four contractors taken at a common test point. We see that the scanning beam errors were generally lower than that of the Doppler scan systems.

Table 4-4 compares the flight data. The flight recording data was not film corrected, and there are some cases of perturbations from other than shadowing. Thus, it is doubtful that any significant conclusion could be developed from the Phase II flight test data.

Several observations can be made regarding the relevance of this data for the ICAO analysis:

1. The aircraft used (see Fig. 4-18) was much larger in terms of fuselage height than that used for the ICAO

TABLE 4-2

COMPARISON OF AZIMUTH ERRORS DUE TO SHADOWING BY TAXIING AIRCRAFT

TEST AIRCRAFT	INTERFERING AIRCRAFT	FLIGHT /RUN	DATE	RANGE OF TEST A/C FROM THRESHOLD	HEIGHT	MLS MAX PK TO PK ERROR	MLS DURA-TION	ILS MAX PK TO PK ERROR	ILS DURA-TION
				nm	feet	degree	sec	degree	sec
Andover	BAC1-11	AA34/2	30.10.75	0·1	120	0·5	18		
Andover	BAC1-11	AA34/4	30.10.75	1·2	386	0·07	7		
Andover	BAC1-11	AA34/7	30.10.75	1·7	527	0·12	20		
BAC1-11	Comet IV	AB08/5	16.4.75	1·5	—	0·04	3		
BAC1-11	Comet IV	AB08/7	16.4.75	1·0	—	0·23	10		
BAC1-11	Comet IV	AB08/9	16.4.75	1·75	—	0·13	5		
BAC1-11	Comet IV	AB08/11	16.4.75	2·0	—	0·11	3		
HS748	VC10	B.5.5.13	11.73	1·0	300	0·52	3	1·06	10
HS748	B.747	B.5.5.14	11.73	2·8	540	0·40	6	0·98	15
HS748	B.707	B.5.5.15	11.73	—	—	—	—	0·26	8
HS748	B.747	B.5.5.16	11.73	2·0	600	0·05	—	1·60	22
HS748	B.707	B.5.5.17	11.73	0·8	—	—	—	0·12	24
HS748	VC10	B.5.5.18	11.73	0·5	150	0·48	1 × 2	0·12	30
HS748	VC10	B.5.5.19	11.73	−0·5	70	0·24	0·2	0·96	12
HS748	VC10	B.5.5.20	11.73	1·5	450	0·48	4·0	0·36	11

DMLS Errors with 0.5° beamwidth FDM System

Test Aircraft	Interfering Aircraft	Flight/ Run	Date	Range of Test A/C From Threshold (nmi)	Height (ft)	MLS Max Error Peak to Peak (deg)	MLS Duration (sec)
DC-6	CV-580	1	10/21/76	-.15	30	0.6°	
"	"	2	"	0.0	50	0.4°	
"	"	3	"	0.0	50	0.5°	
DC-6	CV-880	4	2/8/77	1.1	250	0.3	3
"	"	5	"	0.3	90	.45	6
"	"	6	"	0.3	90	.50	6
"	"	7	"	0.5	107	.45	6
DC-6	CV-880	2	2/18/77	0.4	181	.44	6
"	"	3	"	1.00	364	.40	5
"	"	4	"	1.56	547	.45	4
"	"	5	"	1.64	574	.36	3
"	"	6	"	1.56	547	.37	3
"	"	7	"				
"	"	8	"				
"	"	9	"				
"	"	10	"	0.90	312	.04	2

TRSB Errors with 1° beamwidth TDM System

TABLE 4-3

COMPARISON OF U.S. PHASE II POLE TEST RESULTS
ON CENTERLINE FOR PARKED SHADOWING AIRCRAFT

Pole Height	Doppler Scan (Error in deg)		Scanning Beam (Error in deg)	
	ITT*	Hazeltine	Bendix	TI
5	.134	.07	-.02	-.03
10	.131	-1.0	-.03	-.02
15	.161	-.12	-.07	-.03
20	.140	-.14	-.08	-.04
25	.110	.02	-.03	-.03
30	-.09	.07	-.01	.02
35	-.06	.075	.07	.02
40	.05	.272	-.15	.03
45	.086	-6.06	-.08	.02
50	.084	-.22	-.05	.02
55	.103	-.17		
60	.106	-.10		
65	.106	-.06		
76	.08	-.03		

*Note: mean unshadowed error ~ 0.046°.

TABLE 4-4

COMPARISON OF U.S. PHASE II SHADOWING FLIGHT TESTS

FLIGHT	DOPPLER SCAN		SCANNING BEAM	
	Hazeltine	ITT/G	Bendix	Texas Instruments
1	off scale in both directions* mean = 0.81	NO FLIGHT TEST PRESENTED	.08/-.15	+.1/-.52
2	off scale in both directions* mean = -2.27		.15/-.15	+.2/-.27

*full scale = ± 0.3°

Fig. 4-18. C-124 shadowing viewed from K AZ antenna.

tests.*

2. The use of an identical parked aircraft and pole tests at a standard location helped reduce some of the experimental condition variance -- however, there were still runway layout/profile differences.
3. The principal error mechanism for the scanning beam receivers was the same as that which arises with the proposed TRSB receiver; namely, dwell gate shifts due to the beam envelope distortion.

4. It is not clear how the error mechanism for the Doppler receivers tested compares to that of the proposed DMLS implementation. Hazeltine, using a zero crossing counter which discards the scan amplitude information, had by far the worst performance.

5. The shadowing aircraft location is probably unrealistic operationally since all the US contractors had deemed that location to be a part of the critical area for the azimuth array.

6. From a comparison of the US Phase II scanning beam and Doppler scan shadowing data, one might conclude that Doppler was more susceptible to such effects than scanning beam. However, it is felt that differences in test condition were too great to warrant drawing any definite conclusions.

E. Comparative Simulations of DMLS and TRSB**

In the preceding sections, we have seen that there were considerable experimental condition differences in the shadowing field tests. These differences included:

---

*For example, the C-124 fuselage height is greater than the total height of the BAC-111.

**The DLS technique was not considered in these simulations because the scenario geometry was such (shadowing obstacle in the near field of the 90λ linear array) that the propagation model used for AWOP WG-A studies would not be valid.

1. trial antenna beamwidth vs that proposed
2. ground antenna elevation pattern
3. shadowing by intervening terrain
4. type and location aircraft relative to the LOS
5. flight paths

Consequently, a fairly wide tolerancing band must be applied about each system's field data before direct quantitative comparisons are made.

The multiple component simulations in section C above were more nearly comparable, but it is not clear whether any of those situations will arise or persist in practice. Moreover, we have seen that the past history of the receiver can substantially change the error for a given combination of multipath components.

A more attractive way of obtaining more nearly comparable operationally relevant data was to simulate several operationally relevant scenarios. In this section, we present such comparative simulations for three scenarios:

1. an overflight aircraft situation based on one such overflight in the US January 1977 TRSB tests [129]
2. a taxiing aircraft case based on one of the US February 1977 TRSB tests [129]
3. a case with an aircraft parked parallel to centerline based on the scenario in a UK paper [126]

The TRSB simulation results were shown in Volume II to agree with actual flight test results corresponding to scenarios 1 and 2.

The TRSB and DMLS system models used were those used for the AWOP WG-A scenario simulations, except that the DMLS azimuth array was given the same vertical pattern as that used for the TRSB system. This was done so that the

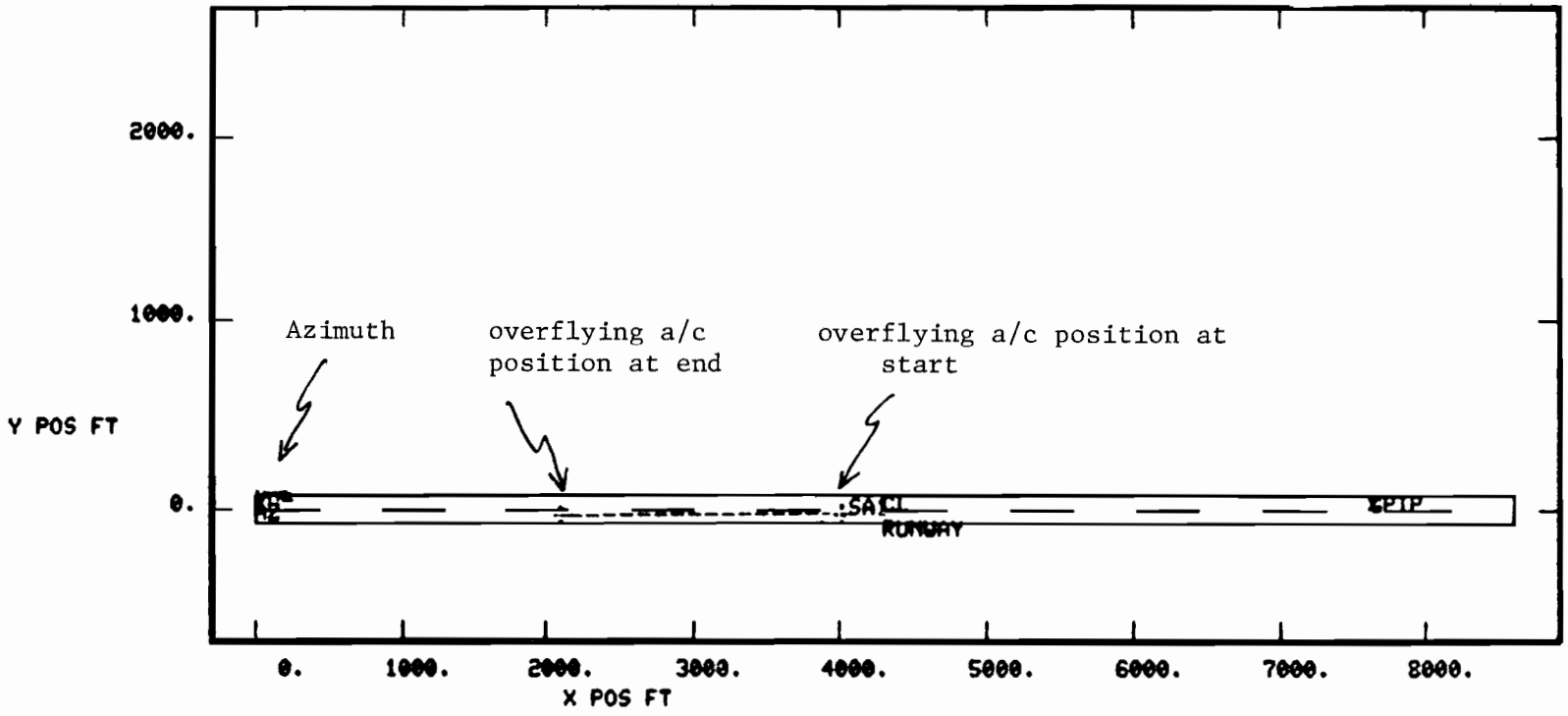

Fig. 4-19. Geometry for overflight simulation.

ground reflection paths would be treated identically for both systems.

1. Blockage by Overflying Aircraft

This scenario was based on a TRSB test conducted January 6, 1977, in which both aircraft were tracked (one by laser and the other by theodolite) so that good position data was available. The blockage occurred when the shadowing CV-880 was ~400 feet from the azimuth transmitter, while the receiver was 0.7 nmi from threshold. Figure 4-19 shows the computer generated map. Figure 4-20 compares the TRSB and DMLS errors. The error waveforms are quite similar.

2. Blockage by Taxiing Aircraft

This scenario is based on a TRSB taxiing aircraft test conducted February 6, 1977. The shadowing CV-880 aircraft rotated approximately 60° on centerline so the the nose and tail were on opposite sides of the centerline and the azimuth site region was visible to the pilot of the landing aircraft. The CV-880 then taxied off the runway.

The computer simulation currently allows the shadowing aircraft to move in a straight line only at fixed velocity. Therefore, the rather complicated taxi maneuver was approximated by having the CV-880 taxi across centerline of an angle of 60° starting with the fuselage across centerline. Figure 4-21 shows the computer generated airport map.

Figure 4-22 compares the TRSB and DMLS simulations for this scenario. The error waveform differences are again small. The TRSB lag in dynamic

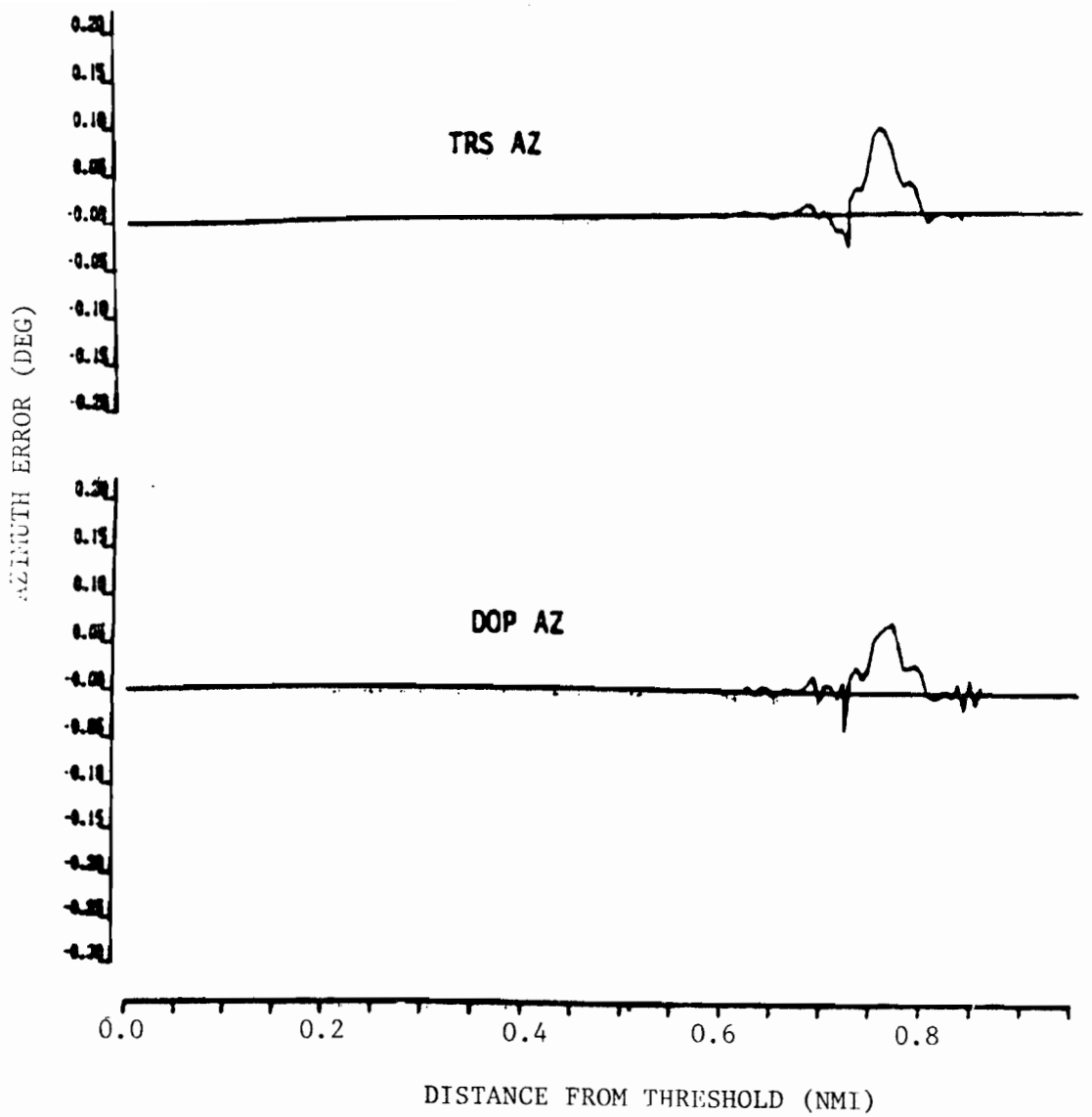

Fig. 4-20. Similarity of simulated raw MLS errors for comparative scenario based on TRSB overflight field test of part II.

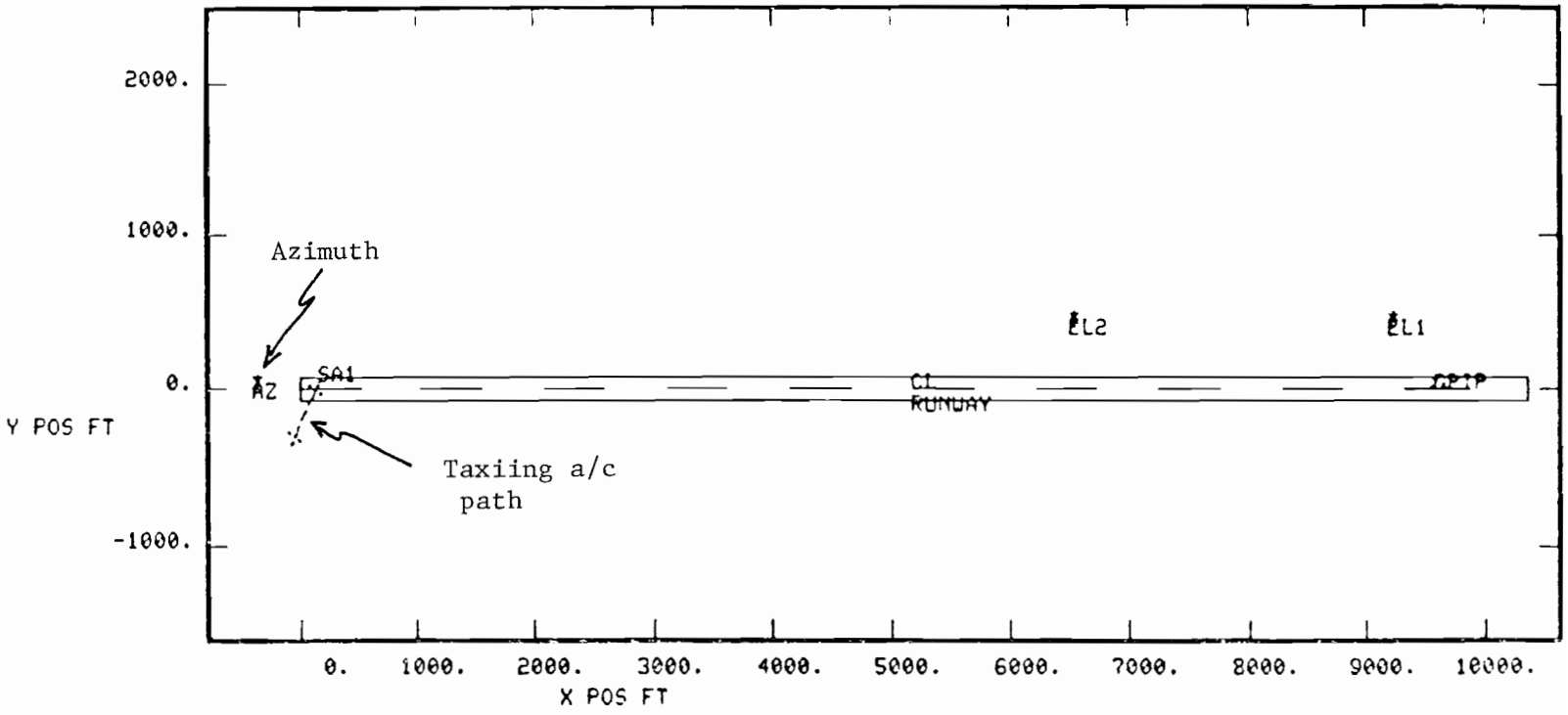

Fig. 4-21. Geometry for taxiing aircraft scenario.

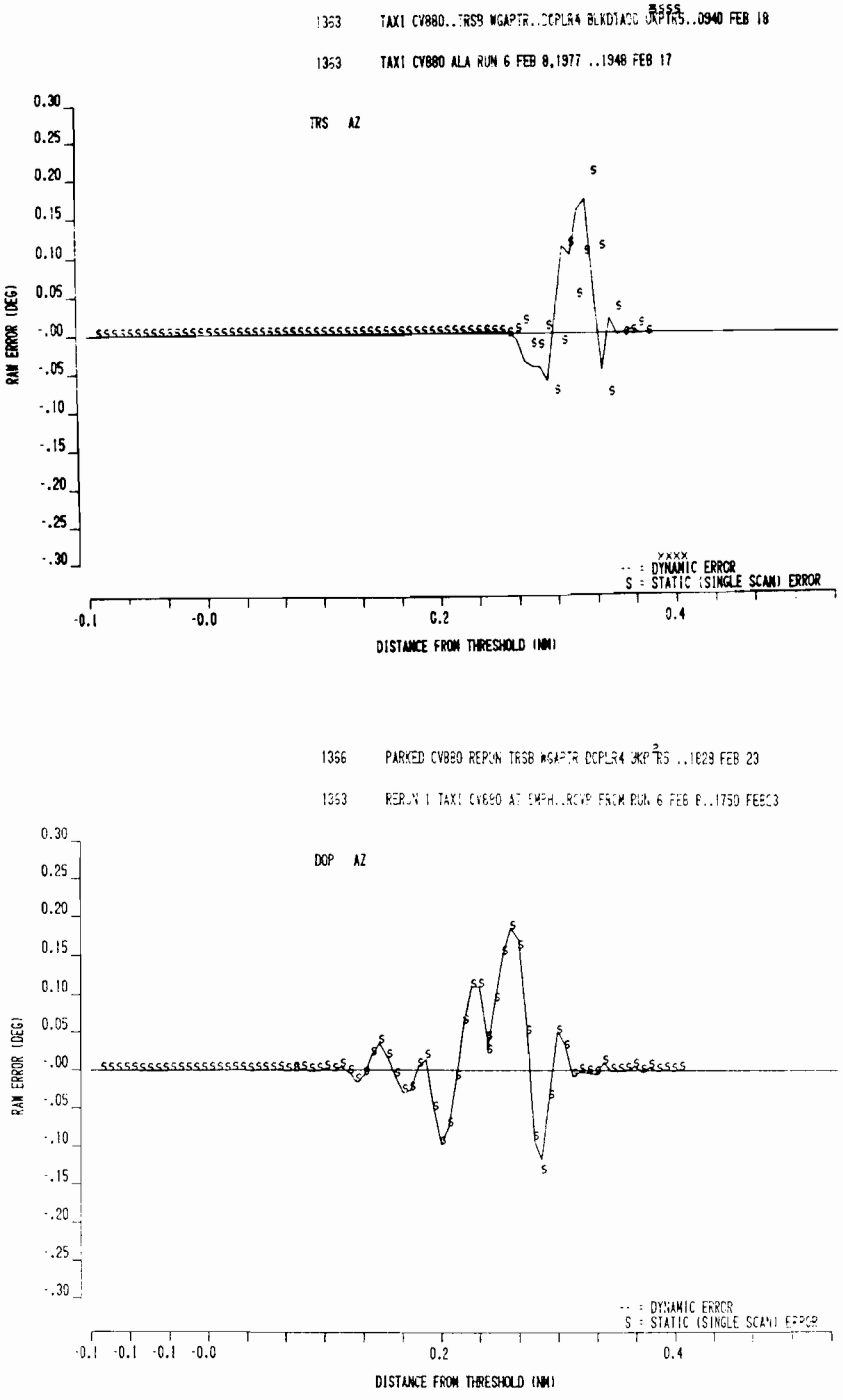

Fig. 4-22. DMLS and TRSB raw errors for shadowing by taxiing aircraft scenario.

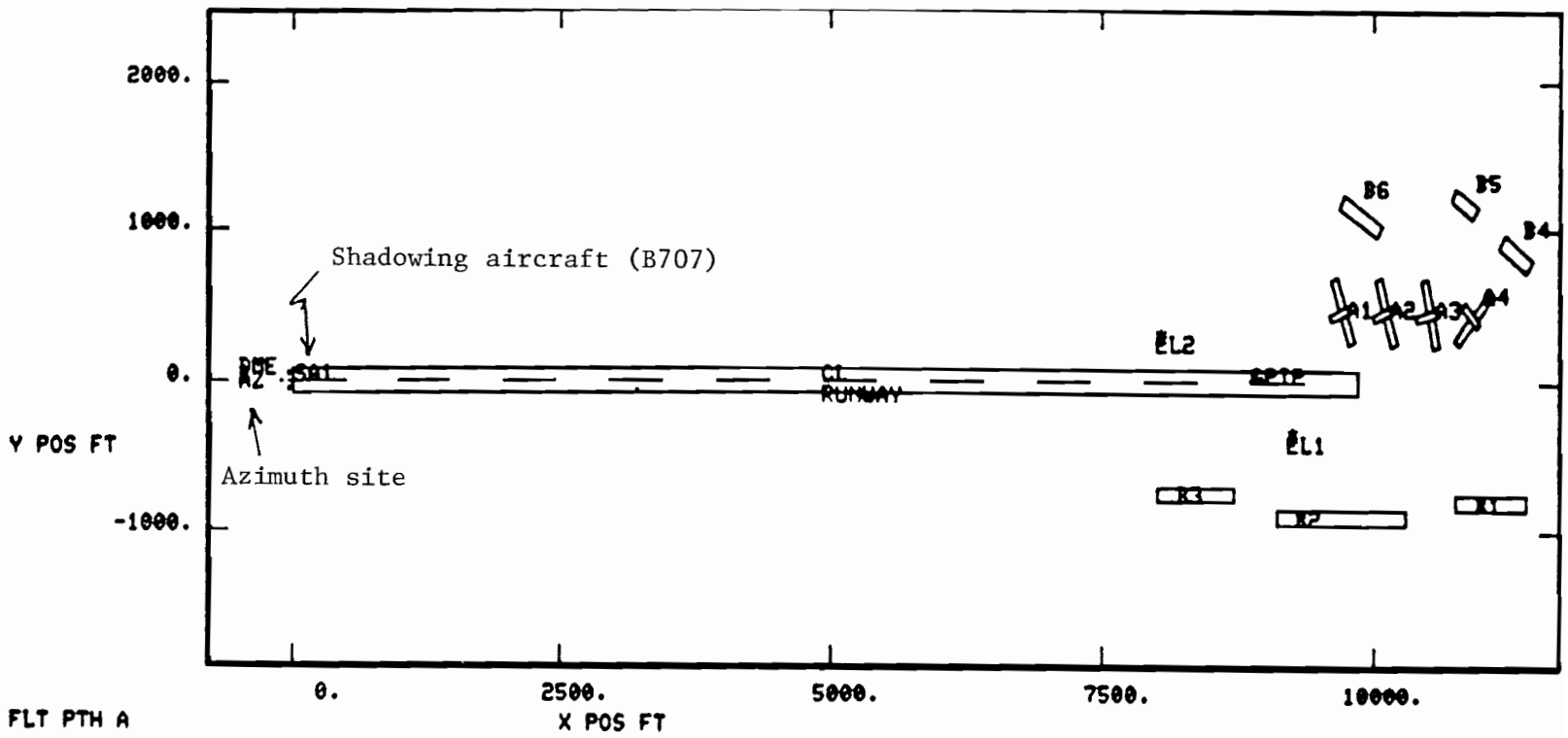

FLT PTH A

AZ SYSTEM

OBST	RANK	AMP	DIST	RDOP
G	11	80	0.0	0.
B1	7	37	6630.7	-110.
B2	5	29	0.0	-6.
B3	3	24	1405.2	-2.
B4	6	30	7377.2	-770.
B5	4	27	7640.7	-740.
B6	1	15	8650.7	-640.
A1	10	70	1317.4	-1.
A2	9	68	9528.9	-2063.
A3	8	55	5708.6	-3.
A4	2	17	7948.1	-1116.
D	0	80	0.0	0.

EL SYSTEM

OBST	RANK	AMP	DIST	RDOP
G	11	80	0.0	0.
B1	1	0	4610.8	-26.
B2	2	1	6542.9	-71.
B3	10	36	9528.9	-374.
B4	9	31	7772.4	-1265.
B5	4	15	8606.7	-1414.
B6	8	30	9177.6	-1070.
A1	3	14	8475.0	-69.
A2	6	17	8299.4	-170.
A3	5	17	5181.6	0.
A4	7	17	8650.7	-1866.
D	0	80	0.0	0.

Fig. 4-23. Computer map of airport for parked shadowing aircraft scenario.

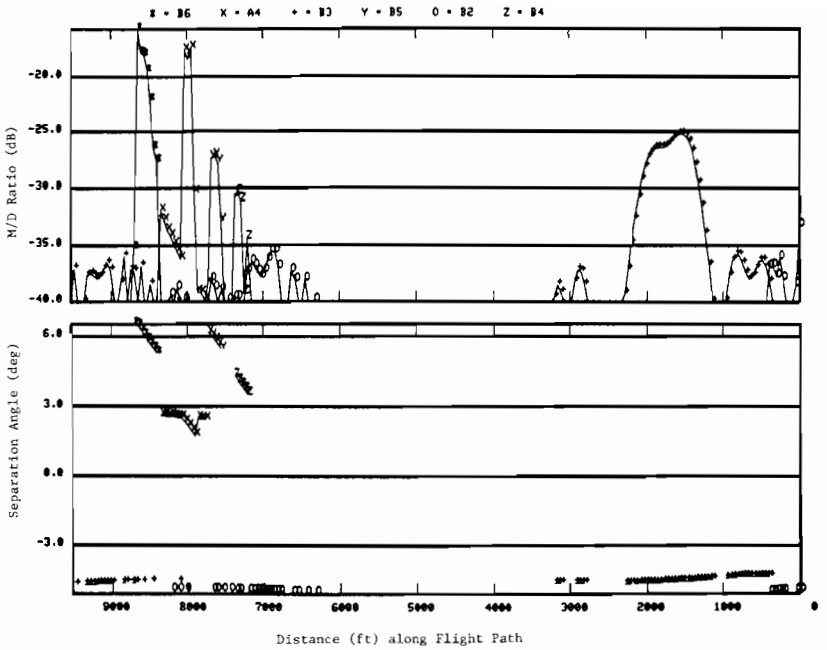

(a)

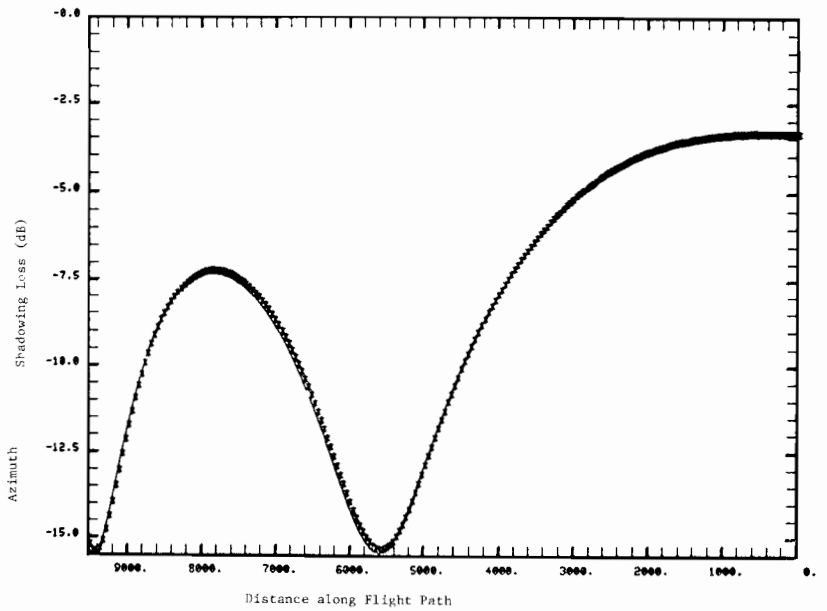

(b)

Fig. 4-24. Azimuth multipath characteristics for parked shadowing aircraft scenario multipath. (a) Reflection multipath characteristics. (b) Shadowing characteristics.

output again is due to the multipath computation.

3. Blockage by Aircraft Parked on Runway

This simulation was based on a scenario described in [126], in which a B-707 is parked on centerline pointing at the azimuth transmitter a distance of 500 feet from the azimuth site. The receiver makes a normal 2.86° approach down to threshold. It should be noted that the shadowing aircraft is parked in the region suggested as being an azimuth array critical area in the DMLS and TRSB proposals to ICAO.

The airport layout and computed multipath characteristics are shown in Figs. 4-23 and 4-24. Analysis of the scenario revealed that ground reflections play an important role in the overall performance, and that the overall effect was sensitive to the elevation pattern of the azimuth array.

Since the proposed DMLS pattern rolled off more slowly than did the proposed TRSB pattern, the simulation used the TRSB elevation pattern for DMLS and TRSB. The raw errors are shown in Fig. 4-25. We see that the DMLS and TRSB performances are quite similar. Simulation of DMLS with the proposed DMLS elevation pattern yielded errors 100% larger than those shown in Fig. 4-25. The fact that the errors for a given system (DMLS) could be changed by 50% by what appear to be small changes in the elevation pattern characteristics illustrates the difficulty in comparing shadowing field trial data.

F. Summary of Results

The comparative analysis results can be summarized as follows:

1. As a consequence of the equivalence of the TRSB received time envelope and the DMLS received spectrum envelope in

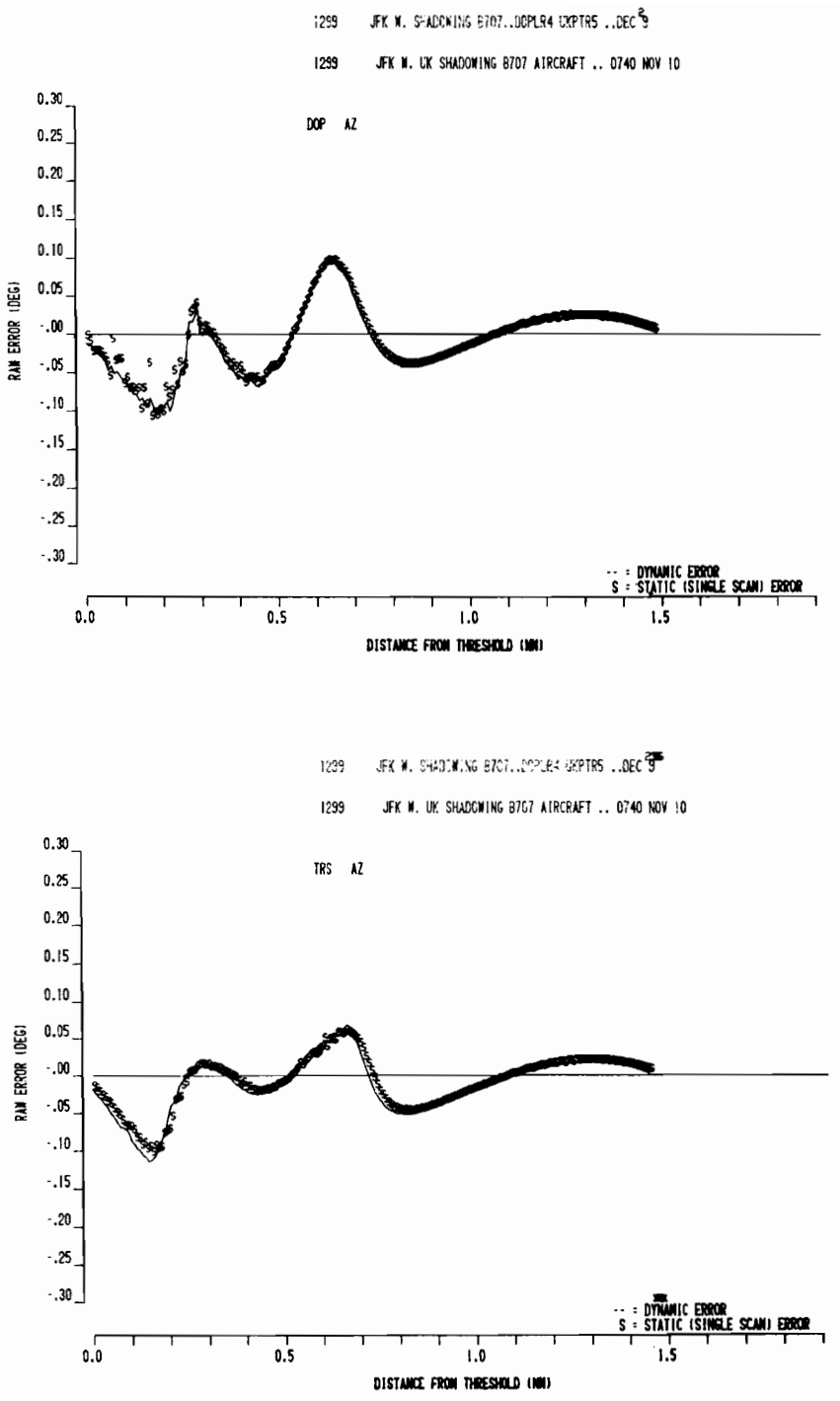

Fig. 4-25. Comparison of TRSB and DMLS raw errors for JFK shadowing scenario with identical elevation patterns.

static conditions, performance differences were expected to be small. Moreover, the proposed DMLS digital correlator is very similar to the TRSB split gate tracker utilized by Australia.

2. Shadowing errors when the line of sight (LOS) is not blocked essentially reduce to the single component multipath problem with an M/D ratio $\leq$ -6 dB. Differences for this case were shown to be small in the bench simulation tests and in simulations of elevation shadowing by an ILS monitor (fig. 4-26)*.
3. Shadowing when the LOS is blocked often becomes a two-component multipath problem where the multipath signals are on either side of the direct signal. The M/D ratio here can be high. It is found that in most cases, the two systems give similar errors. In some cases, DMLS gave a large (0.4°) error, while the Phase III TRSB receiver logic flagged the measurement.

4. The field data suggests that for similar geometries and shadowing aircraft size, the TRSB and DMLS performance was quite similar. The US Phase II contractor data shows larger errors for the Doppler systems, but this probably reflected site conditions and implementation characteristics rather than fundamental differences.

5. Comparative scenarios involving parked, taxiing, and overflying aircraft (based on the US field tests and UK suggestions) yielded quite similar results.

Given the above, it is concluded that shadowing by taxiing and overflying aircraft is a principal MLS multipath error source; however, there was not a significant difference between the DMLS and TRSB techniques in terms of sensitivity to these shadowing effects.

---

*The ILS monitor simulation is based on the Aeroparque (Buenos Aires, Argentina) TRSB elevation shadowing by an ILS glideslope monitor which was described in volume II, chapter 4 of this report.

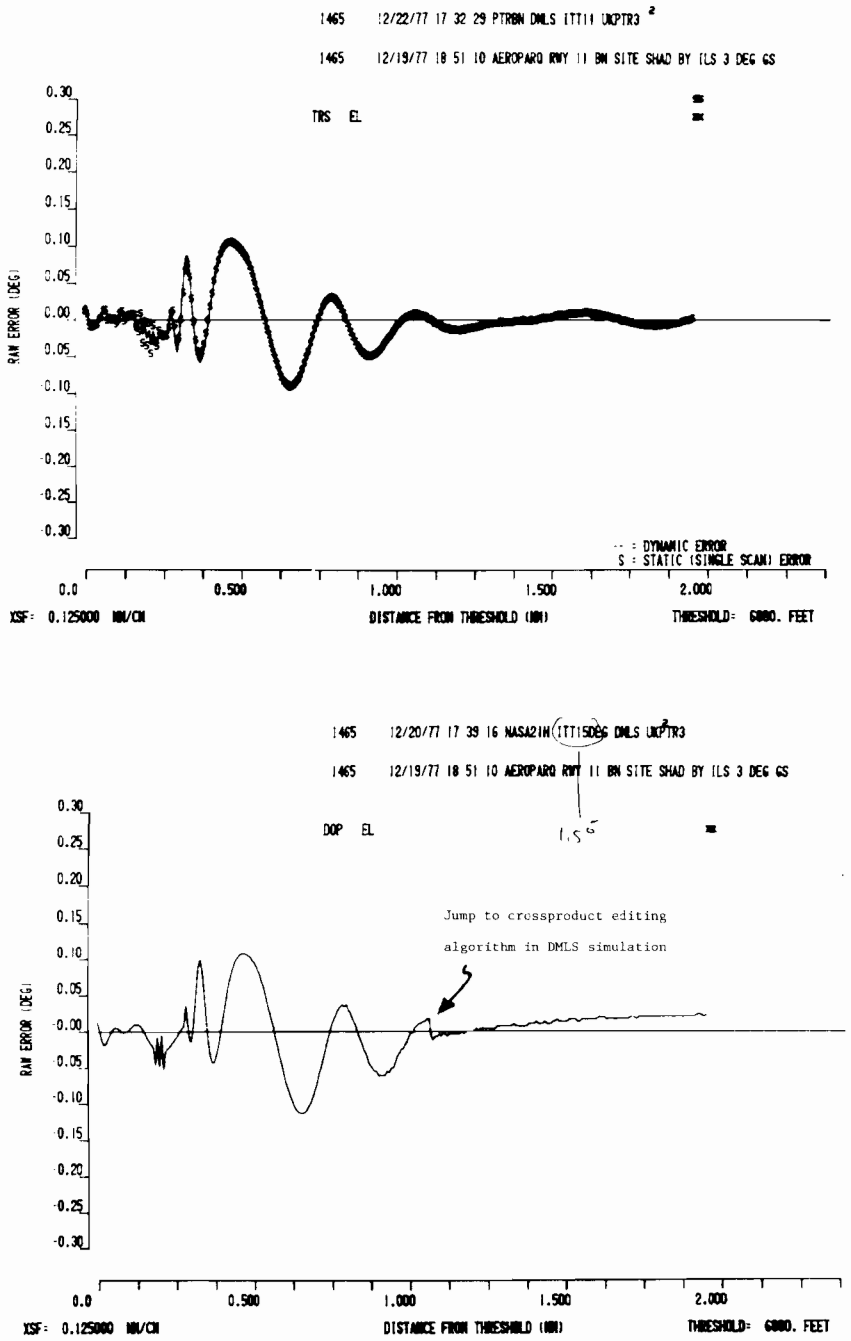

Fig. 4-26. Azimuth errors for shadowing scenario based on Aeroparque (Buenos Aires) field tests.

REFERENCES

1. RTCA SC-117 Final Report, "A New Guidance System for Approach and Landing," RTCA Document DO-148 (Dec. 1970).

2. "National Plan for the Development of the Microwave Landing System," DOT/NASA/DOD Planning Group (July 1971) AD-733268.

3. R.A. Rondini and R.H. McFarland, "Experimental Validation of Boeing 747 ILS Signal Scattering Calculations for Critical Area Determination," FAA SRDS (Jan. 1974) FAA-RD-74-57.

4. "Report of the Seventh Air Navigation Conference," ICAO Doc. 900 4-AN-CONF/7 (April 1972).

5. "Operational Requirements for an Advanced Approach and Landing Guidance System for the Post-1975 Period Prepared by the NATO Industrial Advisory Group (NIAG)," NATO NIAG document NIAG (71) D/1 (March 1971).

6. "The DME-Based-Landing System, DLS," as proposed by the Federal Republic of Germany developed by Standard Elektrik Lorenz AG. and Siemens, AG. (Sept. 1975).

7. "Doppler Microwave Landing Guidance System," proposal submitted by United Kingdom to the International Civil Aviation Organization (Nov. 1975).

8. "Recommendations for Selection of Scanning Beam Technique Using a Time Reference Signal Format for the U.S. Microwave Landing System - Issue Papers and Backup Documentation," Federal Aviation Administration ARD-700 (Jan. 1975).

9. S. Grashoff (chairman) "Report of the Sixth Meeting of the ICAO All-Weather Operations Panel," ICAO Doc. 9200, AWOP/6 (March 1977).

10. T. Breien, "Computer Analysis of MLS in Multipath Environment," IEE Conf. on the Future of All Weather Operations (Nov. 1976).

11. H.A. Wheeler, "Multipath Effects in Doppler MLS," contained in Hazeltine Corp. Report "Microwave Landing System (MLS) Development Plan as proposed by Hazeltine Corp. During the Technique Analysis and Contract Definition Phase of the National MLS Development Program," FAA-RD-73-185 (Sept. 1972).

12. "Microwave Landing System (MLS) Development Plan as Proposed by Texas Instruments, Inc., During the Technique Analysis and Contract Definition Phase of the National MLS Development Program," FAA-RD-74-170 (1 Sept. 1972).

13. ITT/Gilfillan, "Microwave Landing System (MLS) Development Plan as Proposed by ITT/Gilfillan During the Technique Analysis and Contract Definition Phase," FAA-RD-74-118 (Sept. 1972).

14. P. Fombonne, "Position Errors in Microwave Landing Systems," Electronics and Civil Aviation Int. Conf., Paris, France (June 1972).

15. J. Benjamin and G.E.J. Peake, "Contributions to the UK Microwave Landing System Study (Phase 1)," Royal Aircraft Establishment, Tech. Memo RAD 1021 (May 1973).

16. "Interscan," proposal submitted by Australia to International Civil Aviation Organization (December 1975).

17. R. Giles "Study and Test Report on MLS Performance in Shadowing Conditions," ICAO AWOP Paper AWOP/6-BIP.45 (March 1977).

18. B.F. Oreb and J.G. Lucas, "A 1/20th Scale Millimetric Model of the Microwave Landing System," IEE Conf: Future of All Weather Operations (Nov. 1976).

19. L.N. Spinner and V.L. Bencivenga, "Advanced Scanning Beam Guidance System for All Weather Landing," FAA Syst. Res. Dev. Serv., Washington, D.C., RD 68-2 (Feb. 1968), DDC AD-664973.

20. V.L. Bencivenga, "Test and Evaluation of a Portable Scanning Beam Guidance System," (March 1972), FAA-RD-72-16.

21. F.X. Kelly, "Tests of Scanning-Beam Microwave Landing Systems at Difficult Sites," presented at technical seminar "Aviation - A Tool for Economic Development," First International Aerospace Show, Sao Paulo, Brazil (Sept. 1973).

22. Bendix Corp. "Refined Microwave Landing System (MLS) Program Development Plan (Phase III)," (Oct. 1974).

23. Texas Instruments, Inc., "Refined Microwave Landing System (MLS) Development Program Plan," DM74-03-04 (1 Oct. 1974).

24. ITT/Gilfillan, "Five Year MLS Development Program Plan (updated) Microwave Landing System, " MLS-0420 (1 Oct. 1974).

25. Hazeltine Corp., "Refined Microwave Landing System (MLS) Development Program Feasibility Demonstration, Phase II," Report 11009 (1 Oct. 1974).

26. D.A. Shnidman, "The Logan MLS Multipath Experiment," Project Report ATC-55, Lincoln Laboratory, M.I.T. (23 Sept. 1975), DDC AD-A017083, FAA-RD-75-130.

27. D.A. Shnidman, "Airport Survey for MLS Multipath Issues," Project Report ATC-58, Lincoln Laboratory, M.I.T. (15 December 1975), FAA-RD-75-195, DDC AD-A022937/7.

28. J.E. Evans, R. Burchsted, J. Capon, R.S. Orr, D.A. Shnidman, and S.M. Sussman, "MLS Multipath Studies, Volume I: Mathematical Models and Validation; Volume II: Application of Multipath Model to Key MLS Performance Issues," Project Report ATC-63, Lincoln Laboratory, M.I.T. (25 Feb. 1976), FAA-RD-76-3, DDC AD-A023040/9 and DDC AD-A025108/2.

29. J. Capon, "Multipath Parameter Computations for the MLS Simulation Computer Program," Project Report ATC-68, Lincoln Laboratory, M.I.T. (8 April 1976), FAA-RD-76-55, DDC AD-A024350/1.

30. A. Spiridon, "Impact of Obstacle Shadows in Monopulse Azimuth Estimate," Project Report ATC-50, Lincoln Laboratory, M.I.T. (17 July 1975), FAA-RD-75-91, DDC AD-A015139/9.

31. F.L. Frisbie, "Studies of Comparative Shadowing Behavior for DMLS and TRSB," ICAO AWOP Paper AWOP/6-BIP/50 (Feb. 1977).

32. P.S. Demko, "Polarization/Multipath Study," U.S. Army Electro. Command Rep. VL-5-72 (Aug. 1971/June 1972).

33. A.E. Brindley, L.C. Calhoun, and T.N. Patton, (IITRI) "Multipath Environment Evaluation," Air Force Flight Dynamics Laboratory, AFFDL-TR-74-150 (Nov. 1974).

34. ITT Research Institute "A Joint Army/Air Force Investigation of Reflection Coefficient at C and Ku Bands for Vertical, Horizontal, and Circular System Polarizations," AFFDL-TR-76-67 (July 1976).

35. A.E. Brindley, L.E. Calhoun, T.N. Patton, and L. Valcik, "Analysis, Test and Evaluation Support to the USAF Advanced Landing System Program," USAF Flight Dynamics Lab, AFFDL-TR-74-62 (Aug. 1974).

36. E. Bramley and S. Cherry, "Investigation of Microwave Scattering by Tall Buildings," Proc. IEEE, (Aug. 1973).

37. J.G. Lucas and B.F. Oreb, "MLS Modeling Work," Report from Air Navigation Group, School of Electrical Engineering, Univ. of Sydney, Australia, to Australian Dept. of Civil Aviation (1976).

38. B.F. Oreb and J.G. Lucas, "Blocking and Diffraction Due to an ICAO Sheet," personal communication to J. Evans (May 1977).

39. J.E. Evans, D. Karp, R.R. LaFrey, R.J. McAulay, and I.G. Stiglitz, "Experimental Validation of PALM - A System for Precise Aircraft Location," Technical Note 1975-29, Lincoln Laboratory, M.I.T. (29 April 1975), DDC AD-A010112/1.

40. J.E. Evans, "Aperture Sampling Techniques for Precision Direction Finding," paper presented at IEEE Electro 78, Boston, Massachusetts (May 1978).

41. J.E. Evans and S.M. Sussman, "Doppler Azimuth Reference Errors with Out-of-Beam Multipath," ICAO AWOP Working Group A Paper TH.BIP.3 (30 June 1976).

42. T.E. Bernard, "Analytical Studies of Techniques for the Computation of High-Resolution Wavenumber Spectra," Special Report No. 9, Texas Instruments Incorporated, Dallas, Texas (14 May 1969), Project No. VELAT/7701.

43. J. Capon, "High-Resolution Frequency-Wave Number Spectrum Analysis," Proc. IEEE 57, 1408 (1969).

44. N.O. Anderson, "On the Calculations of Filter Coefficients for Maximum Entropy Spectral Analysis," Geophysics 39, 69 (1974).

45. J.P. Burg, "Maximum Entropy Spectral Analysis," Paper presented at the 37th meeting of the Society of Exploration Geophysicists, Oklahoma City, Oklahoma (31 October 1967).

46. R.T. Lacoss, "Data Adaptive Spectral Analysis Methods," Geophysics 56, 661 (1971).

47. R.N. McDonough, "Maximum-Entropy Spatial Processing of Array Data," Geophysics 39, 843 (1974).

48. H.R. Radoski, P.F. Fouger, E.J. Zanalick, "A Comparison of Power Spectral Estimates and Applications of the Maximum Entropy Method," J. Geophy. Res. 80, 619 (1975).

49. T.E. Bernard, "The Maximum Entropy Spectrum and the Burg Technique," Advanced Signal Processing Technical Report No. 1, Texas Instruments Incorporated, Dallas, Texas (25 June 1975), ALEX(03)-TR-75-01.

50. J. Makhoul, "Linear Prediction; A Tutorial Review," Proc. IEEE 63, 561 (1975).

51. T.P. McGarty, "Models of Multipath Propagation Effects in a Ground-to-Air Surveillance System," Technical Note 1974-7, Lincoln Laboratory, M.I.T. (25 February 1974), DDC AD-777241/1.

52. A. Spiridon, "Effects of Local Terrain and Obstacles Upon Near Horizon Gain of L-Band Beacon Antennas," Technical Note 1975-6, Lincoln Laboratory, M.I.T. (17 July 1975), DDC AD-A013732/3.

53. H. Berger and J.E. Evans, "Diversity Techniques for Airborne Communications in the Presence of Ground Reflection Multipath," Technical Note 1972-27, Lincoln Laboratory, M.I.T. (8 September 1972), DDC AD-752249.

54. F. Harris, "On the Use of Windows for Harmonic Analysis with the Discrete Fourier Transform," Proc. IEEE 66, 51 (1978).

55. A. Oppenheim and R. Schafer, Digital Signal Processing (Prentice Hall, New York, L975).

56. A. Brindley, L. Calhoun, T. Patton, and L. Valcik, "Analysis, Test and Evaluation Support to the USAF Advanced Landing System Program Vol. III Part 1 Doppler MLS Guidance Error Data (DOTS Tracking System)," AFFDL-TR-74-62, Vol. III, Part 1 (August 1974).

57. P. Demko, "Propagation Integrity for Microwave Landing Systems," In AGARD Conference Proceedings No. 240 Guidance and Control Design Considerations for Low-Altitude and Terminal-Area Flight (October 1977).

58. "Flight Trials of TRSB/Interscan Equipment at Sydney International Airport, Australia," Paper AWO/78-WP/88 presented by Australia at ICAO AWO Division Meeting. (April 1978).

59. "Tracked Flight Trials of Doppler MLS at Manchester Airport," Paper AWO/78-WP/123 presented by United Kingdom at ICAO AWO division meeting (April 1978).

60. "Tracked Flight Trials of Doppler MLS Azimuth System at Brussels National Airport," Paper AWO/78-WP/12 presented by the United Kingdom at ICAO AWO Division Meeting (January 1977).

61. "Test Results for a Time Reference Scanning Beam (TRSB) 'Basic Narrow' MLS," Paper AWO/78-WO/119, presented by United States at ICAO AWO Division Meeting (April 1978).

62. "DMLS/TRSB Comparative Demonstration Test Results at Brussels National Airport, Brussels, Belgium," Paper AWO/78-WO/141, presented by United States at ICAO AWO Division Meeting (April 1978).

63. DMLS/TRSB Comparative Demonstration Test Results," Paper AWO/78-WP/153 presented by United States at ICAO AWO Division Meeting (April 1978).

64. J.E. Evans and D.A. Shnidman, "Multipath Characteristics of AWOP WG-A Multipath Scenarios," AWOP WG-A Paper TH.BIP/9 also Revision 1 (4 January 1977).

65. "Time Reference Scanning Beam Microwave Landing System," proposal submitted by the United States to the International Civil Aviation Organization (December 1975).

66. R. Butler, (Rappoteur), "Report of the Multipath Subgroup of WG-A Held near Boston, Mass., 11-15 October 1976," L.WP/3 in the report of ICAO AWOP Working Group A, Seventh Meeting, London (Nov. 1-12, 1976).

67. M. Whitney, "UK Presentations and Demonstrations of Doppler MLS Multipath Environments," given at Royal Aircraft Establishment, Bedford, (1 Nov. 1976), CAA Paper 77003 (Feb. 1977).

68. M. Whitney, "DMLS Signal Processing," L.BIP/38 in Report of the Seventh Meeting of ICAO AWOP Working Group A, held in London, U.K. (2-12 Nov. 1976).

69. F. Frisbie, "TRSB Phase III Receiver Functional Description," Paper L.BIP/19 in the report of ICAO AWOP Working Group A, Seventh Meeting, London (Nov. 1976).

70. T. Bohr, "The Proposed DLS Airborne Equipment and DLS System Configuration," L.BIP/42 and L.BIP/43 in Report of ICAO AWOP Working Group A. Seventh Meeting, London (1-12 Nov. 1976).

71. J. Beneke, C. Wightman et al., "Multipath and Performance Tests of TRSB Receivers," FAA-RD-77-66 (March 1977).

72. ICAO All Weather Operations Panel Working Group A, "Report of the Third Meeting Held in Melbourne During the Period 24-28 February 1975" (Feb. 1975).

73. "Validation of Computer Simulation by Comparison with Tests at Operational Airports," Paper AWO/78-WP/135 presented by the United States at ICOA AWO Division meeting (April 1978).

74. "Application and Validation of Computer Simulation to MLS Multipath Performance Assessment," Paper AWO/78-WP/138 presented by the United States at ICAO AWO Division meeting (Jan. 1978).

75. "Performance of Advanced Approach and Landing Systems (AALS)," Electronics Research Laboratory, Univ. of Trondheim, Norwegian Inst. of Tech. (March 1973).

76. "Study of the Radar Reflectivity Characteristics at SSR Frequency of Pilkington 'Insulight' Metallized Glass," Cosser Electronics Limited Report EF/S/055 (Sept. 1973).

77. A. Von Hippel, Dielectric Materials and Applications (Chapman & Hall, Ltd., London,1954).

78. G. Bailey, Personal Communication (Feb. 1977).

79. F.L. Frisbie, "Comparison of DMLS and TRSB Acquisition/Validation in an Azimuth Multipath Environment," ICAO All Weather Operations Panel Working Paper AWOP-WP/322 (March 1977).

80. B.L. Oreb, "Modeling of the Microwave Landing System (MLS) at 104 GHz," PhD Thesis, Univ. of Sydney, Australia, (1978).

81. G.T. Ruck, D.E. Barrick, W.D. Stuart and C. Krichbaum, Radar Cross Section Handbook, Volume 1 (Plenum, New York, 1970).

82. H. Neugebauer and M. Bachynski, "Diffraction by Smooth Cylindrical Mountains," Proc. IRE 41, 1619 (Sept. 1958).

83. I.M. Hunter, "Some Properties of Air-Derived and Ground-Derived Aircraft Landing Guidance Concepts," J. of British Institute of Navigation (1973).

84. K.D. Eckert, "DME Based System for Enroute/Terminal Navigation, All Weather Landing and Air Traffic Control," in AGARD Conference Proc., No. 240 Guidance and Control Design Considerations for Low-Altitude and Terminal Area Flight (Oct. 1977).

85. L. Armijo, K. Daniel, and W. Labuda, "Application of the FFT to Antenna Array Beamforming," EASCON '74 Conference Proceedings, Washington, D.C. (1974).

86. K. Kohler, "Synthetic Radio Direction Finding with Virtual Antenna Patterns," Electric Comm. 48, 299 (1973).

87. W.B. Kendall, "Unambiguous Accuracy of an Interferometric Angle-Measuring System," IEEE Trans. Space Electronics and Telemetry 11, 67 (June 1965).

88. J. Duncan, "The Effect of Ground Reflections on an Interferometric Direction Finder," IEEE Trans. Aerospace Electron. Systems AES-3, 927 (1967).

89. D.K. Barton, "Multipath Error in a Vertical Interferometer," Proc. IEEE 53, 543 (1965).

90. A. Papoulis, The Fourier Integral and Its Applications (McGraw-Hill, New York, 1962).

91. M.F. Whitney, "Simulation of Phased Array Antenna Systems," Working Paper TH.WP-3 presented at the Hague Meeting of AWOP WG-A (July 1976).

92. J. Beneke et al., "TRSB Multimode Digital Processor," Final Report, Calspan Corporation, Report No. FAA-RD-77 (April 1978).

93. Bendix Corp., "Microwave Landing System, Phase III (Basic Narrow and Small Community Configurations) Final Report, Volume 1," Report No. MLS-BCD-R-2801-1 (June 1978).

94. "Report of the All Weather Operations Division Meeting, 1978," International Civil Aviation Organization, Doc. 9242, AWO/78 (April 1978).

95. F. Frisbie, "Out of Coverage Indication (OCI) and Left/Right Guidance," ICAO AWOP Working Group A Background Information Paper L.BIP/20 (Nov. 1976).

96. Hazeltine Corp., "Cost Minimized Phased Array Circuit Technique (COMPACT)," (1976).

97. J. Sebring and J. Ruth, "MLS Scanning-Beam Antenna Implementation," Microwave J. 41 (1974).

98. F. Pogust, "Microwave Landing Systems,"IEEE Spectrum 15, 30 (1978).

99. R. Kelly, H. Redlein and J. Shagena, "Landing Aircraft Under Poor Conditions," IEEE Spectrum 15, 52 (1978).

100. A. Lopez, "Scanning-Beam Microwave Landing System - Multipath Errors and Antenna Design Philosophy," IEEE Trans Antennas Propag. AP-3, 290 (1977).

101. J. Kuznetsov, "Some Questions Concerning Reduction of Multipath Effect on Microwave Landing System Accuracy," ICAO AWOP 6 Paper WP/305 (1977).

102. F.L. Frisbie, "(Latest) Comparison of DMLS Computer Model with January 1977 DMLS Hybrid Simulator Azimuth Multipath Data," ICAO AWOP 6 Paper BIP/62 (1977).

103. H.L. Van Trees, Detection, Estimation and Modulation Theory Part I (John Wiley & Sons, New York, 1968).

104. M. Skolnik, Introduction to Radar Systems (McGraw-Hill, New York, 1962).

105. D.K. Barton and H.R. Ward, Handbook of Radar Measurement (Prentice-Hall, New Jersey, 1969).

106. L. Jolley, Summation of Series (Dover, New York, 1961).

107. R. J. McAulay, "The Effects of Interference on Monopulse Performance," Technical Note 1973-30, Lincoln Laboratory, M.I.T. (1 August 1973), DDC AD-769336/9.

108. Appendix E in "Report of the Seventh Meeting of ICAO AWOP WG-A held in London, UK, Nov. 1-12, 1976" (Dec. 1976).

109. R. Loh, "Preliminary Crows Landing Acceptance Test Data Analysis," MITRE Technical Report MTR-7617 (March 1978).

110. R. Wade, "Effect of TRSB and DMLS Motion Averaged in/beam Multipath from the Elevation System on the Pitch Axis response of a Modern Transport Aircraft on Final Approach," Smith's Industry Report MLS-SI-RW II [presented by M.F. Whitney as AWOP WG-A Background Information Paper W.BIP/1 (May 1976)].

111. S. Grashoff, "Report of the AWOP Working Group A, Fifth Meeting," Washington, D.C. (May 1976).

112. M. Born and E. Wolf, Principles of Optics, 4th edition (Pergamon, London, 1970).

113. S. Grashoff, "Report of AWOP Working Group A, Fourth Meeting," Braunschweig, West Germany (Jan. 1976).

114. S. Grashoff, "Report of AWOP Working Group A, Sixth Meeting," The Hague, Netherlands (July 1976).

115. T. Hagenberg "Modified AWOP WG-A Multipath Scenarios for Simulation with TRSB,"National Aerospace Laboratory NLR The Netherlands memo VV-77-041 L (July 1977).

116. T. Bohr, "Salzburg Scenario for Multipath Simulation Tests,"AWOP Paper AWOP/6 - BIP/52, (March 1977).

117. ICAO Annex 14 Aerodromes Part IV "Obstruction Restriction, Removal and Marking" (18/9/69).

118. "TRSB Microwave Landing System demonstration program at Tegucigalpa, Honduras," Nat. Aviation Facilities Exp. Center Report FAA-NA-78-XX (Feb. 1978).

119. T. Bohr "Multipath Immunity of MLS in Mountainous Sites,"AWOP WG-A Paper L.WP/4 (Nov. 1976).

120. Inst. fur Angewandte Geodasie (Frankfurt), "Salzburg" Map Series M501 Edition 2 - DMG Number NL 33-1 (1966).

121. A.M. Peterson et al., "Low-angle Radar Tracking" Stanford Research Institute Technical Report JSR 74-7 (Feb. 1976).

122. A.R. Lopez, "Scanning beam Microwave Landing System multipath errors and antenna design philosphy," IEEE Trans. Antennas Propag. AP-25, 290 (1977).

123. R.J. Kelly, "Time Reference Microwave Landing System multipath control techniques," Institute of Navigation 31st Annual Meeting, Washington, D.C. (June 1975).

124. R.J. Kelly and E. LaBerge, "Comparison study of MLS airborne signal processing techniques,"NAECOM '78 Proceedings, Dayton, Ohio (May 1978).

125. R.M. Cox and J.R. Sebring, "MLS - a practical application of microwave technology," IEEE Trans. Microwave Theory Tech. MTT-24 , 964 (1976).

126. M. Whitney, "The vulnerability of TRSB MLS to shadowing effects from runway movements," Paper L.P/44 presented at Nov. 1976 (London) meeting of AWOP WG-A.

127. M. Whitney, "TRSB Shadowing -- A Real Problem," Paper L.WP/71 presented at Nov. 1976 (London) meeting of AWOP WG-A.

128. M. Whitney, "Vulnerability of TRSB MLS to Shadowing Effects (Phase II results)," Paper L.BIP/59 presented at Nov. 1976 (London) meeting of AWOP WG-A.

129. F. Frisbie, "TRSB approach azimuth shadowing by taxiing and over-flying aircraft field tests," Paper L.BIP/48 presented at Nov. 1976 (London) meeting of AWOP WG-A.

130. J.B. Keller, "Geometric Theory of Diffraction," J. Opt. Soc. Am. 52, 116 (1972).

131. H. Redlein and R. Masek, "Doppler scanning landing guidance system development," Proc. Inst. Navig. Nat Air Meeting Conf. (April 1971).

132. J. Benjamin and P. Reich, "A survey of microwave landing guidance problems related to the operational requirements," Proc. Inst. Navig. Nat. Air Meeting Conf. (1971).

133. R. Barratt, "The UK approach to MLS," Microwave J. 19, 19 (1976).

134. C. W. Earp, "Doppler techniques employing two-source mobility," presentation to U.S. MLS Assessment Group (Nov., 1974).

135. B. Glance, "Power spectra of multilevel digital phase-modulated signals," Bell Syst. Tech. J. 50 , 2857 (1971).

136. "The limitations of simulation as an aid to MLS selection," ICAO All Weather Operations Divisional Meeting Working Paper AWO/78-WP/128, (April 1978).

137. E. Sherwood and E. Ginzton, "Reflection coefficients of irregular terrain at 10 cm," Proc. IRE 43 , 877 (1955).

138. R. Birgenheier, "Parameter Estimation of Multiple Signals," PhD dissertation, University of California, Los Angeles, 1972.

139. "Computer simulation results for multipath performance comparison," ICAO All Weather Operations Divisional Meeting Paper AWO/78-WP/100, April 1978).

140. I. White, "Reduction of DMLS Bearing Errors Caused by Reference Fading Part I - Ground Equipment Adjustments and Part II - Airborne Equipment Adjustments," Plessey Company Memos 17/76/N130U and 17/76/N131U (Oct. 1976).

141. C. Earp, "Evolution of the commutated Doppler Microwave Landing System," Landing Guidance, Civil Aviation Authority (UK), 1, (1975).

142. D.K. Barton, Radar Resolution and Multipath Effects (Artech House, Dedham, Massachusetts, 1975).

☆U.S. GOVERNMENT PRINTING OFFICE : 1981—700-002/33